Arsenic mobilization processes in inland sediment basins – the example of the Hetao Basin

Zur Erlangung des akademischen Grades einer

DOKTORIN DER NATURWISSENSCHAFTEN (Dr. rer. nat.)

von der KIT-Fakultät für

Bauingenieur-, Geo- und Umweltwissenschaften

des Karlsruher Instituts für Technologie (KIT)

genehmigte

DISSERTATION

von

Dipl.-Geoökol. Hongyan Wang

aus

Shandong, China

Tag der mündlichen Prüfung: 19.02.2021

Referent: Prof. Dr. Stefan Norra

Korreferent: Prof. Dr. HM. Guo

Prof. Dr. Thomas Neumann

Karlsruhe, den 19.02.2021

Erklärung

Hiermit erkläre ich, dass ich die vorliegende Dissertation, abgesehen von der Benutzung der angegebenen Hilfsmittel, selbständig verfasst habe.

Alle Stellen, die gemäß Wortlaut oder Inhalt aus anderen Arbeiten entnommen sind, wurden durch Angabe der Quelle als Entlehnungen kenntlich gemacht.

Diese Dissertation liegt in gleicher oder ähnlicher Form keiner anderen Prüfungsbehörde vor.

Karlsruhe, im März 2021

Hongyan Wang

Acknowledgements

This work could not be completed without the help of the following people:

First and sincerely, I express my deepest gratitude to my supervisor – Prof. Dr. Stefan Norra. Thanks Stefan for taking care of my work and life in Germany. In the life, you always tell me relax and enjoy. In the work, you teach me be patient and precise for what I am doing. The scientific freedom you gave to me enables me to find collaborations and to learn to become an independent scientist. Thanks for the encouragement and tolerance for my PhD! I could not have reached those achievements without you, Stefan! Thanks for the countless greetings during my "dark time", I feel warm with your care staying in Germany.

I would like to thank my co-referees Prof. Dr. Huaming Guo and Prof. Dr. Thomas Neumann. Thanks to Professor Guo for providing me opportunities to learn in his group even before I started my PhD, and gave me the chance to accompany him during his field trips. I started my PhD in his group and learned the fundamentals of research. Thanks to him for providing me samples and so much useful information. His diligence and rigours scholarship inspired me to go forward. Thanks also for the sincere suggestions from Professor Neumann, which let my thesis go smoothly and faster.

Thank the Chinese Scholarship Council (CSC) for giving me a scholarship to study at the Karlsruhe Institute of Technique (KIT), Germany. It is a wonderful and worthful experience to study in Karlsruhe. I never dreamed I could go abroad before I got this scholarship. Further, I like to express my gratitude to Graduate School for Climate and Environment (GRACE) for giving me funding to do experiments outside, and to travel abroad for conferences. Those experiences increased my networks and broadend my horizons. It is helpful for my future career.

My deep and special thanks to Dr. Jörg Göttlicher and Dr. Ralph Steininger. Thank for collecting so many beam times for me and for so many discussions on my experimental details. You taught me a lot of professional knowledge about XAS, and contributed so much to my thesis. Thank you giving me the chance to get closed to such an advanced instrument.

The warm thanks to Dr. Elisabeth Eiche. You gave me constant help for the laboratory work, I could not have survived in the lab without you. Thank you for so many suggestions for my PhD work, and for sharing your experience with me and therein I was able to finish experiment in short time. I am also grateful for your help during applying beam times in SSRL and ALS even though it was not successful. Thanks, Eli!

Thanks as well for Professor Andreas Kappler. You are the first professor to open the collaboration doors to me. I feel so happy and honourable to know and discuss with a professor who has such passion and love for science. You also gave me confidence to look for further collaborators. Thank the funding for collecting Mössbauer spectra for my samples. Thank Dr. James Byrne for countless discussions and numerous simulations for my data. I never met a scientist who is responsible for his/her work like you!

I would like to express my gratitude to Professor Liane Benning. You gave me the chance to do SEM and TEM measurements, also discussed my data and manuscript in depth. Your enthusiasm to science encourages me to do science forever! Thank Dr. Jeffrey Perez, you helped me to collect synchrotron and TEM data even without sleep. You always gave me constructive suggestions for my experiments, and always comfort me when my experiments failed. I am happy to meet a friend and collaborator like you!

Thank Dr. Heidi Höfer providing me funding and support for EPMA analysis. The "old EPMA instrument" helped me a lot to interpret my data! Thank Professor Agnes Kontny for offering me the chance to measure the magnetic susceptibility, which enabled me to know the exciting minerals!

I would like to express my deep gratitude to Ms. Chantalle Kotschenreuther. You can always find something "missed" in the lab. You did not only give help in the lab, but also much more like my sister, gave me help in my life, comfort me when I felt depressed. Thanks, Chantalle! Here, I also thank to all technicians in AGW, Claudia Möβner, Gesine Preuβ, Ralf Wachter, Kristian Nikoloski. Thank you help me analyse countless samples and tolerant my disturbations.

I want to thank Flavia and JingWei and Jia. Thank you always to give me an ear and to listen my complains. Without those ladies, I would not have been so happy to spend the PhD time. Special thanks to Nico. Thank you always try to give solutions for difficulties I met in the experiments.

Thanks, Andrew! Thanks for your help for collecting XAS data. Thank you for the happiness you brought to us. I also want to give thanks to Andre, Andreas, Xiaohui, Jonas, Van. Thank you all to share stories and happy lunch time with me! Thank my friend Yujie, Gai, and Ningyi, thank your company!

Thanks to my family! Words cannot express gratitude to parents. You always gave me support and encouragement. Without you I would not have been able to experience this day . Thank my parents in law, thanks for the help to take care of my child. Special thanks to my husband. Thank you always cheering me up in every dark moment. I could not be a PhD student and study abroad without your support. Thank my lovely child, you give me courage to pursue my future. Here, I dedicate this thesis to all my family members.

Hongyan Wang 王红岩

Karlsruhe

Abstract

Geogenic groundwater arsenic (As) pollution is a worldwide concern that mainly occurs in south and south-east of Asia, including the Ganges-Brahmaputra-Meghna (GBM) plain, the Red River delta and the Mekong delta as well as basins draining the Yellow River and the Yangtze River. In contrast with flood plains in south and southeast of Asia, inland sediment basins show different depositional environment and chemical groundwater compositions, especially regarding high SO_4^{2-} concentrations and pH values. Thus, the mechanisms of As release and transport in the aquifers might be different. However, most of the study focusses on those flood plains based on collecting groundwater and sediment samples. In the north of China, the Hetao Basin is a typical inland basin with As concentrations up to 570 μg/L. Here, the As mobilization is complexed by Fe-S-organic carbon coupled interactions. It provides us a natural laboratory to study the As mobilization in the inland basins.

In this dissertation, I mainly used high-resolution spectroscopy (e.g. XAS and Mössbauer) and microscopy in combination with other geochemical techniques to interpret the Fe–S–As coupled redox profiles in the sediments under depositional frames of the Hetao Basin. Specifically, the objectives of this study were to 1) trace the depositional environment and source of SO_4^{2-} in the Holocene–late Pleistocene aquifers sediments, 2) characterize the Fe-As–S coupled redox minerals in the sediment profiles, 3) indicate the influence of Fe-As-S interaction for groundwater As mobilization and 4) elucidate the impact of organic carbon-rich sediments (peats) for As transport.

Sediments in the Hetao Basin are probably resourced from the Lang Mountains, as indicated by their similar rare earth element (REE) compositions. Weathering of As-enriched minerals from the Lang Mountains may have contributed to the relatively higher sediment As content (11 mg/kg in average) compared to other sediments from south and southeast of Asia. Carbon isotope ($\delta^{13}C$) of organic carbon in combination with C/N ratio revealed that sediments were mainly deposited in the aquatic environment and corresponded to the fluvial-lacustrine deposit, while the sediments at depths of 10-30 m have mostly lacustrine deposit.

The lacustrine depositional environment in the Hetao Basin enables evaporites precipitation. Dissolution of sulfates contributes to the high groundwater SO_4^{2-} concentration. The Fe-S-organic carbon coupled reactions following by sulfates dissolution under redox oscillations further influences the As partitions in the aquifers. Modelling results suggest that thio-As species,

especially thio-arsenate existed in the groundwater and increased As mobilization potentials, while pyrite might form with saturation of FeS_2 and incorporated As into its structure.

Spectroscopy methods in combination with microscopy, and other geochemical techniques were used to further elucidate the As, S and Fe speciation in the sediments. The As K-edge X-ray absorption near-edge structure spectroscopy (XANES) showed the surface sediments are dominated by As(V) species (84%), and a decreasing trend with depth ($R^2 = 0.59$) was revealed. Iron oxides were predominantly goethite and hematite, which also decreased in concentration with depth as indicated by Fe K-edge extended X-ray absorption fine structure (EXAFS). Correlations between the sum of goethite & hematite and desorbable & reducible As ($R^2 = 0.89$) provided the solid evidences that As mainly adsorbed/incorporated on/into Fe(III) oxides in the sediments. Desorption of As from Fe(III) oxides mainly caused As release into groundwater.

Groundwater As contamination in the Hetao Basin shows depth-dependent distribution patterns in general, higher As concentration is found in the unconfined aquifers (10–30 m) (Guo et al., 2008; Cao et al., 2017). The average releasable As content (sum of desorb-able and reducible) (5.4 mg/kg in average) in unconfined aquifers was higher than in aquifers below (3.6 mg/kg in average). It was deduced that higher contents of releasable As in combination with paleolake-derived organic carbon contribute to higher groundwater As concentrations in unconfined aquifers compared to semi-confined aquifers.

Sulfur K-edge XANES fitting results indicated that S in the sediments mainly exists as SO_4^{2-}, also sulfide was detected in most sediments. Iron sulfides and associations with As were detected in particular sediment spots. The As-Fe sulfide associations caused by redox heterogeneity contribute to the heterogeneous groundwater As distribution.

Three organic carbon-rich (peats) sediments were analyzed to elucidate the influence for groundwater As mobilization. Pyrite and metastable greigite as Fe and S transformation end members existed in peats, and they were likely formed in the early diagenetic processes in the water-sediments interface. The Fe–rich phyllosilicates and decaying plants provided an ideal micro-environment for Fe sulfides nucleation, while the organic carbon provided enough electrons for Fe and SO_4^{2-} reduction. Peat layers had the As content up to 250 mg/kg with large proportions (40 to 60 %) of As sequestrated in the Fe sulfides. Pyrite crystallites had up to 1 wt.% As content through the replacement of the S(-I) sites. Greigite crystallites had a relatively constant As content ranging from ~500 to 1400 mg/kg, and As formed As sulfides with sulfide from greigite, analogous

to realgar. The As-associated Fe sulfides performed stable under anoxic conditions. However, part of pyrite was found to oxidize into ferrihydrite, which had average similar As concentrations (~ 4000 mg/kg) compared to pyrite, indicating that As transformed from pyrite crystallites to ferrihydrite. Transformation of pyrite to ferrihydrite retarded As release into groundwater with As incorporating into ferrihydrite structure. However, the groundwater oxidation state is highly variable, which is influenced by the anthropogenic perturbations and seasonal fluctuations. The subsequent ferrihydrite reduction may cause As release into aquifers.

Overall, I investigated the depositional environment in the Hetao Basin, and applied high-resolution spectroscopic techniques to identify and explain the Fe-S-As redox profiles. I contributed to a better understanding of the interplay between Fe-S related redox minerals formation and As mobilization. This dissertation especially contributes to the mechanic study of As mobilization in inland sediment basins.

Zusammenfassung

Die geogene Grundwasserbelastung durch Arsen (As) ist ein weltweites Problem, das hauptsächlich im Süden und Südosten Asiens verbreitet ist, einschließlich des Ganges-Brahmaputra-Meghna (GBM), des Roten Flusses und des Mekongs sowie der Becken, die der Gelbe Fluss und der Jangtse durchfließen. Im Gegensatz zu den Überschwemmungsgebieten im Süden und Südosten Asiens weisen die Sedimentbecken im Landesinneren normalerweise eine andere Ablagerungsumgebung und Grundwasserzusammensetzung auf, insbesondere mit einer hohen SO_4^{2-} Konzentration, so dass die Mechanismen der As-Freisetzung und des As-Transports in den Grundwasserleitern unterschiedlich sein könnten. Die meisten Studien konzentrieren sich jedoch auf diese Überschwemmungsgebiete und basieren auf Grundwasser- und Sedimentproben. Das Hetao-Becken ist ein typisches Binnenbecken im Norden Chinas mit einer As-Konzentration von bis zu 570 µg/L. Die As-Mobilisierung wird durch gekoppelte Fe-S-organischer Kohlenstoff-Wechselwirkungen komplexiert. Das Hetao-Becken stellt ein natürliches Labor dar, um die As-Freisetzung in den Binnenbecken zu untersuchen.

In dieser Dissertation habe ich hauptsächlich hochauflösende Spektroskopie (z.B. XAS und Mössbauer) und Mikroskopie in Kombination mit anderen geochemischen Techniken verwendet, um die Fe-S-As gekoppelten Redoxprofile in den Sedimenten unter Ablagerungsbedingungen des Hetao-Beckens zu interpretieren. Die Ziele dieser Studie waren 1) die Ablagerungsumgebung und die Quelle von SO_4^{2-} in den Sedimenten des holozänen und spätpleistozänen Grundwasserleiters zu ermitteln, 2) die Fe-As-S-gekoppelten Redoxminerale in den Sedimentprofilen zu charakterisieren, 3) den Einfluss der Fe-As-S-Wechselwirkung auf die Mobilisierung von As im Grundwasser aufzuzeigen und 4) den Einfluss der organischen, kohlenstoffreichen Sedimente (Torf) auf die Mobilisierung/Immobilisierung von As im Grundwasser zu klären.

Die Sedimente im Hetao-Becken stammen wahrscheinlich aus dem Lang-Gebirge, was durch die ähnliche Zusammensetzung der Seltenen Erden (REE) angezeigt wird. Die Verwitterung von As-angereicherten Gesteinen aus dem Lang-Gebirge könnte zu dem relativ höheren As-Gehalt im Sediment (durchschnittlich 11 mg/kg) im Vergleich zu Sedimenten aus Süd- und Südostasien beitragen. Das Kohlenstoff-Isotop ($\delta^{13}C$) des organischen Kohlenstoffs in Kombination mit dem C/N-Verhältnis zeigte, dass die Sedimente hauptsächlich in einer aquatischen Umgebung

abgelagert wurden und fluvial-lakustrinen Ablagerungen entsprachen. Die Sedimente aus einer Tiefe von 10-30 m weisen die meisten lakustrinen Ablagerung auf.

Die lakustrine Ablagerungsumgebung im Hetao-Becken ermöglicht die Ausfällung von Evaporiten. Die Auflösung von Sulfaten trägt zur hohen SO_4^{2-} Konzentration im Grundwasser bei. Die Fe-S-organischen Kohlenstoff gekoppelten Reaktionen, die auf die Sulfatauflösung unter Redox-Oszillationen folgen, haben die As-Verteilung in den Aquiferen weiter beeinflusst. Modellierungsergebnisse legen nahe, dass Thio-As-Spezies, insbesondere Thio-Arsenat, im Grundwasser existierten und das As-Mobilisierungspotenzial erhöhten, während sich Pyrit mit der Sättigung von FeS_2 bildete und As in die Struktur einbauen konnte.

Spektroskopien in Kombination mit Mikroskopien und anderen geochemischen Techniken wurden eingesetzt, um die As-, S- und Fe-Speziation in den Sedimenten weiter aufzuklären. Die As-K-Kanten-Röntgenabsorptions-Nahkanten-Strukturspektroskopie (XANES) zeigte, dass die Oberflächensedimente von As(V)-Spezies dominiert sind (84 %), der Gehalt jedoch mit der Tiefe abnimmt ($R^2 = 0,59$). Bei den Eisenoxiden handelte es sich überwiegend um Goethit und Hämatit, deren Konzentrationen ebenfalls mit der Tiefe abnahmen, wie die erweiterte Röntgenabsorptionsfeinstruktur (EXAFS) der Fe-K-Kante zeigte. Korrelationen zwischen der Summe von Goethit und Hämatit sowie desorbierbarem und reduzierbarem As ($R^2 = 0,89$) lieferten solide Beweise dafür, dass As hauptsächlich an Fe(III)-Oxide in den Sedimenten adsorbiert/inkorporiert wurde. Die Desorption von As von Fe(III)-Oxiden ist die Hauptursache für die As-Freisetzung ins Grundwasser.

Die As-Kontamination des Grundwassers im Hetao-Becken zeigt im Allgemeinen tiefenabhängige Verteilungsmuster, wobei höhere As-Konzentrationen in den ungespannten Aquiferen (10-30 m) zu finden sind (Guo et al., 2008; Cao et al., 2017). Der durchschnittliche freisetzbare As-Gehalt (Summe aus desorbierbarem und reduzierbarem As) (im Durchschnitt 5,4 mg/kg) war in den ungespannten Aquiferen höher als in den darunter liegenden Aquiferen (im Durchschnitt 3,6 mg/kg). Daraus kann gefolgert werden, dass ein höherer Gehalt an freisetzbarem As in Kombination mit aus Paläoseen stammendem organischem Kohlenstoff zu höheren Grundwasser-As-Konzentrationen in nicht gespannten Grundwasserleitern beiträgt.

Die Schwefel-K-Kanten-XANES-Anpassung zeigte, dass S in den Sedimenten hauptsächlich als SO_4^{2-} vorliegt, während der reduzierte Schwefel (einschließlich S(-I) und S(-II) und nullwertigem

Schwefel (S0)) in den meisten Sedimenten nachgewiesen wurden. Eisensulfide und Assoziationen mit As wurden an bestimmten Stellen im Sediment nachgewiesen. Die durch Redox-Heterogenität verursachten As-Fe-Sulfid-Assoziationen trugen zur heterogenen As-Verteilung im Grundwasser bei.

Drei organisch kohlenstoffreiche (Torf) Sedimente wurden analysiert, um den Einfluss für die Grundwasser-As-Mobilisierung zu klären. Pyrit und metastabiler Greigit als die Fe- und S-Transformationsendglieder existieren in den Torfen, und sie wurden wahrscheinlich in den frühen diagenetischen Prozessen in der Wasser-Sediment-Grenzfläche gebildet. Die Fe-reichen Schichtsilikate und verrottenden Pflanzen boten eine ideale Mikroumgebung für die Keimbildung von Fe-Sulfiden, wobei der organische Kohlenstoff genügend Elektronen für die Fe- und SO_4^{2-}-Reduktion lieferte. Torfschichten hatten einen As-Gehalt von bis zu 250 mg/kg mit großen Anteilen (40 bis 60 %) von As, das in den Fe-Sulfiden sequestriert war. Pyritkristallite hatten bis zu 1 Gew.-%As-Gehalt durch den Austausch der S(-I)-Stellen. Greigitkristallite hatten einen relativ konstanten As-Gehalt im Bereich von ~500 bis 1400 mg/kg, und das As bildete As-Sulfide mit Sulfid aus Greigit, analog zum Realgar. Die As-assoziierten Fe-Sulfide zeigten sich unter anoxischen Bedingungen stabil. Es wurde jedoch festgestellt, dass ein Teil des Pyrits zu Ferrihydrit oxidierte, der im Durchschnitt ähnliche As-Konzentrationen (~ 4000 mg/kg) wie Pyrit aufwies, was darauf hindeutet, dass As von Pyritkristalliten zu Ferrihydrit transformiert wurde. Die Umwandlung von Pyrit in Ferrihydrit verzögerte die As-Freisetzung ins Grundwasser. Der Oxidationszustand des Grundwassers ist jedoch sehr variabel und wird von anthropogenen Störungen und saisonalen Schwankungen beeinflusst, so dass die anschließende Ferrihydrit-Reduktion eine As-Freisetzung in den Grundwasserleiter verursachen kann.

Zusammenfassend ist zu sagen, dass ich die Ablagerungsumgebung im Hetao-Becken untersucht und hochauflösende spektroskopische Techniken angewendet habe, um die Fe-S-As-Redoxprofile zu identifizieren und zu erklären. Dadurch entwickelte ich ein besseres Verständnis für das Zusammenspiel zwischen der Bildung von Fe-S-verwandten Redoxmineralen und der As-Mobilisierung. Diese Dissertation trägt insbesondere zum Studium der Mechanismen der As-Mobilisierung in den Binnensedimentbecken bei.

Contents

List of Figures

List of Tables

Abbreviations

WHO	World Health Organization
MMA	monomethylarsonate
DMA	dimethylarsinate
AAAS	American Association for the Advancement of Science
ArsC	arsenate reductase
DARP	arsenate-reducing prokaryotes
TDS	total dissolved solids
KIT	Karlsruhe Institute of Technology
WDX	Wavelength Dispersive X-ray Fluorescence Spectrometry
EDX	Energy Dispersive X-ray Fluorescence Spectrometry
HG-FIAS	Hydride Generation Flow Injection Atomic Sorption Spectroscopy
REE	Rare Earth Elements
ICP-MS	Inductively Coupled Plasma Mass Spectrometry
TC	Total Carbon
CSA	Carbon/Sulfur Analyzer
TOC	Total Organic Carbon
XRD	X-ray Diffraction
SEM	Scanning Electron Microscopy
EPMA	Electron Probe Microanalysis
XAS	X-ray Absorption Spectroscopy
EXAFS	Extended X-ray Absorption Fine Structure
XANES	X-ray Absorption Near Edge Structure
LCF	Liner Combination Fitting
VBF	Voigt Based Fitting
HWHM	Half Width at Half Maximum
TS	Total Sulfur
TN	Total Nitrogen

EDX	Energy Diffraction X-ray Spectroscopy
IR-MS	Isotope Ratio Mass Spectrometer
ICP-OES	Inductively Coupled Plasma Atomic Emission Spectroscopy
TEM	Transmission Electron Microscopy
LGM	Last Glacial Maximum
GBM	Ganges-Brahmaputra-Meghna
POC	Particular Organic Carbon
CAOB	Central Asian Orogenic Belt
CUGB	China University of Geoscience (Beijing)
TIC	Total Inorganic Carbon
CIA	Chemical Index of Alteration
UCC	Upper Continental Crust
MREE	Middle Rare Earth Element
GRACE	Graduate School for Climate and Environment
AGW	Applied Geoscience Institute
ESRF	European Synchrotron Radiation Facility

1 Context of this dissertation

1.1 Purposes and whole structure of the dissertation

Arsenic (As), a metalloid, ranks 20th in abundance in the earth's crust (Cullen and Reimer, 1989). As a "killer", the inorganic As can cause disorders of the skin, vascular and nervous systems, as well as cancers (Smith et al., 2000). Drinking As contaminated groundwater is an important way for people to become exposed to As, even though diet, especially rice, also is important. A latest global prediction model estimates that up to 220 million people in the world are potentially exposed to high As groundwater, with more than 90% being in Asia (Podgorski and Berg, 2020).

Geogenic groundwater As contamination mostly occurs in the alluvial sediment aquifers of south and southeast of Asia and inland sediment basins in the Yellow River and the Yangtze River catchment. It shows high heterogeneity, which makes it hard to find As-free supply wells. In general, it is accepted that microbial or chemical reduction of Fe (oxyhydr)oxides release As into groundwater (Islam et al., 2004; Fendorf et al., 2010). But the fate of As is still not fully understood due to the complex biogeochemical cycling in the aquifer, especially in the inland basins which are less studied.

This dissertation aims to indicate the influence of Fe-S-organic carbon coupled sedimentation mineralogy for As partitions in the aquifers, towards for better understanding the heterogenous groundwater As contamination especially in inland basins. The Hetao Basin, located in the middle of the Inner Mongolia, China, is a typical inland basin. The As release in the aquifers is complexed by microbial Fe-S-organic carbon coupled redox recycle. It provides an ideal area to carry out this research.

This dissertation is based on four scientific publications, which are all research articles, and I am the first author for these publications, and corresponding author for three articles. All of these publications are based on the sediment sample characterizations, which were collected from scientific boreholes in the Hetao Basin. Those publications are outlined from chapter 2 to chapter 5.

In order to better understand contents of this dissertation, the research background will be introduced as follows: section 1.2 arsenic properties; section 1.3 worldwide occurrence of groundwater As contamination; section 1.4 As mobility in the groundwater; section 1.5 remediation strategy for groundwater As contamination; section 1.6 open questions; section 1.7

study area; section 1.8 summary of sampling and experimental methods.

Finally, the As mobilization mechanisms in the inland sediment basins are synoptically discussed in chapter 6 according to the results and discussions shown from chapter 2 to chapter 5, and a concept model is generated.

1.2 Arsenic properties

1.2.1 General chemical property and toxicity

Arsenic (As), atomic number 33, is a typical metalloid, which possesses properties of both metals and non-metals. It belongs to group V-A of the periodic table, has an atom. Wt. of 74.92, and chemically resembles phosphorus. The ^{75}As is the only stable isotope in nature, the valence states include As(-III), As(0), As(III), As(V). It covalently bonds with most nonmetals and metals, and forms stable organic compounds in both, its trivalent and pentavalent states. World production of As is estimated to be 75 to 100×10^3 tons annually (Baker and Chesnin, 1975). It is mainly used in agriculture and forestry as pesticides, herbicides, and silvicides.

Inorganic As compounds are highly toxic, it is the most significant chemical contaminant especially in drinking water. Long-term exposure to As via food or drinking water can cause skin cancers, and probably bladder and lung cancers. It may be also associated with developmental effects, diabetes, pulmonary disease, and cardiovascular disease (Jomova et al., 2011). A large area of arsenicosis from drinking groundwater in China was first reported in Kuitun, located in Xinjiang Autonomy region in 1980. In 1989, the Inner Mongolia was reported as another endemic area of severe arsenicosis (Sun, 2004).

1.2.2 Arsenic in the natural environment

1.2.2.1 the As abundance

The As concentration in the earth's crust is around 1.5 mg/kg (Taylor and Mclennan, 1995). It is commonly associated with sulfide in the ores including arsenopyrite (FeAsS), arsenian pyrite ($As(FeS_2)$), realgar (As_4S_4), orpiment (As_2S_3). Even though those minerals are rare in the environment, weathering of pyrite can cause As incorporation into/adsorb onto other minerals such as Fe oxy(hydr)oxides. Arsenic concentrations range from 0.5 to 2.5 mg/kg in most rocks, and 1.5

to 3.0 mg/kg in terrestrial sources (Mandal and Suzuki, 2002). The specific concentrations in various minerals whichare common in the sediments are detailed in **Table 1**.

Table 1 Arsenic content in various minerals.

Minerals	As (mg/kg)	References	Minerals	As (mg/kg)	References
Hematite	<160	(Boyle and Jonasson, 1973)	Illite	10-41	(Pal et al., 2002)
Ilmenite/Magnetite	<1-41	(Baur and Onishi, 1969)	Dolomite	<3	(Boyle and Jonasson, 1973)
Quartz	0.4-1.3	(Baur and Onishi, 1969)	Calcite	1-8	(Boyle and Jonasson, 1973)
Feldspar	<0.1-2.1	(Baur and Onishi, 1969)	Gypsum/Anhydrite	<1-6	(Boyle and Jonasson, 1973)
Arsenopyrite/Arsenian pyrite	100-77,000	(Smedley and Kinniburgh, 2002)	Ferrihydrite	<76,000	(Pichler et al., 1999)
Biotite	1.4	(Baur and Onishi, 1969)	Chlorite	5-50	(Sengupta et al., 2004)

1.2.2.2 Speciation of As in aquatic environment

The As speciation in the aquatic environment mainly depends on the redox (Eh) and pH conditions as well as concentrations of some redox components such as sulfide (Ferguson and Gavis, 1972). As so far, the As speciation in different aquatic environments is still not fully investigated, due to the difficulties of preserving redox-sensitive samples, and limitations of measurement techniques.

The Eh-pH diagram for inorganic As species is shown in **Fig. 1**. Arsenic state shows +V under oxidizing conditions, it exists as H_3AsO_4 at pH < 2, and it co-exists as $H_2AsO_4^-$ and $HAsO_4^{2-}$ species in the pH ranging from 2 to 11. Under anoxic conditions, the uncharged H_3AsO_3 is the dominant speciation with pH less than 9.2. In contrast with other oxyanion-forming elements such as Se, Cr, U, the As is stable over a wide range of redox conditions in the water, therefore considerable mobilization potentials.

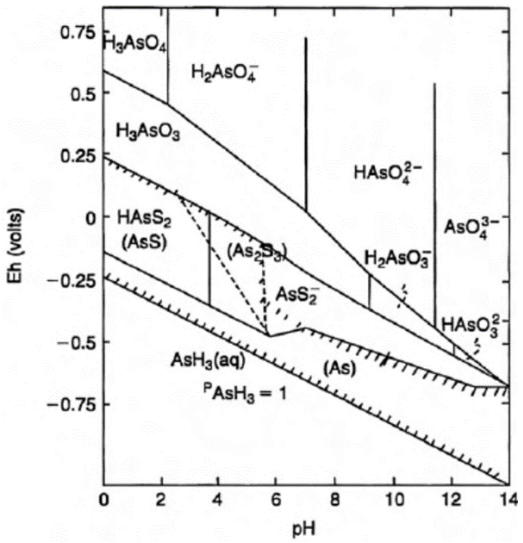

Figure 1 The Eh – pH diagram for As at 25 °C with total As 10^{-5} mol L^{-1} and total sulfur 10^{-3} mol L^{-1}. Solid species are enclosed in the parentheses in cross – hatched area, which indicates solubility less than $10^{-5.3}$ mol L^{-1}. (reproduced from (Ferguson and Gavis, 1972) with permission from Elsevier).

In the sulfidic aquatic environment, the As can substitute S in pyrite (FeS_2), arsenopyrite (FeAsS), or adsorb onto sulfides, or forming sulfide minerals including realgar (As_4S_4) or orpiment (As_2S_3) (Day et al., 2004; Couture et al., 2010; Burton et al., 2011; Le Pape et al., 2017). Two homogenous series of monomeric thio-arsenic species also can exist under sulfidic conditions: (oxy)thioarsenites with As in the oxidation state of +III ($AsO_xS_{3-x}^{3-}$ with x = 0-2) and (oxy)thioarsenates with As oxidation state of +V ($AsO_xS_{4-x}^{3-}$ with x = 0-3). But thioarsenites are sensitive to oxygen and pH variations and easily change to thioarsenates (Wilkin et al., 2003; Planer-Friedrich et al., 2010). Insoluble sulfides (e.g. As_4S_4 and As_2S_3) are mostly formed when As concentrations reach to mg/L (Smedley and Kinniburgh, 2002). However, the As concentration is relatively low in the natural geogenic As contaminated groundwater, normally up to hundreds of µg/L. The thio-As species are often measured and can become the dominant species (> 80%) (Planer-Friedrich et al., 2010; Sigfu et al., 2014; Planer-Friedrich et al., 2018). In addition, methylated organoarsenic compounds including MMA and DMA are also found in the natural water (Oremland and Stolz, 2003), which are generally synthesized by organisms or formed by reacting with constituents of organisms (Ferguson and Gavis, 1972).

Furthermore, the As also can form colloids with metals and dissolved organic carbon. Evidences show As can bind to dissolved organic matter via sulfhydral groups and form ternary

complexes with ferric iron and dissolved organic matter (Langner et al., 2011). The As colloids are not easy to adsorb onto other medias compared to arsenite, therefore increasing its mobility.

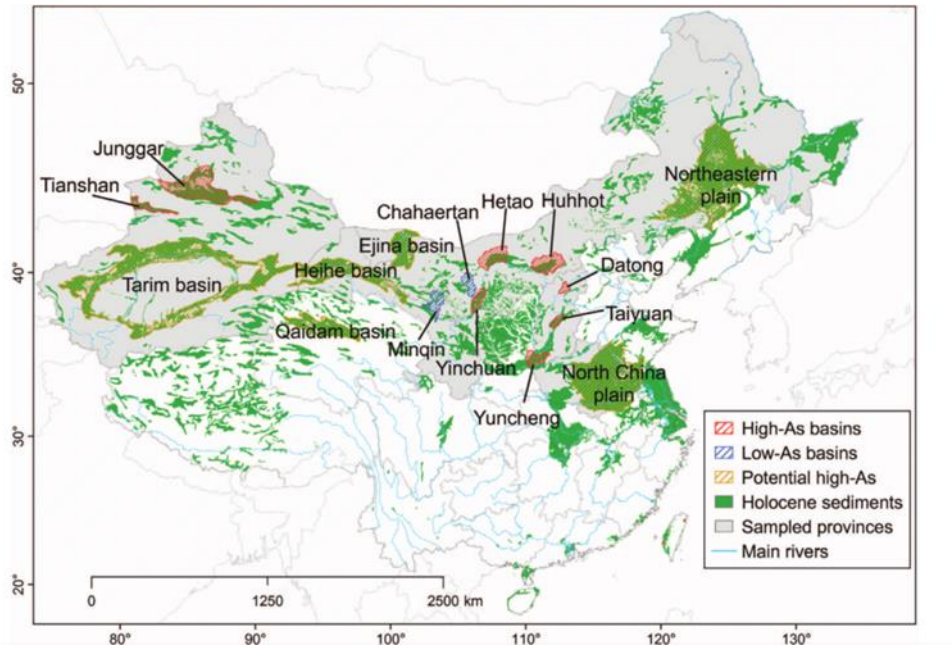

Figure 2 Locations of known and potential As-affected basins in China. (from Rodríguez-lado et al., (2013), reprinted with permission from AAAS).

1.3 Worldwide occurrence of groundwater As contamination

Groundwater As contamination was initially discovered in the Bangladesh. In Bangladesh, surface water was contaminated by the sewage and other organic pollutants. For getting bacteriologically-safe drinking water, government provides tube wells, which abstract water from alluvial fans (Nickson et al., 2000). This achievement reduces the incidence of waterborne disease; however, groundwater was found to be contaminated with As. And this problem threatened a significant proportion of millions of people in Bangladesh.

With the expanding groundwater quality investigation, the As contamination problems gradually became a worldwide concern, mostly reported from Bangladesh, West Bengal, India, Vietnam, Cambodia, Thailand, China, Argentina, USA. The new global prediction map shows that high As groundwater exists on all continents, where 94 million to 220 million people potentially are exposed to high As concentrations in groundwater (Podgorski and Berg, 2020).

Groundwater As contamination in China was recognized in 1960s (Sun, 2004). It mainly occurs in the alluvial/pluvial inland sediment basins of the Yellow River and the Yangtze River

catchment (**Fig. 2**). Around 19.6 million people are estimated to be affected by the consumption of As-contaminated groundwater (Rodríguez-lado et al., 2013).

1.4 Arsenic mobility in groundwater

Most groundwater As contaminations are geogenic processes. In general, two environments can cause geogenic groundwater As contamination: (1) closed basins with semi-arid to arid climate, groundwater normally have alkaline pH conditions, the As desorbs into groundwater via competed OH^- or concentrates result from evaporation, Mexico or Argentine for example (Nordstrom, 2002; Bundschuh et al., 2004; Mar et al., 2011); (2) young alluvial plains, groundwater normally has strong reducing conditions, the As releases into groundwater result from Fe oxy(hydr)oxides reduction, mainly found in south and southeast of Asia such as Vietnam, Bangladesh, Cambodia. Furthermore, geothermal water can have high As concentrations, resulting from high-temperature water that leaches elements out from rocks on the way to the surface. It is widely found in the western USA, Mexico, central America, Japan, New Zealand, Papua New Guinea, Chile, Philippines, Indonesia, Kamchatka, Alaska and Iceland, France (Smedley and Kinniburgh, 2002; Tyrovola et al., 2006).

1.4.1 Groundwater As species

Subsurface sediments return to the anoxic conditions after O_2 is depleted. For detoxifying or gaining energy purpose, the arsenate reductase (ArsC) enzyme catalyzes the reduction of As(V) species to As(III) species (Kumari and Jagadevan, 2016). The major As(V)-respiring bacteria in the groundwater includes *Bacillus, Wolinella, Citrobacter, Clostridium, Sulfurospirillum, and Desulfomicrobiumetc* (Biswas et al., 2019). But As(V) species still can account for proportions of As pool in the sediments, even though under strong reducing conditions, which might be due to that redox reactions in aquifer are kinetically controlled, and do not reach balance. For instance, arsenite can be oxidized by Mn oxides (Suda and Makino, 2016). It also might be biologically controlled. The reduction of As(V) species to As(III) species as occurring in water phases or minerals phases depends on the crystallinity of minerals and microbial communities (Islam et al., 2004; Tufano and Fendorf, 2008; Borch et al., 2010). Microcosm experiments suggest that arsenate reduction likely preceding the Fe oxides reduction, while laboratory experiments indicate that

arsenate reduction can occur before or without Fe oxides reduction even with ferrihydrite presenting in the system (Zobrist et al., 2000; Islam et al., 2004; Tufano and Fendorf, 2008).

Furthermore, arsenite-sulfide species can be dominant species under sulfidic conditions. Experimental results show that arsenite, and thio-As dominate arsenic speciation at sulfide concentrations > $10^{-4.3}$ M under neutral pH (Wilkin et al., 2003). Thio-arsenate (monothioarsenate) was found to occur in most groundwater samples in Bangladesh (Planer-Friedrich et al., 2018). The thio-arsenate species forms via two steps, sulfide exchange for hydroxyl groups forms thioarsenites firstly ($As^{III}S^{-II}_nO_{3-n}{}^{3-}$, with n =1-3), then addition of S_0 causes thio-arsenites that oxidize to thio-arsenates (Planer-Friedrich et al., 2018). With high concentration of humic substance or other organic molecules, the As also can form colloids with those organics and other ions such as Fe, Al (Guo et al., 2011). Furthermore, methylated As is also detected in the groundwater.It is estimated that biomethylation in aquifers has the potential to transform 100 tons of the inorganic As to methylated As species per year (Maguffin et al., 2015), but it seems not to be the major species in groundwater.

1.4.2 Parameters for influencing As mobilization

The worldwide occurrence of groundwater As contamination is mostly a natural process. A small change of partition of As in the sediments can cause significant change of groundwater As concentrations. The release of 0.1 mg/kg As from sediments can cause 200 µg/L As in the groundwater (Geen et al., 2003). However, groundwater As concentration is not simply related to the sediments As content. Over the years, even though several As mobilization mechanisms are put forward, it is still hard to explain the As transport behavior, resulting from complex and heterogeneous sediments compositions, biogeochemical reactions in the groundwater, and hydrogeological conditions. The main As mobilization mechanisms and influencing parameters are outlined in **Fig. 3** and introduced as follows:

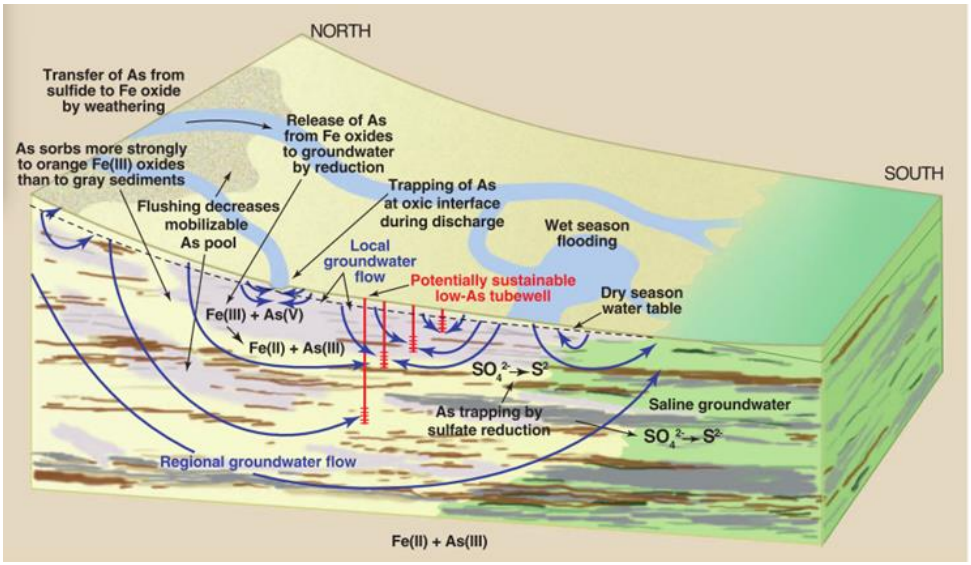

Figure 3 Conceptual diagram to show key processes influencing As distribution in aquifers. from (Fendorf et al., 2010), reprinted with permission from AAAS.

1.4.2.1 Sediments source and depositional environment

The ultimate As source in the sediments of groundwater As contaminated area is still not fully understood. Based on the distribution characters of global groundwater As contaminated areas, it is proposed that sedimentary As in the foreland deltas or basins is resourced from magmatic rocks, which are exposed to the surface via orogenesis (Mukherjee et al., 2014). The As-containing minerals such as pyrite, chlorite, biotite in the Himalaya Mountains were brought to the floodplains of south and southeast of Asia via river debris and weathered to Fe/Mn oxides-As minerals. Arsenic content in sediments is 5-8 mg/kg in average in the floodplains of south and southeast of Asia (Eiche et al., 2008).

Either in the flood plains of south and southeast of Asia or inland basins of the Yellow River and the Yangtze River catchments, groundwater As contamination of both occurs in the late Pleistocene-Holocene aquifer systems. In the late Pleistocene-Holocene epoch, the climate became warmer, and more life broke out in the earth. Therefore the relative higher contents of reactive organic carbon and As following higher weathering intensities were buried in the sediments. Furthermore, the warmer climate creates advantages for metabolisms and developing anoxic conditions. In the floodplains of south and southeast of Asia, the distribution of As contaminated water is influenced by patterns of river intrusion and infilling, which is a response to the glacial sea level changes during quaternary period. The sea level rises after LGM increased the flooding

periods of paleo-channels and therefore increased fine sediments deposits. Co-deposition of fluvial and estuarine organic carbon-rich fine sediments in the paleo-channels induced reducing conditions and increased Fe/Mn oxides-As deposition (McArthur et al., 2008). By contrast, the formation of aquifer systems in the inland basins corresponds to lacustrine-fluvial depositional environments. Sedimentation in those inland basins is influenced by paleo-lakes and river erosions, which are controlled by tectonic movements, volcanic activities and paleoclimatic variations (Wang et al., 2017). But how and to which degree the depositional environment influenced the As mobilization process in the inland sediments basins are still not investigated.

1.4.2.2 Hydrogeological conditions

Groundwater As contamination shows both, spatial and timely heterogeneity, partly influenced by hydrogeological conditions. It is transported with groundwater following the releasing from sediments. The faster groundwater flow favors As flushing out. Groundwater As contamination normally occurs in low-lying areas with gentle groundwater gradient. Furthermore, the relatively older sediments contain less-releasable As, which partly release into groundwater and flush out the system with time (Postma et al., 2012). In the other case, the sluggish groundwater in the low-lying area keeps As in the system, therefore having relatively higher As concentrations. Furthermore, some chemical components, which relate to As transformation such as SO_4^{2-}or dissolved organic carbon can recharge to nearby aquifers via groundwater flow. For instance, the As in the surface sediments can recharge into groundwater by vertically surface water recharge (Stuckey et al., 2015). Thus, the change of hydrological conditions influenced by precipitation or anthropogenic disturbance can influence As concentrations in direct or indirect way.

1.4.2.3 Desorption from minerals surface

Sediments have high abilities to adsorb As either by clay minerals, Fe(III) oxy(hydr)oxides or Mn oxides (Polizzotto et al., 2006; Sø et al., 2018; Gao et al., 2020). The As(III) species (as H_3AsO_3) is free-charged in the groundwater at circum-neutral pH conditions, easily released into groundwater and transport compared to As(V) species under variations of hydrological conditions, even though they show similar adsorption contents to Fe oxides. In contrast, arsenate species easier desorb from mineral surfaces as pH increases especially above 8.5 (Amini et al., 2008). Furthermore, other anions, which are analogous to arsenate such as phosphate (PO_4^{2-}), bicarbonate

(HCO_3^-) and silicate (SiO_4^-) can compete the adsorption site with As, and cause therefore increasing As release (Kim and Haack, 2000; Ciardelli et al., 2008). In contrast, cations such as Ca^{2+} and Mg^{2+} can increase the As adsorption via providing the adsorption bridge to the surface of Fe oxy(hydr)oxides or clay minerals (Fakhreddine et al., 2015).

1.4.2.4 Reductive dissolution of Fe (oxy-hydr)oxides

It is widely accepted that reductive dissolution of Fe oxides causes As desorb into groundwater (Nickson et al., 2000; Islam et al., 2004; Fendorf et al., 2010; Li et al., 2014). Pyrite and other Fe-containing minerals from mountains weathered to the metal oxides, which have high abilities in adsorbing As due to the high abundance of reaction sites. Under reducing conditions, reduction of those phases cause As release into groundwater.

The Mn oxides preceding Fe (oxy-hydr)oxides are reduced in groundwater. But no simple relationship was found about As and Mn concentrations in the groundwater. The groundwater with high Mn concentrations can have low As concentrations (McArthur et al., 2001). In other cases, the As concentration is not positively correlated to Mn, even though they both have high concentrations in the groundwater. Without Fe oxides reduction, released As via Mn oxides reduction can sorb onto Fe oxides, it probably explains this phenomenon (Wang et al., 2017).

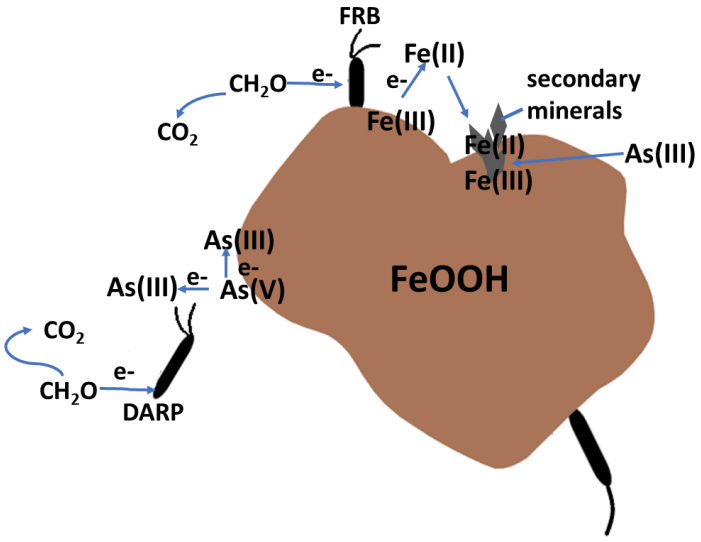

Figure 4 A conceptual model to show reduction of As-containing Fe oxides (Herbel and Fendorf, 2006).

Biotic Fe oxides reduction is widely found in the groundwater of flood plains of south and southeast of Asia (Lear et al., 2007), it is proposed that reduction of As-containing Fe oxides cause

As release into groundwater (**Fig. 4**). The Fe-reducing bacteria mostly live in anoxic environment and are able to use several terminal acceptors such as SO_4^{2-} with organic carbon as electron donors (Bleam, 2012). How much and which kinds of Fe oxides are reduced into groundwater is kinetically controlled by reactivities of Fe oxides and organic carbon. For example, poorly crystalline Fe-phases (e.g. ferrihydrite) are more thermodynamically used by microbes than the crystalline phases (e.g. hematite). It already has been evidenced in the groundwater of Bangladesh, Vietnam, and Cambodia that the Fe oxides reduction process is limited by content of reactive organic carbon (Reza et al., 2010; Eiche et al., 2017; Magnone et al., 2017). Anthropogenic activities, such as groundwater abstraction, induced by surface pollutants including organic matter recharged into groundwater, thereafter accelerating As release into groundwater. In the contamination area of south and southeast of Asia, groundwaters with high concentrations of Fe(II) normally have high As concentration. However, several studies show that Fe(II) concentrations in the groundwater decouple with As concentration (van Geen et al., 2004; Horneman et al., 2004; Mikutta and Rothwell, 2016), indicating that As release and transport process in the groundwater is not simply related with Fe oxides reductions. Other processes must exist to affect the As destiny.

1.4.2.5 Precipitation of secondary minerals

Transformation of redox minerals in aquifers induced by reduction-oxidation process involves As immobilisation or release. Following by ferrihydrite reduction, more crystalline Fe (oxy-hydr)oxides such as goethite, magnetite, lepidocrocite can be formed, and the specific types are controlled by the groundwater geochemical conditions such as pH value, Fe(II) concentration and temperature (Fredrickson et al., 1998; Stolze et al., 2019). The secondary Fe-containing phases including vivianite ($Fe_3[PO_4]_2 \cdot 8H_2O$), green rust or other Fe-containing salts can form in the aquifers with presence of HCO_3^-, PO_4^{2-}. They also show adsorption abilities for As, decreasing the groundwater As concentration (Muehe et al., 2016; Perez et al., 2020).

Iron sulfides are typical minerals formed in the sulfidic aquifers. Upon FeS saturated, mackinawite (FeS) precipitates in the sediments. Mackinawite can transform into pyrite either by polysulfides pathway or H_2S (Hunger and Benning, 2007b). And pyrite shows high capabilities to incorporate As, which already have been evidenced in the organic carbon-rich sediments of Bangladesh and Mekong Delta (Lowers et al., 2007; Wang et al., 2018). With high concentration of As, realgar (AsS) is also found in groundwater under circum-neutral pH conditions (Day et al.,

2004). Under reducing conditions, those sulfides minerals show a stable sink for As. However, the detection of those minerals in the aquifer sediments are limited by poorly crystalline and redox sensitive properties of those minerals, and availabilities of characterization techniques.

1.5 Remediation strategy for groundwater As mobilization

Several methods are proposed to remove As from groundwater under laboratory and field conditions. Commonly reported methods include oxidation, coagulation-flocculation, adsorption, ion-exchange and membrane processes (Mondal et al., 2013). However, seldom there are centralized water supply wells in the rural area such as the Hetao area. So it is hard to deal with groundwater As in personal wells. In Vietnam, people remove As via putting household sand filters in the outlet of the wells. The Fe(II) is oxidized to Fe oxides in the sand filter and thereafter adsorbing As. The sand filter can efficiently remove As with average content up to 80% (Berg et al., 2006). However, the removal efficiency depends on the groundwater Fe(II) concentrations, which means this strategy is adapted for application in the high Fe groundwater. In Bangladesh, people used the groundwater from deep wells which targets to Pleistocene aquifer that contains As-free groundwater due to oxidized properties of aquifers (van Geen et al., 2013). However, this strategy only can supply safe water for short time. As-containing groundwater from shallow wells can recharge into those deep wells. Additionally, some wealthy families are able to buy field kit tests for As measurement to find the safe water (Konhauser and Riding, 2012). In the Hetao Basin, there are still no available methods to remove As until now, due to that the Fe(II) concentrations are relatively low, and As contamination shows both timporal and spatial heterogeneity.

1.6 Open questions

Based on the existing knowledge on As mobilization in the aquifer, open questions are announced in the Hetao Basin:

(1) Where are the As-containing sediments from?
(2) The main As-containing minerals in the sediments should be investigated as well asvariations along with the redox profiles
(3) As speciation in the sediments and groundwater should be re-investigated especially under sulfidic conditions

(4) The key process causing As release into groundwater should be clarified since desorption caused by ion competition and microbial reduction both might contribute to As release

(5) Effective remediation methods for groundwater As contamination should be explored

(6) How and to which degrees As is transported to crops with As groundwater irrigation

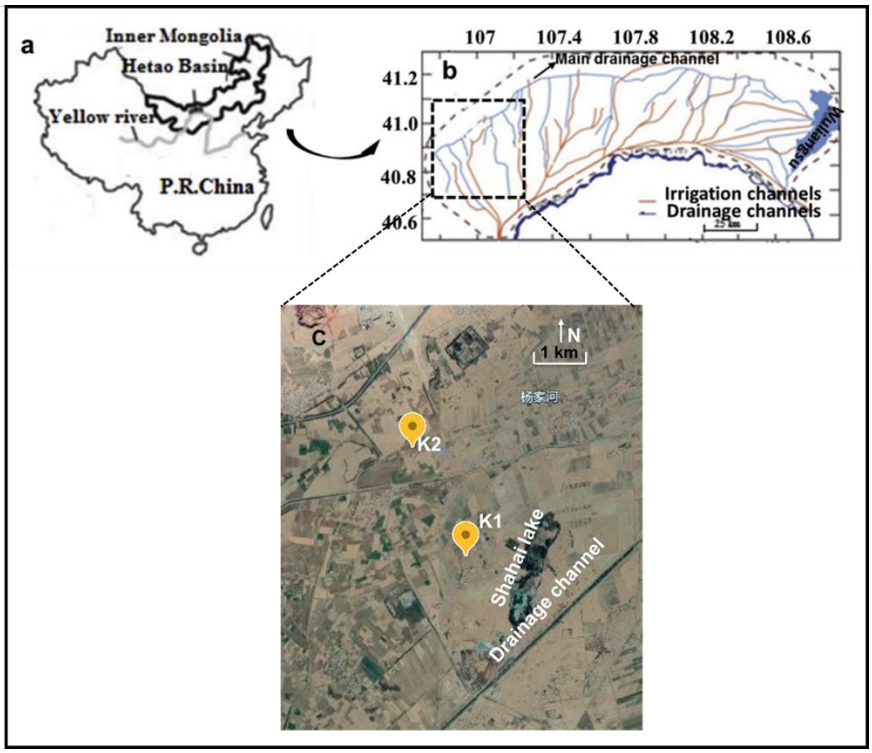

Figure 5 Location of the study area (a, b), the drilled boreholes (c).

1.7 Study area

1.7.1 General geographic information

The Hetao Basin, with an area around 1.16×10^4 km^2, is located in the central Inner Mongolia (**Fig. 5a**), Northern China (40°10′~41°10′N, 106°15′~109°01′). It is bordered by the Lang Mountains in the north and the Yellow River in the South. In the west, it is bordered by the Wulanbuhe desert. In the east, it is bordered by the WuliangSu Lake, which is one of biggest fresh water lakes (**Fig. 5b**) of China.

The Hetao Basin has a typical semi-arid to arid climate. Annual average temperature is around 5.8 ℃, with lowest temperature from December to February (~-20.2 - ~-34.4 ℃), and highest

temperature in the June to August (~31.6 ~38.7 ℃). The annual average precipitation is around 160 mm with most precipitation in summer and fall.

It is an important crop production area such as for corn, wheat and sunflower. In 1988, drainage channels were built to substitute groundwater due to decreasing groundwater table and to resolve the groundwater salinity problem. In the north of the drainage channel, groundwater still is used for irrigation, while the surface water from Yellow River is used for irrigation in the south of drainage channels.

1.7.2 Sedimentation and hydrogeological setting

The Hetao Basin is a typical Cenozoic fault basin that belongs to the Yinchuan-Hetao rift system. It is formed at the end of Jurassic epoch (Liu et al., 2016). A saline lake developed resulting from the dry and relative warm climate in the Jurassic epoch. At the early Pleistocene, the paleo lake developed to a deep lake (Tang et al., 2016), the Yellow River developed its square bend around the Ordos block in the late Miocene-early Pliocene and it flowed through the north of the Hetao Basin to the Wuliangsu lake before this time. In the late Pleistocene, the Yellow River started to migrate to the south, and invaded the paleolake. At the same time, the paleolake started to shrink size until it completely disappeared at around 20 ka before Holocene epoch (Jia et al., 2016). Therefore, the Hetao Basin shows alluvial-lacustrine-fluvial depositional environment. The sediments thickness is around 7000–8000 m in the northwest of the Hetao Basin and gradually decrease to the southeast of the basin.

The study area is located in the Northwest of the Hetao Basin (**Fig. 5b**), which has high As groundwater. Farmers use groundwater for irrigation due to the difficulties to access water from the Yellow River. Groundwater used for irrigation is mainly hold in the sediments within 100 m, which mainly contain late Pleistocene–Holocene silt and fine sand. A clay layer interbedded at ~ 40 m with thickness 1–2 m separates shallow aquifers and deep semi-confined aquifers (**Fig. 6**).

Groundwater in the Hetao Basin is recharged by the Lang Mountains, precipitation, and irrigation water, and discharged via evaporation, irrigation and drainage channels. The groundwater table varies from 20 m in the foot of the mountain to 2 m in the flat plain (Zhang et al., 2020). The groundwater direction generally flows from alluvial fans, through the transition area, to the flat plain (from northwest to southeast), and the flowing speed is relatively slow, from

0.002 to 0.2 m/d due to the gentle topography and low permeability of aquifer sediments (Guo et al., 2016b).

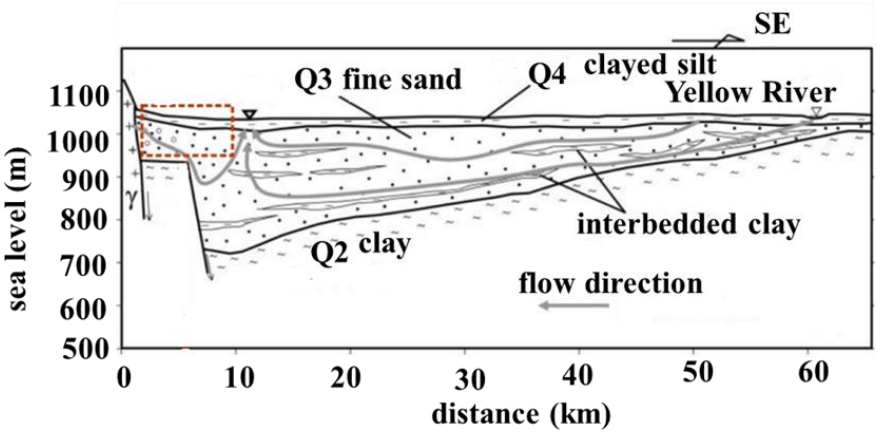

Figure 6 Hydro-geological graph of study area according to Zhang et al., (2019). Study area is marked with dashed yellow square**.**

1.7.3 Groundwater chemistry and As contamination

Groundwater temperatures in the Hetao Basin vary from 9.8 ℃ to 14.7 ℃ (Guo et al., 2008), the pH is circum-neutral to weakly alkaline (7.2-9.3, median: 7.9). Total dissolved solids (TDS) range from ~250 mg/L to ~5000 mg/L, while lower concentration of TDS was observed near the mountains (Jia et al., 2014; Guo et al., 2016a). In general, Ca^{2+} and HCO_3^- are the major cation and anion in the alluvial fans, while Na^+ and Cl^- are major ions in the flat plain. In the study area, the groundwater changes from Ca-SO_4^{2-}-HCO_3^- type in the alluvial fans to Na-SO_4^{2-}-HCO^{3-} type in the flat plain. The groundwater redox values (Eh) range from -153 to 83 mV, and show high heterogeneity. In comparison with groundwater from deltas in south and southeast of Asia, groundwater in the Hetao Basin has in average higher SO_4^{2-} concentrations, ranging from 30 mg/L to 1360 mg/L (Guo et al., 2016a).

Arsenic concentrations in the Hetao Basin vary from 0.58 µg/L to 572 µg/L, with 70% of groundwaters exceeding 10 µg/L (Cao et al., 2017) (**Fig. 7**). High As groundwaters are mainly located at five hotspots, including Shuangmiao-Sandaoqiao, Shahai-Manhui, Bainaobao-Langshan, Taerhu and Shengfeng, which generally occur in the sediments with lacustrine deposits under anoxic conditions. Even though with high As concentrations, the average Fe concentration in the

groundwater is relatively low in comparison with the flood plains in south and southeast of Asia (Horneman et al., 2004; Guo et al., 2013).

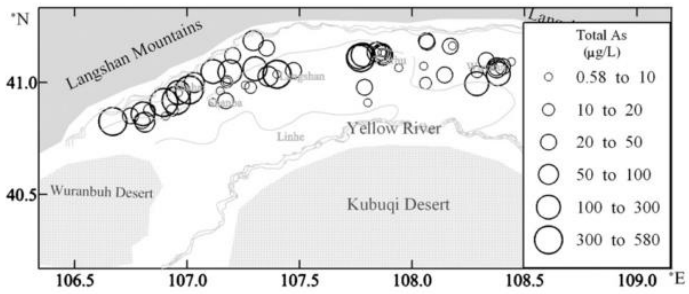

Figure 7 Distribution of groundwater As in the Hetao Basin (Guo et al., 2008 ,. with permission from Elsvier)

1.8 Summary of sampling and experimental methods

An analysis flow chart for sediments samples presents **Fig. 8**. Analysis methods are summarized in **Table 2**. The main methods are described in the following paragraphs:

1.8.1 Sediments sampling

Two deep boreholes (K1 and K2) with depths up to 80 m were drilled using rotary drilling method in the October of 2015 by a team from the China University of Geosciences (Beijing). Sediments were immediately collected after bringing sections to the surface. The sampling interval was around 1.0 m, and additional samples were taken near lithological boundaries. Sediment samples were wrapped with tinfoil, and sealed in sterile plastic bags filled with pure N_2 (> 99.999 %) and kept at -20 ℃. They were stored at -80 ℃ after transporting to the lab. Sub-sections of samples were transported to the Karlsruhe Institute of Technology (KIT) for analysis. Most sediments analysis was done in the Laboratory for Environmental and Raw Materials Analysis (LERA), Geochemistry & Economic Geology (EGG), AGW, KIT.

1.8.2 Major and trace elements analysis

Subsamples of the sediments were freeze-dried and later homogenized by grinding. Major elements including K, Na, Si, Ca, Mg, Fe, Mn, P, Al were analyzed by wavelength dispersive X-ray fluorescence spectrometry (WDX; S4 Explorer, Bruker) using fused beads. Measurement accuracy (within 5%) was checked using the certified standard AVG-1 (USGS) and RGM-1. Trace

elements were analyzed by Energy Dispersive X-ray Fluorescence Spectrometry (EDX; Epsilon 5, PANalytical), accuracy of the measurement was regularly checked by certified materials (SOIL-5, n=4; GXR-6, n=4; GXR-2, n=4; SL-1, n=4). Precision of the repeated standard measurement was better than 5%. Total As content in the sediments was additionally measured by HG-FIAS (hydride generation flow injection atomic absorption spectroscopy) after acid digestion. Digestion recovery (100 ± 5%) for As was checked by including certified standards GXR-5 and RGM-1 into digestion and measurement. Rare earth elements (REE) including Sc, Y, La, Ce, Pr, Nd, Sm, Eu, Gd, Tb, Dy, Ho, Er, Tm, Yb, Lu and Th were measured by ICP-MS after acid digestion. The digestion recovery and measurement accuracy were controlled (100±10% for most REE) using certified standard RGM-1.

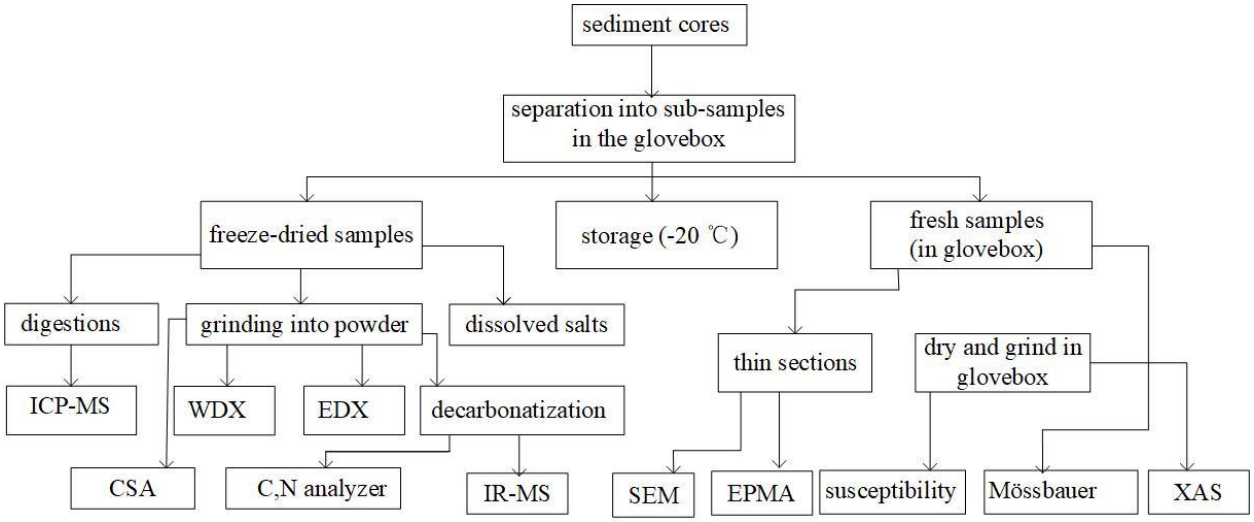

Figure 8 A flow chart representing sample preparation and analyzing process.

The total carbon (TC) content was measured by carbon/sulfur analyzer (CSA; CS 2000 MultiLine F/SET-3, Eltra). Total organic carbon (TOC) was measured after removing inorganic carbon by repeated addition of HCl (20%, suprapure, Merck) at 60 °C. Measurement accuracy (100 ± 2%) was regularly checked by including a steel standard (92400-3050) into the measurement procedure. Further, total carbon and nitrogen contents were measured by de-carbonated samples (2% HCl, Suprapure, Merck) with an elemental analyzer (EuroEA3000, EuroVector). The results of C_{org} and nitrogen content were used to calculate C/N ratio. Measurement accuracy (100 ± 5%) for C and N was checked with reference standards BBOT (HekaTech) and GBW 07043 (office of CRN'S China).

1.8.3 X-ray Diffraction (XRD) analysis

Mineralogy of the sediment was analyzed by X-ray diffraction (XRD) (Kristalloflex D500, Siemens, Germany) at 40 kV and 25 mA. Copper (Cu) Kα-1 radiation was used at angles between 2° and 80°. Clay minerals were analyzed using texturized samples by XRD. After collecting spectra, minerals were identified using calibrated spectra by the EVA program (Bruker) and the database of PDF 2002.

1.8.4 Electron microscopy analysis

A section of sediments was separated from intact cores, and embedded in an arsenic-free resin (Epotek) in the glovebox after drying. Sections of 1-mm thickness were cut and polished to a thickness of 80 μm. Thin sections were carbon-coated and prepared for the scanning electron microscopy (SEM) and electron probe microanalysis (EPMA) analysis.

The SEM images were acquired at German Research Center for Geosciences (GFZ) using Zeiss Ultra Plus FE-SEM at an acceleration voltage of 3 kV with 10 μm aperture distance using an in-lens secondary electron detector. Following by minerals observation using SEM, marked particles and areas were analyzed at Goethe University by wavelength spectrometer electron probe microanalysis (EPMA, JOEL 8900). The operating conditions were 20 keV accelerating voltage and 20 nA beam current. Iron, S, Si, Ca, Mg and As concentrations were quantified using peak counting times of 10 s for Fe, S, Si, Ca, Mg and 60 s for As. Detection limit for As is around 90 mg/kg. For As, S, and Fe mapping, pixel size was set to 0.1 μm × 0.1 μm. Analysis volume for particles was approximately 0.2 – 0.3 μm^3 based on the Monte Carlo simulations.

1.8.5 X-ray absorption spectroscopy

X-ray absorption spectroscopy (XAS) analysis is an important tool of my PhD thesis, to analyze the speciation of Fe, S and As in the sediments. It is a powerful technique in environmental samples analysis especially for samples with complex chemical compositions (Parsons et al., 2002). The XAS consists of two different techniques, extended X-ray absorption fine structure (EXAFS) and X-ray absorption near edge structure (XANES). XANES mainly provides information on the oxidation state, while EXAFS provides information on the coordination environment and local chemical structure. The redox elements in the sediments normally are environmentally sensitive,

they easily changes to other redox states when they are chemically treated. Therefore it is hard to quantify the content of different species. XAS enables to get the information fast without destroying the samples. Furthermore, we cannot get the compositions information in the sediments due to the low abundance, but the EXAFS enables us to semi-quantify each species. In this study, I mainly used the SUL-X beamline from ANKA in Karlsruhe. It is designed for combined measurements with micro-focusing capability, including XRD, XRF, XAS, to get the complex compositions of environmental samples.

Sample mass for Fe K-edge XAS analysis was calculated by the program XAFSmass and mixed with boron nitride to dilute the Fe concentration. Samples for Fe and As K-edge XAS analysis, powdered samples were suspended in deoxygenated water in the glovebox, and drop-casted onto Kapton tape, further sealed using a second piece of Kapton tape. For S K-edge measurement, samples directly were loaded onto Kapton tape to avoid energy attenuation. Spectra were collected using Si (111) crystal pair as a monochromator with a fixed-beam exit. The Fe K-edge spectra was collected in transmission mode with energy calibrated at 7112 eV. The transmission spectra were collected using three ADC IC-Type ionization chambers with Kapton windows. Arsenic and S spectra were collected in fluorescence mode. They are collected at energies at 11874 eV and 2481 eV respectively. The fluorescence spectra were collected using a Gresham 7-element (Li) detector. Arsenic, Fe and S were calibrated with Au foil, Fe metal foil and Na_2SO_4 respectively.

Data reduction and analysis of EXAFS spectra were performed using Athena (Ravel and Newville, 2005). Linear combination fitting (LCF) was conducted on XANES and derivative XANES (-20 eV to 30 eV), and Fe K-edge XAFS (k = 3-10 Å) regions. For all Fe reference compounds, the total number of contributing reference standards was limited to five. The sum was forced to equal 1. For peat samples, the k2-weighted $\chi(k)$ As K-edge EXAFS spectra was Fourier-transformed over a k-range of 3 to 10 Å by a Hanning window with a dk value of 1, afterwards transforming the spectra to R-space.

1.8.6 Mössbauer spectroscopy analysis

A section of samples was separated from each intact core for Mössbauer analysis at the University of Tübingen. Within a glovebox, dried powders of samples were loaded into Plexiglas holders (area 1 cm^2), forming a thin disc. Samples were kept in airtight jars under anoxic conditions

at -20 °C until measurement. Holders were inserted into a closed-cycle exchange gas cryostat (Janis cryogenics) under a backflow of He to minimize exposure to air. Spectra were collected at 20 K using a constant acceleration drive system (WissEL) in transmission mode with a 57Co/Rh source. All spectra were calibrated against a 7 μm thick α-57Fe foil that was measured at room temperature. Analysis was carried out using Recoil (University of Ottawa) and the Voigt Based Fitting (VBF) routine (Rancourt and Ping, 1991). The half width at half maximum (HWHM) was constrained to 0.13 mm/s during fitting. The Mössbauer spectra analysis work was done by James Byrne from Tübingen University.

Table 2 Analysis content and methods for sediments samples

Analysis content	Technique	Instruments
Major elements: Si, K, Ca, Mg, Na, Al, P, Fe, Mn, Ti	Wavelength Dispersive X-ray Fluorescence Spectrometry (WDX)	WDX (S4 Explorer, Bruker)
Trace elements: Ni, Cu, Zn, Rb, Sr, Y, Zr, Nb, Mo, Ba, La, Sr, pb	Energy Dispersive X-ray Fluorescence Spectroscopy (EDX)	EDX (Epsilon 5, PANalytical)
Rare earth elements (REE): Sc, Y, La, Ce, Pr, Nd, Sm, Eu, Gd, Tb, Dy, Ho, Er, Tm, Yb, Lu, Th	Inductively Coupled Plasma Mass Spectrometry (ICP-MS) followed by digestion	Digestion: (START 1500, MLS GmbH) ICP-MS (X-Series 2, Thermo Fisher)
Element As	Hydride Generation Flow Injection Atomic Absorption Spectroscopy (HG-FIAS) followed by digestion	Digestion: (START 1500, MLS GmbH) HG-FIAS (AAnalyst 200, Perkin Elmer)
Total organic carbon (TOC), Total sulfur (TS)	Carbon/sulfur analyzer (CSA)	CSA (CS – 2000, ELTRA)
Total nitrogen (TN)	Elemental analyzer	Elemental Analyzer (EuroEA3000, EuroVector)
Main minerals	X-ray diffraction (XRD) EVA program	XRD (Kristallofles D500, Siemens) EVA program (Bruker) with database 2002
Soluble salts and As in the sediments (Cl^-, Na^+, SO_4^{2-}, Ca^{2+}, Mg^{2+}, K^+)	ICP-MS following by water extraction	ICP-MS (X-Series 2, Thermo Fisher)
Clay minerals analysis	X-ray Diffraction using texturized samples EVA program	XRD (Kristalloflex D8, Siemens) EVA program (Bruker) with database 2002
Specific minerals searching	Field Emission scanning electron microscopy coupled with energy diffraction X-ray spectroscopy (FE-SEM - EDX)	FE-SEM – EDX (Zeiss Ultra Plus)

Carbon isotope ($\delta^{13}C$) and nitrogen isotope ($\delta^{15}N$)	Elemental analyzer in continuous flow mode and connected to an isotope ratio mass spectrometer （IR-MS）	Elemental analyzer (EuroEA3000, EuroVector) IR-MS (IsoPrime, Fa. GV Instrument, UK)
As speciation	ICP-MS following by sequential extractions	ICP-MS (X-Series 2, Thermo Fisher)
	As K-edge X-ray absorption spectroscopy (XAS)	XAS (SUL-X beamline, ANKA, Germany) XAS (BM23 beamline, Grenoble, France)
Fe speciation	Inductively Coupled Plasma Atomic Emission Spectroscopy (ICP-OES) and photometry at 562 nm (ferrozine method) following by 2M HCl extractions Fe K-edge X-ray Absorption Spectroscopy (XAS) ^{57}Fe Mössbauer Spectroscopy at 20 K	ICP-OES (Spectro CirosCCD, Kleve, Germany) Photometry (Lamda2, Perkin Elmer) XAS (SUL-X beamline, ANKA, Germany) Mössbauer spectroscopy (university of Tüebingen)
Magnetic susceptibility	KYL-2 Kappabridge combined with CS-L cryostat and CS-2 furnace (Geofyzika/Agico) with temperature varying from -192 ℃ to 700 ℃.	KYL-2 Kappabridge combined with CS-L cryostat and CS-2 furnace (Geofyzika/Agico)
As content in specific minerals	Electron Probe Microanalysis (EPMA)	EPMA (JEOL 8900)

2 Reconstruction of sedimentation history and influence for As contents in the sediments

Title: Impact of sedimentation history for As distribution in Late Pleistocene – Holocene sediments in the Hetao Basin, China

Authors: Hongyan Wang, Elisabeth Eiche, Huaming Guo, Stefan Norra

In: Journal of Soils and Sediments, **DOI:** http://doi.org/10.1007/s11368-020-02703-2

Journal of Soils and Sediments
https://doi.org/10.1007/s11368-020-02703-2

SEDIMENTS, SEC 2 • PHYSICAL AND BIOGEOCHEMICAL PROCESSES • RESEARCH ARTICLE

Impact of sedimentation history for As distribution in Late Pleistocene-Holocene sediments in the Hetao Basin, China

Hongyan Wang[1] · Elisabeth Eiche[1] · Huaming Guo[2,3] · Stefan Norra[1]

Received: 19 February 2020 / Accepted: 23 June 2020
© The Author(s) 2020

Abstract
Purpose To understand the impact of geochemical sedimentation history for arsenic (As) distribution in the sediment profiles of the Hetao Basin, we (1) evaluated sediments provenance and variations of weathering intensities, (2) attempted to reconstruct the depositional environments, and (3) explored the As and Fe speciation in the sediments. Combining the information above, different sedimentation facies were distinguished in the vertical profiles.
Methods Two sediments cores were drilled up to 80 m depth. Major and trace element compositions, including rare earth elements (REE), were analyzed. Carbon isotope ratios ($\delta^{13}C_{org}$) of embedded organic matter in the sediments were analyzed by isotope ratio mass spectrometry (IR-MS). Arsenic and Fe speciation of the sediments were determined by sequential extractions.
Results and discussion The similar REE geochemistry of rocks from the Lang Mountains and sediments in the Hetao Basin indicated that the sediments originated from the Lang Mountains. The C/N ratio (~ 4 to ~ 10) in combination with $\delta^{13}C_{org}$ (~ 27‰ to ~ 24‰) suggested that sediments were mainly deposited in aquatic environments. The unconfined aquifer equaled the lacustrine deposit with less intensive weathering during last glacial maximum (LGM). Here, the As content (average, 5.4 mg kg^{-1}) was higher than in the aquifer sediments below (average, 3.6 mg kg^{-1}).
Conclusion Higher content of releasable As in combination with paleolake-derived organic matter aquifer sediments probably contributes to higher groundwater As concentration in the unconfined aquifer. This study provides the first insight into the impact of sedimentation history on As distributions in sediment profiles in the Hetao Basin.

Keywords Sediment basin · Sedimentation history · Arsenic provenance · Weathering intensities · Organic carbon isotopic signature · Arsenic speciation

Responsible editor: Tomas Matys Grygar

Electronic supplementary material The online version of this article (https://doi.org/10.1007/s11368-020-02703-2) contains supplementary material, which is available to authorized users.

✉ Hongyan Wang
hongyan.wang@kit.edu

[1] Institute of Applied Geosciences (AGW), Geochemistry & Economic Geology group, Karlsruhe Institute of Technology (KIT), Adenauerring 20 b, 76131 Karlsruhe, Germany
[2] State Key Laboratory of Biogeology and Environmental Geology, China University of Geosciences, Beijing 100083, People's Republic of China
[3] School of Water Resources and Environment, China University of Geosciences, Beijing 100083, People's Republic of China

Published online: 01 July 2020

1 Introduction

Geogenic groundwater arsenic (As) contamination is of global concern. It is mainly reported from floodplains in South and Southeast Asia including the Ganges-Brahmaputra-Meghna (GBM) River delta, the Mekong River delta, the Red River delta, and inland basins located in the Yellow River catchment including the Hetao Basin, the Hohhot Basin, the Datong Basin, and the Yinchuan Basin (Nordstrom 2002; Rodríguez-Lado et al. 2013; Guo et al. 2017). Over 100 million people are exposed to As with concentration higher than 10 μg L^{-1} (the World Health Organization standard) in the drinking water (Ravenscroft et al. 2009).

Studies indicate that in situ microbial organic carbon oxidation processes coupled with reduction of As-bearing Fe oxy(hydr)oxides is the main cause for As release into groundwater (Nickson et al. 1998; McArthur et al. 2001; Islam et al.

Springer

Authorship statement

This peer-reviewed scientific journal article was written and corresponded by Hongyan Wang and was based on the interpretation of the geochemical compositions of sediments and $\delta^{13}C$ isotope analysis; Huaming Guo was contributed to the samples collection; Stefan Norra designed and supervised the whole study.

Abstract

Purpose

To understand the impact of geochemical sedimentation history for arsenic (As) distribution in the sediment profiles of the Hetao Basin, we (1) evaluated sediments provenance and variations of weathering intensities; (2) attempted to reconstruct the depositional environments and (3) explored the As and Fe speciation in the sediments. Combining the information above, different sedimentation facies were distinguished in the vertical profiles.

Methods

Two sediments cores were drilled up to 80 m depth. Major and trace element compositions,

including Rare Earth Elements (REE), were analyzed. Carbon isotope ratios ($\delta^{13}C_{org}$) of embedded organic matter in the sediments were analyzed by Isotope Ratio Mass Spectrometry (IR-MS). Arsenic and Fe speciations of the sediments were determined by sequential extractions.

Results and discussion

The similar REE geochemistry of rocks from the Lang Mountains and sediments in the Hetao Basin indicated that the sediments originated from the Lang Mountains. The C/N ratio (~4 to ~10) in combination with $\delta^{13}C_{org}$ (-27‰ to -24‰) suggest that sediments were mainly deposited in aquatic environments. The unconfined aquifer equalled the lacustrine deposit with less intensive weathering during last glacial maximum (LGM). Here the As content (average 5.4 mg kg^{-1}) was higher than in the aquifer sediments below (average 3.6 mg kg^{-1}).

Conclusion

Higher content of releasable As in combination with paleolake-derived organic matter aquifer sediments probably contributes to higher groundwater As concentration in the unconfined aquifer. This study provides the first insight into the impact of sedimentation history on As distributions in sediment profiles in the Hetao Basin.

The full article is reprinted with permission from Journal of Soils and Sediments in **Appendix 1**. Copyright © 2020 Springer B.V.

3 Evaporite minerals in the sediments and influence for As mobilization

Publication title: Indications that weathering of evaporite minerals affects groundwater salinity and As mobilization in aquifers of the northwestern Hetao Basin, China

Authors: Hongyan Wang, Huaming Guo, Wei Xiu, Jonas Bauer, Guoxin Sun, Xiaohui Tang, Stefan Norra

In: Applied Geochemistry, **DOI**: https://doi.org/10.1016/j.apggeochem.2019.104416

Applied Geochemistry 109 (2019) 104416

Contents lists available at ScienceDirect

Applied Geochemistry

journal homepage: www.elsevier.com/locate/apgeochem

Indications that weathering of evaporite minerals affects groundwater salinity and As mobilization in aquifers of the northwestern Hetao Basin, China

Hong-Yan Wang[a], Hua-Ming Guo[b,c], Wei Xiu[b,*], Jonas Bauer[a], Guo-Xin Sun[d], Xiao-Hui Tang[a], Stefan Norra[a]

ARTICLE INFO

Editorial handling by Prof. M. Kersten

Keywords:
Salinization
Sulphate minerals
pH decrease
Ca^{2+} release
Sulphide
As mobilization

ABSTRACT

Elevated arsenic (As) concentration and salinity (TDS > 1000 mg/L) seriously affect the groundwater quality in the Hetao Basin, China, however, the origin of groundwater salinity and its influence for As mobilization has not been widely studied. In this study, the influence of evaporite minerals weathering on groundwater salinity and As mobilization were investigated by lithological and mineralogical analysis of sediments from two boreholes in combination with groundwater hydrogeochemical characteristics analysis in the northwestern Hetao Basin. Results from a water-leaching method suggest that Na and Ca related sulphates dominate the evaporite minerals in sediment samples. Groundwater salinization mainly results from evaporation and Na^+/Ca^{2+} cation exchange followed by sulphate and silicate minerals weathering. Saturated indices for calcite, dolomite and unsaturated indices for gypsum as well as negative correlation between pH and SO_4^{2-} suggest that groundwater chemistry does not reach equilibrium with continual carbonates precipitation by an excessive Ca supply from Ca related sulphates weathering. The groundwater pH decrease and Ca^{2+} release during weathering of Ca related sulphates can retard As desorption from Fe (oxyhydr)oxides and clay minerals. Furthermore, pyrite minerals were also found in the sediments induced by high sulphide flux and it can cause As sequestration. However, modeling results suggest the occurrence of thio-As species in the study area, which can potentially enhance the As mobilization. This study contributes to the ongoing research into As mobilization in the groundwater of lacustrine basins.

1. Introduction

Co-occurrence of groundwater salinization (with total dissolved solids (TDS) > 1000 mg/L) and As contamination (> 10 μg/L) has been widely found in the aquifers of Argentina, the tidal deltaplain of southwest Bangladesh and many basins in the north of China (Guo and Wang, 2005; Nicolli et al., 2012; Rodríguez-Lado et al., 2013; Xie et al., 2013; Ayers et al., 2016; Li et al., 2016). Reductive dissolution of As-containing Fe (oxyhydr)oxides and/or competitive As desorption are considered critical mechanisms causing groundwater As enrichment (Nordstrom, 2002; Ahmed et al., 2004; Guo et al., 2013a). Possible reasons for groundwater salinization include: saline intrusion, historic marine transgression, evaporite minerals weathering and excessive evaporation of surface water and shallow groundwater (Appelo and Postma, 2005; MacDonald et al., 2016). Since elevated salinity and As concentration are both influenced by groundwater hydrochemical evolution processes, their connection should be highlighted, however, few studies have addressed those two issues until now. Elevated groundwater redox components, especially SO_4^{2-}, which increases during the groundwater salinization processes, can influence the As partitioning process between sediments and groundwater by formation of secondary minerals in the aquifer sediments (Lowers et al., 2007; Buschmann and Berg, 2009; Kao et al., 2011; Guo et al., 2016; Smith et al., 2017), whereas some elevated concentrations of ions such as HCO_3^- and Ca^{2+} can influence the As desorption/adsorption from clay minerals and Fe (oxyhydr)oxides (Brahman et al., 2013; Fakhreddine et al., 2015). Therefore, clarifying the saline source and connection with As contamination is essential for understanding the As

* Corresponding author.
E-mail address: xwuxun@cugb.edu.cn (W. Xiu).

https://doi.org/10.1016/j.apgeochem.2019.104416
Received 12 April 2019; Received in revised form 27 August 2019; Accepted 30 August 2019
Available online 30 August 2019
0883-2927/ © 2019 Published by Elsevier Ltd.

Authorship statement

This peer-reviewed scientific journal article was written by Hongyan Wang and is based on the soluble salts analysis for sediments and statistical analysis of groundwater geochemistry data. Huaming Guo provided the sediments samples and reviewed this article; Jonas Bauer drew the Google map of this study area and reviewed this article; Wei Xiu, Guoxin Sun and Xiaohui Tang reviewed this article; Stefan Norra designed and supervised this study.

Abstract

Elevated arsenic (As) concentration and salinity (TDS > 1,000 mg/L) seriously affect the groundwater quality in the Hetao Basin, China. However, the origin of groundwater salinity and its influence on As mobilization has not been widely studied. In this study, the influence of evaporite minerals weathering on groundwater salinity and As mobilization were investigated by lithological and mineralogical analysis of sediments from two boreholes in combination with groundwater

hydrogeochemical characteristics analysis in the northwestern Hetao Basin. Results from a water- leaching method suggest that Na and

Ca related sulphates dominate the evaporite minerals in sediment samples. Groundwater salinization mainly results from evaporation and Na^+/Ca^{2+} cation exchange followed by sulphate and silicate minerals weathering. Saturated indices for calcite, dolomite and unsaturated indices for gypsum as well as negative correlation between pH and SO_4^{2-} suggest that groundwater chemistry does not reach equilibrium with continual carbonates precipitation by an excessive Ca supply from Ca related sulphates weathering. The groundwater pH decrease and Ca^{2+} release during weathering of Ca related sulphates can retard As desorption from Fe (oxy-hydr)oxides and clay minerals. Furthermore, pyrite minerals were also found in the sediments induced by high sulphide flux and it can cause As sequestration. However, modeling results suggest the occurrence of thio-As species in the study area, which can potentially enhance the As mobilization. This study contributes to the ongoing research into As mobilization in the groundwater of lacustrine basins.

The full article is reprinted with the permission from Applied geochemistry shown in **Appendix 2**
Copyright © 2019, Elsevier.

4 Vertical redox zones of Fe-S-As coupled mineralogy in the sediments of the Hetao Basin

Publication title: Vertical redox zones of Fe-S-As coupled mineralogy in the sediments of Hetao Basin – constraints for groundwater As contamination

Authors: Hongyan Wang, Jörg Göttlicher, James Byrne, Huaming Guo, Liane Benning, Stefan Norra

In: Journal of Hazardous Materials https://doi.org/10.1016/j.jhazmat.2020.124924

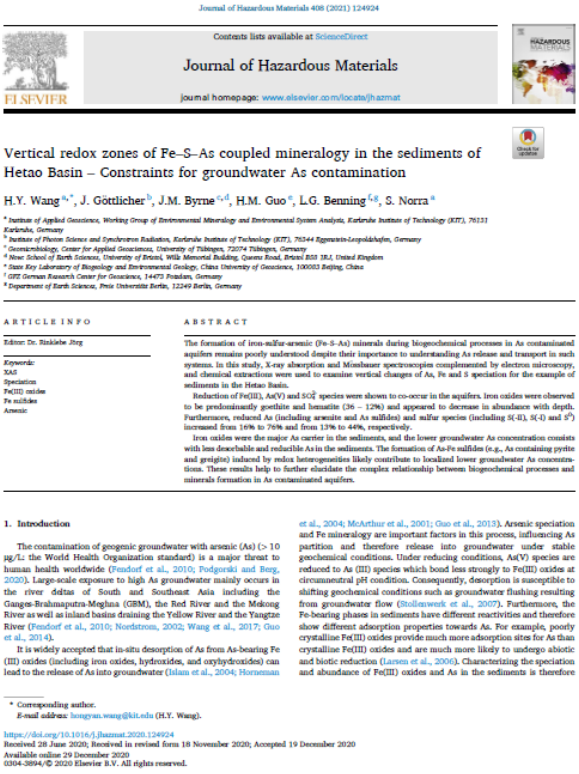

Journal of Hazardous Materials 408 (2021) 124924

Contents lists available at ScienceDirect

Journal of Hazardous Materials

journal homepage: www.elsevier.com/locate/jhazmat

Vertical redox zones of Fe–S–As coupled mineralogy in the sediments of Hetao Basin – Constraints for groundwater As contamination

H.Y. Wang [a,*], J. Göttlicher [b], J.M. Byrne [c,d], H.M. Guo [e], L.G. Benning [f,g], S. Norra [a]

[a] Institute of Applied Geosciences, Working Group of Environmental Mineralogy and Environmental System Analysis, Karlsruhe Institute of Technology (KIT), 76131 Karlsruhe, Germany
[b] Institute of Photon Science and Synchrotron Radiation, Karlsruhe Institute of Technology (KIT), 76344 Eggenstein-Leopoldshafen, Germany
[c] Geomicrobiology, Center for Applied Geosciences, University of Tübingen, 72074 Tübingen, Germany
[d] Near School of Earth Sciences, University of Bristol, Wills Memorial Building, Queens Road, Bristol BS8 1RJ, United Kingdom
[e] State Key Laboratory of Biogeology and Environmental Geology, China University of Geosciences, 100083 Beijing, China
[f] GFZ German Research Center for Geosciences, 14473 Potsdam, Germany
[g] Department of Earth Science, Freie Universität Berlin, 12249 Berlin, Germany

ARTICLE INFO

Editor: Dr. Rinklebe Jörg

Keywords:
XAS
Speciation
Fe(III) oxides
Fe sulfides
Arsenic

ABSTRACT

The formation of iron-sulfur-arsenic (Fe-S-As) minerals during biogeochemical processes in As contaminated aquifers remains poorly understood despite their importance to understanding As release and transport in such systems. In this study, X-ray absorption and Mössbauer spectroscopies complemented by electron microscopy, and chemical extractions were used to examine vertical changes of As, Fe and S speciation for the example of sediments in the Hetao Basin.

Reduction of Fe(III), As(V) and SO_4^{2-} species were shown to co-occur in the aquifers. Iron oxides were observed to be predominantly goethite and hematite (26 – 12%) and appeared to decrease in abundance with depth. Furthermore, reduced As (including arsenite and As sulfides) and sulfur species (including S(-II), S(-I) and S^0) increased from 16% to 76% and from 13% to 44%, respectively.

Iron oxides were the major As carrier in the sediments, and the lower groundwater As concentration coexists with less desorbable and reducible As in the sediments. The formation of As-Fe sulfides (e.g., As containing pyrite and greigite) induced by redox heterogeneities likely contribute to localized lower groundwater As concentrations. These results help to further elucidate the complex relationship between biogeochemical processes and minerals formation in As contaminated aquifers.

1. Introduction

The contamination of geogenic groundwater with arsenic (As) (> 10 μg/L; the World Health Organization standard) is a major threat to human health worldwide (Fendorf et al., 2010; Podgorski and Berg, 2020). Large-scale exposure to high As groundwater mainly occurs in the river deltas of South and Southeast Asia including the Ganges-Brahmaputra-Meghna (GBM), the Red River and the Mekong River as well as inland basins draining the Yellow River and the Yangtze River (Fendorf et al., 2010; Nordstrom, 2002; Wang et al., 2017; Guo et al., 2014).

It is widely accepted that in-situ desorption of As from As-bearing Fe (III) oxides (including iron oxides, hydroxides, and oxyhydroxides) can lead to the release of As into groundwater (Islam et al., 2004; Horneman et al., 2004; McArthur et al., 2001; Guo et al., 2013). Arsenic speciation and Fe mineralogy are important factors in this process, influencing As partition and therefore release into groundwater under stable geochemical conditions. Under reducing conditions, As(V) species are reduced to As (III) species which bond less strongly to Fe(III) oxides at circumneutral pH condition. Consequently, desorption is susceptible to shifting geochemical conditions such as groundwater flushing resulting from groundwater flow (Stollenwerk et al., 2007). Furthermore, the Fe-bearing phases in sediments have different reactivities and therefore show different adsorption properties towards As. For example, poorly crystalline Fe(III) oxides provide much more adsorption sites for As than crystalline Fe(III) oxides and are much more likely to undergo abiotic and biotic reduction (Larsen et al., 2006). Characterizing the speciation and abundance of Fe(III) oxides and As in the sediments is therefore

* Corresponding author.
E-mail address: hongyan.wang@kit.edu (H.Y. Wang).

https://doi.org/10.1016/j.jhazmat.2020.124924
Received 28 June 2020; Received in revised form 18 November 2020; Accepted 19 December 2020
Available online 29 December 2020
0304-3894/© 2020 Elsevier B.V. All rights reserved.

Authorship statement:

Hongyan Wang wrote and corresponded this article. This article mainly investigated the Fe-S-As coupled redox profiles based on the data collected with high resolution X-ray spectroscopies and microscopies as well as extractions. Jörg Göttlicher as a beam scientist, helped me to collect the Fe, As and S XAS data; James Byrne collected and interpreted the Mössbauer spectrum; Liane Benning helped to collect the SEM – EDX data; Huaming Guo and Stefan Norra designed and supervised this study.

Abstract

The formation of iron-sulfur-arsenic (Fe-S-As) minerals during biogeochemical processes in As contaminated aquifers remains poorly understood despite their importance to understanding As release and transport in such systems. In this study, X-ray absorption and Mössbauer spectroscopies complemented by electron microscopy, and chemical extractions were used to examine vertical changes of As, Fe and S speciation for the example of sediments in the Hetao Basin.

Reduction of Fe(III), As(V) and SO_4^{2-} species were shown to co-occur in the aquifers. Iron oxides were observed to be predominantly goethite and hematite (36 – 12%) and appeared to decrease in abundance with depth. Furthermore, reduced As (including arsenite and As sulfides) and sulfur species (including S(-II), S(-I) and S^0) increased from 16% to 76% and from 13% to 44%, respectively.

Iron oxides seem to be the major As carrier in the sediments, and the less desorbable and reducible As in the depth intervals consists with lower groundwater As concentration. The formation of As-Fe sulfides (e.g pyrite and greigite) caused by redox heterogeneity probably contributes to localized lower groundwater As concentrations. These results help to further elucidate the complex relationship between biogeochemical processes and minerals formation in As contaminated aquifers.

The full article is reprinted with the permission from Journal of Hazardous Material shown in **Appendix 3** Copyright © 2020, Elsevier.

5 Fe-S-As coupled diagenetic minerals formation in the peat layers

Publication title: Arsenic sequestration in pyrite and greigite in the buried peat of As-contaminated aquifers

Authors: Hongyan Wang, James Byrne, Jeffrey Perez, Andrew Thomas, Jörg Göttlicher, Heidi Höfer, Satish Mayanna, Agnes Kontny, Andreas Kappler, Huaming Guo, Liane Benning, Stefan Norra

In: Geochimica et Cosmochimica Acta, **DOI**: http://doi.org/10.1016/j.gca.202006.021

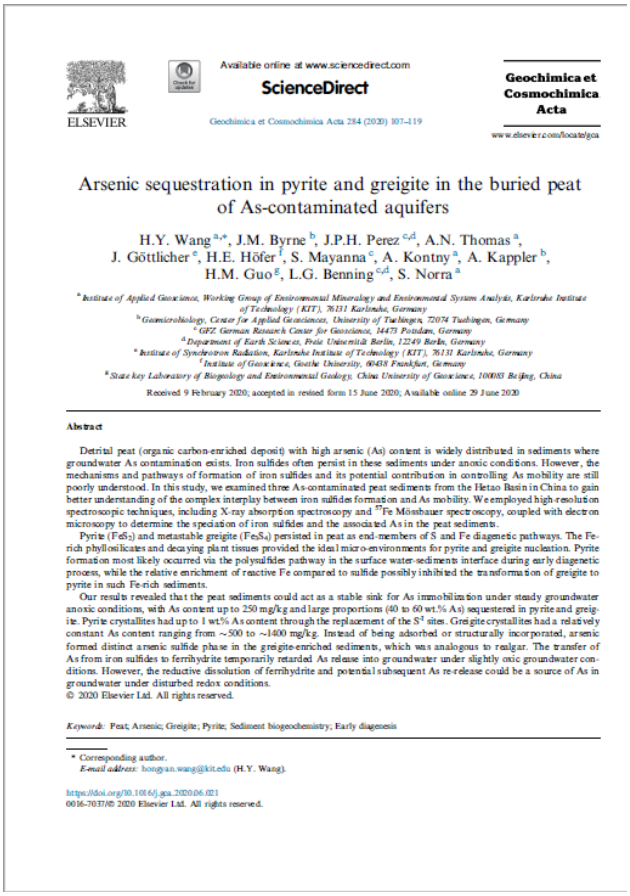

Available online at www.sciencedirect.com
ScienceDirect
Geochimica et Cosmochimica Acta 284 (2020) 107–119
Geochimica et Cosmochimica Acta
www.elsevier.com/locate/gca

Arsenic sequestration in pyrite and greigite in the buried peat of As-contaminated aquifers

H.Y. Wang [a,*], J.M. Byrne [b], J.P.H. Perez [c,d], A.N. Thomas [a], J. Göttlicher [e], H.E. Höfer [f], S. Mayanna [c], A. Kontny [a], A. Kappler [b], H.M. Guo [g], L.G. Benning [c,d], S. Norra [a]

[a] Institute of Applied Geosciences, Working Group of Environmental Mineralogy and Environmental System Analysis, Karlsruhe Institute of Technology (KIT), 76131 Karlsruhe, Germany
[b] Geomicrobiology, Center for Applied Geosciences, University of Tuebingen, 72074 Tuebingen, Germany
[c] GFZ German Research Center for Geosciences, 14473 Potsdam, Germany
[d] Department of Earth Sciences, Freie Universität Berlin, 12249 Berlin, Germany
[e] Institute of Synchrotron Radiation, Karlsruhe Institute of Technology (KIT), 76131 Karlsruhe, Germany
[f] Institute of Geoscience, Goethe University, 60438 Frankfurt, Germany
[g] State key Laboratory of Biogeology and Environmental Geology, China University of Geosciences, 100083 Beijing, China

Received 9 February 2020; accepted in revised form 15 June 2020; Available online 29 June 2020

Abstract

Detrital peat (organic carbon-enriched deposit) with high arsenic (As) content is widely distributed in sediments where groundwater As contamination exists. Iron sulfides often persist in these sediments under anoxic conditions. However, the mechanisms and pathways of formation of iron sulfides and its potential contribution in controlling As mobility are still poorly understood. In this study, we examined three As-contaminated peat sediments from the Hetao Basin in China to gain better understanding of the complex interplay between iron sulfides formation and As mobility. We employed high-resolution spectroscopic techniques, including X-ray absorption spectroscopy and ^{57}Fe Mössbauer spectroscopy, coupled with electron microscopy to determine the speciation of iron sulfides and the associated As in the peat sediments.

Pyrite (FeS_2) and metastable greigite (Fe_3S_4) persisted in peat as end-members of S and Fe diagenetic pathways. The Fe-rich phyllosilicates and decaying plant tissues provided the ideal micro-environments for pyrite and greigite nucleation. Pyrite formation most likely occurred via the polysulfides pathway in the surface water-sediments interface during early diagenetic process, while the relative enrichment of reactive Fe compared to sulfide possibly inhibited the transformation of greigite to pyrite in such Fe-rich sediments.

Our results revealed that the peat sediments could act as a stable sink for As immobilization under steady groundwater anoxic conditions, with As content up to 250 mg/kg and large proportions (40 to 60 wt.% As) sequestered in pyrite and greigite. Pyrite crystallites had up to 1 wt.% As content through the replacement of the S^{-1} sites. Greigite crystallites had a relatively constant As content ranging from ~500 to ~1400 mg/kg. Instead of being adsorbed or structurally incorporated, arsenic formed distinct arsenic sulfide phase in the greigite-enriched sediments, which was analogous to realgar. The transfer of As from iron sulfides to ferrihydrite temporarily retarded As release into groundwater under slightly oxic groundwater conditions. However, the reductive dissolution of ferrihydrite and potential subsequent As re-release could be a source of As in groundwater under disturbed redox conditions.
© 2020 Elsevier Ltd. All rights reserved.

Keywords: Peat; Arsenic; Greigite; Pyrite; Sediment biogeochemistry; Early diagenesis

* Corresponding author.
E-mail address: hongyan.wang@kit.edu (H.Y. Wang).

https://doi.org/10.1016/j.gca.2020.06.021
0016-7037/© 2020 Elsevier Ltd. All rights reserved.

Authorship statement: Hongyan Wang wrote and corresponded this article. This article was written based on the data collected from X-ray spectroscopies, Mössbauer spectroscopy as well as the microscopies. James Byrne and Andreas Kappler collected and interpreted the Mössbauer data; Jeffrey Perez, Jörg Göttlicher and Andrew Thomas helped collecting the synchrotron data; Liane Benning and Satish Myanna performed the SEM analysis; Agnes Kontny organized the magnetic suspension analysis; Heidi Höfer performed the EPMA analysis; Huaming Guo and Stefan Norra designed and supervised this study.

Abstract

Detrital peat (organic carbon-enriched deposit) with high arsenic (As) content is widely distributed in sediments where groundwater As contamination exists. Iron sulfides often persist in these sediments under anoxic conditions. However, the mechanisms and pathways of formation of iron sulfides and its potential contribution in controlling As mobility are still poorly understood. In this study, we examined three As-contaminated peat sediments from the Hetao

Basin in China to gain better understanding
of the complex interplay between iron

sulfides formation and As mobility. We employed high-resolution spectroscopic techniques, including X-ray absorption spectroscopy and ^{57}Fe Mössbauer spectroscopy, coupled with electron microscopy to determine the speciation of iron sulfides and the associated As in the peat sediments.

Pyrite (FeS_2) and metastable greigite (Fe_3S_4) persisted in peat as end-members of S and Fe diagenetic pathways. The Fe-rich phyllosilicates and decaying plant tissues provided the ideal micro-environments for pyrite and greigite nucleation. Pyrite formation most likely occurred via the polysulfides pathway in the surface water-sediments interface during early diagenetic process, while the relative enrichment of reactive Fe compared to sulfide possibly inhibited the transformation of greigite to pyrite in such Fe-rich sediments.

Our results revealed that the peat sediments can act as a stable sink for As immobilization under steady groundwater anoxic conditions, with As content up to 250 mg/kg and large proportions (40 to 60 wt.% As) sequestered in pyrite and greigite. Pyrite crystallites had up to 1 wt.% As content through the replacement of the S^{-I} sites. Greigite crystallites had a relatively constant As content ranging from ~500 to ~1,400 mg/kg. Instead of being adsorbed or structurally incorporated, arsenic formed distinct arsenic sulfide phase in the greigite-enriched sediments, which was analogous to realgar. The transfer of As from iron sulfides to ferrihydrite temporarily retarded As release into groundwater under slightly oxic groundwater conditions. However, the reductive dissolution of ferrihydrite and potential subsequent As re-release can be a source of As in groundwater under disturbed redox conditions.

The full article is reprinted with the permission from Journal of Hazardous Material shown in **Appendix 4** Copyright © 2020, Elsvier

6 Synoptic discussions on As mobilization process in the inland sediment basins

Combining the results and discussions from chapter 2 to chapter 5, a conceptual model was built for As mobilization processes in the inland sediment basins (**Fig. 9**). Synoptic discussions based on the comparison between inland sediment basins and flood deltas are shown in the following.

Inland sedimentary basins were formed by hundreds of millions of years with depositions of eroded rocks, precipitation of minerals and carbon debris. Groundwater bodies in aquifers, which develop subsequently to the disappearance of paleolakes/oceans, normally have different chemical compositions in comparison to flood deltas, especially in regard to higher pH and SO_4^{2-} concentrations. My study tries to further answer open questions concerning the groundwater As mobilization in the inland basins based on the geochemical investigations of sediments from the Hetao Basin.

The first question arises from how As is transported to the inland sediment basins, which is important for understanding As-carrying minerals and enrichment processes in the sediments. This study suggests that the surrounding mountains are the sediment sources; the As-containing minerals such as biotite, pyrite are weathered to Fe oxides and thereafter buried in the sediments. This finding is consistent with higher As contents found in the sediments of inland basins such as the Hetao Basin or the Datong Basin than in river deltas (Xie et al., 2008). A previous study also suggests that the As source in foreland basins is more complex, obviously influenced by nearby mountains (Raychowdhury et al., 2014). The weathering intensities of those minerals contribute to the As reactivities in the sediments, and obviously increased after the Last Glacial Maximum (LGM) (**chapter 2**).

Arsenic transport and distribution in the aquifers followed by weathering of As-bearing bedrocks and minerals is strongly influenced by the specific depositional environment (Wang et al., 2017). In south and south-east of Asia, the depositional environment is mostly pluvial and alluvial. The sedimentation shows successive characters, and is controlled by river pattern intrusions and sea level change, which is influenced by climate change. The co-deposition of fluvial and estuary organic carbon-rich sediments in the paleo-channels after the Last Glacial

Maximum (LGM) created favorable conditions for As release. In contrast, the oxidized paleo-soil formed in Pleistocene time protects the minerals from reduction (McArthur et al., 2008). The sedimentation in inland sediment basins is influenced by alluvial-lacustrine deposit in the Pleistocene-Holocene epoch. Organic carbon derived from paleo-lakes has a high reactivity to help to build reducing conditions. In contrast, sediments brought by the Yellow River have poor-sorting characters and have less releasable As (**chapter 2**). Lithostratigraphic investigations of the Hetao Basin reveal that the locations of paleo-lakes are coincident with high-As groundwater bands (Wang et al., 2004). Because of a discontinuity of clay layers in the inland basin, multi-aquifer systems develop and sediment lithologies show a high degree of heterogeneity, making it hard to predict and monitor aquifer conditions. Therefore, it is difficult to know As concentrations at every spot.

The strong evaporation in the inland basins causes precipitation of evaporates. Thus, the genesis of groundwater is strongly influenced by dissolution of the evaporites. Sulfates dissolution and strong evaporations cause high SO_4^{2-} concentration in the groundwater (**chapter 3**). Further, subsequent redox reactions of SO_4^{2-} largely influence the As partitions in aquifers.

Iron oxides occurring in the sediments are mainly hematite, showing a similar scenario with river deltas. The good correlation between Fe oxides content and releasable As content suggests that Fe oxides are the main As carriers (**chapter 4**). However, Fe-reducing bacteria are rarely detected in the groundwater of inland basins, while SO_4^{2-}-reducing microbial communities dominate under reducing conditions and are well positively related to As concentrations in the groundwater (Li et al., 2013; Li et al., 2017). This difference is possibly related to the different groundwater compositions (such as high pH and SO_4^{2-} concentration). Furthermore, secondary Fe-containing precipitates such as siderite, vivianite or magnetite were not detected in the sediments of inland basins. The possible reason is that the slight alkaline groundwater pH condition causes most Fe^{2+} to adsorb in-situ back to the clay minerals, instead of further reacting with other anions in the groundwater (**chapter 4**).

Abiotic reduction of Fe oxides by H_2S can be present in the aquifers, which has already been evidenced in the experimental column experiments (Burton et al., 2011). Elemental S was detected in the interbedded clay samples. It indicates active redox reactions occurring in the clayey aquitard. The reductive dissolution of Fe oxides by H_2S might be an ongoing process, and vertical recharge

of groundwater causes elevated As concentration (**chapter 4**). Previous laboratory studies also suggest that reductive dissolution of Fe oxides by H_2S oxidation releases As in the reducing-clay lenses (Kumar et al., 2020). Mono Fe sulfide (FeS) is detected in the primary sediment of the Hetao Basin with negligible As sulfide concentrations, which might be related to the fast groundwater flow (Day et al., 2004; Burton et al., 2011). The FeS (mackinawite) is a metastable mineral (Benning et al., 2000; Hunger and Benning, 2007a) and can transform to greigite/pyrite over time (**chapter 4**). Neither of the latter minerals was detected in the primary sediments. This could be because the conversion of mackinawite to greigite/pyrite is thermodynamically unfavorable with limited elemental sulfur/H_2S flux. In contrast, pyrite/greigite was found in the organic carbon-rich sediments and high sulfide flux resulting from sulfates reduction produces abundant elemental sulfur and therefore simulating FeS transform to latter minerals (**chapter 5**). Greigite/pyrite provides a stable sink for As via scavenging to its structures. The in-situ degraded organics heterogeneously distribute in the sediments, therefore As-pyrite/greigite was heterogeneously found, contributing to the heterogenic groundwater As contamination (**chapter 4, chapter 5**). By this way, we may inject reactive organic carbon to remediate groundwater As pollution by fixing As in the sediments. This needs further laboratory and field studies. Furthermore, thio-As probably present in the inland basins as indicated by modelling studies (**chapter 3**) can largely increase the As mobility potentials.

Laboratory batch experiments observed that desorption of As(III) species from sediments obviously increases after pH exceeding 8 (**chapter 3**). The field study in the Hetao Basin also demonstrates that groundwater As concentrations obviously increase with pH increase. High groundwater As concentrations caused by elevated groundwater pH are widely found in arid to semi-arid plains/basins (e.g. Indus plain and South America) (Podgorski et al., 2017). However, both, reductive dissolution of Fe oxides and competitive desorption contribute to As release. It is important for further mitigation solutions to understand which one is the key process.

In semi-arid to arid sediment basins, surface water normally is limited to develop the agriculture. The anthropogenic groundwater abstraction in addition to seasonal surface recharge complexes the As transport, resulting in temporal variations of As concentrationsin groundwater. For example, the vertical recharge of oxygen-containing groundwater increases As fixation in the sediments during irrigation/surface water recharge seasons, which has evidenced in the Yangtze

River Basin and the Hetao Basin (Schaefer et al., 2016; Zhang et al., 2020). In contrast, penetration of O_2 causes the localized Fe sulfides to oxidize to Fe oxides. Even though transformation to subsequent minerals can inhibit As mobilization in short time, it still has risks to release As while groundwater turns anoxic (**chapter 5**). Furthermore, recharge of organics and redox elements from the surface into the groundwater will influence the electrons balance and thus redox reactions including Fe oxides and As. I propose that monitoring wells should be built in those areas to enhance groundwater monitoring. This would be helpful for looking for safe-drinking groundwater.

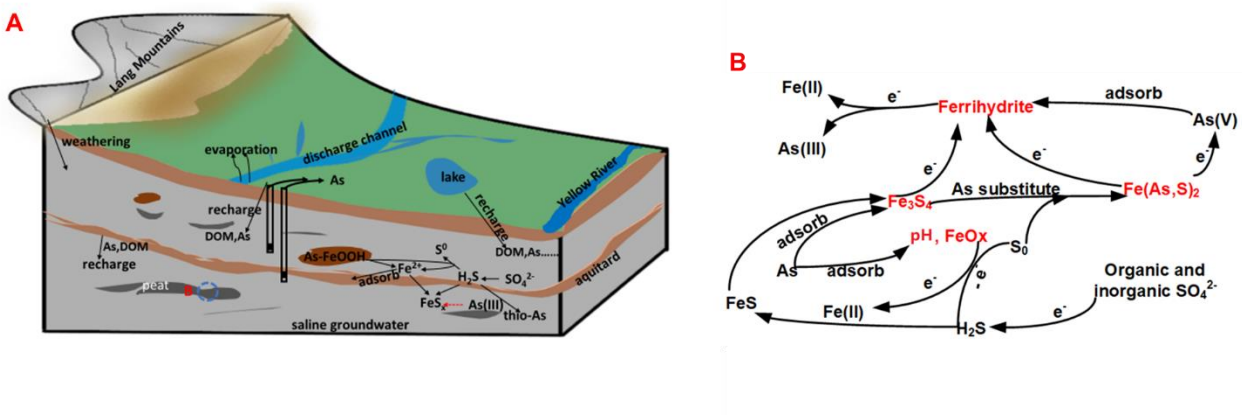

Figure 9 A conceptual model to show As mobilization mechanisms in the inland sediment Basin.

7 Conclusions and outlook

The Hetao Basin is a typical inland Basin in the north of China thatbelongs to the Yellow River catchment. Groundwater in the Hetao Basin has an As contamination problem with As concentrations up to 570 µg/L. The Fe-As-S complex interactions in the aquifers are still not fully investigated . Limitations of detailed mineral characterization in the aquifers hinders efforts to explain the high As concentration and predict As partitions in the aquifers as well as taking effective remediation strategy. In this study, I mainly used isotopes combined with geochemical data to indicate the deposition environment of the Hetao Basin, and applied high resolution spectroscopies in combination with microscopies and other geochemical techniques to study the Fe–As–S coupled redox minerals in sediments. Based on scientific results, conclusions are summarized in the section 7.1, and new scientific questions are put forward in the section 7.2.

7.1 Conclusions

Sediments in the Hetao Basin show average higher As contents than in the flood plains in south and south east of Asia, indicating that sediments in Hetao Basin have a different origin. The similar REE compositions between the Hetao Basin and the Lang Mountains, which are located in the north of the Hetao Basin, suggest that sediments in the Hetao Basin are resourced from the Lang Mountains. Weathering of As–contains minerals contributes to high As content in the sediments.

Carbon isotope signals ($\delta^{13}C$) of organic carbon in combination with C_{org}/N ratios shows that sediments are mainly of aquatic origin. The unconfined aquifer sediments (at depths between 10 – 30 m) correspond to lacustrine deposits, and have higher releasable As (PO_4^{2-}desorbable and iron oxides-reducible) contents than sediments below. The higher content of releasable As in combination with paleo-lake derived organic carbon causes higher As concentrations in unconfined aquifers.

Due to the lacustrine deposits, evaporite minerals can be found in these sediments. Evaporite minerals identified in the sediments mainly include Na and Ca related sulfates. The sulfates dissolution and silicates weathering control groundwater geochemical compositions. Furthermore, the groundwater pH decreases and Ca^{2+} release resulting from weathering of Ca related sulfates

can retard As desorption from sediments, while the redox reaction coupled with SO_4^{2-} has opposing influence on As mobilizations in aquifers.

Further, I applied high-resolution X-ray spectroscopies in combination with microscopies and extractions to investigate the Fe-S-As coupled redox minerals in the depth profiles and indicated the influences on As mobilizations in the aquifers. In the surface silt/clay layers, sediments are dominated by oxidized species, such as As(V) species, SO_4^{2-}, and Fe(III). Underlying the groundwater table, reduction of SO_4^{2-}, Fe(III) and As(V) species co-occurs. The Fe(III) oxides and As(V) species show negative correlations with depths, which means that Fe(III) oxides and As(V) species gradually decreases with depths independently to groundwater redox conditions, while the SO_4^{2-} reduction is much more prevalent in deep zones. The Fe(III) oxides mainly including hematite, show similar compositions in comparison to sediments from flood plains in southeast of Asia. Releasable As contents in sediments show positive correlations with Fe(III) oxides contents, which is quantified by XAS. This provides the solid evidence that As is mobilized into groundwater via desorption from Fe(III) oxides. The reduced FeS was detected in the primary sediments, but with scarce abilities to adsorb As. Pyrite and greigite were detected in particular depths, which most likely were formed with enriched organic carbon supply.

Organic carbon-rich layers (peat) were separated from bulk sediments to examine Fe and S diagenetic pathways and to explain the complex interplay between Fe sulfides formation and As mobilization. Fe sulfides nucleate in the decaying plant tissues and phyllosilicates, and likely are formed in the early diagenetic process in the water-sediment interface. Pyrite and greigite are respectively as S and Fe diagenetic end members. Pyrite forms likely via polysulfides pathways, and excessive Fe(II) compared to sulfide due to lower sulfide flux potentially inhabits pyrite formation. Those peat sediments reveal a stable sink for As under anoxic aquifer conditions, with significant ratio of As incorporating into pyrite/greigite. Arsenic incorporates into pyrite structure by replacing S(-I), while precipitates with S form minerals analogous to realgar. Part of pyrite was found to oxidize into ferrihydrite which have average similar As content as pyrite, indicating that oxidation of pyrite into ferrihydrite can retard As release into groundwater. In the Hetao Basin, groundwater redox conditions frequently experience oscillations due to anthropogenic perturbations and seasonal fluctuations of groundwater table. The possibly induced reduction of ferrihydrite has the potential to release As since pyrite formation is limited by sulfide flux.

7.2 Outlook

After performing this research, some open questions are put forward and need to be studied in the future:

(1) This study indicates that higher releasable As content in the unconfined aquifer in combination with paleo-lake derived organic matter probably causes As release into groundwater. The difference between organic matter buried in unconfined aquifers and confined aquifers needs to be studied, especially from molecular aspects.

(2) The Fe-S-organic carbon coupled biogeochemical mineralization pathways need to be studied in detail in the laboratory scale. The Fe sulfides formation would be controlled by the ratio of reactive Fe to sulfide flux, which is further controlled by availabilities of SO_4^{2-} and organic carbon. Whether sulfide incorporates into functional groups of organic carbon or reacts with Fe (II) also depends on the ratios of Fe(II) to sulfide and reactive sites of organic carbon. Those different reaction pathways can further influence As species. Based on this assumption, experiments in laboratory scale need to be studied.

(3) Groundwater As species need to be measured. The thio-As species recently is proven to account for large proportions of As species in the paddy soils. In inland basins, higher sulfide concentrations and alkaline pH conditions favor for thio-As formation. However, it is still unknown how large proportions of thio-As are in groundwater resulting from instabilities of thio-As species and limitations of groundwater sampling techniques.

(4) This study checks Fe-As-S coupled minerals in sediments in detail. Based on the results, further modelling studies are needed to couple with other geochemical parameters to model As reaction behavior in the aquifers.

(5) The results of this PhD study show that As incorporates with S into the surface of greigite, and the precipitates resemble realgar. However, the structure could not be characterized due to complexities of sediments and low quality of XAS spectra. In the future, there is a need to clarify this in the lab scale. It also has to be shown whether greigite is an environmentally friendly and effective adsorbent for As either in the soil or water.

(6) Lacustrine deposits in the upper aquifers provide more Fe oxides and releasable As. Further work is needed to investigate whether this is related to the depositional environment or less flushing history.

References

Amini M., Abbaspour K. C., Berg M., Winkel L., Hug S. J., Hoehn E., Yang H. and Johnson C. A. (2008) Statistical modeling of global geogenic arsenic contamination in groundwater. *Environ. Sci. Technol.* **42**, 3669–3675.

Bauer, W. O., Onishi, B. M. H. (1969) Arsenic. In Wedepohl, K.H.(ed). Handbook of Geochemistry. Springer, Berlin.

Baker D. E. and Chesnin L. (1975) Chemical monitoring of soils for environmental quality and animal and human health., *ADV AGRON.***27**, 305-374.

Benning L. G., Wilkin R. T. and Barnes H. L. (2000) Reaction pathways in the Fe – S system below 100 °C. *Chem. Geol.,* 167, 25-51.

Berg M., Luzi S., Trang P. T. K., Viet P. H., Giger W. and Stüben D. (2006) Arsenic removal from groundwater by household sand filters: Comparative field study, model calculations, and health benefits. *Environ. Sci. Technol.* **40**, 5567–5573.

Biswas R., Majhi A. K. and Sarkar A. (2019) The role of arsenate reducing bacteria for their prospective application in arsenic contaminated groundwater aquifer system. *Biocatal. Agric. Biotechnol.* **20**, 101218. Available at: https://doi.org/10.1016/j.bcab.2019.101218.

Bleam W. F. (2012) Redox Chemistry. *Soil Environ. Chem.*, 321–370.

Borch T., Kretzschmar R., Skappler A., Van Cappellen P., Ginder-Vogel M., Voegelin A. and Campbell K. (2010) Biogeochemical redox processes and their impact on contaminant dynamics. *Environ. Sci. Technol.* **44**, 15–23.

Boyle R. W. and Jonasson I. R. (1973) the Geochemistry of Arsenic and Its Use As an Indicator. *J. Geochemical Explor.* **2**, 251–296.

Bundschuh J., Farias B., Martin R., Storniolo A., Bhattacharya P., Cortes J., Bonorino G. and Albouy R. (2004) Groundwater arsenic in the Chaco-Pampean Plain, Argentina: Case study from Robles county, Santiago del Estero Province. *Appl. Geochemistry* **19**, 231–243.

Burton E. D., Johnston S. G. and Bush R. T. (2011) Microbial sulfidogenesis in ferrihydrite-rich environments: Effects on iron mineralogy and arsenic mobility. *Geochim. Cosmochim. Acta* **75**, 3072–3087. Available at: http://dx.doi.org/10.1016/j.gca.2011.03.001.

Cao W., Guo H., Zhang Y., Ma R., Li Y., Dong Q., Li Y. and Zhao R. (2017) Controls of paleochannels on groundwater arsenic distribution in shallow aquifers of alluvial plain in the Hetao Basin, China. *Sci. Total Environ.* **613–614**, 958–968. Available at: http://linkinghub.elsevier.com/retrieve/pii/S0048969717325330%0Ahttp://www.ncbi.nlm.nih.gov/pubmed/28946383.

Ciardelli M. C., Xu H. and Sahai N. (2008) Role of Fe(II), phosphate, silicate, sulfate, and carbonate in arsenic uptake by coprecipitation in synthetic and natural groundwater. *Water Res.* **42**, 615–624.

Couture R. M., Gobeil C. and Tessier A. (2010) Arsenic, iron and sulfur co-diagenesis in lake sediments. *Geochim. Cosmochim. Acta* **74**, 1238–1255.

Cullen W. R. and Reimer K. J. (1989) Arsenic Speciation in the Environment. *Chem. Rev.* **89**, 713–764.

Day P. A. O., Vlassopoulos D., Root R. and Rivera N. (2004) The influence of sulfur and iron on dissolved arsenic concentrations in the shallow subsurface under changing redox conditions. *Proceeding Natl. Acad. Sci.*

Eiche E., Berg M., Hönig S. M., Neumann T., Lan V. M., Pham T. K. T. and Pham H. V. (2017) Origin and availability of organic matter leading to arsenic mobilisation in aquifers of the Red River Delta, Vietnam. *Appl. Geochemistry* **77**, 184–193.

Eiche E., Neumann T., Berg M., Weinman B., van Geen A., Norra S., Berner Z., Trang P. T. K., Viet P. H. and Stüben D. (2008) Geochemical processes underlying a sharp contrast in groundwater arsenic concentrations in a village on the Red River delta, Vietnam. *Appl. Geochemistry* **23**, 3143–3154. Available at: http://dx.doi.org/10.1016/j.apgeochem.2008.06.023.

Fakhreddine S., Dittmar J., Phipps D., Dadakis J. and Fendorf S. (2015) Geochemical Triggers of Arsenic Mobilization during Managed Aquifer Recharge. *Environ. Sci. Technol.* **49**, 7802–7809.

Fendorf S., Michael H. A. and van Geen A. (2010) Spatial and Temporal Variations of Groundwater Arsenic in South and Southeast Asia. *Science (80-.).* **328**, 1123–1127. Available at: http://www.sciencemag.org/cgi/content/abstract/328/5982/1123.

Ferguson J. F. and Gavis J. (1972) A review of the arsenic cycle in natural waters. *Water Res.* **6**, 1259–1274.

Fredrickson J. K., Zachara J. M., Kennedy D. W., Dong H., Onstott T. C., Hinman N. W. and Li S. M. (1998) Biogenic iron mineralization accompanying the dissimilatory reduction of hydrous ferric oxide by a groundwater bacterium. *Geochim. Cosmochim. Acta* **62**, 3239–3257.

Gao Z., Guo H., Zhao B., Wang A., Han S. and Dong H. (2020) Experiment-based geochemical modeling of Arsenic (V) and Arsenic (III) adsorption onto aquifer sediments from an inland basin. *J. Hydrol.* **588**, 125094. Available at: https://doi.org/10.1016/j.jhydrol.2020.125094.

van Geen A., Bostick B. C., Thi Kim Trang P., Lan V. M., Mai N.-N., Manh P. D., Viet P. H., Radloff K., Aziz Z., Mey J. L., Stahl M. O., Harvey C. F., Oates P., Weinman B., Stengel C., Frei F., Kipfer R. and Berg M. (2013) Retardation of arsenic transport through a Pleistocene aquifer. *Nature* **501**, 204–207. Available at: http://www.nature.com/doifinder/10.1038/nature12444.

van Geen A., Rose J., Thoral S., Garnier J. M., Zheng Y. and Bottero J. Y. (2004) Decoupling of As and Fe release to Bangladesh groundwater under reducing conditions. Part II: Evidence from sediment incubations. *Geochim. Cosmochim. Acta* **68**, 3475–3486.

Geen A. Van, Zheng Y., Versteeg R., Stute M., Horneman A., Dhar R., Steckler M., Gelman A., Small C., Ahsan H., Graziano J. H., Hussain I. and Ahmed K. M. (2003) Spatial variability of arsenic in 6000 tube wells in a 25 km 2 area of Bangladesh. **39**, 1–16.

Guo H., Jia Y., Wanty R. B., Jiang Y., Zhao W., Xiu W., Shen J., Li Y., Cao Y., Wu Y., Zhang D., Wei C., Zhang Y., Cao W. and Foster A. (2016a) Contrasting distributions of groundwater arsenic and uranium in the western Hetao basin, Inner Mongolia: Implication for origins and fate controls. *Sci. Total Environ.* **541**, 1172–1190. Available at: http://dx.doi.org/10.1016/j.scitotenv.2015.10.018.

Guo H., Liu C., Lu H., Wanty R. B., Wang J. and Zhou Y. (2013) Pathways of coupled arsenic and iron cycling in high arsenic groundwater of the Hetao basin, Inner Mongolia, China: An iron isotope approach. *Geochim. Cosmochim. Acta* **112**, 130–145. Available at:

http://dx.doi.org/10.1016/j.gca.2013.02.031.

Guo H., Yang S., Tang X., Li Y. and Shen Z. (2008) Groundwater geochemistry and its implications for arsenic mobilization in shallow aquifers of the Hetao Basin, Inner Mongolia. *Sci. Total Environ.* **393**, 131–144.

Guo H., Zhang B. and Zhang Y. (2011) Applied Geochemistry Control of organic and iron colloids on arsenic partition and transport in high arsenic groundwaters in the Hetao basin , Inner Mongolia. *Appl. Geochemistry* **26**, 360–370. Available at: http://dx.doi.org/10.1016/j.apgeochem.2010.12.009.

Guo H., Zhou Y., Jia Y., Tang X., Li X., Shen M., Lu H., Han S., Wei C., Norra S. and Zhang F. (2016b) Sulfur Cycling-Related Biogeochemical Processes of Arsenic Mobilization in the Western Hetao Basin, China: Evidence from Multiple Isotope Approaches. *Environ. Sci. Technol.*, acs.est.6b03460. Available at: http://pubs.acs.org/doi/abs/10.1021/acs.est.6b03460.

Herbel M. and Fendorf S. (2006) Biogeochemical processes controlling the speciation and transport of arsenic within iron coated sands. *Chem. Geol.* **228**, 16–32.

Horneman A., van Geen A., Kent D. V., Mathe P. E., Zheng Y., Dhar R. K., O'Connell S., Hoque M. A., Aziz Z., Shamsudduha M., Seddique A. A. and Ahmed K. M. (2004) Decoupling of As and Fe release to Bangladesh groundwater under reducing conditions. Part I: Evidence from sediment profiles. *Geochim. Cosmochim. Acta* **68**, 3459–3473.

Hunger S. and Benning L. G. (2007a) Greigite : a true intermediate on the polysulfide pathway to pyrite. **20**, 1–20.

Hunger S. and Benning L. G. (2007b) Greigite: A true intermediate on the polysulfide pathway to pyrite. *Geochem. Trans.* **8**, 1–20.

Islam F. S., Gault A. G., Boothman C., Polya D. a, Charnock J. M., Chatterjee D. and Lloyd J. R. (2004) Role of metal-reducing bacteria in arsenic release from Bengal delta sediments. *Nature* **430**, 68–71.

Jia L., Zhang X., Ye P., Zhao X., He Z., He X., Zhou Q., Li J., Ye M., Wang Z. and Meng J. (2016) Development of the alluvial and lacustrine terraces on the northern margin of the Hetao Basin, Inner Mongolia, China: Implications for the evolution of the Yellow River in

the Hetao area since the late Pleistocene. *Geomorphology* **263**, 87–98. Available at: http://dx.doi.org/10.1016/j.geomorph.2016.03.034.

Jia Y., Guo H., Jiang Y., Wu Y. and Zhou Y. (2014) Hydrogeochemical zonation and its implication for arsenic mobilization in deep groundwaters near alluvial fans in the Hetao Basin, Inner Mongolia. *J. Hydrol.* **518**, 410–420. Available at: http://dx.doi.org/10.1016/j.jhydrol.2014.02.004.

Jomova K., Jenisova Z., Feszterova M., Baros S., Liska J., Hudecova D., Rhodes C. J. and Valko M. (2011) Arsenic: Toxicity, oxidative stress and human disease. *J. Appl. Toxicol.* **31**, 95–107.

Kim M. and Haack S. (2000) Carbonate Ions and Arsenic Dissolution by Groundwater. **34**, 3094–3100.

Konhauser K. and Riding R. (2012) Chapter 6 – The global iron cycle. , 65–92.

Kumar N., Noël V., Planer-friedrich B., Besold J., Lezama J., Bargar J. R., Brown G. E., Fendorf S. and Boye K. (2020) Redox Heterogeneities Promote Thioarsenate Formation and Release into Groundwater. *Environ. Sci. Technol.*

Kumari N. and Jagadevan S. (2016) Genetic identification of arsenate reductase and arsenite oxidase in redox transformations carried out by arsenic metabolising prokaryotes – A comprehensive review. *Chemosphere* **163**, 400–412. Available at: http://dx.doi.org/10.1016/j.chemosphere.2016.08.044.

Langner P., Mikutta C. and Kretzschmar R. (2011) Arsenic sequestration by organic sulphur in peat. *Nat. Geosci.* **5**, 66–73. Available at: http://dx.doi.org/10.1038/ngeo1329.

Lear G., Song B., Gault A. G., Polya D. A. and Lloyd J. R. (2007) Molecular analysis of arsenate-reducing bacteria within Cambodian sediments following amendment with acetate. *Appl. Environ. Microbiol.* **73**, 1041–1048.

Li P., Jiang Z., Wang Y., Deng Y., Van Nostrand J. D., Yuan T., Liu H., Wei D. and Zhou J. (2017) Analysis of the functional gene structure and metabolic potential of microbial community in high arsenic groundwater. *Water Res.* **123**, 268–276. Available at: http://dx.doi.org/10.1016/j.watres.2017.06.053.

Li P., Wang Y., Jiang Z., Jiang H., Li B., Dong H. and Wang Y. (2013) Microbial Diversity in High Arsenic Groundwater in Hetao Basin of Inner Mongolia, China. *Geomicrobiol. J.* **30**, 897–909. Available at: http://www.tandfonline.com/doi/abs/10.1080/01490451.2013.791354.

Li Y., Guo H. and Hao C. (2014) Arsenic release from shallow aquifers of the Hetao basin, Inner Mongolia: evidence from bacterial community in aquifer sediments and groundwater. *Ecotoxicology* **23**, 1900–1914.

Liu M., Zhang D., Xiong G., Zhao H., Di Y., Wang Z. and Zhou Z. (2016) Zircon U-Pb age, Hf isotope and geochemistry of Carboniferous intrusions from the Langshan area, Inner Mongolia: Petrogenesis and tectonic implications. *J. Asian Earth Sci.* **120**, 139–158. Available at: http://dx.doi.org/10.1016/j.jseaes.2016.01.005.

Lowers H. A., Breit G. N., Foster A. L., Whitney J., Yount J., Uddin M. N. and Muneem A. A. (2007) Arsenic incorporation into FeS2 pyrite and its influence on dissolution: A DFT study>. *Geochim. Cosmochim. Acta* **71**, 2699–2717.

Magnone D., Richards L. A., Polya D. A., Bryant C., Jones M. and Van Dongen B. E. (2017) Biomarker-indicated extent of oxidation of plant-derived organic carbon (OC) in relation to geomorphology in an arsenic contaminated Holocene aquifer, Cambodia. *Sci. Rep.* **7**.

Maguffin S. C., Kirk M. F., Daigle A. R., Hinkle S. R. and Jin Q. (2015) Substantial contribution of biomethylation to aquifer arsenic cycling. *Nat. Geosci.* **8**, 290–293.

Mar L., Gutiérrez M., Alarcón-herrera M. T. and Lourdes M. De (2011) Chemosphere Occurrence and treatment of arsenic in groundwater and soil in northern Mexico and southwestern USA. *Chemosphere* **83**, 211–225. Available at: http://dx.doi.org/10.1016/j.chemosphere.2010.12.067.

McArthur J. M., Ravenscroft P., Banerjee D. M., Milsom J., Hudson-Edwards K. A., Sengupta S., Bristow C., Sarkar A., Tonkin S. and Purohit R. (2008) How paleosols influence groundwater flow and arsenic pollution: A model from the Bengal Basin and its worldwide implication. *Water Resour. Res.* **44**.

McArthur J. M., Ravenscroft P., Safiulla S. and Thirlwall M. F. (2001) Arsenic in groundwater: Testing pollution mechanisms for sedimentary aquifers in Bangladesh. *Water Resour. Res.*

37, 109–117.

Mikutta C. and Rothwell J. J. (2016) Peat Bogs as Hotspots for Organoarsenical Formation and Persistence. *Environ. Sci. Technol.* **50**, 4314–4323.

Mondal P., Bhowmick S., Chatterjee D., Figoli A. and Van der Bruggen B. (2013) Remediation of inorganic arsenic in groundwater for safe water supply: A critical assessment of technological solutions. *Chemosphere* **92**, 157–170. Available at: http://dx.doi.org/10.1016/j.chemosphere.2013.01.097.

Muehe E. M., Morin G., Scheer L., Le Pape P., Esteve I., Daus B. and Kappler A. (2016) Arsenic(V) Incorporation in Vivianite during Microbial Reduction of Arsenic(V)-Bearing Biogenic Fe(III) (Oxyhydr)oxides. *Environ. Sci. Technol.* **50**, 2281–2291.

Mukherjee A., Verma S., Gupta S., Henke K. R. and Bhattacharya P. (2014) Influence of tectonics, sedimentation and aqueous flow cycles on the origin of global groundwater arsenic: Paradigms from three continents. *J. Hydrol.* **518**, 284–299. Available at: http://dx.doi.org/10.1016/j.jhydrol.2013.10.044.

Mukherjee S. S. Æ. P. K. and Shome Æ. T. P. Æ. S. (2004) Nature and origin of arsenic carriers in shallow aquifer sediments of Bengal Delta , India. , 1071–1081.

Nickson R. T., Mcarthur J. M., Ravenscroft P., Burgess W. G. and Ahmed K. M. (2000) Mechanism of arsenic release to groundwater, Bangladesh and West Bengal. *Appl. Geochemistry* **15**, 403–413.

Nordstrom D. K. (2002) Worldwide Occurrences of Arsenic in Ground Water. *Science (80-.).* **296**, 64–65.

Pal T., Mukherjee P. K., Sengupta S., Bhattacharyya A. K. and Shome S. (2002) Arsenic Pollution in Groundwater of West Bengal , India - An Insight into the Problem by Subsurface Sediment Analysis. , 501–512.

Le Pape P., Blanchard M., Brest J., Boulliard J. C., Ikogou M., Stetten L., Wang S., Landrot G. and Morin G. (2017) Arsenic Incorporation in Pyrite at Ambient Temperature at Both Tetrahedral S-I and Octahedral FeII Sites: Evidence from EXAFS-DFT Analysis. *Environ. Sci. Technol.* **51**, 150–158.

Parsons J. G., Aldrich M. V. and Gardea-Torresdey J. L. (2002) Environmental and biological applications of extended X-ray absorption fine structure (EXAFS) and X-ray absorption near edge structure (XANES) spectroscopies. *Appl. Spectrosc. Rev.* **37**, 187–222.

Perez J. P. H., Freeman H. M., Brown A. P., Van Genuchten C. M., Dideriksen K., S'Ari M., Tobler D. J. and Benning L. G. (2020) Direct Visualization of Arsenic Binding on Green Rust Sulfate. *Environ. Sci. Technol.* **54**, 3297–3305.

Pichler T., Veizer J. A. N. and Hall G. E. M. (1999) Natural Input of Arsenic into a Coral-Reef Ecosystem by Hydrothermal Fluids and Its Removal by Fe (III) Oxyhydroxides. **33**, 1373–1378.

Planer-Friedrich B., Schaller J., Wismeth F., Mehlhorn J. and Hug S. J. (2018) Monothioarsenate Occurrence in Bangladesh Groundwater and Its Removal by Ferrous and Zero-Valent Iron Technologies. *Environ. Sci. Technol.* **52**, 5931–5939.

Planer-Friedrich B., Suess E., Scheinost A. C. and Wallschläger D. (2010) Arsenic speciation in sulfidic waters: Reconciling contradictory spectroscopic and chromatographic evidence. *Anal. Chem.* **82**, 10228–10235.

Podgorski J. and Berg M. (2020) Global threat of arsenic in groundwater. *Science (80-.).* **850**, 1–31.

Podgorski J. E., Eqani S. A. M. A. S., Khanam T., Ullah R., Shen H. and Berg M. (2017) Extensive arsenic contamination in high-pH unconfined aquifers in the Indus Valley. *Sci. Adv.* **3**.

Polizzotto M. L., Harvey C. F., Li G., Badruzzman B., Ali A., Newville M., Sutton S. and Fendorf S. (2006) Solid-phases and desorption processes of arsenic within Bangladesh sediments. **228**, 97–111.

Postma D., Larsen F., Thai N. T., Trang P. T. K., Jakobsen R., Nhan P. Q., Long T. V., Viet P. H. and Murray A. S. (2012) Groundwater arsenic concentrations in Vietnam controlled by sediment age. *Nat. Geosci.* **5**, 656–661. Available at: http://dx.doi.org/10.1038/ngeo1540.

Rancourt D. G. and Ping J. Y. (1991) Voigt-based methods for arbitrary-shape static hyperfine parameter distributions in Mössbauer spectroscopy. *Nucl. Inst. Methods Phys. Res. B* **58**, 85–97.

Ravel B. and Newville M. (2005) ATHENA, ARTEMIS, HEPHAESTUS: Data analysis for X-ray absorption spectroscopy using IFEFFIT. *J. Synchrotron Radiat.* **12**, 537–541.

Raychowdhury N., Mukherjee A., Bhattacharya P., Johannesson K., Bundschuh J., Sifuentes G. B., Nordberg E., Martin R. A. and Storniolo A. del R. (2014) Provenance and fate of arsenic and other solutes in the Chaco-Pampean Plain of the Andean foreland, Argentina: From perspectives of hydrogeochemical modeling and regional tectonic setting. *J. Hydrol.* **518**, 300–316. Available at: http://dx.doi.org/10.1016/j.jhydrol.2013.07.003.

Reza A. H. M. S., Jean J. S., Lee M. K., Liu C. C., Bundschuh J., Yang H. J., Lee J. F. and Lee Y. C. (2010) Implications of organic matter on arsenic mobilization into groundwater: Evidence from northwestern (Chapai-Nawabganj), central (Manikganj) and southeastern (Chandpur) Bangladesh. *Water Res.* **44**, 5556–5574. Available at: http://linkinghub.elsevier.com/retrieve/pii/S0043135410006330 [Accessed August 5, 2017].

Rodríguez-lado L., Sun G., Berg M., Zhang Q., Xue H., Zheng Q. and Johnson C. A. (2013) Throughout China. **341**, 866–869. Available at: http://www.sciencemag.org/content/341/6148/866.full.pdf.

Schaefer M. V., Ying S. C., Benner S. G., Duan Y., Wang Y. and Fendorf S. (2016) Aquifer Arsenic Cycling Induced by Seasonal Hydrologic Changes within the Yangtze River Basin. *Environ. Sci. Technol.* **50**, 3521–3529.

Sigfu B., Keller N. S. and Stefa A. (2014) ScienceDirect Arsenic speciation in natural sulfidic geothermal waters. **142**, 15–26.

Smedley P. L. and Kinniburgh D. G. (2002) A review of the source, behaviour and distribution of arsenic in natural waters. *Appl. Geochemistry* **17**, 517–568.

Smith A., Lingas E. and Rahman M. (2000) Contamination of drinking-water by arsenic in Bangladesh: a public health emergency: RN - Bull. W.H.O., v. 78, p. 1093-1103. *Bull. World Health Organ.* **78**, 1093–1103.

Sø H. U., Postma D., Vi M. L., Pham T. K. T., Kazmierczak J., Dao V. N., Pi K., Koch C. B., Pham H. V. and Jakobsen R. (2018) Arsenic in Holocene aquifers of the Red River floodplain, Vietnam: Effects of sediment-water interactions, sediment burial age and groundwater residence time. *Geochim. Cosmochim. Acta* **225**, 192–209. Available at:

https://doi.org/10.1016/j.gca.2018.01.010.

Stolze L., Zhang D., Guo H. and Rolle M. (2019) Model-Based Interpretation of Groundwater Arsenic Mobility during in Situ Reductive Transformation of Ferrihydrite. *Environ. Sci. Technol.* **53**, 6845–6854.

Stuckey J. W., Schaefer M. V, Kocar B. D., Benner S. G. and Fendorf S. (2015) Arsenic release metabolically limited to permanently water-saturated soil in Mekong Delta. *Nat. Geosci.* **advance on**, 1–9. Available at: http://dx.doi.org/10.1038/ngeo2589%5Cn10.1038/ngeo2589%5Cnhttp://www.nature.com/ngeo/journal/vaop/ncurrent/abs/ngeo2589.html#supplementary-information.

Suda A. and Makino T. (2016) Functional effects of manganese and iron oxides on the dynamics of trace elements in soils with a special focus on arsenic and cadmium: A review. *Geoderma* **270**, 68–75. Available at: http://dx.doi.org/10.1016/j.geoderma.2015.12.017.

Sun G. (2004) Arsenic contamination and arsenicosis in China. *Toxicol. Appl. Pharmacol.* **198**, 268–271.

Tufano K. J. and Fendorf S. (2008) Confounding impacts of iron reduction on arsenic retention. *Environ. Sci. Technol.* **42**, 4777–4783.

Tyrovola K., Nikolaidis N. P., Veranis N., Kallithrakas-kontos N. and Koulouridakis P. E. (2006) Arsenic removal from geothermal waters with zero-valent iron — Effect of temperature , phosphate and nitrate. **40**, 2375–2386.

Wang Y., Le Pape P., Morin G., Asta M., King G., Bartova B., Suvorova E., Frutschi M., Ikogou M., Pham V. H. C., Vo P. Le, Herman F., Charlet L. and Bernier-Latmani R. (2018) Arsenic speciation in Mekong Delta sediments depends on their depositional environment. *Environ. Sci. Technol.*, acs.est.7b05177. Available at: http://pubs.acs.org/doi/10.1021/acs.est.7b05177.

Wang Y., Pi K., Fendorf S., Deng Y. and Xie X. (2017) Sedimentogenesis and hydrobiogeochemistry of high arsenic Late Pleistocene-Holocene aquifer systems. *Earth-Science Rev.*, 0–1. Available at: http://dx.doi.org/10.1016/j.earscirev.2017.10.007.

Wilkin R. T., Wallschläger D. and Ford R. G. (2003) Speciation of arsenic in sulfidic waters. *Geochem. Trans.* **4**, 1–7.

Xie X., Wang Y., Su C., Liu H., Duan M. and Xie Z. (2008) Arsenic mobilization in shallow aquifers of Datong Basin: Hydrochemical and mineralogical evidences. *J. Geochemical Explor*. **98**, 107–115.

Zhang Z., Guo H., Liu S., Weng H., Han S. and Gao Z. (2020) Mechanisms of groundwater arsenic variations induced by extraction in the western Hetao Basin, Inner Mongolia, China. *J. Hydrol.* **583**, 124599. Available at: https://doi.org/10.1016/j.jhydrol.2020.124599.

Zhang Z., (2019) Variation and its driving mechanismes of groundwater arsenic induced by intensive groundwater extraction. phD thesis

Zobrist J., Dowdle P. R., Davis J. A. and Oremland R. S. (2000) Mobilization of arsenite by dissimilatory reduction of adsorbed arsenate. *Environ. Sci. Technol.* **34**, 4747–4753.

List of Publications and presentations

Publications

H.Y. Wang*, E. Eiche, H.M. Guo, S. Norra, Impact of sedimentation history for As distribution in Late Pleistocene-Holocene sediments in the Hetao Basin , China, Journal of Soils and sediments (2020). https://doi.org/10.1007/s11368-020-02703-2

H.Y. Wang, H.M. Guo, W. Xiu*, J. Bauer, G.X. Sun, X.H. Tang, S. Norra, Indications that weathering of evaporite minerals affects groundwater salinity and As mobilization in aquifers of the northwestern Hetao Basin, China, Applied Geochemistry. (2019) https://doi.org/10.1016/j.apgeochem.2019.104416

H.Y. Wang*, J. Göttlicher, J.M. Byrne, H.M. Guo, L.G. Benning, S. Norra, Vertical redox zones of Fe-S-As coupled mineralogy in the sediments of Hetao Basin – constraints for groundwater As contamination. *Journal of hazardous materia*ls (2020). https://doi.org/10.1016/j.jhazmat.2020.124924

H.Y. Wang*, J.M. Byrne, J.P.H. Perez, A.N. Thomas, J. Göttlicher, S. Mayanna, A. Kontny, A. Kappler, H.M. Guo, L.G. Benning, Arsenic sequestration in pyrite and greigite in the buried peat of As-contaminated aquifers, Geochimica et Cosmochimica Acta (2020). https://doi.org/10.1016/j.gca.2020.06.021

Presentations

H.Y. Wang*, J.M. Byrne, J.P.H. Perez, A. Thomas, L.G. Benning, S. Mayanna, H.E. Höfer, A. Kontny, E. Eiche, H.M. Guo, A. Kappler, S. Norra. Arsenic speciation and distribution in peat deposits of the Hetao Basin, China. Barcelona, presentation (oral) and poster, **Goldschmidt 2019**.

H.Y. Wang*. Hydrogeological and geochemical comparison of high and low arsenic groundwater in the Hetao Basin, Inner Mongolia. Beijing, presentation (poster), **As 2018**.

Appendix 1 Imapct of sedimentation history for As distribution in Late Pleistocene-Holocene sediments in the Hetao Basin, China

Journal of Soils and Sediments
https://doi.org/10.1007/s11368-020-02703-2

SEDIMENTS, SEC 2 • PHYSICAL AND BIOGEOCHEMICAL PROCESSES • RESEARCH ARTICLE

Impact of sedimentation history for As distribution in Late Pleistocene-Holocene sediments in the Hetao Basin, China

Hongyan Wang [1] · Elisabeth Eiche [1] · Huaming Guo [2,3] · Stefan Norra [1]

Received: 19 February 2020 / Accepted: 23 June 2020
© The Author(s) 2020

Abstract

Purpose To understand the impact of geochemical sedimentation history for arsenic (As) distribution in the sediment profiles of the Hetao Basin, we (1) evaluated sediments provenance and variations of weathering intensities, (2) attempted to reconstruct the depositional environments, and (3) explored the As and Fe speciation in the sediments. Combining the information above, different sedimentation facies were distinguished in the vertical profiles.

Methods Two sediments cores were drilled up to 80 m depth. Major and trace element compositions, including rare earth elements (REE), were analyzed. Carbon isotope ratios ($\delta^{13}C_{org}$) of embedded organic matter in the sediments were analyzed by isotope ratio mass spectrometry (IR-MS). Arsenic and Fe speciation of the sediments were determined by sequential extractions.

Results and discussion The similar REE geochemistry of rocks from the Lang Mountains and sediments in the Hetao Basin indicated that the sediments originated from the Lang Mountains. The C/N ratio (~ 4 to ~ 10) in combination with $\delta^{13}C_{org}$ (− 27‰ to −2 4‰) suggested that sediments were mainly deposited in aquatic environments. The unconfined aquifer equaled the lacustrine deposit with less intensive weathering during last glacial maximum (LGM). Here, the As content (average, 5.4 mg kg^{-1}) was higher than in the aquifer sediments below (average, 3.6 mg kg^{-1}).

Conclusion Higher content of releasable As in combination with paleolake-derived organic matter aquifer sediments probably contributes to higher groundwater As concentration in the unconfined aquifer. This study provides the first insight into the impact of sedimentation history on As distributions in sediment profiles in the Hetao Basin.

Keywords Sediment basin · Sedimentation history · Arsenic provenance · Weathering intensities · Organic carbon isotopic signature · Arsenic speciation

1 Introduction

Geogenic groundwater arsenic (As) contamination is of global concern. It is mainly reported from floodplains in South and Southeast Asia including the Ganges-Brahmaputra-Meghna (GBM) River delta, the Mekong River delta, the Red River delta, and inland basins located in the Yellow River catchment including the Hetao Basin, the Hohhot Basin, the Datong Basin, and the Yinchuan Basin (Nordstrom 2002; Rodríguez-Lado et al. 2013; Guo et al. 2017). Over 100 million people are exposed to As with concentration higher than 10 μg L^{-1} (the World Health Organization standard) in the drinking water (Ravenscroft et al. 2009).

Studies indicate that in situ microbial organic carbon oxidation processes coupled with reduction of As-bearing Fe oxy(hydr)oxides is the main cause for As release into groundwater (Nickson et al. 1998; McArthur et al. 2001; Islam et al.

Responsible editor: Tomas Matys Grygar

Electronic supplementary material The online version of this article (https://doi.org/10.1007/s11368-020-02703-2) contains supplementary material, which is available to authorized users.

✉ Hongyan Wang
hongyan.wang@kit.edu

[1] Institute of Applied Geosciences (AGW), Geochemistry & Economic Geology group, Karlsruhe Institute of Technology (KIT), Adenauerring 20 b, 76131 Karlsruhe, Germany

[2] State Key Laboratory of Biogeology and Environmental Geology, China University of Geosciences, Beijing 100083, People's Republic of China

[3] School of Water Resources and Environment, China University of Geosciences, Beijing 100083, People's Republic of China

Published online: 01 July 2020

2004; Van Geen et al. 2004; Stuckey et al. 2015). The adsorbed or incorporated As in the Fe oxy(hydr)oxides is believed to originate from weathering of As-bearing minerals in the source region of the sediments (Zheng et al. 2005; Mukherjee et al. 2014; Xie et al. 2014). Saunders et al. (2005) proposes that intensive weathering of As-bearing bedrocks from the Himalaya in the Holocene epoch increases the As flux into deltas in the South and Southeast of Asia. Already trace or normal concentrations of As in the sediments can induce groundwater As contamination. Therefore, slight differences in the As contents, and more importantly the As speciation, may cause great differences in groundwater As concentration (Guilliot and Charlet 2007; Van Geen et al. 2008; Mukherjee et al. 2014). However, studies about source of As and weathering degrees in different geological settings are insufficient yet.

The depositional environments strongly control the sediment (bio)geochemistry, and thus influence the groundwater As biogeochemical cycling (Dowling et al. 2002; Quicksall et al. 2008; Winkel et al. 2008; McArthur et al. 2011; Wang et al. 2018). In the Mekong Delta, organic carbon and sulfur-enriched sediments formed in a paleo-Mangrove depositional environment after the last glacial maximum (LGM). This type of sediment is seen as an important sink for dissolved As. Here, arsenic is either sequestered by the formation of less mobile organic As or incorporated into pyrite (Wang et al. 2018). In West Bengal, the impermeable paleosol of red clay formed during LGM largely protects the underlying aquifer from vertical recharge of As-rich water or dissolved organic matter (McArthur et al. 2011). Depositional environments can be traced by a combined interpretation of C/N ratios and $\delta^{13}C_{org}$ signatures of organic matter embedded in the sediments (Krishnamurthy et al. 1986; Lamb et al. 2006; Neidhardt et al. 2013; Eiche et al. 2017). Organic matter originating from terrestrial C3 ($\delta^{13}C_{org} \sim -31$ to $-24‰$) and C4 plants ($\delta^{13}C_{org} \sim -16$ to $-12‰$) clearly differs in their $\delta^{13}C_{org}$ signatures but has similar C/N ratios (> 15). The terrestrial material and freshwater organic carbon (POC) can mainly be differentiated by C_{org}/N ratio, which are much lower in the latter case (Fritz and Fontes 1980; Salomons and Mook 1981; Fry and Sherr 1984; Barth et al. 1998). However, systematic research that uses these indicators to better understand the depositional environment in the groundwater As contaminated area is still limited.

The Hetao Basin is a typical arid to semi-arid basin located in the Inner Mongolia (Northern China). The unconfined aquifer (mainly at depths between 10 and 30 m), which is the aquifer used for drinking water supply, is severely affected by dissolved As contamination. Here, more than 70% of groundwater samples exceed 10 μg L^{-1} (Guo et al. 2008; Wen et al. 2013; Cao et al. 2018; Wang et al. 2018). Aquifer sediments deposited in the Late Pleistocene to Holocene are mainly composed of Yellow River bed-load sediments carried from upstream or alluvial/fluvial deposit from the surrounding Lang Mountains, which both can have different weathering intensities (Cai et al. 2019). Furthermore, the aquifer system in the Hetao Basin is influenced by fluvial-alluvial-lacustrine sedimentation dynamics that took place during the Quaternary epoch (Jia et al. 2016; Yang et al. 2018; Cai et al. 2019). The complex sedimentary framework provides ideal opportunities to study the influence of sedimentation history on As accumulation in or release from the sediments.

Based on the assumption that weathering of As-enriched rocks and the depositional environment will influence the sediment As content and speciation, we want to (1) evaluate the sediment provenance and variations in the weathering intensities by analyzing major and trace element compositions in the sediments, (2) attempt to reconstruct the depositional environments based on the combined interpretation of C/N ratio and $\delta^{13}C_{org}$ signatures of organic matter embedded in the sediments, and (3) explore the As and Fe speciation in the sediments by applying sequential extraction experiments. The final aim is to distinguish different sedimentation facies throughout the sediment profiles and their relation to sediments As in the respective depth.

2 Material and methods

2.1 Study area

The Hetao Basin, which covers an area of around 13,000 km^2, is located in the Middle part of the Inner Mongolia (Fig. 1a). It is a Cenozoic fault basin that belongs to the Yinchuan-Hetao rift system. It was formed at the end of the Jurassic epoch (Liu et al. 2016). The Hetao Basin is bordered by the Yellow River in the south, the Lang Mountains in the north, the Ulanbuh Desert in the west, and the Wuliangsu Lake in the east (Fig. 1b). The Lang Mountains, which are part of the Central Asian Orogenic Belt (CAOB), are mainly composed of Archean-Mesoproterozoic metamorphic rocks including gneiss, schist, phyllite, slate, and late Paleozoic igneous rocks such as granite and diorite (Wang et al. 2016).

Paleoclimate change and tectonic movement during the Quaternary epoch strongly influenced the sediment deposition in the Hetao Basin. Sediments thickness in the Northwest of the basin (Hangjinhouqi) is in the range of 7000–8000 m. During the Tertiary epoch, red or brown sediments were formed in a shallow paleo lake. This lake developed into the deep lake until the early Pleistocene (Tang et al. 1996). The Yellow River developed its square bend around the Ordos block in the late Miocene-early Pliocene. It flowed through the North of the basin to the Wuliangsu Lake until the onset of the late Pleistocene. Then, it started to flow out of the basin at the beginning of late Pleistocene. As a consequence, the paleolake started to shrink the size until it completely disappeared (Li et al. 2017; Yang et al. 2018).

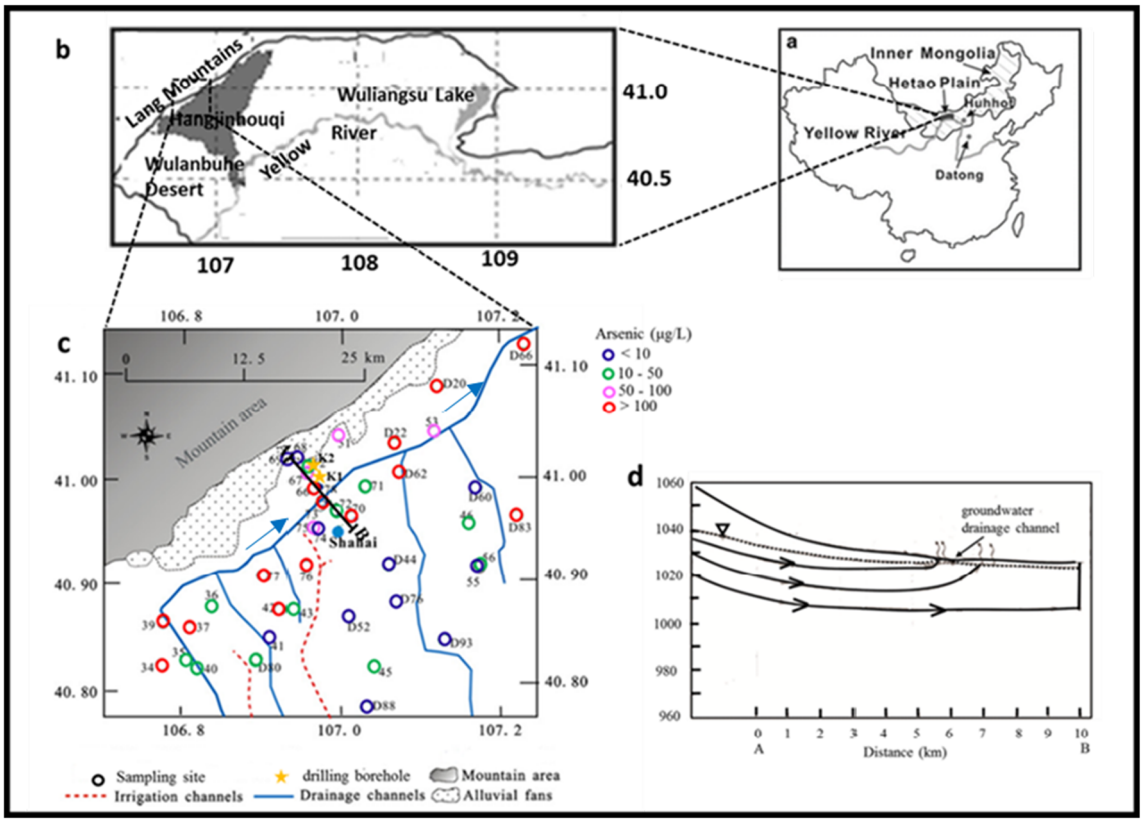

Fig. 1 **a** Location of the Hetao Basin; **b** Hetao Basin with Hangjinhouqi, an often-studied area, marked in gray color. **c** The known distribution of dissolved As in the study area. The groundwater was collected from hand-tube wells at depth between 13 and 100 m; the data was previously published by Guo et al. (2012) and partly by Deng et al. (2009). The location of the two sediment cores (K1 and K2) is marked in the map. **d** Profile A–B showing the groundwater flow direction in the drilling area. The groundwater flow direction was cited from Guo et al. (2011)

Today, the Hetao Basin has a semi-arid to arid climate with annual precipitation of around 200 mm. For detailed hydrogeological information, refer to Zhang et al. (2020). Our study area is located in Shahai (217 km^2), an area with serious groundwater As contamination with As concentration up to 720 μg L^{-1} (Fig. 1c). Groundwater that is high in dissolved As is mainly found at depth between 10 and 30 m (Guo et al. 2008; Cao et al. 2018).

2.2 Sediments collection

Two multilevel wells (K1 and K2) were drilled by the CUGB group using rotary drilling equipment in October 2015. Both sites (K1 and K2) are located in the flat plain area, so similar hydrogeological conditions are assumable (Fig. 1c). At the surface, the cores were split into sections of 10 cm length, capped and placed into N_2 purged Mylar bags to avoid oxidation. Aliquots of the sediment samples were transported to Karlsruhe Institute of Technology (KIT) and kept frozen until further analysis. All sediments characterization was done in the Institute of Applied Geoscience at KIT.

2.3 Major and trace element analysis

Subsamples of the sediments were freeze-dried and homogenized by mechanical grinding. The trace element geochemistry was determined by means of Energy Dispersive X-ray Fluorescence Spectrometry (EDX; Epsilon 5, PANanalytical). The accuracy (better than 10% for all elements) of the method was regularly checked by certified standard materials (SOIL-5, $n = 4$; GXR-6, $n = 4$; GXR-2, $n = 4$; SL-1, $n = 4$). Precision of the repeated standard measurements was better than 5%. The major element geochemistry (K, Na, Si, Ca, Mg, Fe, Mn, P, Al) was analyzed by wavelength dispersive X-ray fluorescence spectrometry (WDX; S4 Explorer, Bruker) using fused beads. The measurement accuracy (within 5%) was checked using the certified standard AGV-1 (USGS) and RGM-1.

Total As content in the sediments was additionally determined by HG-FIAS (hydride generation flow injection atomic absorption spectroscopy) measurements after acid digestion. The results of the HG-FIAS were partly crosschecked by measurements using inductively coupled plasma mass spectrometry (ICP-MS) (X-Series, Thermo

Fisher). Cross-correlation of As concentration determined by HG-FIAS and ICP-MS was $r^2 = 0.99$ (Fig. S1). A detailed description of the acid digestion method is provided in the supplement material. Digestion recovery (100 ± 5%) for As was checked by including the certified standards GXR-5 and RGM-1 into the digestion and measurement procedure. Rare earth elements (REE) including Sc, Y, La, Ce, Pr, Nd, Sm, Eu, Gd, Tb, Dy, Ho, Er, Tm, Yb, Lu, and Th were also measured by ICP-MS after acid digestion. The digestion recovery and measurement accuracy (100 ± 10% for most REE) was checked using the certified standard RGM-1.

The total carbon (TC) content was determined by a carbon/sulfur analyzer (CSA; CS 2000 MultiLine F/SET-3, Eltra). Total organic carbon (TOC) was measured with the same instrument after removing inorganic carbon by repeated addition of HCl (20%, suprapure, Merck) at 60 °C. The total inorganic carbon (TIC) content was calculated by subtracting the carbon content of decarbonized material (TOC) from untreated material (TC). Measurement accuracy (100 ± 2%) was regularly checked by including a steel standard (92400–3050) into the measurement procedure.

2.4 Clay mineralogy

The clay mineralogy was determined using texturized samples by X-ray diffraction (XRD) (Bruker D8, Karlsruhe, Germany). For each selected sample, about 10 g of sediments was treated with 1% HNO_3 (sub-boiled) and ammonia solution in the test tubes. After 15 min in the ultrasonic bath, the samples were left for 3 h until no muddy deposit was visible. Then, the suspensions were pipetted to glass slides using a 1-mL pipette. Three subsamples were produced. One was air-dried, a second was treated with glycol (60 °C for 24 h), and the third one was heated at 550 °C. The XRD pattern was recorded at angles between 2° to 22°. The $CuK_{\alpha 1}$-radiation was used at 40 kV and 25 mA. Minerals were identified using calibrated spectra by the EVA program (Bruker) and the database of PDF 2002.

2.5 Extraction method for Fe and As

A five-step sequential extraction scheme was used to investigate the Fe and As partitioning in the sediments (Table 1). The modified sequential procedure was based on Keon et al. (2001) and Poulton and Canfield (2005). The 0.5 g of fresh sediment was weighed into centrifuge tubes. In each extraction step, the appropriate amount of deoxygenated leaching solution was added. Then the sediment-solution mixture was shaken at 300 rpm at room temperature (Table 1). After centrifugation at 4500 rpm for 15 min, all solutions were filtrated using 0.45 μm cellulose acetate filters (whatman), and acidified if necessary. Arsenic and Fe concentrations in the leachate were measured by ICP-MS (X-Series, Thermo Fisher). The water content of the sediments was determined gravimetrically after freeze-drying.

2.6 Analysis of C/N ratios and $\delta^{13}C_{org}$ signatures

The determination of carbon/nitrogen (C/N) ratios and organic carbon isotope ($\delta^{13}C_{org}$) signature was done in accordance with Neidhardt et al. (2013) and Eiche et al. (2017). Total nitrogen (TN) and carbon content of de-carbonated samples (2% HCl, Suprapure, Merck) was measured with an elemental analyzer (EuroEA3000, EuroVector). The results of C_{org} and TN measurements were used to calculate molar C/N ratios. The measurement accuracy (100 ± 5%) for C and N was checked with the reference standards BBOT (HekaTech) and GBW 07043 (office of CRN′S China).

The $\delta^{13}C_{org}$ signature for de-carbonated samples was measured using an elemental analyzer (EuroEA3000, EuroVector) in continuous flow mode, which was connected to an isotope ratio mass spectrometer in an open split mode (IR-MS, IsoPrime, Fa. GV Instrument, UK). All $\delta^{13}C_{org}$ values of de-carbonated samples were reported relative to the Vienna Pee Dee Belemnite (‰ VPDB). The measurement precision, which was controlled by repeated sample (triplicate) and standard (UREA, $n = 12$; USGS 24, $n = 44$; NBS 18, $n = 12$) measurements, was better than ± 0.1‰. The measurement accuracy (100 ± 5%) was controlled using the standard reference values.

2.7 Calculation method for weathering intensity

The chemical index of alteration (CIA) is used as a proxy to predict the weathering intensities. It was calculated as follows:

$$CIA = Al_2O_3/(Al_2O_3 + Na_2O + K_2O + CaO^*) \times 100$$

(Nesbitt and Young 1982)

where CaO* is CaO hosted in silicates only. The CIA index was calculated empirically by assuming the same mobilization abilities for Na and Ca. The CaO* was assumed to be equivalent to Na_2O if the remaining number of CaO moles (after CaO corrected for phosphate using P_2O_5) is greater than Na_2O (Mclennan 1993). The content of Na_2O was a sum in the sediments including Na content in the soluble salts, the CaO content in the sediments of Hetao Basin was greater than the Na_2O after correcting using P_2O_5, therefore CaO* was assumed to be equivalent to Na_2O.

Table 1 Sequential extraction scheme used for As and Fe leaching

Step	Target phase	Extractant	Conditions	Reference
S1	Ionically bonded and strongly adsorbed	1.0 M NaH_2PO_4	40 mL, 24 h, pH 4–5, one repetition of each time duration, one water wash (40 mL)	[1]
S2	Co-precipitated with acid volatile sulfides, carbonates	1 M CH_3COONa/CH_3COOH	40 mL, 1 h, pH 4.5, one repetition, one water wash (40 mL)	[2]
S3	Co-precipitated with amorphous iron oxides and magnetite	0.2 M ammonium oxalate/0.17 M oxalic acid	40 mL, 2 h, pH 3, dark (wrapped in Al-foil), one repetition, one water wash (40 mL)	[1]
S4	Co-precipitated with crystalline Fe oxides	DCB: 0.5 M Na-Citrate +1 M $NaHCO_3$; 0.5 g $Na_2S_2O_4xH_2O$	35 mL Na-Citrate +2.5 mL $NaHCO_3$ (heating to 85 °C), addition of 0.5 g $Na_2S_2O_4xH_2O$, 15 min at 80 °C, one repetition, one water wash (40 mL)	[1]
S5	Co-precipitated with pyrite and part of sheet silicates	16 M HNO_3	20 ml 16 M HNO_3, 2 h, 25 °C, one repetition, one water wash (40 mL)	[1]

[1] Keon et al. (2001), [2] Poulton and Canfield (2005)

3 Result

3.1 Lithology, mineralogy, and geochemical composition of the sediments

The aquifer sediments that were covered by silty clay or clay layers (K1, 0 ~ 10 m; K2, 0 ~ 14 m) were mainly composed of silt to fine sand. A clay layer at 40 m depth separated the unconfined aquifer from the semi-confined aquifer (Fig. 2). The major minerals in the sediments of study area included quartz and feldspar, with minor contributions from carbonates including calcite and dolomite, mica, and clay minerals (Wang et al. 2019a, b). The clay minerals were mainly composed of chlorite and illite (Fig. S2).

Major element geochemistry was dominated by SiO_2 (ranging from 45.6 to 85.5 wt% with an average value of 66.7 wt%), followed by Al_2O_3 (ranging from 7.9 to 17.6 wt% with an average value of 11.2 wt%) and CaO (ranging from 1.6 to 7.2 wt% with an average value of 3.7 wt%). The average Fe_2O_3 and MnO content was 3.7% and 0.06%, respectively. Discriminant function analysis of major elements showed that sediments were plotted in the quartz sedimentary and felsic igneous region (Fig. 3).

The As content in the sediments ranged from 4.7 to 40.3 mg kg^{-1} with an average value of 11.2 mg kg^{-1} (except for peat layers) (Table 2). Cluster analysis showed that As was grouped together with major elements including Fe, Mn, Mg, Al, and trace elements including Pb, Zn, Cu, and Ni (Euclidean distance ≤ 5) (Fig. 4). The REE composition of the sediments was summarized in the Table 3. It showed enrichment of the light rare earth elements ($(La/Yb)_{chondrite}$ = 9.6). A significant Eu anomaly (δEu = 0.70) was visible in comparison with chondrite.

The investigated sediments were depleted in Na and enriched Ca compared with the upper continental crust (UCC). Trace element concentrations including Rb, Pb, Mo, and As were higher in the investigated sediments compared to the UCC composition. The As enrichment ranged from 0.98 times to 8.4 times the UCC value with an average of 2.3 (Fig. 5a). In comparison with the UCC, the REE content showed a flat distribution pattern with a slightly depleted abundance (Fig. 5b).

3.2 Proxies of sediment weathering and deposition

The CIA was applied to understand variation of mineral weathering intensities along the depth profile (Fig. 2).

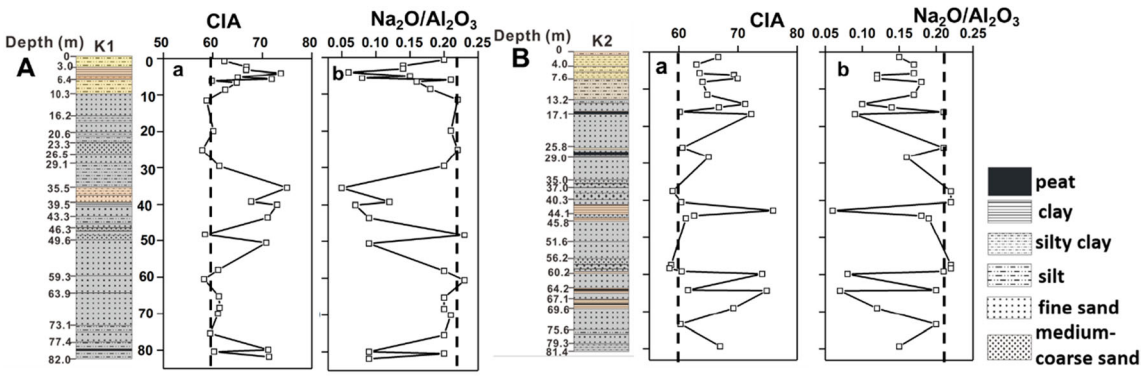

Fig. 2 Chemical index of alteration (CIA) (a) and Na_2O/Al_2O_3 ratio (b) in the depth profiles of K1 (**a**) and K2 (**b**)

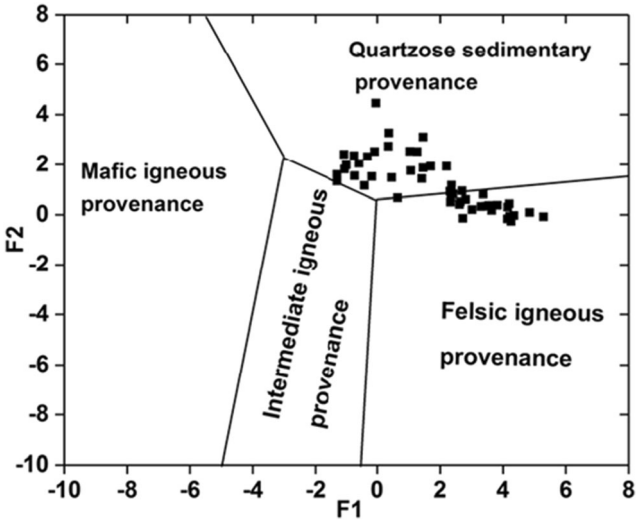

Fig. 3 Discrimination diagram for sedimentary provenance. F1 = 30.638 TiO_2/Al_2O_3–12.541 $Fe_2O_{3(Total)}/Al_2O_3$ + 7.329 MgO/Al_2O_3 + 12.031 Na_2O/Al_2O_3 + 35.402 K_2O/Al_2O_3–6.382, F2 = 56.5 TiO_2/Al_2O_3–10.897 $Fe_2O_{3(Total)}/Al_2O_3$ + 30.875 MgO/Al_2O_3–5.404 Na_2O/Al_2O_3 + 11.112 K_2O/Al_2O_3–3.89. The discrimination analysis is cited from Roser and Korsch (1988)

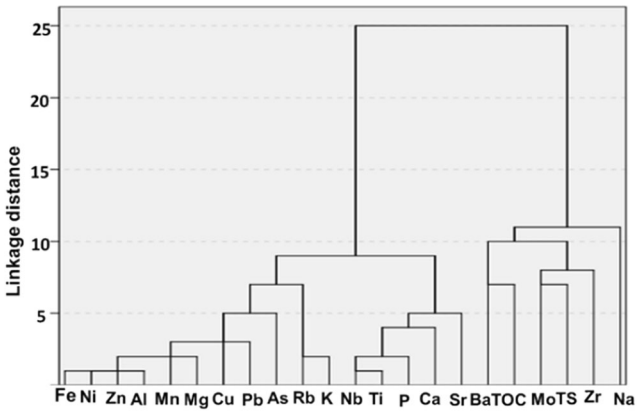

Fig. 4 Dendrogram for 22 variables expressing the statistical distance of different elements in the sediments of K1 and K2 (except peat samples)

Systematic mineral weathering changing from incipient (CIA = 50–60) over intermediate (CIA = 60–80) to extreme (CIA > 80) weathering could be concluded by the CIA (Fedo et al. 1995). The CIA values of the investigated sediments ranged from 58 to 76, indicating incipient to intermediate weathering of the sediments. Ratio of Na_2O/Al_2O_3 showed coherent variations with CIA signatures (Fig. 2), suggesting that sediments were dominated by silicate weathering (e.g., plagioclase) connected to Na^+ removal which was consistent with the Na depletion in comparison to UCC values (Fig. 2). Chemical weathering in the Hetao Basin was controlled by the climate (especially precipitation and temperatures). This is further indicated by the chlorite and illite as the main clay minerals in the sequence, which formation was limited to semi-arid to arid climate (Fig. S2) (Robert and Kennett 1994).

Higher CIA values were obtained in the top silty clay and clay layers of K1 and K2 (depth less than ~ 10 m in K1 and ~ 14 m in K2) with an average value of 66 (Fig. 2). Stronger weathering intensities could be related to the warm and humid climate in the Holocene (Lambeck et al. 2014) when sediment age at a depth of 6 m (~ 8 ka) and 9 m (~ 12 ka) from previous studies was taken into account (Guo et al. 2011; Liu et al. 2014) (Table S1). The unconfined aquifer sediments lying between ~ 10 m- ~ 30 m showed slightly lower weathering intensities (average CIA = 60). This could be the result of cold climate conditions during the LGM from ~ 10 to ~30 ka assuming that the deposition rate was 1 m ka^{-1}. The peat layers formed at depth of 16.7 m and 28.4 m could be related to buried plant material, which was deposited during LGM induced by paleolake regression (Fig. 2). Sediments from a depth of ~ 30 m to ~ 75 m in K1 and K2 were composed of a mixture of fine-medium/coarse sand with interbedded clay layers (average CIA = 64). Hydraulic sorting could cause the poorly sorted grain sizes, which was influenced by bursting and flooding of the Yellow River-connected paleolake (Jia et al. 2016; Yang et al. 2018; Cai et al. 2019).

Table 2 Major and trace element geochemical composition of sediments from K1 and K2 (except peat sediments) in the Hetao Basin

Element	SiO_2 (wt%)	K_2O (wt%)	Na_2O (wt%)	Al_2O_3 (wt%)	CaO (wt%)	MgO (wt%)	P_2O_5 (%)	Fe_2O_3 (wt%)	MnO (wt%)	TiO_2 (wt%)	Nb (mg kg^{-1})	As (mg kg^{-1})
Min	45.6	1.76	0.92	7.88	2.18	0.74	0.05	1.61	0.02	0.19	5	4.7
Max	85.5	3.56	2.35	17.60	9.39	3.87	0.19	7.15	0.12	0.66	15	40.3
Average	65.7	2.42	1.66	11.2	5.34	1.85	0.10	3.72	0.06	0.43	9	11.2
Element	Zr (mg kg^{-1})	Pb (mg kg^{-1})	Mo (mg kg^{-1})	Sr (mg kg^{-1})	Ni (mg kg^{-1})	Zn (mg kg^{-1})	Cu (mg kg^{-1})	Rb (mg kg^{-1})	Ba (mg kg^{-1})	TOC (wt%)	TS (wt%)	
Min	74	15	0.6	155	10	26	15	68	387	0.045	0.009	
Max	227	37	6.4	428	47	107	45	177	692	0.896	0.544	
Average	137	23	1.4	222	25	57	27	108	472	0.224	0.040	

Table 3 Rare earth elements (REE) concentrations (mg kg^{-1}) in the sediments of K1 and K2 from the Hetao Basin

Element	La	Ce	Pr	Nd	Sm	Eu	Gd	Tb	Dy	Y	Ho	Er	Tm	Yb	Lu	La_N/Yb_N
Min	11.1	21.4	2.6	9.5	1.8	0.5	1.6	0.3	1.5	8.7	0.3	0.9	0.1	0.9	0.1	8.3
Max	33.7	80.5	8.1	29.9	5.7	1.2	4.9	0.8	4.4	26.9	0.9	2.6	0.4	2.5	0.4	11.9
Average	22.6	46.9	5.3	19.6	3.8	0.8	3.2	0.5	2.9	17.1	0.6	1.7	0.2	1.6	0.2	9.6

3.3 Characteristics of organic matter in the sediments

The TOC content in the near surface clay or silty clay layers (TOC, 0.11–0.60 wt% in K1; 0.08–0.90 wt% in K2) was higher compared to the aquifer sediments below. The $\delta^{13}C_{org}$ values showed an increasing trend towards the surface in these layers (ranging from − 24.73 to −23.53 ‰ in K1 and − 25.96 to −23.11‰ in K2) (Fig. 6c). Aquifer sediments had a relatively low organic matter with content around 0.05 wt%, the $\delta^{13}C_{org}$ values ranged between − 27 and −24‰. The C/N ratios in the analyzed samples of both sediment profiles had a relatively narrow range between ~ 4 and ~ 10 (Figs. 6a and 7).

Slightly depleted $\delta^{13}C_{org}$ values were measured in the unconfined aquifer in the depth range of ~ 10 m to ~ 30 m (average, − 26.1‰) compared to sediments from depths ~ 40 m to ~ 75 m (average, − 24.9‰). The highest TOC content (9.5 wt%) was accompanied by the highest C/N ratio (up to 32) in the peat layer at a depth of 28.4 m. The $\delta^{13}C_{org}$ values in peat layers from different depths varied from − 26 to −18‰ (Fig. 6c).

3.4 Arsenic and Fe in the sequential sediment extractions

The extractable As in the sediments mainly included strongly adsorbed As (PO_4^{2-}-extractable) and As associated with Fe oxy(hydr)oxides (sum of $C_2O_4^{2-}$-extractable and DCB-extractable) (Table 4). The clay sediments had much higher contents of strongly adsorbed As (8.3 mg kg^{-1} on average) and Fe oxy(hydr)oxides associated As (8.9 mg kg^{-1}) compared to aquifer sand/silt (strongly-adsorbed As, 2.0 mg kg^{-1}, As associated with Fe oxy(hydr)oxides: 2.8 mg kg^{-1}). The releasable As and Fe was calculated as its sum in S1 to S4 since pyrite and phyllosilicate-incorporated As were relatively stable at anoxic conditions (Stuckey et al. 2015). The releasable As content, especially the strongly adsorbed As, was slightly higher in the unconfined aquifer sediments (depth, ~ 10 m to ~ 30 m; average 5.4 mg kg^{-1}) than in semi-confined aquifer sediments (depth, ~ 40 m to ~ 75 m; average 3.6 mg kg^{-1}). In contrast, the releasable Fe was slightly lower in the unconfined aquifer sediments, on average (average 4000 mg kg^{-1} in the unconfined aquifer and 4500 mg kg^{-1} in the semi-confined aquifer). Extractable As content had the highest concentration in the peat layers with up to 250 mg kg^{-1} and 140 mg kg^{-1}, respectively (Fig. 6d). In both sediment profiles (K1 and K2), the ratio of releasable As/Fe ratio (mmol mol^{-1}) increased towards to the surface (ranging from ~ 0.5 to ~ 1.5) (Fig. 6e).

4 Discussion

4.1 Sediments and arsenic provenance

Sediments in the Hetao Basin have a higher average As content (11 mg kg^{-1}) in comparison with sediments from other river deltas in South and Southeast of Asia including the Ganges-Brahmaputra-Meghna delta, the Mekong delta, and the Red River delta that suffer from groundwater As contamination (Smedley and Kinniburgh 2002; Eiche et al. 2008; Neidhardt et al. 2013). This indicates that the As-bearing sediments in the Hetao Basin may have a different provenance

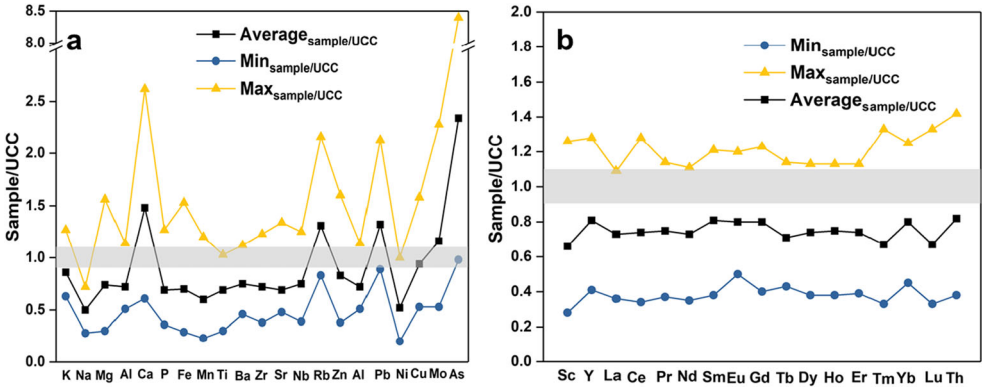

Fig. 5 Major and trace elements (**a**) as well as rare earth elements (REE) (**b**) in the sediments from K1 and K2 normalized to the mean concentration in the upper continental crust (UCC). The UCC value of each element was obtained from Rudnick and Gao (2003)

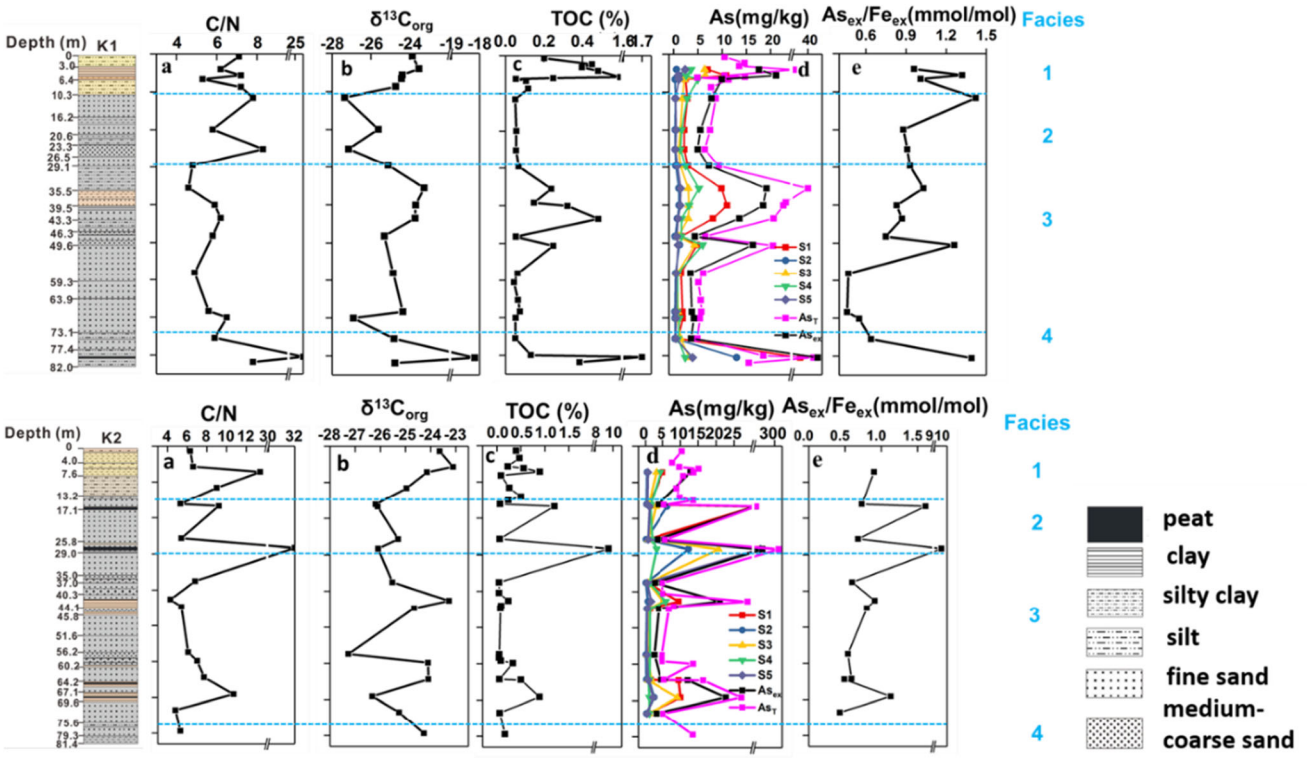

Fig. 6 Depth related variation of the C_{org}/N ratio (**a**), $\delta^{13}C_{org}$ signature (**b**), TOC content (**c**), extractable As content in each sequential extraction step and the sum of As extracted in S1 to S4 (**d**), as well as As_{ex}/Fe_{ex} ratio (mmol mol^{-1}) (**e**) in selected samples. Lithology colors are displayed according to the visualized color in field. For more details on extraction chemicals and extractable phases in S1–S5 please refer to Table 1

compared to the other mentioned river deltas. Sediments provenance can be traced, amongst others, by REE pattern due to their strong resistance to geological processes including weathering, transport and sorting (André et al. 1986; Roddaz et al. 2006; Hofer et al. 2013). The small range of La/$Yb_{chondrite}$(8.3–11.9) indicates that sediments of different depths originate from similar source rocks. Discriminant function analysis of major element geochemistry is independent of grain sizes (Roser and Korsch 1988). In our case, it shows that sediments in the Hetao Basin are mainly of felsic igneous origin and experienced different sedimentary reworking.

The sediments have a similar REE content to gneiss and granite rocks from the Lang Mountains. More precise, the range of La/$Yb_{chondrite}$ with depleted Eu anomaly in comparison with chondrite is similar (Wang et al. 2016). However, bed-load sediments from the Yellow River have, on average, a

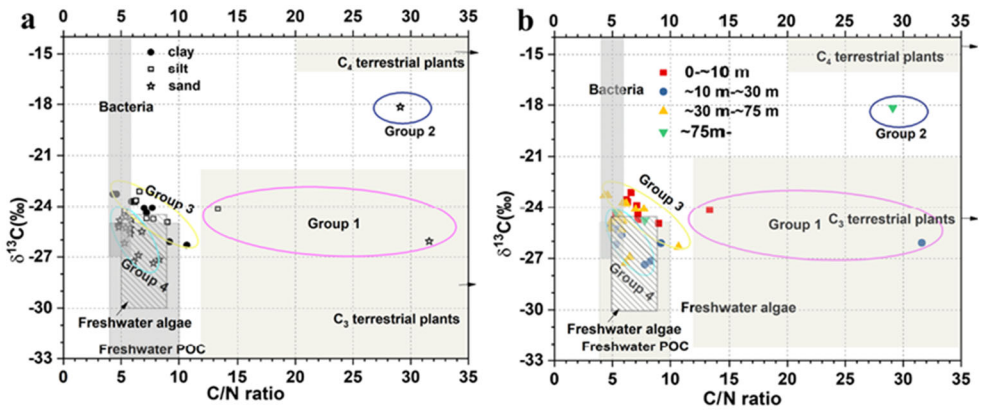

Fig. 7 Grouping of sediment samples based on $\delta^{13}C_{org}$ signatures and C_{org}/N ratios. In group 1, C3 terrestrial plants are the main organic matter source. Organic matter in group 2 gets contributions from C3 plants and C4 plants. Group 3 sediments have mixtures of freshwater POC and C3 terrestrial plants. Group 4 indicates freshwater POC as major organic matter component in the sediment. The predominance fields of different sources of organic carbon are based on Lamb et al. (2006). **a** Samples from K1 and K2 boreholes are grouped according to lithologies. **b** Samples from K1 and K2 boreholes are grouped according to depths

Table 4 Extractable As and Fe contents in each sequestration step (except peat layers)

Extraction phases	sand/silt ($n = 18$) (average ± SD)		Silty clay/clay ($n = 7$) (average ± SD)	
	As (mg kg^{-1})	Fe (wt%)	As (mg kg^{-1})	Fe (wt%)
S1 (strongly adsorbed)	2.0 ± 1.8	0.046 ± 0.009	8.3 ± 2.7	0.038 ± 0.0102
S2 (volatile sulfides, carbonates-precipitated)	0.3 ± 0.2	0.037 ± 0.019	0.9 ± 0.3	0.007 ± 0.002
S3 (amorphous iron oxides and magnetite-precipitated)	1.2 ± 0.6	0.202 ± 0.155	4.5 ± 1.5	0.583 ± 0.228
S4 (crystalline Fe oxides-precipitated)	1.6 ± 0.6	0.186 ± 0.041	4.4 ± 1.4	0.413 ± 0.135
S5 (pyrite and part of sheet silicates-precipitated)	0.6 ± 0.2	0.123 ± 0.056	1.3 ± 0.6	0.436 ± 0.139
Total extractable content	5.7	0.594	18.1	1.477
Total sediments content	7.3	2.470	23.7	6.485

higher REE content and middle earth element (MREE) enrichment in comparison with UCC (Yang et al. 2002). Therefore, the sediments from Hetao Basin originate most likely from the Lang Mountains. Total As contents in gneiss and granite from the Lang Mountains range from 9.0 to 33 mg kg^{-1}. Arsenic is mainly incorporated in Fe-containing minerals such as biotite and pyrite (Guo et al. 2016a; Liu et al. 2016). The indications here are consistent with previous suggestions that most groundwater As-enriched areas in or near sediment basins can be adjacent to orogenic belts with rocks containing As-enriched minerals (Mukherjee et al. 2008; Nordstrom 2009). Weathering of As-containing minerals from the Lang Mountains transfers As into Fe oxy(hydr)oxides or Mn oxides and clay minerals in the sediments. This is indicated by the clustering of As and major elements like Fe, Mn, Mg, Al, and trace elements Ni, Zn, Cu, and Pb. Iron and Mn are the major components of Fe oxy(hydr)oxides and Mn oxides, the Mg and Al of chlorite and illite. Furthermore, trace elements including Ni, Zn, Cu, and Pb can be incorporated into Fe oxy(hydr)oxides or clay minerals (Fakhreddine et al. 2015).

4.2 Depositional environment of the sediments

The origin of organic carbon in the sediments of the Hetao Basin can be deduced based on the associations between C/N ratio and $\delta^{13}C_{org}$ values of embedded organic matter (Lamb et al. 2006) (Fig. 7). In total, four different groups were distinguishable (Fig. 7). In general, organic matter embedded in the aquifer sediments results from freshwater particular organic matter (POC) or algae, indicating the aquatic deposit environment (Fig. 7a). Organic matter embedded in the depth interval from ~ 10 to ~30 m was plotted in the algae or POC region (except peat layers), indicating sole aquatic origin (Fig. 7b). The decrease in the C/N ratio with depths could be related to microbial decomposition, as microbes oxidize organic carbon to inorganic CO_2. In this form, carbon can leave the aquifer (Meyers and Benson 1988). Slightly enriched $\delta^{13}C_{org}$ values in the sediments at ~30 m - ~75 m depth can be related to the terrestrial input from C3 plants, which were deposited by the paleo Yellow River during flooding period (Fig. 7b). This is consistent with the poor sorting of the grain sizes in these sediments. Sediment samples from surface or interbedded clay layers mostly plot in the group 3 (Fig. 7b), suggesting a considerable influence from terrestrial C3 plant input. These findings go in line with previous studies in the Red River and Mekong River delta (Eiche et al. 2017; Magnone et al. 2017). The increasing $\delta^{13}C_{org}$ signatures towards the surface in the top silty clay or clay layers can be related to C4 plant debris input, as maize is the main C4 crop in the Hetao Basin nowadays.

Peat layers embedded in the sediments are dominated by terrestrial input (group 1 and group 2) (Fig. 7a). Peat bands at a depth of 16.7 m and 28.4 m in core K2 developed as response to the paleolake regression during LGM. The temporary lowering of the water table of local paleolakes in the LGM period allowed plant growth followed by burial within the sediments. Previous studies confirm that the peat layers with visually dark color are widely distributed at depth between 15 m and 30 m in the Hetao Basin (Deng 2008; Deng et al. 2011; Guo et al. 2016a, b). Pollen analysis of sediments deposited during the late Pleistocene also revealed that marsh areas developed locally resulting from lake level drop (Cai et al. 2019). While the peat layer in the unconfined aquifer at a depth of 28.4 m is influenced from C3 terrestrial input, the peat layer at a depth of 80.4 m is mainly composed of C4 terrestrial input. The change of vegetation type could be caused by climate change (Cai et al. 2019). It further indicates that the depositional environment of sediments at around 80 m is different compared to the sediments above.

4.3 Facies interpretation and implications for As mobilization to the aquifer

Based on similarities and differences in weathering intensities, geochemical composition, and depositional environment, the sediment profiles can be subdivided into four facies (Fig. 6).

4.3.1 Facies 1

The surface and near surface sediments (0 ~10 m) are mainly composed of silty clay and clay. Stronger weathering intensities during the Holocene lead to a higher proportion of As that is adsorbed onto or incorporated into Fe oxy(hydr)oxides and clay minerals, consistent with higher As contents in the surface sediments (Fig. 6d). The oxic conditions in the surface sediments largely protect Fe oxy(hydr)oxides from reduction and thus strongly minimize the As release into porewater/groundwater. However, fluctuations in the groundwater table resulting from anthropogenic perturbations or seasonal fluctuations in the Hetao Basin (Guo et al. 2013) could cause frequent flooding of the surface sediments. As a consequence, occasional reduction of Fe oxy(hydr)oxides caused by a decreased redox potential may cause As release into porewater/groundwater, as indicated in other area such as Mekong Delta (Guo et al. 2013; Van Geen et al. 2013; Stuckey et al. 2015; Xiu et al. 2020).

4.3.2 Facies 2

Sediments in the depth interval from ~ 10 to ~30 m were most likely formed during the LGM period with reduced chemical weathering intensities. The higher amount of releasable As, especially of strongly adsorbed As, in this facies compared to underlying sediments suggests that adsorption-desorption processes are important for controlling As concentrations in the groundwater (Radloff et al. 2011; Richards et al. 2019) (Fig. 6c). This goes in line with the generally higher groundwater As concentration (70% of groundwater with As higher than 10 μg L^{-1}) in the unconfined aquifer in this depth interval (Guo et al. 2008; Cao et al. 2018).

Organic matter embedded in this facies mainly results from in situ paleolake algae or POC (Fig. 7b). The in situ produced organic matter is more labile and thus more easily decomposed by microbes compared to terrestrial plant material (Nguyen et al. 2005). Microcosm experiments as well as groundwater microbial community studies suggested that microbial reduction of Fe oxy(hydr)oxides and As(V) species cause As to desorb from sediments into groundwater (Li et al. 2014; Guo et al. 2015; Stolze et al. 2019; Xiu et al. 2020). Therefore, the reactive organic carbon and peat produced within paleolakes provide an easily available electron source for microbial reduction of Fe oxy(hydr)oxides (McArthur et al. 2001; Fendorf et al. 2010; Guo et al. 2019). This is consistent with the higher Fe^{2+} concentration in the groundwater that is high in dissolved As (Zhang et al. 2020; Qiao et al. 2020).

4.3.3 Facies 3 and Facies 4

Sediments in a depth from ~ 30 to ~ 75 m are strongly influenced by fluvial deposition as indicated by the poor sorting of the grain sizes. The slightly higher content of releasable Fe can be related to the stronger weathering, which increases the release of Fe from Fe-containing silicates such as biotite. The released Fe can be reprecipitated as Fe oxy(hydr)oxides, therefore increasing the releasable Fe content. The formation of Fe oxy(hydr)oxides can incorporate As or provide As adsorption sites which further retards the As release into groundwater.

The interpretation of facies 4 is constrained by the limited number of samples and the unknown thickness of the layer. These sediments both from K1 and K2 are composed of silt or silty clay. Previous studies showed that a deep paleolake that was connected to the Yellow river existed in Hetao Basin between ~ 60 and ~ 54 ka (Chen et al. 2008; Yang et al. 2018). Sediments of the area have an age of 55.4 ± 2.4 ka at a depth of 76 m (Liu et al. 2014) (Table S1). Thus, facies 4 would fit to the typical paleolake sedimentation environment. The fine-grained sediments have to be considered as aquitard, and only limited wells in the Hetao Basin are target to this depth. Consequently, no significant influence on the dissolved As concentration in groundwater can be expected from this facies. Still, further drilling is necessary to better characterize this facies.

5 Conclusion

The As content in sediments from the Hetao Basin ranges from ~ 5 to ~ 280 mg kg^{-1} with highest As contents in the peat layers. The REE pattern in the sediments indicates a possible origin sediment material from the Lang Mountains. Incipient to intermediate weathering of As-bearing rocks causes the As release from the Lang Mountains and its accumulation in the Hetao Basin sediments. More than 70% of As is PO_4^{3-}-displaceable or released by Fe oxy(hydr)oxides reduction indicates its high potential mobility. Ratios of C_{org}/N combined with $\delta^{13}C_{org}$ signatures show that organic matter that is embedded in the sediments was mainly produced in fresh water environments.

Four sediment facies can be distinguished. Sediments from a depth of ~ 30 m to ~ 75 m are significantly influenced by the fluvial deposition. Arsenic is less releasable in this facies. The sediments at depth of ~ 10 to ~ 30 m is believed to be deposited during LGM where paleolakes regressed. Less reactive Fe phases with a higher content of releasable As presents in this facies. The higher content of potentially mobile As may explain the generally higher groundwater As concentration in this unconfined aquifer. Furthermore, reactive organic matter produced within the paleolake that makes up sediments of the unconfined aquifer probably simulates the reduction of Fe oxy(hydr)oxides and As(V) species, therefore increasing groundwater As concentration.

Acknowledgments The authors give special thanks to students from China University of Geoscience (Beijing) for recording sediments properties in the field. We are also grateful for the measurements from N. Gill, G. Preuß, M. Kull, C. Mössner, and B. Oetzel from Karlsruhe Institute of Technology. We give thanks to the Graduate school for Climate and Environment (GRACE) in Karlsruhe Institute of Technology. Ms. Hongyan Wang is founded by China Scholarship Council. Furthermore, the authors are grateful for the constructive suggestions from editor Philip N. Owens and two reviewers.

Funding Information Open Access funding provided by Projekt DEAL.

Compliance with ethical standards

Conflict of interest The authors declare that they have no conflict of interest.

Research involving human participants and/or animals Human participants and animals are not involved in the research

Open Access This article is licensed under a Creative Commons Attribution 4.0 International License, which permits use, sharing, adaptation, distribution and reproduction in any medium or format, as long as you give appropriate credit to the original author(s) and the source, provide a link to the Creative Commons licence, and indicate if changes were made. The images or other third party material in this article are included in the article's Creative Commons licence, unless indicated otherwise in a credit line to the material. If material is not included in the article's Creative Commons licence and your intended use is not permitted by statutory regulation or exceeds the permitted use, you will need to obtain permission directly from the copyright holder. To view a copy of this licence, visit http://creativecommons.org/licenses/by/4.0/.

References

André L, Deutsch S, Hertogen J (1986) Trace-element and Nd isotopes in shales as indexes of provenance and crustal growth: the early Paleozoic from the Brabant Massif (Belgium). Chem Geol 57(1–2):101–115

Barth JA, Veizer J, Mayer B (1998) Origin of particulate organic carbon in the upper St. Lawrence: isotopic constraints. Earth Planet Sci Lett 162(1–4):111–121

Cai MT, Ye P, Yang X, Li C (2019) Vegetation and climate change in the Hetao Basin (northern China) during the last interglacial-glacial cycle. J Asian Earth Sci 171:1–8

Cao W, Guo HM, Zhang Y, Ma R, Li Y, Dong Q, Li Y, Zhao R (2018) Controls of paleochannels on groundwater arsenic distribution in shallow aquifers of alluvial plain in the Hetao Basin, China. Sci Total Environ 613:958–968

Chen FH, Fan YX, Chun X, Madsen DB, Oviatt CG, Zhao H, Yang LP, Sun Y (2008) Preliminary research on Megalake Jilantai-Hetao in the arid areas of China during the late quaternary. Chin Sci Bull 53:1725–1739

Deng Y (2008) Geochemical process of high arsenic groundwater system at western Hetao Basin. Dissertation China University of Geoscience

Deng Y, Wang Y, Ma T (2009) Isotope and minor element geochemistry of high arsenic groundwater from Hangjinhouqi, the Hetao Plain, Inner Mongolia. Appl Geochem 24(4):587–599

Deng YM, Wang Y, Ma T, Yang H, He J (2011) Arsenic associations in sediments from shallow aquifers of northwestern Hetao Basin, Inner Mongolia. Environ Earth Sci 64(8):2001–2011

Dowling CB, Poreda J, Basu AR, Peters SL, Aggarwal PK (2002) Geochemical study of arsenic release mechanisms in the Bengal Basin groundwater. Water Resour Res 38(9):1–12

Eiche E, Neumann T, Berg M, Weinman B, van Geen A, Norra S, Berner Z, Thi Kim Trang P, Hung Viet P, Stüben D (2008) Geochemical processes underlying a sharp contrast in groundwater arsenic concentrations in a village on the Red River delta, Vietnam. Appl Geochem 23(11):3143–3154

Eiche E, Berg M, Hönig SM, Neumann T, Lan VM, Pham TKT, Pham HV (2017) Origin and availability of organic matter leading to arsenic mobilisation in aquifers of the Red River Delta, Vietnam. Appl Geochem 77:184–193

Fakhreddine S, Dittmar J, Phipps D, Dadakis J, Fendorf S (2015) Geochemical Triggers of Arsenic Mobilization during Managed Aquifer Recharge. Environ Sci Technol 49(13):7802–7809

Fedo CM, Wayne Nesbitt H, Young GM (1995) Unraveling the effects of potassium metasomatism in sedimentary rocks and paleosols, with implications for paleo weathering conditions and provenance. Geol 23(10):921–924

Fendorf S, Michael HA, Van Geen A (2010) Spatial and temporal variations of groundwater arsenic in. South Southeast Asia Sci 328(5982):1123–1127

Fritz P, Fontes JC (1980) Handbook of environmental isotope geochemistry. In: Deines P (ed) The isotopic composition of reduced carbon. Elsevier, Amsterdam, pp 329–406

Fry B, Sherr EB (1984) $\delta^{13}C$ measurements as indicators of carbon flow in marine and freshwater ecosystems. Contrib Mar Sci 27:13–47

Guilliot S, Charlet L (2007) Bengal arsenic, an archive of Himalaya orogency and paleohydrology. J Environ Sci Health A 42:1785–1794

Guo H, Yang S, Tang X, Li Y, Shen Z (2008) Groundwater geochemistry and its implications for arsenic mobilization in shallow aquifers of the Hetao Basin, Inner Mongolia. Sci Total Environ 393(1):131–144

Guo H, Zhang B, Li Y, Berner Z, Tang X, Norra S, Stüben D (2011) Hydrogeological and biogeochemical constrains of arsenic mobilization in shallow aquifers from the Hetao basin, Inner Mongolia. Environ Pollut 159(4):876–883

Guo HM, Zhang Y, Xing L, Jia YF (2012) Spatial variation in arsenic and fluoride concentrations of shallow groundwater from the town of Shahai in the Hetao basin, Inner Mongolia. Appl Geochem 27(11):2187–2196

Guo HM, Liu C, Lu H, Wanty RB, Wang J, Zhou YZ (2013) Pathways of coupled arsenic and iron cycling in high arsenic groundwater of the Hetao basin, Inner Mongolia, China: an iron isotope approach. Geochim Cosmochim Acta 112:130–145

Guo HM, Liu ZY,Ding SS, Hao CB, Xiu W, Hou WG (2015) Arsenate reduction and mobilization in the presence of indigenous aerobic bacteria obtained from high arsenic aquifers of the Hetao basin, Inner Mongolia. Environmental Pollution 203:50–59

Guo HM, Jia Y, Wanty RB, Jiang Y, Zhao W, Xiu W, Shen J, Li Y, Cao Y, Wu Y, Zhang D, Wei C, Zhang Y, Cao W, Foster A (2016a) Contrasting distributions of groundwater arsenic and uranium in the western Hetao basin, Inner Mongolia: implication for origins and fate controls. Sci Total Environ 541:1172–1190

Guo HM, Zhou Y, Jia Y, Tang X, Li X, Shen M, Lu H, Han S, Wei C, Norra S, Zhang F (2016b) Sulfur cycling-related biogeochemical processes of arsenic mobilization in the western Hetao Basin, China: evidence from multiple isotope approaches. Environ Sci Technol 50(23):12650–12659

Guo HM, Zhang D, Ni P, Cao Y, Li F, Jia Y, Li H, Wan L, Wang G (2017) On the scalability of hydrogeochemical factors controlling arsenic mobility in three major inland basins of PR China. Appl Geochem 77:15–23

Guo HM, Li X, Xiu W, He W, Cao Y, Zhang D, Wang A (2019) Controls of organic matter bioreactivity on arsenic mobility in shallow aquifers of the Hetao Basin, PR China. J Hydrol 571:448–459
Hofer G, Wagreich M, Neuhuber S (2013) Geochemistry of fine-grained sediments of the upper Cretaceous to Paleogene Gosau Group (Austria, Slovakia): implications for paleoenvironmental and provenance studies. Earth Sci Front 4(4):449–468
Islam FS, Gault AG, Boothman C, Polya DA, Charnock JM, Chatterjee D, Lloyd JR (2004) Role of metal-reducing bacteria in arsenic release from Bengal delta sediments. Nature 430:68–71
Jia L, Zhang X, Ye P, Zhao X, He Z, He X, Zhou Q, Li J, Ye M, Wang Z, Meng J (2016) Development of the alluvial and lacustrine terraces on the northern margin of the Hetao Basin, Inner Mongolia, China: implications for the evolution of the Yellow River in the Hetao area since the late Pleistocene. Geomorphology 263:87–98
Keon NE, Swartz CH, Brabander DJ, Harvey C, Hemond HF (2001) Validation of an arsenic sequential extraction method for evaluating mobility in sediments. Environ Sci Technol 35(13):2778–2784
Krishnamurthy RV, Bhattacharya SK, Kusumgar S (1986) Palaeoclimatic changes deduced from 13C/12C and C/N ratios of Karewa lake sediments, India. Nature 323(6084):150–152
Lamb AL, Wilson GP, Leng MJ (2006) A review of coastal palaeoclimate and relative sea-level reconstructions using δ13C and C/N ratios in organic material. Earth-Sci Rev 75(1–4):29–57
Lambeck K, Rouby H, Purcell A, Sun Y, Sambridge M (2014) Sea level and global ice volumes from the Last Glacial Maximum to the Holocene. Proc Natl Acad Sci 111(43):15296–15303
Li Y, Guo HM, Hao C (2014) Arsenic release from shallow aquifers of the Hetao basin, Inner Mongolia: evidence from bacterial community in aquifer sediments and groundwater. Ecotoxicol 23(10): 1900–1914
Li B, Sun D, Xu W, Wang F, Liang B, Ma Z, Wang X, Li Z, Chen F (2017) Paleomagnetic chronology and paleoenvironmental records from drill cores from the Hetao Basin and their implications for the formation of the Hobq Desert and the Yellow River. Quat Sci Rev 156:69–89
Liu Z, Zhao H, Wang C, Ji Y, Zhang Y, Liu L, Zhao H, Bi Z, Liu H (2014) OSL ages of sedimentary layers in Linhe Depression since Late Pleistocene. Arid Land Geogr 37(3):439–446 Chinese with English abstract
Liu M, Zhang D, Xiong G, Zhao H, Di Y, Wang Z, Zhou Z (2016) Zircon U–Pb age, Hf isotope and geochemistry of carboniferous intrusions from the Langshan area, Inner Mongolia: Petrogenesis and tectonic implications. J Asian Earth Sci 120:139–158
Magnone D, Richards LA, Polya DA, Bryant C, Jones M, van Dongen BE (2017) Biomarker-indicated extent of oxidation of plant-derived organic carbon (OC) in relation to geomorphology in an arsenic contaminated Holocene aquifer, Cambodia. Sci Rep 7(1):1–12
McArthur JM, Ravenscroft P, Safiulla S, Thirlwall MF (2001) Arsenic in groundwater: testing pollution mechanisms for sedimentary aquifers in Bangladesh. Water Resour Res 37(1):109–117
McArthur JM, Nath B, Banerjee DM, Purohit M, Grassineau N (2011) Palaeosol Control on Groundwater Flow and Pollutant Distribution: The Example of Arsenic. Environ Sci Technol 45(4):1376–1383
McLennan SM (1993) Weathering and global denudation. J Geol 101(2): 295–303
Meyers PA, Benson LV (1988) Sedimentary biomarker and isotopic indicators of the paleoclimatic history of the Walker Lake basin, western Nevada. Org Geochem 13(4–6):807–813
Mukherjee A, Bhattacharya P, Savage K, Foster A, Bundschuh J (2008) Distribution of geogenic arsenic in hydrologic systems: controls and challenges. J Contam Hydrol 99:1–7
Mukherjee A, Verma S, Gupta S, Henke KR, Bhattacharya P (2014) Influence of tectonics, sedimentation and aqueous flow cycles on the origin of global groundwater arsenic: paradigms from three continents. J Hydrol 518:284–299
Neidhardt H, Biswas A, Freikowski D, Majumder S, Chatterjee D, Berner ZA (2013) Reconstructing the sedimentation history of the Bengal Delta Plain by means of geochemical and stable isotopic data. Appl Geochem 36:70–82
Nesbitt H, Young GM (1982) Early Proterozoic climates and plate motions inferred from major element chemistry of lutites. Nature 299(5885):715–717
Nguyen ML, Westerhoff P, Baker L, Hu Q, Esparza-Soto M, Sommerfeld M (2005) Characteristics and reactivity of algae-produced dissolved organic carbon. J Environ Eng (N Y) 131(11):1574–1582
Nickson R, McArthur J, Burgess W, Ahmed KM, Ravenscroft P, Rahman M (1998) Arsenic poisoning of Bangladesh groundwater. Nature 395:338
Nordstrom DK (2002) Worldwide occurrences of arsenic in ground water. Sci 296(5576):2143–2145
Nordstrom DK (2009) Natural arsenic enrichment: effects of diagenetic tectonichydrothermal cycle. Geol Soc Am Abstracts Progr 41(7): 217
Poulton SW, Canfield DE (2005) Development of a sequential extraction procedure for iron: implications for iron partitioning in continentally derived particulates. Chem Geol 214(3–4):209–221
Qiao W, Guo HM, He C, Shi Q, Xiu W, Zhao B (2020) Molecular evidence of arsenic mobility linked to biodegradable organic matter. Environ Sci Technol 54:7280–7290. https://doi.org/10.1021/acs.est.0c00737
Quicksall AN, Bostick BC, Sampson ML (2008) Linking organic matter deposition and iron mineral transformations to groundwater arsenic levels in the Mekong delta, Cambodia. Appl Geochem 23(11): 3088–3098
Radloff KA, Zheng Y, Michael HA, Stute M, Bostick BC, Mihajlov I, Bounds M, Huq MR, Choudhury I, Rahman MW, Schlosser P (2011) Arsenic migration to deep groundwater in Bangladesh influenced by adsorption and water demand. Nat Geosci 4(11):793–798
Ravenscroft P, Brammer H, Richards K (2009) Arsenic pollution: a global synthesis. Wiley-Blackwell, Chichester
Richards LA, Casanueva-Marenco MJ, Magnone D, Sovann C, Dongen BE, Polya DA (2019) Contrasting sorption behaviors affecting groundwater arsenic concentration in Kandal Province, Cambodia. Geosci Front 10:1701–1713
Robert C, Kennett JP (1994) Antarctic subtropical humid episode at the Paleocene-Eocene boundary: clay-mineral evidence. Geology 22(3):211–214
Roddaz M, Viers J, Brusset S, Baby P, Boucayrand C, Hérail G (2006) Controls on weathering and provenance in the Amazonian foreland basin: insights from major and trace element geochemistry of Neogene Amazonian sediments. Chem Geol 226(1–2):31–65
Rodríguez-Lado L, Sun G, Berg M, Zhang Q, Xue H, Zheng Q, Johnson CA (2013) Groundwater arsenic contamination throughout China. Sci 341(6148):866–868
Roser BP, Korsch RJ (1988) Provenance signatures of sandstone-mudstone suites determined using discriminant function analysis of major-element data. Chem Geol 67(1–2):119–139
Rudnick RL, Gao S (2003) The crust. Treatise Geochem 3:1–64
Salomons W, Mook WG (1981) Field observations of the isotopic composition of particulate organic carbon in the south- ern North Sea and adjacent estuaries. Mar Geol 41:11–20
Saunders JA, Lee MK, Uddin A, Mohammad S, Wilkin RT, Fayek M, Korte NE (2005) Natural arsenic contamination of Holocene alluvial aquifers by linked tectonic, weathering, and microbial processes. Geochem Geophys Geosyst 6(4):1–7
Smedley PL, Kinniburgh DG (2002) A review of the source, behaviour and distribution of arsenic in natural waters. Appl Geochem 17(5): 517–568
Stolze L, Zhang D, Guo H, Rolle M (2019) Surface complexation modeling of arsenic mobilization from goethite: interpretation of an in-situ experiment. Geochim Cosmochim Acta 248:274–288

Stuckey JW, Schaefer MV, Benner SG, Fendorf S (2015) Reactivity and speciation of mineral-associated arsenic in seasonal and permanent wetlands of the Mekong Delta. Geochim Cosmochim Acta 171: 143–155

Tang J, Lin NF, Bian JM, Liu WZ, Zhang ZL (1996) Environmental geochemistry of arsenism areas in the Hetao plain, inner Mongolia. Hydrogeol Eng Geol 1:49–54 (In Chinese with English abstract)

Van Geen A, Rose J, Thoral S, Garnier JM, Zheng Y, Bottero JY (2004) Decoupling of As and Fe release to Bangladesh groundwater under reducing conditions. Geochim Cosmochim Acta 68:3475–3468

Van Geen A, Zheng Y, Goodbred S Jr, Horneman A, Aziz Z, Cheng Z, Stute M, Mailloux B, Weinman B, Hoque MA, Seddique A, Hossain M, Chowdhury S, Ahmed K (2008) Flushing history as a hydrogeological control on the regional distribution of arsenic in shallow groundwater of the Bengal Basin. Environ Sci Technol 42(7):2283–2288

Van Geen A, Bostick BC, Trang PTK, Lan VM, Mai NN, Manh PD, Viet PH, Radloff K, Aziz Z, Mey JL, Stahl MO, Harvey CF, Oates P, Weinman B, Stengel C, Frei F, Kipfer R, Berg M (2013) Retardation of arsenic transport through Pleistocene aquifer. Nature 501:204–207

Wang ZZ, Han BF, Feng LX, Liu B, Zheng B, Kong LJ (2016) Tectonic attribution of the Langshan area in western Inner Mongolia and implications for the Neoarchean–Paleoproterozoic evolution of the Western North China Craton: Evidence from LA-ICP-MS zircon U–Pb dating of the Langshan basement. Lithos 261:278–295

Wang Y, Le Pape P, Morin G, Asta MP, King G, Bártová B, Suvorova E, Frutschi M, Ikogou M, Pham V, Vo P, Herman F, Charlet L (2018) Arsenic speciation in Mekong Delta sediments depends on their depositional environment. Environ Sci Technol 52(6):3431–3439

Wang HY, Guo HM, Xiu W, Bauer J, Sun GX, Tang XH, Norra S (2019a) Indications that weathering of evaporite minerals affects groundwater salinity and As mobilization in aquifers of the northwestern Hetao Basin, China. Appl Geochem 109:104416

Wang YH, Pi KF, Fendorf S, Deng YM, Xie XJ (2019b) Sedimentogenesis and hydrobiogeochemistry of high arsenic Late Pleistocene-Holocene aquifer systems. Earth-Sci Rev 189:79–98

Wen D, Zhang F, Zhang E, Wang C, Han S, Zheng Y (2013) Arsenic, fluoride and iodine in groundwater of China. J Geochem Explor 135:1–21

Winkel L, Berg M, Amini M, Hug SJ, Johnson CA (2008) Predicting groundwater arsenic contamination in Southeast Asia from surface parameters. Nat Geosci 1(8):536–542

Xie X, Wang Y, Ellis A, Liu C, Duan M, Li J (2014) Impact of sedimentary provenance and weathering on arsenic distribution in aquifers of the Datong basin, China: constraints from elemental geochemistry. J Hydrol 519:3541–3549

Xiu W, Lloyd J, Guo HM, Dai W, Nixon S, Bassil NM, Ren C, Zhang CR, Ke TT, Polya D (2020) Linking microbial community composition to hydrogeochemistry in the western Hetao Basin: potential importance of ammonium as an electron donor during arsenic mobilization. Environ Int 136:105489

Yang SY, Jung HS, Choi MS, Li CX (2002) The rare earth element compositions of the Changjiang (Yangtze) and Huanghe (Yellow) river sediments. Earth Planet Sci Lett 201(2):407–419

Yang X, Cai M, Ye P, Yang Y, Wu Z, Zhou Q, Li C, Liu X (2018) Late Pleistocene paleolake evolution in the Hetao basin, inner Mongolia, China. Quat Int 464:386–395

Zhang Z, Guo HM, Liu S, Weng HC, Han SB, Gao ZP (2020) Mechanisms of groundwater arsenic variations induced by extraction in the western Hetao Basin, Inner Mongolia, China. J Hydrol 583:124599

Zheng Y, Van Geen A, Stute M, Dhar R, Mo Z, Cheng Z, Horneman A, Gavrieli I, Simpson H, Versteeg R, Steckler M, Grazioli-Venier A, Goodbred S, Shahnewaz M, Shamsudduha M, Hoque M, Ahmed K (2005) Geochemical and hydrogeological contrasts between shallow and deeper aquifers in two villages of Araihazar, Bangladesh: implications for deeper aquifers as drinking water sources. Geochim Cosmochim Acta 69(22):5203–5218

Publisher's note Springer Nature remains neutral with regard to jurisdictional claims in published maps and institutional affiliations.

Supplementary materials

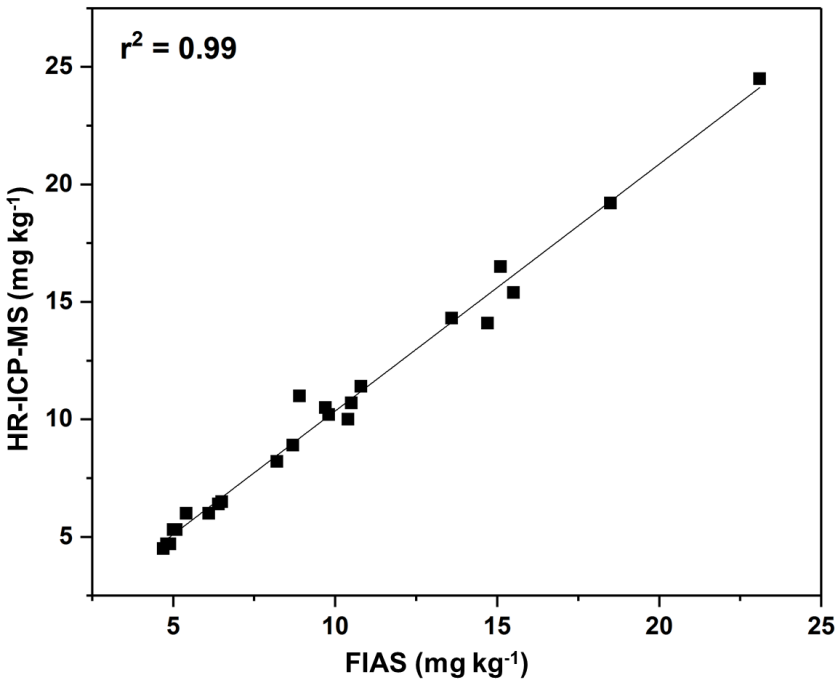

Fig. S1 Cross correlation plot for results from As content after acid digestion measured by ICP-MS and FIAS analysis.

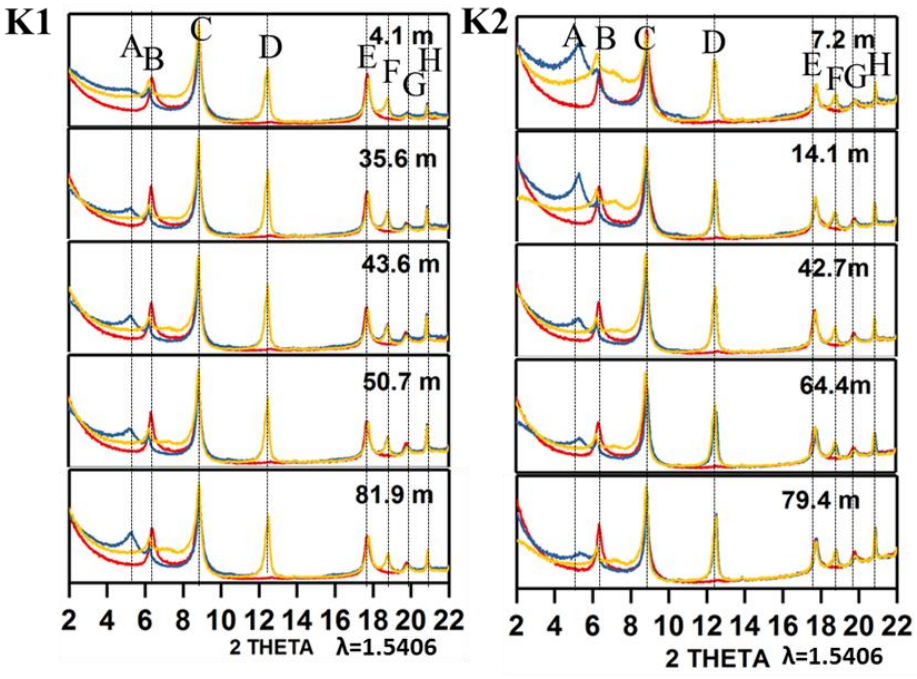

peak	interpretation
A	glycol-solvated smectite
B	chlorite + smectite
C	illite + heat-treated smectite
D	chlorite/kaolinite
E	illite
F	chlorite
G	illite
H	quartz

Fig. S2 Diffractograms and interpretation of orientated clay mineral analysis in the sediments from different depth of K1 and K2.

Acid digestion method used to determine As in the sediment

0.1 g of dried and grinded sample material was weighted into 100 mL Teflon tubes. 0.05 g GXR-5 (Soil, USGS) and RGM-1 (Rhyolite, USGS) were additionally digested as certified references to check for accuracy. Two blank samples were digested at same time as control. Firstly, 1 mL Milli-Q water was added into tubes for avoiding heavy reactions of sediments with acid. Afterwards, 2 ml 65% HNO_3 (subboiled) was added and heated at 80 ℃ for around 10 minutes. Then 1 mL $HClO_4$ (70%, normapure) and 5 mL HF (40%, suprapure) were added into tubes for digesting with cover at 120 ℃ for 18 h. Afterwards, the acid was evaporated until near dryness. Then 2 mL 65% HNO_3 (subboiled) were added and evaporated until dryness. This last step was repeated for 3 times. Finally, 2 mL HNO_3 were added and the final volume was adjusted to 50 mL in flasks using MiliQ-water.

Table S1 The sediment age dating results in the Shahai Town cited from Liu et al. (2014) and Guo et al. (2011)

Area	Depth (m bls)	Age (ka)	Material	Analysis method	Reference
ShaHai	6.1	8.4 ± 0.3	Qz	OSL	Liu et al. (2014)
Town	65.1	52.6 ± 0.8	Qz	OSL	
	76.1	55.4 ± 2.4	Qz	OSL	
	128.1	91.2 ± 3.8	Qz	OSL	
	~9.0	~12.0	sediment	^{14}C	Guo et al. (2011)
	~23.0	~23.0	sediment	^{14}C	

Reference

Liu Z, Zhao H, Wang C, Ji Y, Zhang Y, Liu L, Zhao H, Bi Z, Liu H, (2014) OSL ages of sedimentary layers in Linhe Depression since Late Pleistocene, Arid Land Geography 37(3):439-446. Chinese with English abstract

Guo H, Zhang B, Li Y, Berner Z, Tang X, Norra S, Stüben D (2011) Hydrogeological and biogeochemical constrains of arsenic mobilization in shallow aquifers from the Hetao basin, Inner Mongolia. Environ Pollut 159(4):876-883.

Appendix 2 Indications that weathering of evaporite minerals affects groundwater salinity and As mobilization in aquifers of the northwestern Hetao Basin, China

Applied Geochemistry 109 (2019) 104416

Contents lists available at ScienceDirect

Applied Geochemistry

journal homepage: www.elsevier.com/locate/apgeochem

Indications that weathering of evaporite minerals affects groundwater salinity and As mobilization in aquifers of the northwestern Hetao Basin, China

Hong-Yan Wang[a], Hua-Ming Guo[b,c], Wei Xiu[b,*], Jonas Bauer[a], Guo-Xin Sun[d], Xiao-Hui Tang[a], Stefan Norra[a]

[a] Working Group of Environmental Mineralogy and Environmental System Analysis, Institute of Applied Geosciences, Karlsruhe Institute of Technology (KIT), Adenauerring 20 b, 76131, Karlsruhe, Germany
[b] State Key Laboratory of Biogeology and Environmental Geology, China University of Geosciences, Beijing, 100083, PR China
[c] School of Water Resources and Environment, China University of Geosciences, Beijing, 100083, PR China
[d] State Key Laboratory of Urban and Regional Ecology, Research Center for Eco-Environmental Sciences, The Chinese Academy of Sciences, Beijing, 100085, PR China

ARTICLE INFO

Editorial handling by Prof. M. Kersten

Keywords:
Salinization
Sulphate minerals
pH decrease
Ca^{2+} release
Sulphide
As mobilization

ABSTRACT

Elevated arsenic (As) concentration and salinity (TDS > 1000 mg/L) seriously affect the groundwater quality in the Hetao Basin, China, however, the origin of groundwater salinity and its influence for As mobilization has not been widely studied. In this study, the influence of evaporite minerals weathering on groundwater salinity and As mobilization were investigated by lithological and mineralogical analysis of sediments from two boreholes in combination with groundwater hydrogeochemical characteristics analysis in the northwestern Hetao Basin. Results from a water-leaching method suggest that Na and Ca related sulphates dominate the evaporite minerals in sediment samples. Groundwater salinization mainly results from evaporation and Na^+/Ca^{2+} cation exchange followed by sulphate and silicate minerals weathering. Saturated indices for calcite, dolomite and unsaturated indices for gypsum as well as negative correlation between pH and SO_4^{2-} suggest that groundwater chemistry does not reach equilibrium with continual carbonates precipitation by an excessive Ca supply from Ca related sulphates weathering. The groundwater pH decrease and Ca^{2+} release during weathering of Ca related sulphates can retard As desorption from Fe (oxyhydr)oxides and clay minerals. Furthermore, pyrite minerals were also found in the sediments induced by high sulphide flux and it can cause As sequestration. However, modeling results suggest the occurrence of thio-As species in the study area, which can potentially enhance the As mobilization. This study contributes to the ongoing research into As mobilization in the groundwater of lacustrine basins.

1. Introduction

Co-occurrence of groundwater salinization (with total dissolved solids (TDS) > 1000 mg/L) and As contamination (> 10 μg/L) has been widely found in the aquifers of Argentina, the tidal deltaplain of southwest Bangladesh and many basins in the north of China (Guo and Wang, 2005; Nicolli et al., 2012; Rodríguez-Lado et al., 2013; Xie et al., 2013; Ayers et al., 2016; Li et al., 2016). Reductive dissolution of As-containing Fe (oxyhydr)oxides and/or competitive As desorption are considered critical mechanisms causing groundwater As enrichment (Nordstrom, 2002; Ahmed et al., 2004; Guo et al., 2013a). Possible reasons for groundwater salinization include: saline intrusion, historic marine transgression, evaporite minerals weathering and excessive evaporation of surface water and shallow groundwater (Appleo and Postma, 2005; MacDonald et al., 2016). Since elevated salinity and As concentration are both influenced by groundwater hydrochemical evolution processes, their connection should be highlighted, however, few studies have addressed those two issues until now. Elevated groundwater redox components, especially SO_4^{2-}, which increases during the groundwater salinization processes, can influence the As partitioning process between sediments and groundwater by formation of secondary minerals in the aquifer sediments (Lowers et al., 2007; Buschmann and Berg, 2009; Kao et al., 2011; Guo et al., 2016; Smith et al., 2017), whereas some elevated concentrations of ions such as HCO_3^- and Ca^{2+} can influence the As desorption/adsorption from clay minerals and Fe (oxyhydr)oxides (Brahman et al., 2013; Fakhreddine et al., 2015). Therefore, clarifying the saline source and connection with As contamination is essential for understanding the As

* Corresponding author.
E-mail address: xwsuron@cugb.edu.cn (W. Xiu).

https://doi.org/10.1016/j.apgeochem.2019.104416
Received 12 April 2019; Received in revised form 27 August 2019; Accepted 30 August 2019
Available online 30 August 2019
0883-2927/ © 2019 Published by Elsevier Ltd.

mobilization process as well as safe groundwater exploration.

Groundwater salinization processes in the semi-arid to arid inland basins of the Yellow River catchment have recently attracted increased attention, these include the Hetao Basin, the Datong Basin and the Huhhot Basin (Smedley et al., 2003; Deng et al., 2009; Xie et al., 2012; Li et al., 2016; Jia et al., 2017). Groundwater with TDS > 1000 mg/L approximately accounts for 91% of total groundwater samples (n = 634) in the Hetao Basin (Gao et al., 2014). Deng et al. (2009) suggested that evaporation caused the elevated salinity, whereas Jia et al. (2017) proposed that evaporite dissolution might contribute to groundwater salinization. However, there is no comprehensive study to show the influence of evaporites dissolution on the groundwater salinization process. In general, three processes can contribute solutes to groundwater, these include: evaporite dissolution, carbonate dissolution and silicates weathering (MacKenzie and Garrels 1971). The most distinctive geologic feature of the Hetao Basin is the lacustrine deposit, which is known to contain evaporite minerals (Eugster, 1980; Smoot and Lowenstein, 1991). Evaporite minerals can drive salinization since chlorides and sulphates are more dissoluble than carbonates and both show higher weathering rates than silicates (MacKenzie and Garrels 1971), whereas weathering of rock-forming aluminosilicates in the typical clastic sediments of Hetao Basin contribute to an enrichment of different cations in groundwater (Wang et al., 2009). During the late Pleistocene epoch, the shrinking of a paleolake might has accumulated evaporites in the sediments of the Hetao Basin, though it is presently unclear as to which specific evaporite minerals (Jia et al., 2016). In this study, the distribution of evaporite minerals in depth profiles were investigated using a water-extraction method. Afterwards, the groundwater salinization process is analyzed with emphasis on the influence of evaporite mineral dissolution.

Historically, research into the groundwater hydrochemistry of the Hetao Basin has focused far more on As contamination than salinization (Gao, 1999; Guo et al., 2008; Deng et al., 2009; Rodríguez-Lado et al., 2013). Microbial reduction of Fe (oxyhydr)oxides releasing As into groundwater is thought to be the most important mechanism for As mobilization (Guo et al., 2008, 2013a; Li et al., 2014), though fewer studies have been conducted into the influence of desorption-adsorption processes, which can be largely affected by divalent cations (Ca^{2+}, Mg^{2+}) and competing anions (HCO_3^-, OH^-, SiO_4^{4-}) (Smedley and Kinniburgh, 2002; Wang et al., 2009; Fakhreddine et al., 2015). Evaporites accumulated in Pleistocene epoch can significantly influence As mobilization/immobilization in the aquifer of Hetao Basin. Firstly, evaporite minerals are thought to be an important sink for trace elements such as As, B and F (Thiede and Cameron, 1978; Tabelin et al., 2017). For example, gypsum ($CaSO_4{\cdot}2H_2O$) and calcite ($CaCO_3$) can incorporate As into the their structures (Winkel et al., 2013; Zhang et al., 2015). Secondly, dissolution of evaporites can largely influence the groundwater pH and alkalinity conditions, which are key parameters for As desorption from Fe (oxyhydr)oxides and clay minerals (Plummer et al., 1990; Nordstrom, 2002; Podgorski et al., 2017). Furthermore, sulphide formation resulting from sulphate reduction can influence As partitioning between groundwater and sediments as described above (Kirk et al., 2004; Planer-Friedrich et al., 2018). This study focus on the influence of evaporite minerals weathering on As mobilization.

Based on the assumption that evaporites weathering will contribute to the elevated groundwater salinity and influence As mobilization processes, the objectives of this study are: 1) to clarify the distribution of evaporite minerals in the study area and their influence on groundwater hydrochemical composition; and 2) to evaluate the effects of the evaporites weathering on As mobilization.

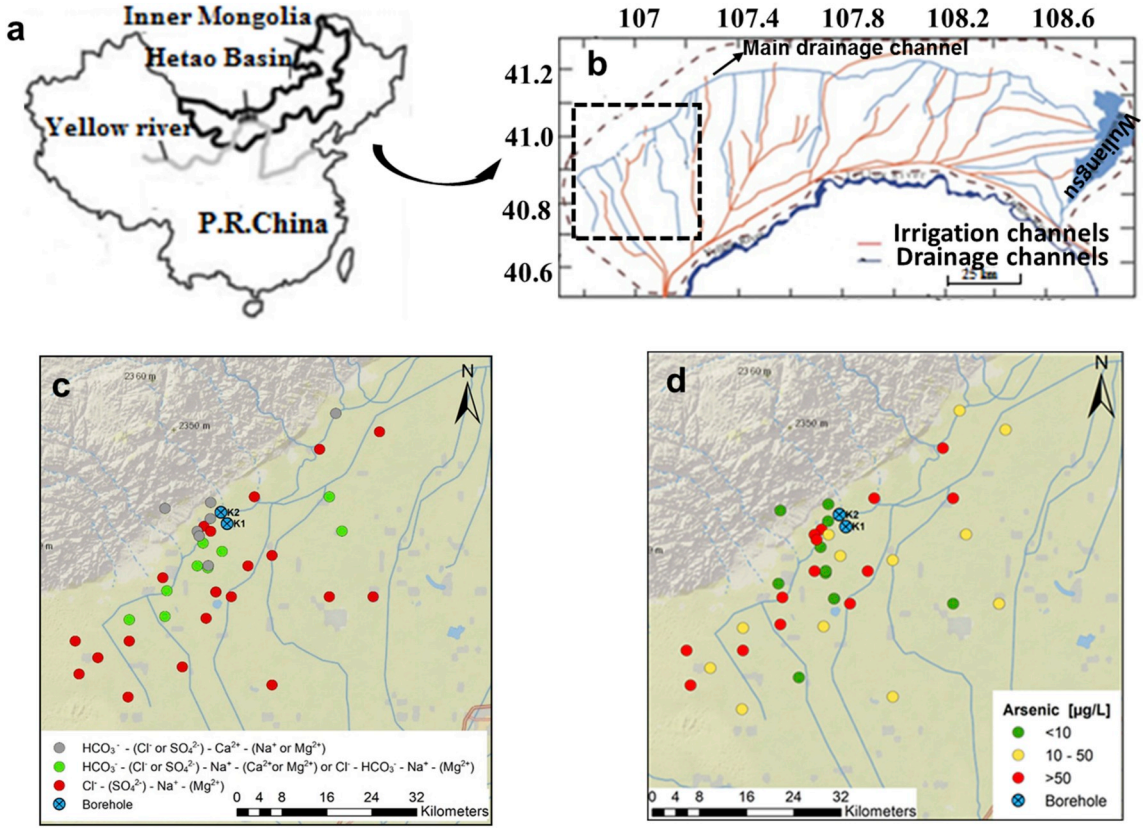

Fig. 1. Description for study area: a) geography position of the Hetao Basin, b) landscape of the Hetao Basin with labeled study area, the graph is modified from Jia et al. (2014), c) Google map of study area with groundwater samples, labeled groundwater chemistry types and boreholes area, d) Google map of study area with groundwater samples, labeled groundwater As concentration range and borehole area. Part of groundwater data is cited from Guo et al. (2011) with detailed information showed in Table S1.

2. Overview of the study area

The research area (Fig. 1) is located in the Hangjinhouqi, the northwest part of the Hetao Basin, near the paleolake sedimentation center. It is also one of most serious As contamination area in the Hetao Basin (Deng et al., 2011).

The Hetao Basin (13,000 km^2) is located in the middle of Inner Mongolia (Fig. 1). It is a Cenozoic rift basin bordered by the Langshan Mountains in the north and the Kubuqi desert towards the south, stretching from Ulan Buh desert in the west to Wuliangsu Lake in the east. The Yellow River flows through from west to east along the southern margin of the basin, which is around 60 km away from the Lang Mountains. The Hetao Basin has typical semi-arid to arid continental climate. Precipitation mainly falls between June to September with an average monthly value of 200 mm and evaporation varies from 2000 to 2500 mm per year.

The Langshan Mountains, located in the north of the Hetao Basin, are mainly composed of Archen-Mesoproterozoic metamorphic rocks including gneiss, schist, phyllite, slate, and late Paleozoic igneous rocks mainly granite and diorite (Liu et al., 2016). In the early late Pleistocene epoch (~120 ka), alluvial-lacustrine sediments were developed while the Yellow River gradually migrated from the pediments of the Langshan Mountains to the south of the basin (Jia et al., 2016). Paleolakes gradually dried out after further 50 ka (Yang et al., 2018).

In the study area, the groundwater table ranges from ~1 m to 10 m (Guo et al., 2012). For irrigation and drinking, groundwater is mainly supplied from the Holocene-late Pleistocene fluvial/alluvial-lacustrine aquifer at up to 100 m depth. In general, the study area consists of an unconfined aquifer and a semi-confined aquifer separated by a clay layer at ~40 m depth (Inner Mongolia Institute of Hydrogeology, 1982; Jia et al., 2014).

3. Methods

3.1. Groundwater sampling and analysis

Thirty-seven groundwater samples from hand-pumped tube wells at depths < 100 m and one rain water sample were collected (7 samples were collected in 2017 and 30 groundwater and rain water samples are cited from Guo et al. (2011)). Detailed measurement information for published data was shown in Guo et al. (2011). Groundwater samples from October of 2017 were collected by the CUGB (China University of Geoscience (Beijing)) group and the KIT (Karlsruhe Institute of Technology) group. The sampling followed the same procedure as in Guo et al. (2011) except that groundwater was run through solid phase extraction (SPE) (Meng et al., 2001) and measured by HG-FIAAS (Hydride Generation Flow Injection Atomic Absorption Spectroscopy) with a PerkinElmer Analyst 200 coupled with a FIMS-400 Hydride Generation System and Auto sampler. Detection limit of FIAAS is around 0.1 μg/L. The groundwater samples were analyzed within one month after sampling. All groundwater sampling area and chemistry types used for hydrochemistry process analysis are shown in Fig. 1. Detailed results show in Table S1.

3.2. Multi-level well installations

Two multilevel wells (K1 and K2) were drilled by the CUGB group using circulatory drilling method in October 2015. K2 is located in the transition area, north of K1 with a distance of around 2 km, while K1 is located in the flat plain (Fig. 1). After cores were brought to the surface, they were sectioned into 10 cm lengths, capped, and placed into N_2 purged bags according to lithology and color variations observed by eye. Sub-samples of the sediments were transported to the KIT group.

The multi-level samplers were installed by CUGB group in October of 2015. Each well has 7 sampling levels placed at depths ranging from 15 to 80 m. Groundwater samples were collected from each depth of K1 and K2 and hydrochemical characteristics were analyzed by the CUGB group according to the method mentioned above.

3.3. Sediments characterization

Geochemical and mineralogical analysis of the sediments samples was performed at AGW (Institute of Applied Geoscience) of KIT in 2017. Samples were freeze-dried and homogenized by manual grinding. Mineralogy of the core samples was determined by X–ray diffraction (XRD) (Kristalloflex D500, Siemens, Germany) at 40 kV and 25 mA. Cu Kα1-radiation was used at angles between 2° and 80°. Major minerals were identified using calibrated spectra by the software EVA program (Bruker) using the database of PDF 2002. Afterwards, the spectra were semi-quantified using known mineral compositions (Snyder and Bish, 1989; Norra et al., 2005).

Trace element composition in the sediments were determined by means of Energy Dispersive X-ray Spectrometry (EDX; Epsilon 5, PANanalytical). Results were regularly checked and corrected by standard material (SOIL-5, n = 4; GXR-6, n = 4; GXR-2, n = 4; SL-1 n = 4) with a precision better than 5%. Major elements (K, Na, Si, Ca, Mg, Fe, Mn) were analyzed by Wavelength Dispersive X-ray Spectrometry (WDX; S4 Explorer, Bruker AXS) with glass beads. The measurement accuracy (within 5%) was regularly checked by standard material AGV-1 (USGS).

Total sulphur (TS) and carbon (TC) content in the sediments were measured by Carbon-Sulphur-Analyzer (CS-2000, Leybold Heraeus, Germany) and total organic carbon (TOC) was measured after inorganic carbon removal by repeated addition of 20% HCl (Suprapure, Merke) at 60 °C. Detection limits for C and S are both 0.1 mg/kg. The measurement accuracy (± 0.5%) was controlled by reference material Cast Iron 92400–3100 (%C 4.20 ± 0.03 and %S 0.023 ± 0.001, USGS) and Steel 92400–3050 (%C 0.147 ± 0.002 and %S 0.027 ± 0.001, USGS).

3.4. Soluble salts in the sediments

The chemical composition of soluble salts were determined by a water-extraction method slightly modified from Tabelin et al. (2014) and analyzed at AGW of KIT. Four grams of each sediment sample was added into 20 mL of Milli-Q water. The extraction was performed in centrifuge tubes with mixing speed 300 r/min for 24 h. Afterwards, samples were centrifuged for 30 min at 4000 rpm and the pH and electrical conductivity (EC) were measured in the supernatant solution using pH and EC meters (WTW). The alkalinity was measured using a titration method with bromocresol green-methyl red indicator (Merck). Samples for cation and As concentration analysis were filtrated using 0.45 μm filters (cellulose acetate) and preserved by adding 1% 6 M HNO_3 (Superpure, Merck). Cations (Ca^{2+}, Mg^{2+}, Na^{+}, K^{+}) were measured by ICP-OES (Varian 715 ES), while anions (SO_4^{2-}, Cl^{-}) were analyzed using Ion Chromatography (Dionex, ICS-1000). The measurement accuracy (± 2%) was controlled by River Water reference (RW-LGC6020). Arsenic concentrations from extracted samples were analyzed with HG-FIAS.

3.5. Geochemical modeling and statistical analysis

Saturation indices (SI) for dolomite ($CaMg(CO_3)_2$), calcite ($CaCO_3$) and gypsum ($CaSO_4{\cdot}2H_2O$) as well as As species calculation were modelled using PHREEQC with Wateq4f database, which was updated for As species according to Helz and Tossell (2008). The modeling temperature was assumed to be 10 °C according to the groundwater temperature ranging from 5.5 °C to 15.6 °C in the Hetao Basin (Li et al., 2013). The pH value, element concentration as well as As species (As (III) and As(V)) are known from measurement results. Statistical analysis for water as well as sediments data was done using IBM SPSS statistics.

Table 1
Semi-quantitative mineral abundance of sediments with different lithology from K1 and K2 borehole (except peat layers). Detailed information for single sample can be found in Table S2.

Mineral	Sand (wt %) (n = 22)	Silt (wt %) (n = 14)	Clay/silty clay (wt %) (n = 14)
Quartz	52 ± 4	39 ± 5	31 ± 3
Plagioclase	26 ± 2	30 ± 5	28 ± 8
K-feldspar	14 ± 3	12 ± 5	13 ± 8
Calcite	3 ± 1	8 ± 3	11 ± 6
Mica	4 ± 1	7 ± 2	12 ± 6
Dolomite	< 1	< 1	1
Chlorite/Kaolinite	< 1	2 ± 1	4 ± 3

4. Results

4.1. Sediments lithology and bulk chemical composition

Sediments from both K1 and K2 boreholes are dominated by fine sand and silt (Fig. S1). Quartz and feldspar (plagioclase and K-feldspar) are major minerals in the sediments (> 70%), while carbonates (calcite, dolomite), mica and clay minerals are minor phases (Table 1). The TIC content in the sediments ranges from ~0.6% to 1.5%, while the CaO and MgO content ranges from ~3.2% to ~7.1% and ~1.0%–~2.8%, respectively. Positive correlations between CaO and total inorganic carbon (TIC) ($R^2 = 0.97$) and between MgO and total inorganic carbon (TIC) ($R^2 = 0.83$) indicate that Ca^{2+} and Mg^{2+} mostly exist as carbonates (Fig. S2). Evaporite mineral content is below the detection limit of the XRD characterization except trace amounts of gypsum together with pyrite detected in a peat layer at a depth of 28.4 m in K2 (Table S2).

The average sulphur content in the sediments is 480 mg/kg for clayed or silt samples and 230 mg/kg for sandy samples (Table 2). However, no observable correlation between TS and TOC (0.045 %–0.597%) combined with the low content of sulphides or polysulphides (evidenced by S K-edge XAS measurement; unpublished data) suggest that sulphur (S) mainly exists in form of sulphates in the sediments.

Arsenic content in the solid phases (except peat layers) ranges from 5 mg/kg to 41 mg/kg (Table 2) with an average content of 14 mg/kg. It is related with Fe content ($R^2 = 0.87$) (Fig. S3) rather than the TOC content, indicating that As mainly bonds/adsorbs into Fe related (oxyhydro)oxides and Fe-containing clay minerals in the sediments. Peat sediments (sediments with high content of organic matter) have higher As content up to 328 mg/kg at a depth of 28.4 m.

4.2. Soluble salts in sediments

Higher content of soluble salts (EC > 1000 μS/cm^3) was found in the near-surface sediments (< 4 m) compared to deeper sediments and mostly originate from sulphates and chlorides (Fig. 2). The lowest EC value was observed at a depth around 6 m (98 μS/cm^3) in K1, suggesting that the accumulative soluble salts in deeper sediments are rarely sourced from top sediments. EC of Milli-Q water extracts for clayed/silty clayed samples (average 330 μS/cm^3) is slightly higher than that in silty/sandy samples (200 μS/cm^3). Moreover, sandy/silty samples from K1 have higher EC values (228 μS/cm^3) than that of sandy/silty samples from K2 (174 μS/cm^3) (Fig. 2). The pH values of sediments vertically vary from 8.0 to 9.8 (Fig. 2). Such alkaline pH values are characteristic for saline or saline-sodic sediments and soils in arid and semi-arid regions as well as many fresh lakes (Inoue et al., 1998).

Water-extractable SO_4^{2-} content in sediments (at depth > 4 m) ranges from 56 to 555 mg/kg with an average value of 177 mg/kg, more than 5 times higher than the soluble Cl^- (from 8 to 92 mg/kg with an average value of 33 mg/kg). In both K1 and K2, the sediments at depth between ~10 m and ~40 m have higher soluble SO_4^{2-} content than sediments in the lower parts (Fig. 2). Average equivalent abundances of water-soluble cations of K1 sediments decrease in the order: Na^+ (56%) > Ca^{2+} (28%) > Mg^{2+} (14%) > K^+ (2%). Linear regression analysis shows that [SO_4^{2-}] positively correlates with [$Na^+ + Ca^{2+}$] ($R^2 = 0.55$) (Fig. 3a), it hints to the potential occurrence of glauberite ($Na_2Ca(SO_4)_2$) in K1. In the borehole K2, average Ca^{2+} equivalent abundance of total cations (60%) is higher than that of the Na^+ (26%) followed by Mg^{2+} (11%) and K^+ (3%). Positive correlations between soluble SO_4^{2-} and Ca^{2+} contents of K2 sediments ($R^2 = 0.50$) with the molar ratio of SO_4^{2-}/Ca^{2+} close to 1 (Fig. 3a) indicates that SO_4^{2-} mainly exists as Ca-sulphates (gypsum or anhydrite ($CaSO_4$)). The sulphates dissolution system is buffered by carbonates dissolution, which is indicated by correlations between [$Ca^{2+} + Mg^{2+}$] and [HCO_3^-] ($R^2 = 0.37$), [Ca^{2+}] and pH ($R^2 = 0.65$) (Fig. 3b, c). Peat sediments leach out higher amount of SO_4^{2-} and Ca^{2+} with contents up to 5240 mg/kg and 1770 mg/kg at a depth of 28.4 m in K2, which is consistent with the gypsum/anhydrite detected by XRD.

4.3. Water-soluble As in the sediments

Water-soluble As is generally low in sediments from both K1 and K2. Arsenic concentration in the extraction solution (except peat layers) generally ranges from 0.3 μg/L to 7.4 μg/L with an average value of 2.5 μg/L (average 13 μg/kg in sediments), which only accounts for less than 0.1% of total As content in the sediments (average 14 mg/kg) (Fig. 2). An exception is that the As concentration in extraction solute is 23 μg/L (115 μg/kg) at a depth of 11.5 m of K1 aquifer sand, more than 10 times higher than average value. Noticeably, arsenic release in the sand samples depends on the sediments pH conditions ($R^2 = 0.74$) (Fig. 3d).

4.4. Groundwater chemistry

All groundwater samples show a neutral or weakly alkaline condition with pH values ranging from 7.1 to 8.9. The detailed groundwater hydro-chemical characteristics analysis is shown in Guo et al. (2011).

Table 2
Major and trace elements composition from sediments depth profiles of K1 and K2 (except peat layers). Detailed information for single sample can be found in Table S3.

Lithology	Number	SiO_2 (wt %)	Na_2O (wt %)	CaO (wt %)	MgO (wt %)	K_2O (wt %)	Al_2O_3 (wt %)	MnO (wt %)	Fe_2O_3 (wt %)
clay/silty clay	14	53.9 ± 6.4	1.4 ± 0.4	7.1 ± 1.8	2.8 ± 0.5	3.0 ± 0.3	14.3 ± 1.5	0.09 ± 0.02	5.6 ± 1.0
silt	14	62.0 ± 6.5	1.7 ± 0.2	6.6 ± 1.4	2.2 ± 0.7	2.3 ± 0.3	11.4 ± 1.5	0.07 ± 0.02	4.1 ± 1.0
sand	22	77.0 ± 3.1	1.8 ± 0.1	3.2 ± 0.7	1.0 ± 0.2	2.1 ± 0.2	8.8 ± 0.6	0.04 ± 0.01	3.2 ± 0.7

Lithology	Number	TOC (wt %)	TIC (wt %)	TS (wt %)	As (mg/kg)	Sr (mg/kg)	Ba (mg/kg)	Rb (mg/kg)
clay/silty clay	14	0.402 ± 0.198	1.537 ± 0.463	0.048 ± 0.017	21 ± 8	263 ± 56	513 ± 85	146 ± 17
silt	14	0.229 ± 0.147	1.401 ± 0.398	0.048 ± 0.025	14 ± 5	241 ± 65	456 ± 45	105 ± 17
sand	22	0.058 ± 0.011	0.578 ± 0.175	0.023 ± 0.005	7 ± 2	176 ± 9	450 ± 37	83 ± 9

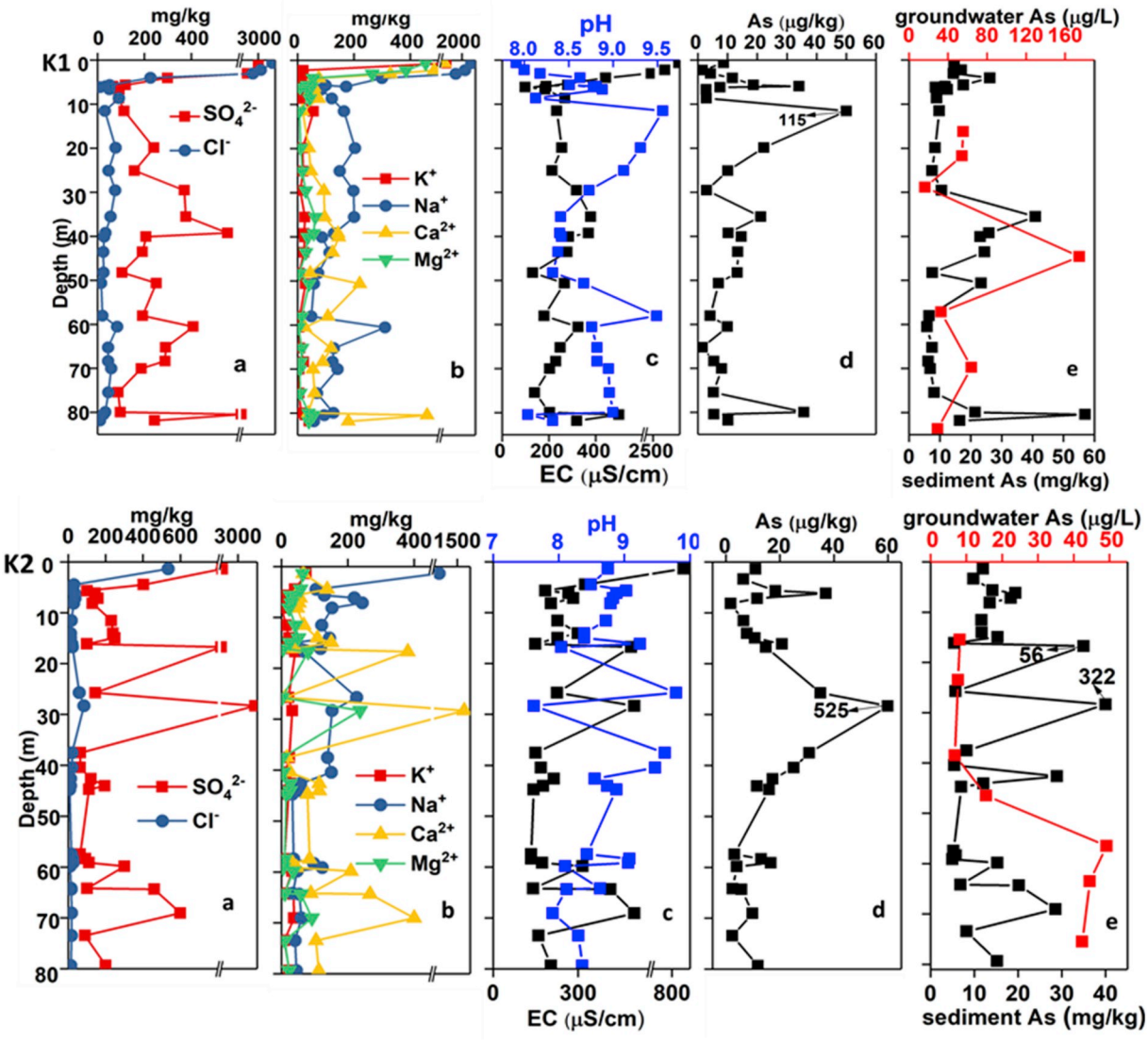

Fig. 2. Depth profiles of soluble salts from the sediments of K1 and K2. (a) content of soluble anions in the sediments: SO_4^{2-} and Cl^-, (b) content of soluble cations in the sediments: K^+, Na^+, Ca^{2+}, Mg^{2+}, (c) pH and electrical conductivity (EC) values in the sediments extraction solution, (d) soluble As content in the sediments, (e) arsenic content in the sediments as well as As concentration in the groundwater. The measurement values are provided in Table S4.

Isotopic compositions (δ^2D and $\delta^{18}O$) show that groundwater is of meteoric origin (Guo et al., 2011). Samples collected from alluvial fans and transition area have HCO_3^- or SO_4^{2-} as main the anions, and Ca^{2+} or Na^+ as the main cations (Fig. 1). In the flat plain, most groundwater samples are of the HCO_3^--Na^+ type or Cl^--Na^+ type, the latter near the main drainage channel (Fig. 1). More than 70% of analyzed groundwater samples are saline groundwater with TDS values (from 420 to 6730 mg/L) higher than 1000 mg/L. The depths profiles of TDS show that most saline groundwater occurs in the unconfined aquifer with depths between 10 m and 30 m (Fig. S4). SO_4^{2-} concentration ranges from near < 0.1 mg/L to 1260 mg/L, accounting for 18% of total anions in average.

Arsenic concentrations range from < 1 μg/L to 666 μg/L with an average concentration of 142 μg/L in the study area (Guo et al., 2011). High TDS groundwater (84%) occurs concurrently with As concentrations above 10 μg/L, even though no direct correlation between TDS and As is observed. Arsenic concentrations in investigated groundwater samples are negatively correlated with SO_4^{2-} and Ca^{2+} concentration as well as ORP values (reducing conditions), while it is positively correlated with pH values (Table 3).

5. Discussion

5.1. Origin of groundwater chemical composition

Mineralogical analysis combined with mass-balance calculation yields important information on groundwater chemical composition for groundwater chemical composition (Mukherjee et al., 2009; Wang et al., 2009; Xie et al., 2013). Plots of $[Mg^{2+}/Na^+]$ vs $[Ca^{2+}/Na^+]$ and $[HCO^{3-}/Na^+]$ vs $[Ca^{2+}/Na^+]$ in groundwater are presented in Fig. 4a and b along the mixing line with silicate, evaporite and carbonate minerals as end-numbers obtained from Gaillardet et al. (1997, 1999). Results show that groundwater chemistry evolution is mainly controlled by incongruent silicate and evaporite minerals weathering. Molar ratio of $[Na^+ + K^+]$ to total cations (varying from 0.34 to 0.97 with an average value of 0.72) is much higher than $[Ca^{2+} + Mg^{2+}]$ (varying from 0.03 to 0.66 with an average value of 0.28) (Fig. 4c). Combined with lithological analysis, Na^+ and K^+ in the groundwater primarily provided from incongruent dissolution of feldspar and mica. In addition, sulphate minerals accumulated in soils or sediments might recharge Na^+ into groundwater (Jalali, 2007; Li et al., 2016), however, halite (NaCl) in sediment profiles is rare and limited leaching from

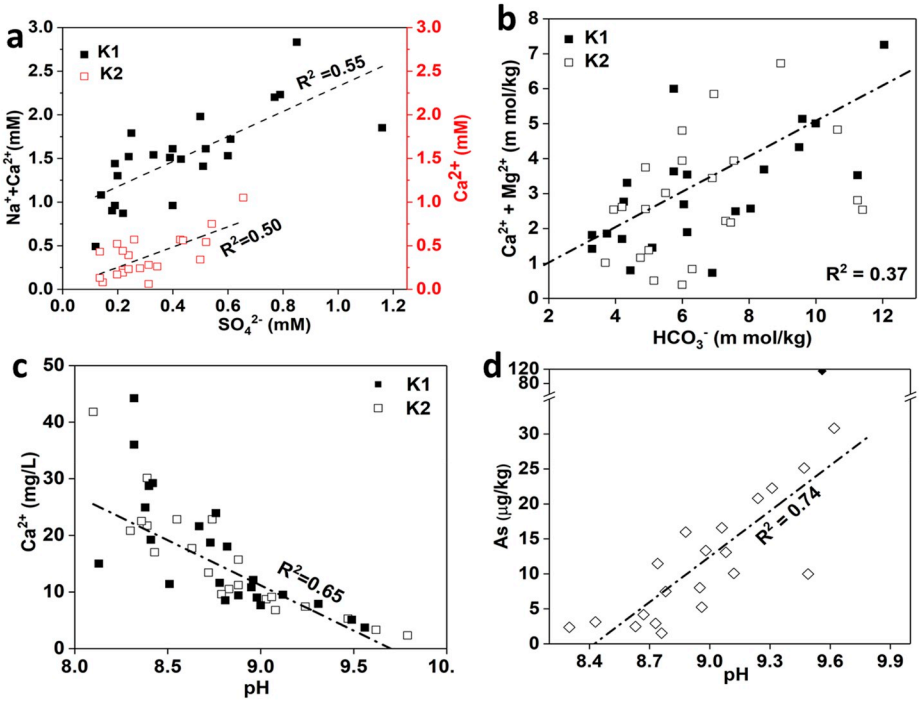

Fig. 3. Regression liner analysis of soluble salts in the sediments samples at depth > 4 m (except peat layers). (a) correlation between soluble SO_4^{2-} concentration and Na^+ as well as Ca^{2+} concentration in the extraction solution, (b) correlation between soluble HCO_3^- concentration and Mg^{2+} as well as Ca^{2+} concentration in the extraction solution, (c) relationship between sediments pH and soluble Ca^{2+}, (d) regression liner analysis to show As leaching in the sand samples depending the sediments pH. The filled square symbol stands for one outlier samples with high leached As content (115 μg/kg) at depth 11.5 m of K1 borehole.

Table 3
Pearson's correlation matrices for geochemical parameters showing marked correlations at a significant level $p < 0.01$. Part of groundwater data was cited from Guo et al. (2011).

	pH	ORP	EC	NH_4^+	Cl^-	SO_4^{2-}	HCO_3^-	K^+	Na^+	Mg^{2+}	Ca^{2+}	As(III)	As_T	Fe(II)	Fe_T	DOC	H_2S
pH	1																
ORP (mV)		1															
EC (μS/cm³)			1														
NH_4^+ (mg/L)				1													
Cl^- (mg/L)			0.95		1												
SO_4^{2-} (mg/L)	−0.64	0.51	0.66		0.54	1											
HCO_3^- (mg/L)			0.73		0.65	0.50	1										
K^+ (mg/L)			0.63		0.64			1									
Na^+ (mg/L)			0.94		0.93	0.55	0.82	0.47	1								
Mg^{2+} (mg/L)	−0.49		0.82		0.77	0.71	0.48	0.73	0.64	1							
Ca^{2+} (mg/L)	−0.76					0.53				0.54	1						
As(III) (μg/L)	0.58	−0.68				−0.53					−0.48	1					
As_T (μg/L)	0.61	−0.68				−0.58					−0.47	0.97	1				
Fe(II) (mg/L)														1			
Fe_T (mg/L)		−0.54										0.51	0.43	0.78	1		
DOC (mg/L)																1	
H_2S (μg/L)		−0.51				−0.44							0.48				1

surface soil, shown by the TDS values in the soluble salts profile.

The effects of cation exchange are evaluated by an equivalent plot of corrected bivalent Ca^{2+} and Mg^{2+} versus corrected Na^+ (Fig. 4d). Groundwater samples from the study area form a slope near −1.0, indicating that Na^+/Ca^{2+} cation exchange is an important process for groundwater chemistry evolution (Mukherjee et al., 2009). Besides Na^+/Ca^{2+} exchange, the positive correlation between $[Cl^-]$ and TDS ($R^2 = 0.89$) shows that strong evaporation probably occurs in the study area (Fig. 4e). However, there is no correlation between $\delta^{18}O$ and Cl^- concentration (Fig. 4f), which might be due to the fact that non-direct evaporation processes such as plant transpiration are contributing to the Cl^- enrichment, while the isotope compositions remain unchanged (Zimmermann et al., 1967). The deuterium excess further indicated that non-direct evaporation contributes to the groundwater salinity (Jia et al., 2017).

Compared with other high As alluvial systems in south and southeast Asia, SO_4^{2-} concentration in groundwater of the Hetao Basin is relatively high (Berg et al., 2007; Guo et al., 2016). Molar ratio of SO_4^{2-} to Cl^- is up to 1.11, while the average SO_4^{2-}/Cl^- ratio in the precipitation is 0.72. Lithological and soluble salt analysis reveals that SO_4^{2-} concentration can partly be attributed to the Na- and Ca-related sulphates which are among main evaporite minerals found in the sediments.

5.2. Contribution of evaporite minerals weathering to groundwater chemistry

Evaporite minerals found in the sediments are mainly Na and Ca related sulphates occurring as gypsum or anhydrite and most likely as glauberite. The weathering of Ca-sulphates can induce the groundwater dedolomitization process (Bischoff et al., 1994; Atekwana and Seeger, 2015), the total mass transfer of the dedolomitization process is given by the reaction (Appleo and Postma, 2005):

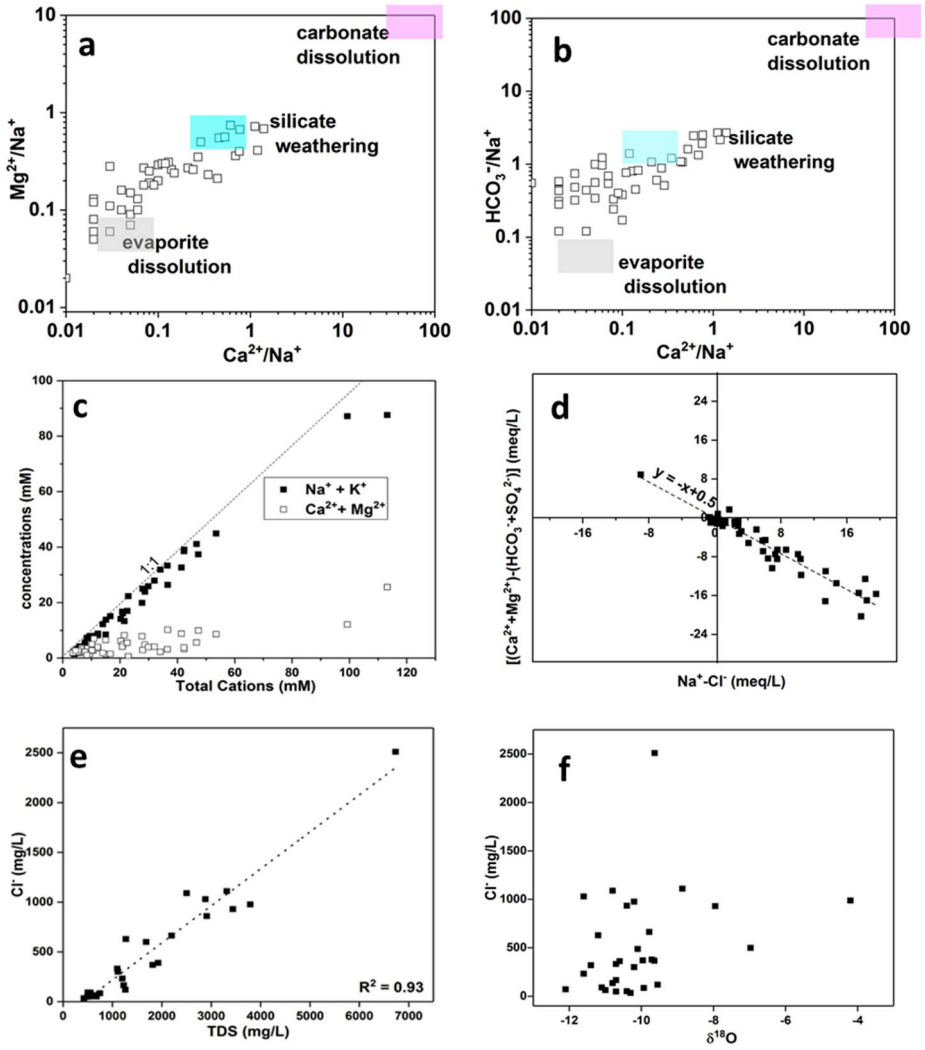

Fig. 4. Bivariate plots of ion analysis in groundwater. (a), Na-normalized Mg^{2+} (μM/μM) versus Ca^{2+} (μM), (b), Na-normalized (μM/μM) and HCO_3^- versus Ca^{2+} (μM), (c), molar ratio of Ca^{2+} and Mg^{2+} as well as Na^+ and K^+ versus total cations (Na^+, K^+, Ca^{2+}, Mg^{2+}) in groundwater samples (d), Ca^{2+} and Mg^{2+} less HCO_3^- and SO_4^{2-} against Na^+ less Cl^- to indicate cation exchange (e), concentration of Cl^- versus TDS, (f), concentration of Cl^- versus $\delta^{18}O$. The weathering end members of silicates, carbonate and evaporites are cited from Gaillardet et al. (1997, 1999). Part of groundwater data is cited from Guo et al. (2011).

$$1.8\ CaSO_4 + 0.8\ CaMg(CO_3)_2 \rightarrow 1.6\ CaCO_3 + Ca^{2+} + 0.8\ Mg^{2+} + 1.8\ SO_4^{2-} \quad (1)$$

The theoretical molar ratios of $[Ca^{2+}]/[SO_4^{2-}]$ and $[Mg^{2+}]/[SO_4^{2-}]$ are 1:1.8 and 0.8:1.8, respectively. All groundwater samples in the study area are undersaturated with respect to gypsum, indicating the potential of Ca sulphates dissolution (Fig. 5). The Ca^{2+} and Mg^{2+} concentrations of groundwater simultaneously increase with increasing SO_4^{2-} concentration (Table 3**).** However, molar ratios of Mg^{2+} or Ca^{2+} to SO_4^{2-} are not strictly along the theoretical ratio line (Fig. 6a). The saturation index shows most groundwater samples are supersaturated with dolomite and saturated with calcite, this possibly suggests that the dedolomitization process may not further influence the hydrochemical conditions. Co-increased Ca^{2+} and Mg^{2+} concentrations with SO_4^{2-} concentration can be related to carbonate precipitation inhibitors, which are related to the Mg disturbance for the calcite crystal growth (Berner, 1975). Hydrogen (H^+) release resulting from precipitation of carbonates driven by gypsum can induce pH decrease (Back et al., 1983; Hanshaw and Hallet, 1978). The negative relationship between pH and SO_4^{2-} and between pH and Ca^{2+} further indicates that the carbonate precipitation is driven by gypsum (or anhydrite) or glauberite dissolution still actively happens in the research area (Fig. 6b and Table 3).

For evaluating the influence of soluble sulphates for groundwater salinity, soluble SO_4^{2-} is converted to groundwater SO_4^{2-} concentration based on the assumption that aquifer porosity is 0.2 and mass density of sediments is 2.65 g/cm^3, which are typical values for sediments (Francis and Brinkley, 1976) (Fig. 7a). Higher concentrations of both solid-phase and liquid phase SO_4^{2-} are observed at K1 borehole compared to the K2 borehole, this supports the hypothesis that groundwater SO_4^{2-} originates from the sediments. In general, groundwater SO_4^{2-} concentration is related to the water-soluble fractions of the SO_4^{2-} within sediments at the similar depth from both K1 and K2 borehole (R^2 = 0.67) (Fig. 7b), which also supports the hypothesis that part of SO_4^{2-} in the groundwater originates from evaporite minerals. Seasonal variation of groundwater SO_4^{2-} concentrations was monitored in the study area and found that most wells showed increasing trends from 2006 to 2010 (Guo et al., 2013b), confirming that sulphate minerals are still contributing SO_4^{2-} to the groundwater and weathering rate of sulphate minerals would be faster than the SO_4^{2-} reduction rate in general.

5.3. Potential effect of soluble evaporite minerals on As mobilization

More than 80% of high TDS groundwater is contaminated with As

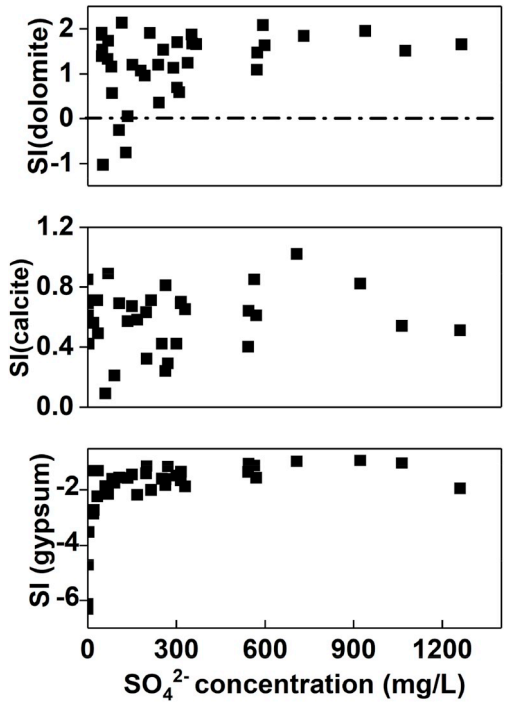

Fig. 5. Comparison of calcite ($CaCO_3$), dolomite ($CaMg(CO_3)_2$), and gypsum ($CaSO_4{\cdot}2H_2O$) saturation indices as a function of SO_4^{2-} concentration. Part of groundwater data was cited from Guo et al. (2011).

(> 10 μg/L). Evaporation can cause enrichment of elements, therefore possibly causing typical elevated As concentrations which is known to occur in groundwater in semi-arid to arid regions (Deverel and Millard, 1988; Nickson et al., 2005; Karroum et al., 2017). However, there is no significant correlation between the concentrations of major ions (except for SO_4^{2-} and Ca^{2+} and Mg^{2+}) and As concentrations (Table 3), indicating that As immobilization/mobilization in the groundwater is mainly influenced by factors other than evaporations.

Water-soluble As only accounts for a minor percentage of the total As content in sediments and is independent of soluble salts, while it is related to the pH conditions in the leaching solution. In the Hetao Basin, arsenic is mainly incorporated into/adsorbed onto Fe containing minerals including Fe (oxyhydr)oxides and clay minerals. The adsorption abilities of those minerals are significantly influenced by solute pH conditions. With elevated solute pH, As species especially $HAsO_4^{2-}$, can be desorbed from iron oxides or clay mineral surfaces to the solution (Schwertmann and Cornell, 1992; Dixit and Hering, 2003; Bhattacharyya and Gupta, 2008). The pH-dependent As concentration in the leaching solution suggests that the As release from the sediments matrix could be influenced by the groundwater pH conditions in the Hetao Basin. The spatial patterns in groundwater hydrochemistry show that pH decreases with the continual carbonate precipitation, which is driven by Ca related sulphates dissolution. On one hand, the decreased pH can retard As desorption from (oxyhydr)oxides and clay minerals. Furthermore, the divalent cation-Ca^{2+} can increase the positive surface charge of clay minerals (Fakhreddine et al., 2015), the adsorption potential of clay minerals for As will increase. The positive correlation between groundwater pH and As concentration, as well as the negative correlation between Ca^{2+} concentration and As concentration reinforces this hypothesis. The pH-dependent As release has already been evidenced in the La Pampa Basin of Argetina (Smedley et al., 2005). Furthermore, previous studies suggest that As could be incorporated into the crystal structures of precipitating carbonates, but mostly with pH > 9 (Goldberg and Glaubig, 1988; Fakhreddine et al., 2015), it would have minor influence for weakly alkaline pH conditions of groundwater in the Hetao Basin.

Redox cycles of sulphur and iron in the groundwater can promote sulphides formation, and therefore influencing the As mobilization in the groundwater. In the Hetao Basin, arsenic concentration generally increases with the increasing sulphide concentration under relatively low sulphide flux (< 50 μg/L) (Table 3 and Fig. 8a). This could be related to that As release from sediments increases with stronger groundwater reducing conditions, which occurs simultaneously with SO_4^{2-} reduction. In addition, the modeling results show that sulphide can form thio-As species, especially with As(V) ($HAsO_4^{2-}$) in the groundwater. In comparison with As(V) or As(III) species, thio-As species are much more stable in the groundwater, which can potentially increase the As mobilization in the aquifer (Sø et al., 2018) (Fig. 8b**).** This is consistent with previous suggestions that sulphide could stabilize As by formation of thio-As species under a subsurface alkaline environment (Stucker et al., 2014; Mladenov et al., 2014). Furthermore, Fe (oxyhydr)oxides can be thermodynamically reduced by sulphide (Poulton et al., 2004; Sun et al., 2016). However, it is unexpected with such high amount of reactive Fe in the sediment matrix under low sulphide flux, reaction of sulphide with Fe^{2+} from microbial reduction of Fe (oxyhydr)oxides inhibits the reaction between H_2S and Fe (oxyhydr)oxides. However, some samples with high sulphide concentrations (≥ 50 μg/L) have relatively lower As concentration was found in Hetao basin (Fig. 8a). This possibly suggests that As could incorporate into pyrite, which is confirmed in the peat sample with high content of As at depth 28.4 m of K2, and pyrite together with gypsum are being characterized (Table S2). The reactive organic carbon leached from detrital

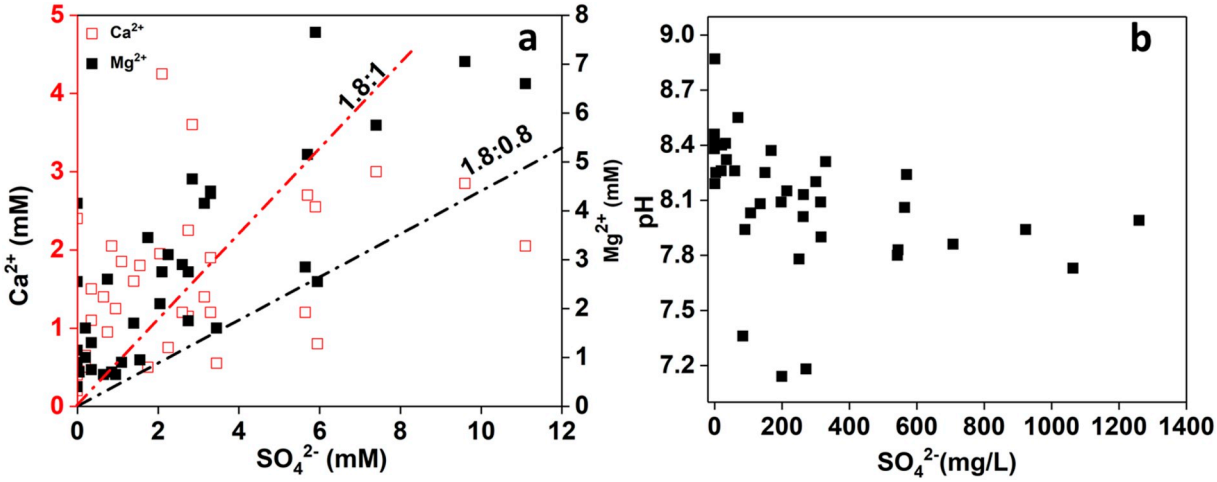

Fig. 6. Bivariate plots of Ca^{2+} and Mg^{2+} versus SO_4^{2-} (a) and pH versus SO_4^{2-}, (b) part of the groundwater data was cited from Guo et al. (2011).

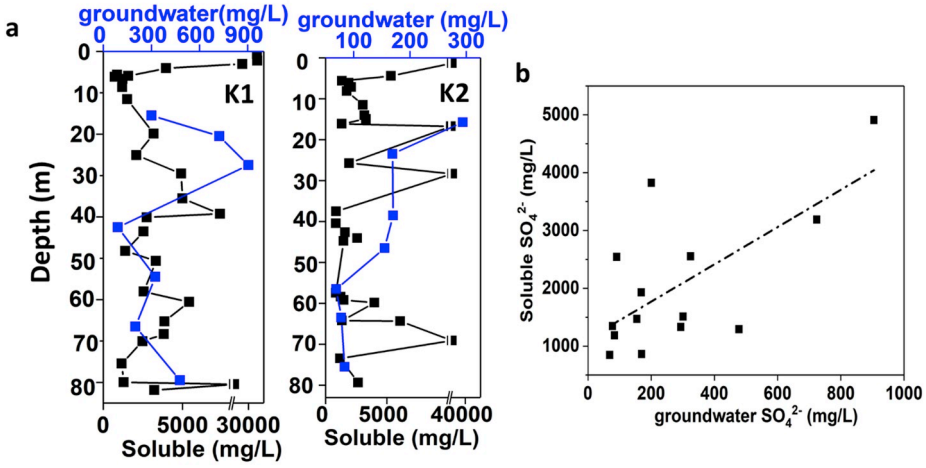

Fig. 7. Depth profile of sediments soluble SO_4^- and groundwater SO_4^{2-} (a) and correlation (b) (soluble SO_4^{2-} in sediments is converted into groundwater SO_4^{2-} concentration basing on assumption that aquifer porosity is 0.2 and mass density of sediments is 2.65 g/cm^3).

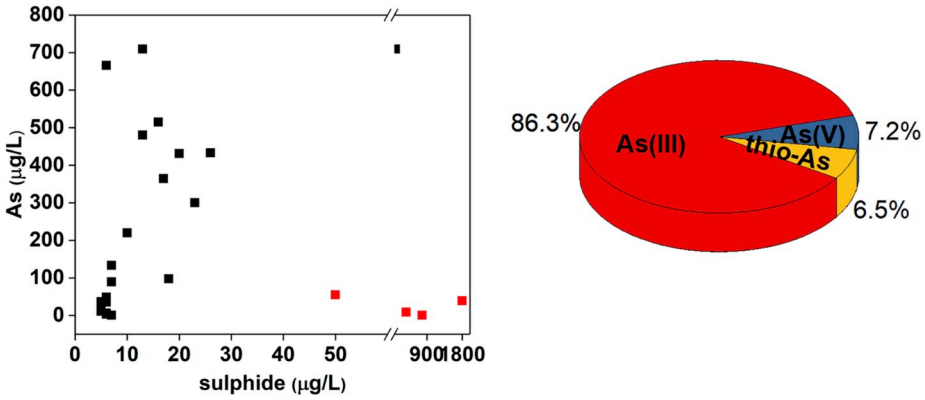

Fig. 8. Influence of sulphide concentration for As mobilization: (a) bivariate plots of As versus sulphide, the red filled squares show groundwater samples with higher sulphide concentration and relatively low As concentration (< 100 μg/L), (b) example of modeling results for As species (As concentration: 515 μg/L, sulphide concentration: 16 μg/L). Thio-As species stands for As-sulphide complex, As content for respective species was calculated if the concentration is higher than 1 μg/L. Part of the groundwater data is cited from Guo et al. (2011). (For interpretation of the references to color in this figure legend, the reader is referred to the Web version of this article.)

peat layers or recharged from surface provides enough electrons for SO_4^{2-} and Fe^{3+} reduction (Guo et al., 2019), and therefore promoted formation of arsenianpyrite/arsenopyrite in the aquifer. Similarly, the significant role of pyrite for As sequestration has already been evidenced in the Mekong River Delta and Bangladesh (Lowers et al., 2007; Stuckey et al., 2015).

6. Conclusions

In the study area, more than 70% of groundwater shows salinization properties with TDS > 1000 mg/L. In combination with lithological analysis, major ion ratios show that the groundwater salinization is mainly caused by evaporation and Na^+/Ca^{2+} cation exchange followed by silicate and evaporite minerals weathering.

Water-extraction experiments show that evaporites mainly include sulphates. Whereas evaporite mineral dissolution only releases less than 0.1% of total As in sediments, it can influence As concentration via groundwater salinization processes. Saturation indices of gypsum, calcite and dolomite and negative correlation between pH and SO_4^{2-} suggest that groundwater chemistry does not achieve equilibrium with carbonate precipitation and Ca sulphates weathering. The pH decrease and Ca^{2+} release induced by Ca sulphates weathering can retard As desorption from the Fe (oxyhydr)oxides and clay minerals. Furthermore, arsenic can be incorporated into the structure of pyrites which forms following by SO_4^{2-} reduction, which is evidenced by XRD characterization in peat (organic carbon-rich) layers. However, modeling results suggest that trace sulphide may form thio-As species with $HAsO_4^{2-}$, which would be much more stable in comparison with H_3AsO_3 and $HAsO_4^{2-}$ species in the groundwater. Further research should be attempted to model the quantification effects of sulphates dissolution on groundwater salinization and As mobilization process in the Hetao Basin.

Acknowledgement

The study was financially supported by the National Natural Science Foundation of China (grant Nos. 41825017, 41702272 and 41672225). We express the special thanks to Graduate School for PhD students of KIT-center Climate and Environment (GRACE) at Karlsruhe Institute of Technology for the field trip funding to go to Hetao Basin. We are grateful for the help for analytical supports from our colleagues B. Oetzel (XRD, XRF and CSA) and G. Preuss (ICP-OES and FIAS), C. Moessner (IC) and XRD spectra analysis support from G. Ott. We also appreciate the help from CUGB group during the field trip to the Hetao Basin. We are grateful for the language update from M.S. O. Moore and Dr. S. Islam in University of Manchester. We especially give thanks to the editor and reviewers for giving valuable suggestions and comments.

Appendix A. Supplementary data

Supplementary data to this article can be found online at https://doi.org/10.1016/j.apgeochem.2019.104416.

References

Ahmed, K.M., Bhattacharya, P., Hasan, M.A., Akhter, S.H., Alam, S.M., Bhuyian, M.H.,

Imam, M.B., Khan, A.A., Sracek, O., 2004. Arsenic enrichment in groundwater of the alluvial aquifers in Bangladesh: an overview. Appl. Geochem. 19 (2), 181–200.
Appleo, C.A.J., Postma, D., 2005. Geochemistry, Groundwater and Pollution, second ed. CRC.
Atekwana, E.A., Seeger, E.J., 2015. Carbonate and carbon isotopic evolution of groundwater contaminated by produced water brine with hydrocarbons. Appl. Geochem. 63, 105–115.
Ayers, J.C., Goodbred, S., George, G., Fry, D., Benneyworth, L., Hornberger, G., Roy, K., Karim, M.R., Akter, F., 2016. Sources of salinity and arsenic in groundwater in southwest Bangladesh. Geochem. Trans. 17 (1), 4.
Back, W., Hanshaw, B.B., Plummer, L.N., Rahn, P.H., Rightmire, C.T., Rubin, M., 1983. Process and rate of dedolomitization: mass transfer and ^{14}C dating in a regional carbonate aquifer. Geol. Soc. Am. Bull. 94 (12), 1415–1429.
Berg, M., Stengel, C., Trang, P.T.K., Viet, P.H., Sampson, M.L., Leng, M., Samreth, S., Fredericks, D., 2007. Magnitude of arsenic pollution in the Mekong and red river deltas-Cambodia and Vietnam. Sci. Total Environ. 372 (2–3), 413–425.
Berner, R.A., 1975. The role of magnesium in the crystal growth of calcite and aragonite from sea water. Geochem. Cosmochim. Acta 39 (4), 489–504.
Bhattacharyya, K.G., Gupta, S.S., 2008. Adsorption of a few heavy metals on natural and modified kaolinite and montmorillonite: a review. Adv. Colloid Interface Sci. 140 (2), 114–131.
Bischoff, J.L., Juliá, R., Shanks III, W.C., Rosenbauer, R.J., 1994. Karstification without carbonic acid: bedrock dissolution by gypsum-driven dedolomitization. Geology 22 (11), 995–998.
Brahman, K.D., Kazi, T.G., Afridi, H.I., Naseem, S., Arain, S.S., Ullah, N., 2013. Evaluation of high levels of fluoride, arsenic species and other physicochemical parameters in underground water of two sub districts of Tharparkar, Pakistan: a multivariate study. Water Res. 47 (3), 1005–1020.
Buschmann, J., Berg, M., 2009. Impact of sulfate reduction on the scale of arsenic contamination in groundwater of the Mekong, Bengal and Red River deltas. Appl. Geochem. 24 (7), 1278–1286.
Deng, Y., Wang, Y., Ma, T., 2009. Isotope and minor element geochemistry of high arsenic groundwater from Hangjinhouqi, the Hetao Plain, Inner Mongolia. Appl. Geochem. 24 (4), 587–599.
Deng, Y., Wang, Y., Ma, T., Yang, H., He, J., 2011. Arsenic associations in sediments from shallow aquifers of northwestern Hetao Basin, Inner Mongolia. Environ. Earth Sci. 64 (8), 2001–2011.
Deverel, S.J., Millard, S.P., 1988. Distribution and mobility of selenium and other trace elements in shallow groundwater of the western San Joaquin Valley, California. Environ. Sci. Technol. 22 (6), 697–702.
Dixit, S., Hering, J.G., 2003. Comparison of arsenic (V) and arsenic (III) sorption onto iron oxide minerals: implications for arsenic mobility. Environ. Sci. Technol. 37 (18), 4182–4189.
Eugster, H.P., 1980. Geochemistry of evaporitic lacustrine deposits. Annu. Rev. Earth Planet Sci. 8 (1), 35–63.
Fakhreddine, S., Dittmar, J., Phipps, D., Dadakis, J., Fendorf, S., 2015. Geochemical triggers of arsenic mobilization during managed aquifer recharge. Environ. Sci. Technol. 49 (13), 7802–7809.
Francis, C.W., Brinkley, F.S., 1976. Preferential adsorption of ^{137}Cs to micaceous minerals in contaminated freshwater sediment. Nature 260 (5551), 511.
Gaillardet, J., Dupre, B., Allegre, C.J., Négrel, P., 1997. Chemical and physical denudation in the Amazon river basin. Chem. Geol. 142 (3–4), 141–173.
Gaillardet, J., Dupré, B., Louvat, P., Allegre, C.J., 1999. Global silicate weathering and CO_2 consumption rates deduced from the chemistry of large rivers. Chem. Geol. 159 (1–4), 3–30.
Gao, Q.R., 1999. Research on the mechanism of arsenic pollution in groundwater in the Hetao Plain, Inner Mongolia, China. Chin. J. Geol. Hazard Control 10, 25–32 (in Chinese with English title).
Gao, C.R., Liu, W.B., Feng, C.E., 2014. Distribution characteristics of saline groundwater and high-arsenic groundwater in the Hetao Plain, Inner Mongolia. Acta Geol. Sin. 35 (2), 139–148 (in Chinese with English Abstract).
Goldberg, S., Glaubig, R.A., 1988. Anion sorption on a calcareous, montmorillonitic soil-arsenic. Soil Sci. Soc. Am. J. 52 (5), 1297–1300.
Guo, H., Wang, Y., 2005. Geochemical characteristics of shallow groundwater in Datong basin, northwestern China. J. Geochem. Explor. 87 (3), 109–120.
Guo, H., Li, X., Xiu, W., He, W., Cao, Y., Zhang, D., Wang, A., 2019. Controls of organic matter bioreactivity on arsenic mobility in shallow aquifers of the Hetao Basin, PR China. J. Hydrol. 571, 448–459.
Guo, H., Liu, C., Lu, H., Wanty, R.B., Wang, J., Zhou, Y., 2013a. Pathways of coupled arsenic and iron cycling in high arsenic groundwater of the Hetao basin, Inner Mongolia, China: an iron isotope approach. Geochem. Cosmochim. Acta 112, 130–145.
Guo, H., Yang, S., Tang, X., Li, Y., Shen, Z., 2008. Groundwater geochemistry and its implications for arsenic mobilization in shallow aquifers of the Hetao Basin, Inner Mongolia. Sci. Total Environ. 393 (1), 131–144.
Guo, H., Zhang, B., Li, Y., Berner, Z., Tang, X., Norra, S., Stüben, D., 2011. Hydrogeological and biogeochemical constrains of arsenic mobilization in shallow aquifers from the Hetao Basin, Inner Mongolia. Environ. Pollut. 159 (4), 876–883.
Guo, H., Zhang, Y., Jia, Y., Zhao, K., Li, Y., Tang, X., 2013b. Dynamic behaviors of water levels and arsenic concentration in shallow groundwater from the Hetao Basin, Inner Mongolia. J. Geochem. Explor. 135, 130–140.
Guo, H., Zhang, Y., Xing, L., Jia, Y., 2012. Spatial variation in arsenic and fluoride concentrations of shallow groundwater from the town of Shahai in the Hetao basin, Inner Mongolia. Appl. Geochem. 27 (11), 2187–2196.
Guo, H., Zhou, Y., Jia, Y., Tang, X., Li, X., Shen, M., Lu, H., Han, S., Wei, C., Norra, S., Zhang, F., 2016. Sulfur cycling-related biogeochemical processes of arsenic mobilization in the western Hetao Basin, China: evidence from multiple isotope approaches. Environ. Sci. Technol. 50 (23), 12650–12659.
Hanshaw, B.B., Hallet, B., 1978. Oxygen isotope composition of subglacially precipitated calcite: possible paleoclimatic implications. Science 200 (4347), 1267–1270.
Helz, G.R., Tossell, J.A., 2008. Thermodynamic model for arsenic speciation in sulfidic waters: a novel use of ab initio computations. Geochem. Cosmochim. Acta 72 (18), 4457–4468.
Inner Mongolia Institute of Hydrogeology, 1982. Hydrogeological Setting and Remediation Approaches of Soil Salinity in the Hetao Basin, Inner Mongolia. Scientific report. (in Chinese).
Inoue, K., Saito, M., Naruse, T., 1998. Physicochemical, mineralogical, and geochemical characteristics of lacustrine sediments of the Konya Basin, Turkey, and their significance in relation to climatic change. Geomorphology 23 (2–4), 229–243.
Jalali, M., 2007. Salinization of groundwater in arid and semi-arid zones: an example from Tajarak, western Iran. Environ. Geol. 52 (6), 1133–1149.
Jia, L., Zhang, X., Ye, P., Zhao, X., He, Z., He, X., Zhou, Q., Li, J., Ye, M., Wang, Z., Meng, J., 2016. Development of the alluvial and lacustrine terraces on the northern margin of the Hetao basin, inner Mongolia, China: implications for the evolution of the Yellow River in the Hetao area since the late Pleistocene. Geomorphology 263, 87–98.
Jia, Y., Guo, H., Jiang, Y., Wu, Y., Zhou, Y., 2014. Hydrogeochemical zonation and its implication for arsenic mobilization in deep groundwaters near alluvial fans in the Hetao Basin, Inner Mongolia. J. Hydrol. 518, 410–420.
Jia, Y., Guo, H., Xi, B., Jiang, Y., Zhang, Z., Yuan, R., Xue, X., 2017. Sources of groundwater salinity and potential impact on arsenic mobility in the western Hetao Basin, Inner Mongolia. Sci. Total Environ. 601, 691–702.
Kao, Y.H., Wang, S.W., Liu, C.W., Wang, P.L., Wang, C.H., Maji, S.K., 2011. Biogeochemical cycling of arsenic in coastal salinized aquifers: evidence from sulfur isotope study. Sci. Total Environ. 409 (22), 4818–4830.
Karroum, M., Elgettafi, M., Elmandour, A., Wilske, C., Himi, M., Casas, A., 2017. Geochemical processes controlling groundwater quality under semi arid environment: a case study in central Morocco. Sci. Total Environ. 609, 1140–1151.
Kirk, M.F., Holm, T.R., Park, J., Jin, Q., Sanford, R.A., Fouke, B.W., Bethke, C.M., 2004. Bacterial sulfate reduction limits natural arsenic contamination in groundwater. Geology 32 (11), 953–956.
Li, J., Wang, Y., Xie, X., 2016. Cl/Br ratios and chlorine isotope evidences for groundwater salinization and its impact on groundwater arsenic, fluoride and iodine enrichment in the Datong basin, China. Sci. Total Environ. 544, 158–167.
Li, P., Wang, Y., Jiang, Z., Jiang, H., Li, B., Dong, H., Wang, Y., 2013. Microbial diversity in high arsenic groundwater in Hetao Basin of Inner Mongolia, China. Geomicrobiol. J. 30 (10), 897–909.
Li, Y., Guo, H., Hao, C., 2014. Arsenic release from shallow aquifers of the Hetao Basin, Inner Mongolia: evidence from bacterial community in aquifer sediments and groundwater. Ecotoxicology 23 (10), 1900–1914.
Liu, M., Zhang, D., Xiong, G., Zhao, H., Di, Y., Wang, Z., Zhou, Z., 2016. Zircon U–Pb age, Hf isotope and geochemistry of Carboniferous intrusions from the Langshan area, Inner Mongolia: petrogenesis and tectonic implications. J. Asian Earth Sci. 120, 139–158.
Lowers, H.A., Breit, G.N., Foster, A.L., Whitney, J., Yount, J., Uddin, M.N., Muneem, A.A., 2007. Arsenic incorporation into authigenic pyrite, Bengal Basin sediment, Bangladesh. Geochem. Cosmochim. Acta 71 (11), 2699–2717.
MacDonald, A.M., Bonsor, H.C., Ahmed, K.M., Burgess, W.G., Basharat, M., Calow, R.C., Dixit, A., Foster, S.S.D., Gopal, K., Lapworth, D.J., Lark, R.M., 2016. Groundwater quality and depletion in the Indo-Gangetic Basin mapped from in situ observations. Nat. Geosci. 9 (10), 762.
Mackenzie, Fred T., Garrels, R.M., 1971. Evolution of Sedimentary Rocks. Norton, New York.
Meng, X., Korfiatis, G.P., Jing, C., Christodoulatos, C., 2001. Redox transformations of arsenic and iron in water treatment sludge during aging and TCLP extraction. Environ. Sci. Technol. 35 (17), 3476–3481.
Mladenov, N., Wolski, P., Hettiarachchi, G.M., Murray-Hudson, M., Enriquez, H., Damaraju, S., Galkaduwa, M.B., McKnight, D.M., Masamba, W., 2014. Abiotic and biotic factors influencing the mobility of arsenic in groundwater of a through-flow island in the Okavango Delta, Botswana. J. Hydrol. 518, 326–341.
Mukherjee, A., Bhattacharya, P., Shi, F., Fryar, A.E., Mukherjee, A.B., Xie, Z.M., Jacks, G., Bundschuh, J., 2009. Chemical evolution in the high arsenic groundwater of the Huhhot basin (Inner Mongolia, PR China) and its difference from the western Bengal basin (India). Appl. Geochem. 24 (10), 1835–1851.
Nickson, R.T., McArthur, J.M., Shrestha, B., Kyaw-Myint, T.O., Lowry, D., 2005. Arsenic and other drinking water quality issues, Muzaffargarh District, Pakistan. Appl. Geochem. 20 (1), 55–68.
Nicolli, H.B., Bundschuh, J., Blanco, M.D.C., Tujchneider, O.C., Panarello, H.O., Dapeña, C., Rusansky, J.E., 2012. Arsenic and associated trace-elements in groundwater from the Chaco-Pampean plain, Argentina: results from 100 years of research. Sci. Total Environ. 429, 36–56.
Nordstrom, D. Kirk, 2002. Worldwide occurrences of arsenic in groundwater. Science 2143–2145.
Norra, S., Berner, Z.A., Agarwala, P., Wagner, F., Chandrasekharam, D., Stüben, D., 2005. Impact of irrigation with as rich groundwater on soil and crops: a geochemical case study in West Bengal Delta Plain, India. Appl. Geochem. 20 (10), 1890–1906.
Planer-Friedrich, B., Schaller, J., Wismeth, F., Mehlhorn, J., Hug, S.J., 2018. Monothioarsenate occurrence in Bangladesh groundwater and its Removal by ferrous and zero-valent iron technologies. Environ. Sci. Technol. 52 (10), 5931–5939.
Plummer, L.N., Busby, J.F., Lee, R.W., Hanshaw, B.B., 1990. Geochemical modeling of the Madison aquifer in parts of Montana, Wyoming, and South Dakota. Water Resour. Res. 26 (9), 1981–2014.

Podgorski, J.E., Eqani, S.A.M.A.S., Khanam, T., Ullah, R., Shen, H., Berg, M., 2017. Extensive arsenic contamination in high-pH unconfined aquifers in the Indus Valley. Sci. Adv. 3 (8), e1700935.
Poulton, S.W., Krom, M.D., Raiswell, R., 2004. A revised scheme for the reactivity of iron (oxyhydr) oxide minerals towards dissolved sulfide. Geochem. Cosmochim. Acta 68 (18), 3703–3715.
Rodríguez-Lado, L., Sun, G., Berg, M., Zhang, Q., Xue, H., Zheng, Q., Johnson, C.A., 2013. Groundwater arsenic contamination throughout China. Science 341 (6148), 866–868.
Schwertmann, U., Cornell, R.M., 1992. Iron Oxides in the Laboratory. John Wiley & Sons p.12.
Smedley, P.L., Kinniburgh, D.G., 2002. A review of the source, behavior and distribution of arsenic in natural waters. Appl. Geochem. 17 (5), 517–568.
Smedley, P.L., Kinniburgh, D.G., Macdonald, D.M.J., Nicolli, H.B., Barros, A.J., Tullio, J.O., Pearce, J.M., Alonso, M.S., 2005. Arsenic associations in sediments from the loess aquifer of La Pampa, Argentina. Appl. Geochem. 20 (5), 989–1016.
Smedley, P.L., Zhang, M., Zhang, G., Luo, Z., 2003. Mobilization of arsenic and other trace elements in fluviolacustrine aquifers of the Huhhot Basin, Inner Mongolia. Appl. Geochem. 18 (9), 1453–1477.
Smith, R.L., Kent, D.B., Repert, D.A., Böhlke, J.K., 2017. Anoxic nitrate reduction coupled with iron oxidation and attenuation of dissolved arsenic and phosphate in a sand and gravel aquifer. Geochem. Cosmochim. Acta 196, 102–120.
Smoot, J.P., Lowenstein, T.K., 1991. Depositional environments of non-marine evaporites. Dev. Sedimentol. 50, 189–347.
Snyder, R.L., Bish, D.L., 1989. Quantitative analysis. Rev. Mineral. 20, 101.
Sø, H.U., Postma, D., Vi, M.L., Pham, T.K.T., Kazmierczak, J., Dao, V.N., Pi, K., Koch, C.B., Pham, H.V., Jakobsen, R., 2018. Arsenic in Holocene aquifers of the Red River floodplain, Vietnam: effects of sediment-water interactions, sediment burial age and groundwater residence time. Geochem. Cosmochim. Acta 225, 192–209.
Stucker, V.K., Silverman, D.R., Williams, K.H., Sharp, J.O., Ranville, J.F., 2014. Thioarsenic species associated with increased arsenic release during biostimulated subsurface sulfate reduction. Environ. Sci. Technol. 48 (22), 13367–13375.
Stuckey, J.W., Schaefer, M.V., Kocar, B.D., Dittmar, J., Pacheco, J.L., Benner, S.G., Fendorf, S., 2015. Peat formation concentrates arsenic within sediment deposits of the Mekong Delta. Geochem. Cosmochim. Acta 149, 190–205.
Sun, J., Quicksall, A.N., Chillrud, S.N., Mailloux, B.J., Bostick, B.C., 2016. Arsenic mobilization from sediments in microcosms under sulfate reduction. Chemosphere 153, 254–261.
Tabelin, C.B., Hashimoto, A., Igarashi, T., Yoneda, T., 2014. Leaching of boron, arsenic and selenium from sedimentary rocks: II. pH dependence, speciation and mechanisms of release. Sci. Total Environ. 473, 244–253.
Tabelin, C.B., Sasaki, R., Igarashi, T., Park, I., Tamoto, S., Arima, T., Ito, M., Hiroyoshi, N., 2017. Simultaneous leaching of arsenite, arsenate, selenite and selenate, and their migration in tunnel-excavated sedimentary rocks: I. Column experiments under intermittent and unsaturated flow. Chemosphere 186, 558–569.
Thiede, D.S., Cameron, E.N., 1978. Concentration of heavy metals in the Elk Point evaporite sequence, Saskatchewan. Econ. Geol. 73 (3), 405–415.
Wang, Y., Shvartsev, S.L., Su, C., 2009. Genesis of arsenic/fluoride-enriched soda water: a case study at Datong, northern China. Appl. Geochem. 24 (4), 641–649.
Winkel, L.H., Casentini, B., Bardelli, F., Voegelin, A., Nikolaidis, N.P., Charlet, L., 2013. Speciation of arsenic in Greek travertines: Co-precipitation of arsenate with calcite. Geochem. Cosmochim. Acta 106, 99–110.
Xie, X., Wang, Y., Ellis, A., Su, C., Li, J., Li, M., Duan, M., 2013. Delineation of groundwater flow paths using hydrochemical and strontium isotope composition: a case study in high arsenic aquifer systems of the Datong basin, northern China. J. Hydrol. 476, 87–96.
Xie, X., Wang, Y., Su, C., Li, J., Li, M., 2012. Influence of irrigation practices on arsenic mobilization: evidence from isotope composition and Cl/Br ratios in groundwater from Datong Basin, northern China. J. Hydrol. 424, 37–47.
Yang, X., Cai, M., Ye, P., Yang, Y., Wu, Z., Zhou, Q., Li, C., Liu, X., 2018. Late Pleistocene paleolake evolution in the Hetao basin, inner Mongolia, China. Quat. Int. 464, 386–395.
Zhang, D., Yuan, Z., Wang, S., Jia, Y., Demopoulos, G.P., 2015. Incorporation of arsenic into gypsum: relevant to arsenic removal and immobilization process in hydrometallurgical industry. J. Hazard Mater. 300, 272–280.
Zimmermann, U., Ehhalt, D., Münnich, K.O., 1967. Soil-water movement and evapotranspiration: changes in the isotopic composition of the water. In Isotopes in hydrology. In: Proceedings of a Symposium. 38, 38061083 27.

Appendix 3 Vertical redox zones of Fe-S-As coupled mineralogy in the sediments of Hetao Basin – Constraints for groundwater As contamination

Journal of Hazardous Materials 408 (2021) 124924

Contents lists available at ScienceDirect

Journal of Hazardous Materials

journal homepage: www.elsevier.com/locate/jhazmat

Vertical redox zones of Fe–S–As coupled mineralogy in the sediments of Hetao Basin – Constraints for groundwater As contamination

H.Y. Wang [a,*], J. Göttlicher [b], J.M. Byrne [c,d], H.M. Guo [e], L.G. Benning [f,g], S. Norra [a]

[a] Institute of Applied Geoscience, Working Group of Environmental Mineralogy and Environmental System Analysis, Karlsruhe Institute of Technology (KIT), 76131 Karlsruhe, Germany
[b] Institute of Photon Science and Synchrotron Radiation, Karlsruhe Institute of Technology (KIT), 76344 Eggenstein-Leopoldshafen, Germany
[c] Geomicrobiology, Center for Applied Geosciences, University of Tübingen, 72074 Tübingen, Germany
[d] Now: School of Earth Sciences, University of Bristol, Wills Memorial Building, Queens Road, Bristol BS8 1RJ, United Kingdom
[e] State Key Laboratory of Biogeology and Environmental Geology, China University of Geoscience, 100083 Beijing, China
[f] GFZ German Research Center for Geoscience, 14473 Potsdam, Germany
[g] Department of Earth Sciences, Freie Universität Berlin, 12249 Berlin, Germany

ARTICLE INFO

Editor: Dr. Rinklebe Jörg

Keywords:
XAS
Speciation
Fe(III) oxides
Fe sulfides
Arsenic

ABSTRACT

The formation of iron-sulfur-arsenic (Fe–S–As) minerals during biogeochemical processes in As contaminated aquifers remains poorly understood despite their importance to understanding As release and transport in such systems. In this study, X-ray absorption and Mössbauer spectroscopies complemented by electron microscopy, and chemical extractions were used to examine vertical changes of As, Fe and S speciation for the example of sediments in the Hetao Basin.

Reduction of Fe(III), As(V) and SO_4^{2-} species were shown to co-occur in the aquifers. Iron oxides were observed to be predominantly goethite and hematite (36 – 12%) and appeared to decrease in abundance with depth. Furthermore, reduced As (including arsenite and As sulfides) and sulfur species (including S(-II), S(-I) and S^0) increased from 16% to 76% and from 13% to 44%, respectively.

Iron oxides were the major As carrier in the sediments, and the lower groundwater As concentration consists with less desorbable and reducible As in the sediments. The formation of As-Fe sulfides (e.g., As containing pyrite and greigite) induced by redox heterogeneities likely contribute to localized lower groundwater As concentrations. These results help to further elucidate the complex relationship between biogeochemical processes and minerals formation in As contaminated aquifers.

1. Introduction

The contamination of geogenic groundwater with arsenic (As) (> 10 μg/L: the World Health Organization standard) is a major threat to human health worldwide (Fendorf et al., 2010; Podgorski and Berg, 2020). Large-scale exposure to high As groundwater mainly occurs in the river deltas of South and Southeast Asia including the Ganges-Brahmaputra-Meghna (GBM), the Red River and the Mekong River as well as inland basins draining the Yellow River and the Yangtze River (Fendorf et al., 2010; Nordstrom, 2002; Wang et al., 2017; Guo et al., 2014).

It is widely accepted that in-situ desorption of As from As-bearing Fe (III) oxides (including iron oxides, hydroxides, and oxyhydroxides) can lead to the release of As into groundwater (Islam et al., 2004; Horneman et al., 2004; McArthur et al., 2001; Guo et al., 2013). Arsenic speciation and Fe mineralogy are important factors in this process, influencing As partition and therefore release into groundwater under stable geochemical conditions. Under reducing conditions, As(V) species are reduced to As (III) species which bond less strongly to Fe(III) oxides at circumneutral pH condition. Consequently, desorption is susceptible to shifting geochemical conditions such as groundwater flushing resulting from groundwater flow (Stollenwerk et al., 2007). Furthermore, the Fe-bearing phases in sediments have different reactivities and therefore show different adsorption properties towards As. For example, poorly crystalline Fe(III) oxides provide much more adsorption sites for As than crystalline Fe(III) oxides and are much more likely to undergo abiotic and biotic reduction (Larsen et al., 2006). Characterizing the speciation and abundance of Fe(III) oxides and As in the sediments is therefore

* Corresponding author.
E-mail address: hongyan.wang@kit.edu (H.Y. Wang).

https://doi.org/10.1016/j.jhazmat.2020.124924
Received 28 June 2020; Received in revised form 18 November 2020; Accepted 19 December 2020
Available online 29 December 2020
0304-3894/© 2020 Elsevier B.V. All rights reserved.

helpful for understanding the potential for As release into the groundwater.

Upon reduction of Fe(III) oxides, the formation of secondary Fe(II)-containing minerals can also influence the partitioning of As between sediments and groundwater (Horneman et al., 2004; Postma et al., 2007; Postma et al., 2016). With large surface to volume ratios, Fe(II)-bearing minerals such as Fe sulfides (pyrite, FeS_2 or greigite, Fe_3S_4), Fe-carbonates (siderite, $FeCO_3$), Fe-phosphates (vivianite, $Fe_3(PO_4)_20.8H_2O$), or Fe oxides (e.g., magnetite, Fe_3O_4) are each also able to sorb As to varying degrees, and can therefore retard As mobilization in groundwater (Wang et al., 2018; Kocar et al., 2010; Perez et al., 2020; Perez et al., 2021). For example, magnetite has been reported as the main secondary oxide and As carrier in Bangladesh sediments (Polizzotto et al., 2006). The formation of secondary Fe(II)-bearing minerals largely depends on the redox conditions in subsurface sediments and these influence the fate of heavy metals and metalloids (Lemonte et al., 2017; Shaheen et al., 2016; Frohne et al., 2011). It is necessary to develop a holistic understanding of the differences in Fe solid phases between redox zones to better understand heterogenous groundwater As contamination.

Recently, the influence of biogeochemical Fe–S–As cycling for As release and speciation in subsurface settings have been increasingly studied (Pi et al., 2018; Jeong et al., 2010; Kumar et al., 2020; Lemonte et al., 2017). The reduction of SO_4^{2-} and Fe(III) oxides can simultaneously occur at redox interfaces especially at neutral or slightly alkaline groundwater pH conditions (Bethke et al., 2011). On the one hand, saturation of Fe(II) and H_2S cause precipitation of Fe sulfides such as mackinawite (nominally FeS), pyrite (FeS_2), which can incorporate or adsorb As (Pi et al., 2017; Kocar et al., 2010; Mihaljevic, 2019). Furthermore, extra sulfide/S^0 may reduce poorly crystalline iron(III) oxides or produce As thiolations in porewaters, further increasing As mobilization potential in groundwater (Sun et al., 2016; Guo et al., 2016). To date, the majority of published studies on sediments collected from the flood deltas/basins from South and Southeast of Asia focused on the relationship between Fe mineralogy and As speciation. These high-As containing groundwater typically have extreme low or undetectable SO_4^{2-} concentrations. In contrast As contaminated groundwaters in inland basins, especially those with arid/semi-arid climate e.g. Hetao Basin, have high SO_4^{2-} concentrations (Wang et al., 2017). Such inland basins therefore represent the most suitable location to develop understanding of the interplay between Fe–S–As redox reactions and groundwater As concentration.

The Hetao Basin in North China is a typical alluvial-lacustrine inland basin draining the Yellow River. Groundwater As concentrations vary between $<$ 1 μg/L and 900 μg/L, with 70% of analyzed groundwater samples being higher than 10 μg/L (Guo et al., 2008). Groundwater SO_4^{2-} concentration is up to 3000 mg/L with median values around 90 mg/L (Guo et al., 2016). Previous isotopic and hydro-chemical studies showed that As mobilization was closely linked to the reduction of Fe (III) oxides and SO_4^{2-} (Guo et al., 2013; Guo et al., 2016; Jia et al., 2014). However, there is so far no detailed mineralogical evidence about Fe–S–As coupled reactions in the sediments. In this study, we analyzed sediments from the Hetao Basin with a range of geochemical based techniques with spectroscopic (XAS, ^{57}Fe Mössbauer) and electron microscopic techniques to (1) identify different redox zones along a sediment core depth profile (2) examine vertical changes in the coupling between mineral phases and As, Fe and S speciation, and (3) understand the influence of Fe-S-As coupled minerals on groundwater As concentrations.

2. Material and methods

2.1. Field area

The Hetao Basin, covering an area of 13,000 km^2, is one of the typical alluvial-lacustrine Quaternary inland basins in northern China within the Yellow River catchment area. Groundwater is mainly extracted from depths $<$ 100 m for irrigation usage, with family-based drinking water mainly obtained from depths of 20–30 m. Groundwater tables are vulnerable to irrigations, and have been shown to drop as a result of extraction (from mid-April to early September) (Zhang et al., 2020). The study area (Shahai) is located in the flat plain of the Hetao Basin, and it is one of the areas' most seriously affected by groundwater As contamination. Further information about the study area is detailed in (Zhang et al., 2020; Wang et al., 2020).

2.2. Well installation, sediments sampling and groundwater sampling

A multi-level well (K1) was drilled by CUGB (China University of Geoscience, Beijing) in October 2015 using a circulatory drilling method. After the core sections were brought to the surface, sediments were cut into 10 cm segments and immediately wrapped with tinfoil, and sealed in N_2-purged bags. Subsamples (5 cm segments) were transported to Karlsruhe Institute of Technology (KIT) and stored at − 80 °C. The physical parameters and chemical compositions of the groundwater were monitored from April to November 2016 (six times during the non-irrigation season and eleven times during irrigation season) by members of China University of Geosciences (Beijing) (CUGB). Further details about sediment sampling, and groundwater monitoring as well as water samples analyses are detailed in (Zhang et al., 2020; Wang et al., 2020).

2.3. Bulk sediment characterization

Part of each sample was freeze-dried and ground into a powder. The basic characterization of the sediments described in Wang et al. (2020) was complemented in the current study with detailed analyses. For this, iron content in the sediments was analyzed by wavelength dispersive X-ray spectrometry (WDX, S4 Explorer, Bruker AXS) with measurement accuracy (within ± 5%) being regularly controlled with a standard material (AGV-1, USGS). Total sulfur (TS) and organic carbon (TOC) content were measured by carbon-sulfur-analyzer (CS-2000, Leybold Heraeus, Germany) with TOC obtained after removing inorganic carbon by repeated addition of 20% HCl (Superpure, Merke). The measurement accuracy and precision (100 ± 2%) was regularly checked with a steel standard 92400-3050 (Eltra). Arsenic contents in the sediments was determined by digestion prior to measurement by Hydride Generation Flow Injection Atomic Absorption Spectroscopy (HG-FIAS). The details about acid digestion method is provided in Supplementary text 1. The recovery (100 ± 5%) was regularly checked by including standards GXR-5 and RGM-1 into the digestion workflow. The detection limit of the HG-FIAS analyses was 0.1 μg/L.

2.4. Sequential extractions for As and 2 M HCl extractions

A five-step sequential extraction was used to analyze As partitioning in the sediments. The extraction procedure is shown in Table S1 and is based on Keon et al. Keon et al., (2001) and Poulton and Canfield (Poulton and Canfield, 2005): (1) "ligand-displaceable" (1.0 M $H_2PO_4^-$, pH = 5.0, S1), (2) "AVS (acid volatile sulfides), carbonates-precipitated" (1.0 M $CHCOO^-$, pH = 4.5, S2), (3) "amorphous Fe oxides and magnetite-precipitated" (0.17 M oxalic acid, pH = 3.0, S3), (4) "crystalline Fe oxides-precipitated" (citrate-bicarbonate-dithionite (CBD), S4), and (5) "Fe(II) sulfides-precipitated nominally from dissolution of pyrite" (12 M HNO_3, S5). For the extraction, 0.5 g of fresh sediments was weighed into centrifuge tubes and shaken at 300 rpm followed by addition of an appropriate amount of deoxygenated chemical solution. After each extraction step, solutions were filtered using 0.45 μm cellulose acetate filters (Whatman) followed by centrifugation at 4500 rpm for 15 min. Resulting, samples were washed once using 50 mL ultrapure water. Arsenic and Fe concentrations were measured by inductively coupled plasma mass spectrometry (ICP-MS, X-Series, Thermo Fisher),

and the resulting extracted As from each step was converted into As content in the dried bulk sediments.

In a second extraction mode, we used HCl extraction with fresh sediments to obtain the reactive Fe phases (Schaefer et al., 2017). For this extraction, around 2 g sediments were weighed into centrifuge tubes, mixed with 15 mL 2 M HCl (Superpure, Merck) and shaken. After 20 h, the solutions were filtered through 0.45 μm cellulose acetate filters (Whatman). Total Fe concentration was measured by inductively coupled plasma-optical emission spectrometry (ICP-OES, Spectro CirosCCD, Kleve, Germany). The Fe(II) concentration in the resulting extracts was measured by photometry at 562 nm using the ferrozine method (Viollier et al., 2000).

2.5. Electron microscopy

Parts of the sediment samples were separated from intact cores and embedded in an As free-resin (Araldite, 2020) and dried in a glovebox (Jacomex, 100% Ar). Sections of 1-mm thickness were cut and polished down to a thickness of 80 μm. Thin sections were stored in the glovebox until analysis. Carbon-coated thin sections were imaged and spectrally analyzed at the GFZ Research Center for Geosciences in Potsdam, Germany, using field emission scanning electron microscope (FE-SEM, Zeiss Ultra Plus) equipped with an energy dispersive X-ray (EDX) detector for qualitative elemental analyses. Images were acquired at an acceleration voltage of 3 kV using a 10 mm aperture distance using an In-lens secondary electron detector.

2.6. ^{57}Fe Mössbauer spectroscopy

Selected sediments were analyzed using ^{57}Fe Mössbauer spectroscopy at the University of Tübingen, Germany. Approximately 100 mg sediments were separated from each intact core for analysis. Inside a glovebox (100% N_2 atmosphere), dried sample powders were loaded into Plexiglas holders (area 1 cm^2), forming a thin disc. Samples were kept in airtight jars under anoxic conditions at − 20 °C until measurement. Holders were inserted into a closed-cycle exchange gas cryostat (Janis cryogenics) under a backflow of He to minimize exposure to air. Spectra were collected at 20 K using a constant acceleration drive system (WissEL) in transmission mode with a ^{57}Co/Rh source. All spectra were calibrated against a 7 μm thick α-^{57}Fe foil that was measured at room temperature. The analysis was carried out using Recoil (University of Ottawa) and the Voigt Based Fitting (VBF) routine (Rancourt and Ping, 1991), with the half width at half maximum (HWHM) constrained to 0.13 mm/s during fitting.

2.7. Bulk X-ray absorption spectroscopy

The speciation of As, S and Fe in selected sediment samples were measured using X-ray absorption spectroscopy (XAS) analysis at the SUL-X beamline at the synchrotron radiation facility of the KIT. Samples were ground into powder after drying in a glovebox (Jacomex, 100% Ar) with O_2 level less than 1 ppm). A sample mass for Fe K-edge XAS analysis, calculated by the program XAFSmass, was mixed with boron nitride (Sigma-Aldrich) before analysis. For As and Fe K-edge XAS analysis, powdered samples were suspended in deoxygenated water in the glovebox, drop-casted onto Kapton tape, and sealed using a second piece of Kapton tape. For S K-edge XAS measurements, dried samples were directly loaded onto the Kapton tape surface. Prepared samples were stored in the N_2-filled bags to protect from O_2 before transferring into the measurement chamber. Samples are analyzed under ultra-vacuum conditions in the beam chamber. At least three scans were collected per sample for each As, Fe and S K-edge XAS spectrum. During the data collection, line shapes and peak positions were monitored, with no difference between scans for each sample, indicating no redox change during analyses. Data reduction and analysis of the XAS spectra were performed using the Athena software package (Ravel and Newville, 2005). Experimental and data analysis procedures are outlined in the Supplementary text 2. Besides the samples analyses here, we also compared our data with XAS spectra and Mössbauer spectra for sample from another depth (80.5 m) that had been previously analyzed (Wang et al., 2020).

3. Results

3.1. Vertical profile of groundwater chemical compositions and As concentration

Groundwater monitoring data in the well are detailed in Zhang et al. (2020). The data shows that in the shallow zone SO_4^{2-} concentrations increased from 400 mg/L to 1000 mg/L from 15 to 16 m to 27–28 m, but that it stabilized at around 200 mg/L in the deeper zone. Arsenic concentration also generally decreased with depths. Specifically, it increased from 90 μg/L at depth of 15–16 m to 120 μg/L at depth of 20–21 m and slightly decreased to 90 μg/L at depth of 27–28 m in the shallow zone, while it was less than 50 μg/L in the deep zone (Fig. 1).

3.2. Sediments profile characterization

A ~ 2 m thick clay layer located at a depth of 39.5 m separated the shallow and deep groundwater zone. Aquifer sediments were mainly composed of fine sand and silt, and the color varied from gray to dark gray. In general, sediments from the deep zone had a darker color than the shallow zone. A thin peat layer was identified at a depth of around 80 m with dark color (Fig. 1). Lithology profile of the borehole presents general sedimentation textures in the Hetao Basin (Guo et al., 2016; Guo et al., 2016).

Total organic carbon (TOC) contents ranged from 0.04% to 0.59% with lower TOC contents in the aquifer sediments (~0.05%). Surface sediments had higher S content (~ 1000 mg/kg) than aquifer sediments (average 285 mg/kg). Iron content in the sediments ranged from ~1% to ~ 6% with lower Fe content shown in silt/sand. Sediments had As contents ranging from 5 mg/kg to 46 mg/kg, while primary aquifer sand/silt contained 5 mg/kg to 9 mg/kg (Fig. 2). Highest As contents were found in sediment samples from ~29 m (38 mg/kg) and 80 m (46 mg/kg).

3.3. Sediments mineralogy and iron speciation

Predominant minerals in the sediments included quartz, feldspars, mica and clay minerals (Wang et al., 2019). Additional clastic trace minerals including hornblende, augite and ilmenite were qualitatively identified by SEM-EDX analysis (data not shown). Iron oxides which might have different morphologies were identified (Fig. 3a, b and c). In most cases, the Fe oxides were surrounded by or coated on the surface of clay minerals. In addition, Fe sulfides (nominally FeS_2, pyrite as shown in the EDX spectra) were identified in samples from 29 m (Fig. 3d). A previous study identified the presence of greigite in the peats (at depth of 80 m) (Wang et al., 2020) (Fig. 3e).

Mössbauer spectroscopic analysis suggested that Fe was present in several phases including: Fe(II), silicate-bound Fe(III), or goethite/hematite (Fig. 4**a** and Table S3). The hyperfine parameters of the Fe(II) phase (isomer shift: 1.19–1.27 mm/s and quadrupole splitting: 2.34–2.85 mm/s) are potentially indicative of the phyllosilicates shown in the sediments. A narrow doublet (isomer shift: 0.41–0.48 mm/s, quadrupole splitting: 0.77–1.16 mm/s) was also required for an accurate fit which is indicative of ferric ions (Fe^{3+}) that could correspond to a phyllosilicates, though the presence of short range ordered phases (e.g. ferrihydrite) or low spin ferrous ion (Fe^{2+}) phases (e.g. pyrite) cannot be ruled out (Davey et al., 1988). From the Liner combination fitting (LCF) of the Fe K-edge EXAFS spectra, it was revealed that goethite and hematite comprised 12–35% (mol%) of the Fe speciation in the sediments (Fig. 4b and Table 1). The difference between the Fe K-edge EXAFS fits

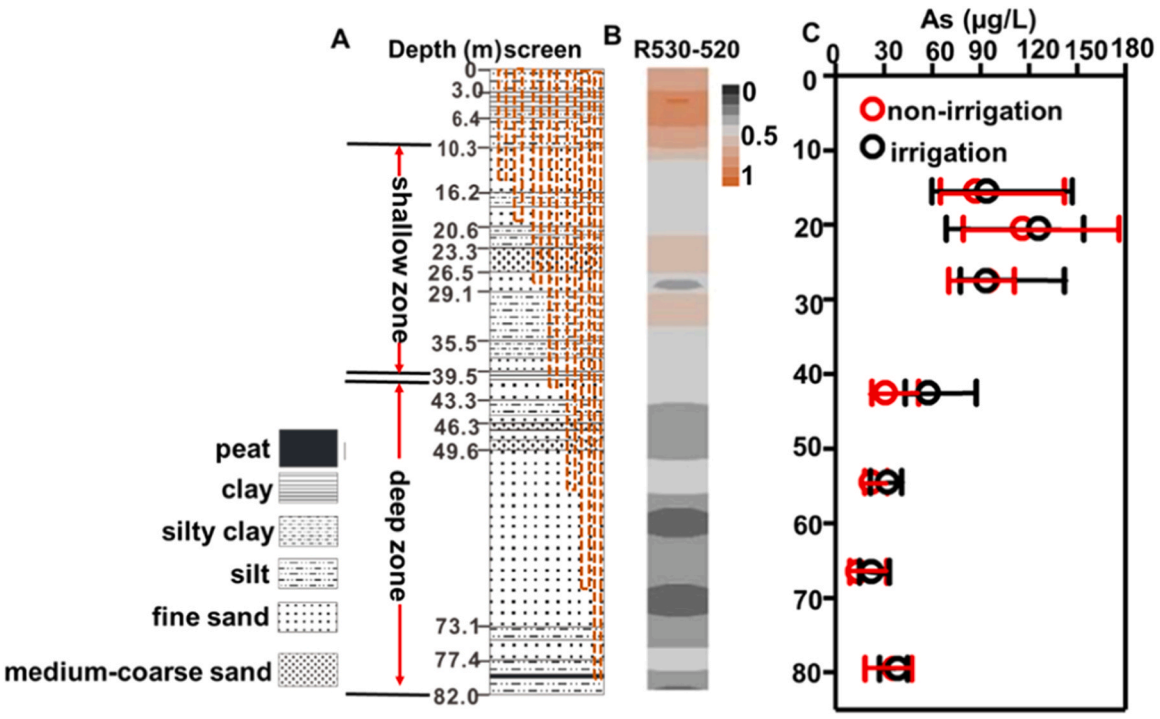

Fig. 1. Plots of sediments lithologies (A), depths of screens, difference in reflectance at 530 nm and 520 nm for the sediments (B), and monitoring data for groundwater As concentration (C). Difference in reflectance between 530 nm and 520 nm indicated the color of collected sediments (Horneman et al., 2004). The center circle showed the median value of As concentration in each screen, while the edge of bars showed the min and max values. The reflectance data and groundwater As monitoring data are previously shown in Zhang et al. (2020).

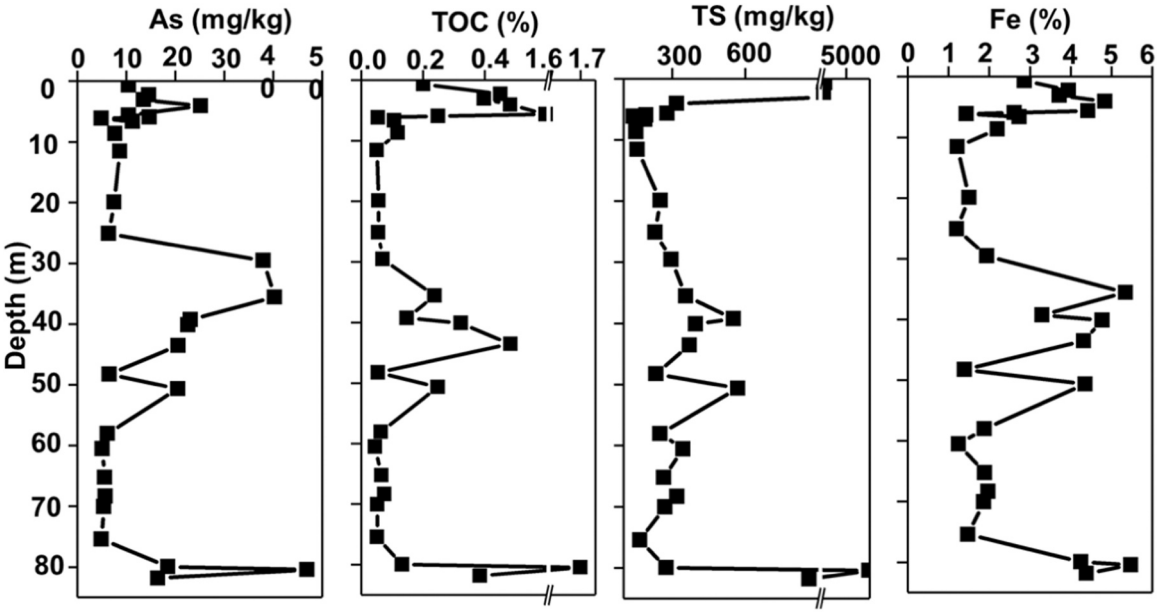

Fig. 2. Depth profile of As, total organic carbon (TOC), total sulfur (TS) and Fe content in the sediments. The data is referred to Wang et al. (2020).

and the Mössbauer fits in terms of Fe(III) oxides contents was less than 10% and which is considered acceptable (Thomasarrigo et al., 2014) (Table 1 and Table S3).

Iron sulfides were shown as mono FeS (mackinawite) in most aquifer sediments with primarily low content indicated by Fe K-edge EXAFS fitting (Fig. 4b). However, pyrite was not detected at the depth of 29 m as revealed by SEM-EDX, likely due to an abundance of pyrite is lower than the detection limit of Fe EXAFS fits, which has been estimated to be 5% by fitting a set of mixed standards with known fractions (Chen et al., 2017; Shaheen et al., 2016).

The redox characteristics of Fe phases was deduced from the combined 2 M HCl extractions and Fe K-edge XANES. The reactive Fe extracted by 2 M HCl included poorly crystalline Fe(III) oxides, acid volatile sulfides (AVS), carbonates as well as part of Fe adsorbed or incorporated in the silicates (Horneman et al., 2004; Eiche et al., 2009; Wallmann et al., 1993). This extractable Fe comprised 28–51% of total Fe in the sediments (Table S5), while the Fe(II) content ranged from 29% to 72% of total extractable Fe (except peat layer) (Fig. 5a). Noticeably,

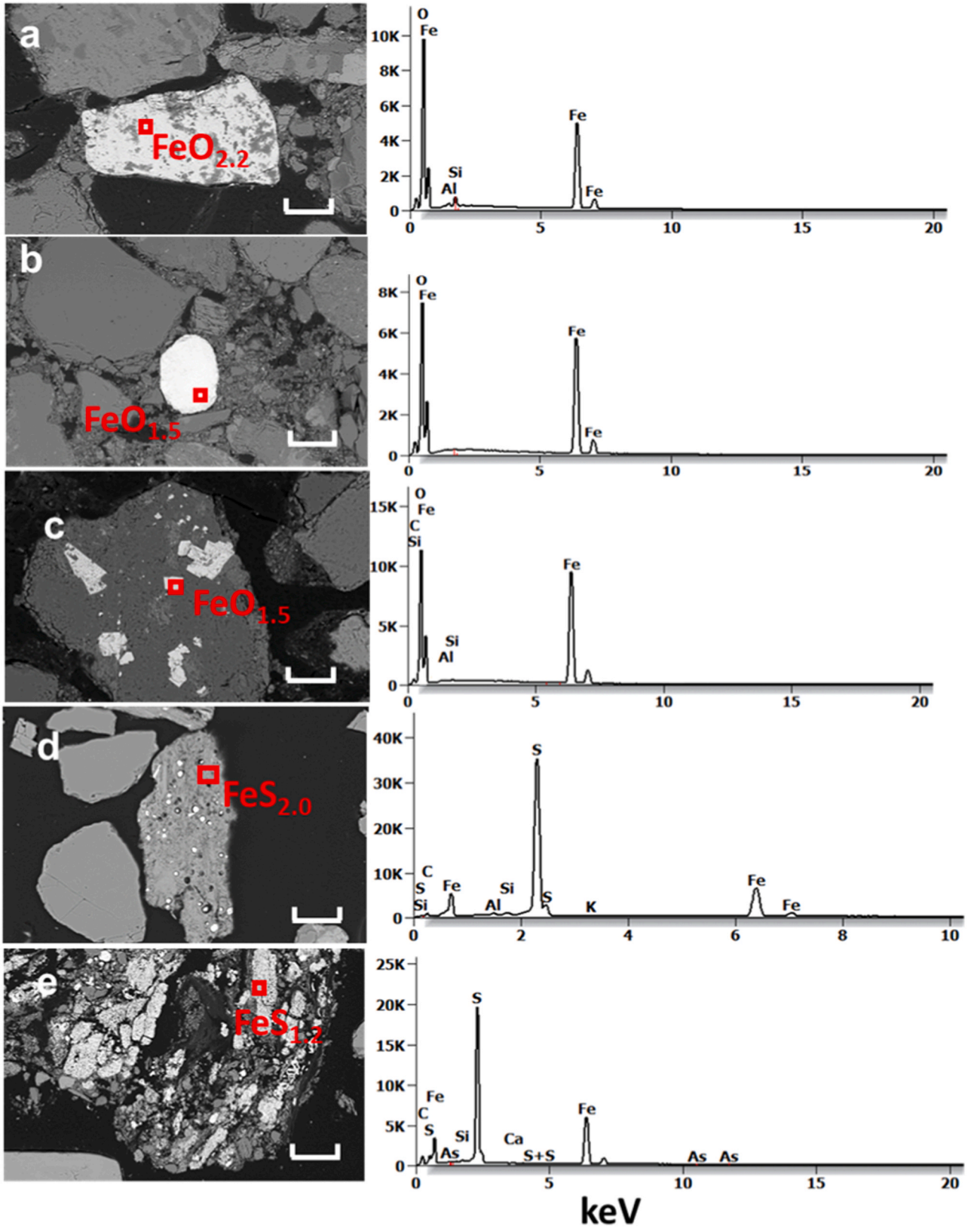

Fig. 3. Iron oxides/Fe sulfides characterized by SEM-EDX. The Fe oxides shown in primary sediments (a, b, c), Fe sulfides shown at depth of 29 m and 80 m (d, e). The EDX spectra corresponded to chemical compositions of minerals marked with the red square in the SEM images and the EDX data was shown in Table S2. The scale bar in each image represents 40 μm.

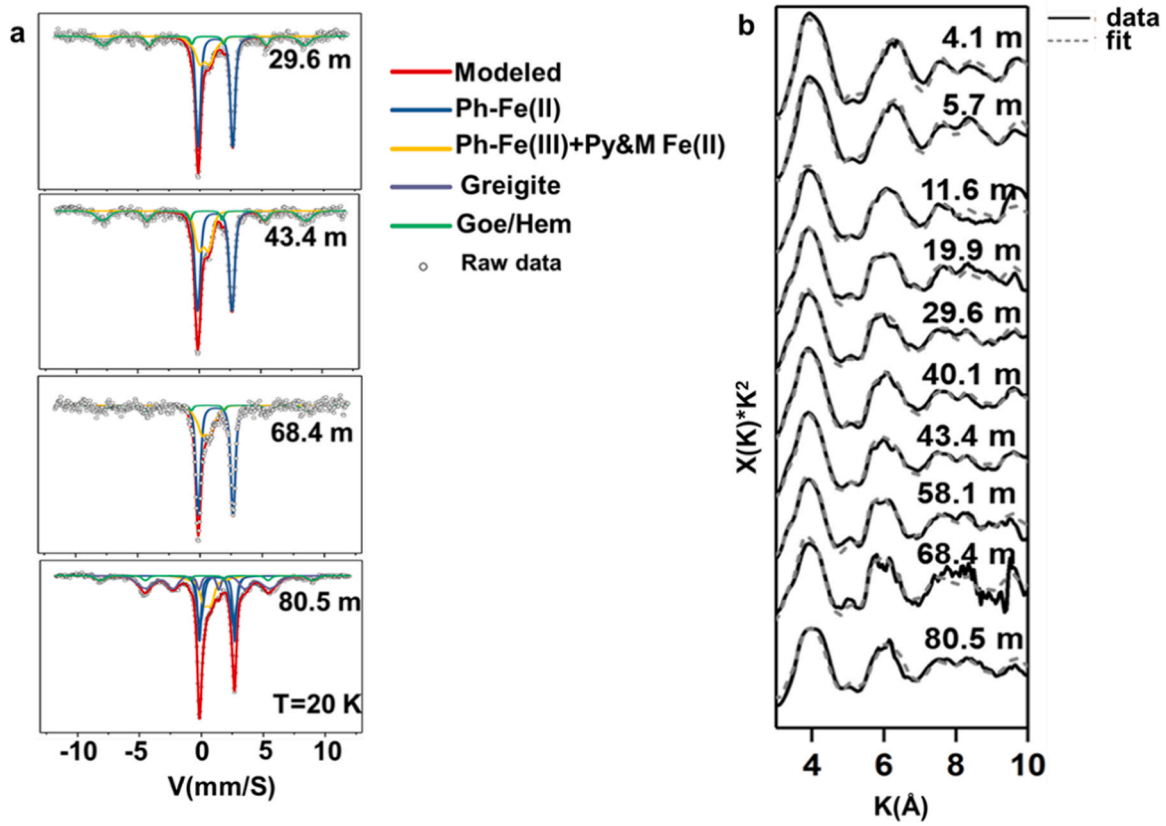

Fig. 4. The ^{57}Fe Mössbauer spectra was collected at 20 K for sediments (a), pH phyllosilicates; py: pyrite; M: mackinawite; Goe: goethite; Hem: hematite. Liner combination fitting (LCF) results of Fe K-edge EXAFS spectra (b), black lines represented experimental data for samples and model compound spectra used for fitting, and gray dashed lines represented LCF. Fe K-edge EXAFS reference spectra are shown in Fig. S1. Mössbauer and Fe K-edge EXAFS spectra for sediments from depth of 80.5 m are referred from Wang et al., (2020).

Table 1
Summary of S, Fe and As K-edge XANES or EXAFS LCF fitting results.

Depth (m)	Mineralogical composition (% mol Fe)								
	EXAFS								
	illite	biotite /chlorite		hematite	goethite	Fe sulfide			R^2
4.1	53 (0.4)	10 (2.0)		12 (1.9)	24 (5.8)	–			0.0521
5.7	56 (4.4)	10 (2.2)		10 (2.0)	25 (5.7)	–			0.0471
11.6	30 (6.2)	34 (4.7)		10 (2.9)	18 (10.3)	8 (4.9)			0.1219
19.9	24 (4.8)	41 (3.6)		11 (2.3)	16 (4.2)	10 (3.8)			0.0809
29.6	18 (3.2)	55 (4.7)		7 (1.5)	20 (2.9)	–			0.0467
40.1	31 (4.8)	42 (1.3)		9 (1.0)	15 (2.3)	–			0.0240
43.4	26 (2.9)	43 (2.2)		5 (1.4)	17 (4.5)	–			0.0305
58.1	23 (7.9)	46 (3.3)		–	14 (3.9)	15 (3.5)			0.0743
68.4	31 (7.2)	49 (13)		–	12 (6.3)	5 (5.7)			0.1711
80.5	37 (4.4)	19 (2.4)		–	–	39 (3.3)			0.0911
Depth (m)	Mineralogical composition (% mol As)					Mineralogical composition (% mol S)			
	XANES first-derivative					XANES			
	realgar	arsenopyrite	As (III)-Fh	As (V)-Fh	R^2	sulfates	sulfides	S_0	R
4.1	–	–	16 (2.5)	84 (0)	0	–	–	–	–
5.7	–	–	46 (0.6)	54 (0.6)	0.0057	87 (1.6)	–	13 (1.6)	0.0575
11.6	–	–	38 (4.5)	62 (1.0)	0.0170	61 (7.7)	23 (5.4)	16 (5.4)	0.0416
19.9	7 (0.9)	–	44 (1.4)	49 (0.6)	0.0074	89 (0.8)	11 (1.3)	–	0.0160
29.6	–	62 (3.7)	21 (0.7)	17 (0.5)	0.0102	93 (1.8)	7.3 (0.9)	–	0.0185
40.1	–	–	76 (0.6)	24 (0.8)	0.0072	70 (1.5)	6.5 (8.3)	23 (8)	0.0710
43.4	–	–	70 (3.4)	30 (1.0)	0.0213	79 (2.0)	–	21 (1.4)	0.0534
58.1	9 (1.5)	–	63 (1.3)	28 (0.8)	0.0123	49 (0.8)	51 (7.6)	–	0.0368
68.4	–	–	60 (0.9)	40 (0.9)	0.0195	56 (9.4)	23 (7)	21 (7)	0.0680
80.5	40 (5.0)		50 (1.8)	10 (1.1)	0.0197	2 (0.7)	92 (0.7)	6 (0.6)	0.0058

–: samples not measured, -: not detected or abundance lower than 5%. Values within brackets indicate standard deviation, Fe sulfide exists as FeS, except it shows as greigite in the depth of 80.4 m. Results for samples from depth of 80.5 m are referred to Wang et al., (Wang et al., 2020).

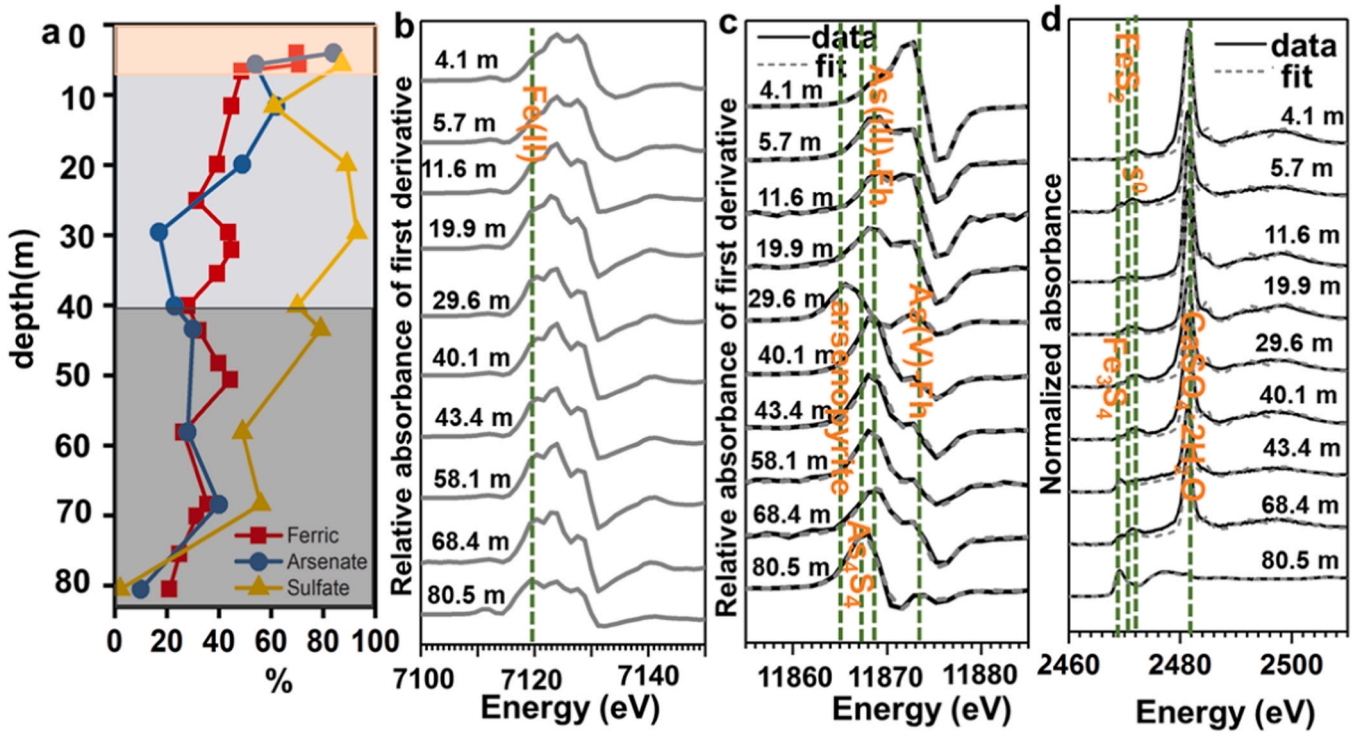

Fig. 5. Depth patterns of ferric fraction from 2 M HCl extraction, arsenate fraction (mol%) resulting from As K-edge derivative XANES fitting, and sulfate fraction (mol%) from S K-edge XANES fitting (a). 1st derivative of Fe K-edge XANES data (b), 1st derivative of As K-edge XANES data and fits (c), sulfur K-edge XANES data and fits (d), vertical dashed lines corresponded to peak positions of respective speciation/reference spectra. The reference spectra are shown in Fig. S1. The As K-edge derivative XANES data and sulfur K-edge XANES data for sample from depth of 80.5 are cited from previous study (Wang et al., 2020).

the Fe(II)/Fe ratio obtained from the 2 M HCl extractions is not comparable to the Mössbauer result, as Mössbauer results showed all Fe in the sediments instead of reactive Fe. Depth patterns of the leached Fe (II)/Fe_{total} showed increasing trend with depth (R^2 = 0.55, Fig. 6a), while it sharply increased from 30% to 50% at a depth of 7 m (Fig. 5**a**). In the Fe K-edge XANES spectra, a peak at an energy of ~7120 keV suggests the presence of Fe(II) phases (Chen et al., 2017; O'Day et al., 2004), the intensity of these generally increased with depth, consistent with the results from the 2 M HCl extractions. Furthermore, Fe K-edge EXAFS showed that the proportion of Fe(III) oxides decreased with depth (R^2 = 0.94) (Fig. 6b), comprising of 35 mol% of the Fe species in the top sediments (~ 7 m), decreasing to 27–28% in the shallow zone and further decreasing to 22–12% in the deep zone. Unfortunately, Mössbauer result cannot be used to indicate the redox profile, when only few samples were analyzed.

3.4. Arsenic extractability

Desorbable (ligand-reducible) As (1.0–11 mg/kg) accounted for 23–56% of the total extractable As in the sediments, while reducible As (sum of ammonium oxalate and CBD extractable) (2.0–10.4 mg/kg) accounted for 32–65% of total extractable As (Table 2). Only a limited amount of As was extracted by $CHCOO^-$ (< 1.2 mg/kg) and HNO_3 (< 1.4 mg/kg) (except for peat layers). The contents of desorbable and reducible As were positively correlated to Fe(III) oxides (R^2 = 0.89, Fig. 6c), showing a decreasing trend with depth. Noticeably, the extractable As content at a depth of 29 m was much lower than 38 mg/kg, and no pyrite-associated As could be extracted by HNO_3, which further suggests that pyrite was low in abundance and heterogeneously distributed in the sediments.

3.5. Arsenic and sulfur speciation

The LCF of the As K-edge XANES spectra (Fig. 5c and Table 1) revealed that arsenate comprised 28–84% of the total As in the primary sediments, but that its abundance sharply declined from 84% at a depth of 4 m to 54% at a depth of 6 m, and further decreasing with depth (R^2 = 0.59, Fig. 6d). Conversely, the arsenite content increased with depth. At a depth of 29 m, 62% of As was present as As sulfides (arsenian pyrite/arsenopyrite), consistent with the pyrite found in the sediments. The As sulfides accounted for 41% of total As in the peat layer (Fig. 5c and Table 1). Finally, sulfur K-edge XANES LCF showed that S mainly existed as SO_4^{2-} (vary from 49% to 93%). Reduced sulfur (including S(-I) and S(-II)) and zero-valent sulfur (S^0) was detected at most depths except in the surface sediments at 4 m. The ratio of reduced sulfur was generally higher in the deep zone than the shallow zone (Fig. 5d and Table 1).

4. Discussion

4.1. Sediment profile redox zonation

The surface sediments were dominated by oxidized phases including sulfates, As(V) species and Fe(III)-containing solid phases, due to oxygen penetration into sediments pores. Reduction of As(V) species, Fe(III), and SO_4^{2-} is present near the groundwater table (6–7 m). The co-occurrence of reduction reactions were independent of the thermodynamic redox ladder, which suggested the electron accepting process followed the order of As(V) > Fe(III) > SO_4^{2-} (Lovley et al., 1994; Borch et al., 2009). These observations are consistent with previous suggestions that Fe(III) and SO_4^{2-} reduction co-occur in near neutral or slightly alkaline subsurface environments (Bethke et al., 2011). Underlying the aquitard (~ 40 m), SO_4^{2-} reduction generally increases with relatively higher ratio of reduced sulfur species, which is consistent with lower redox values in the groundwater of deep zone (Zhang et al., 2020). These results together indicate that redox zones in the alluvial-lacustrine sediments of the Hetao Basin are generally controlled by the physiographic properties, including the groundwater table and sediment depths. In contrast, the aquifer redox conditions in the floodplain of

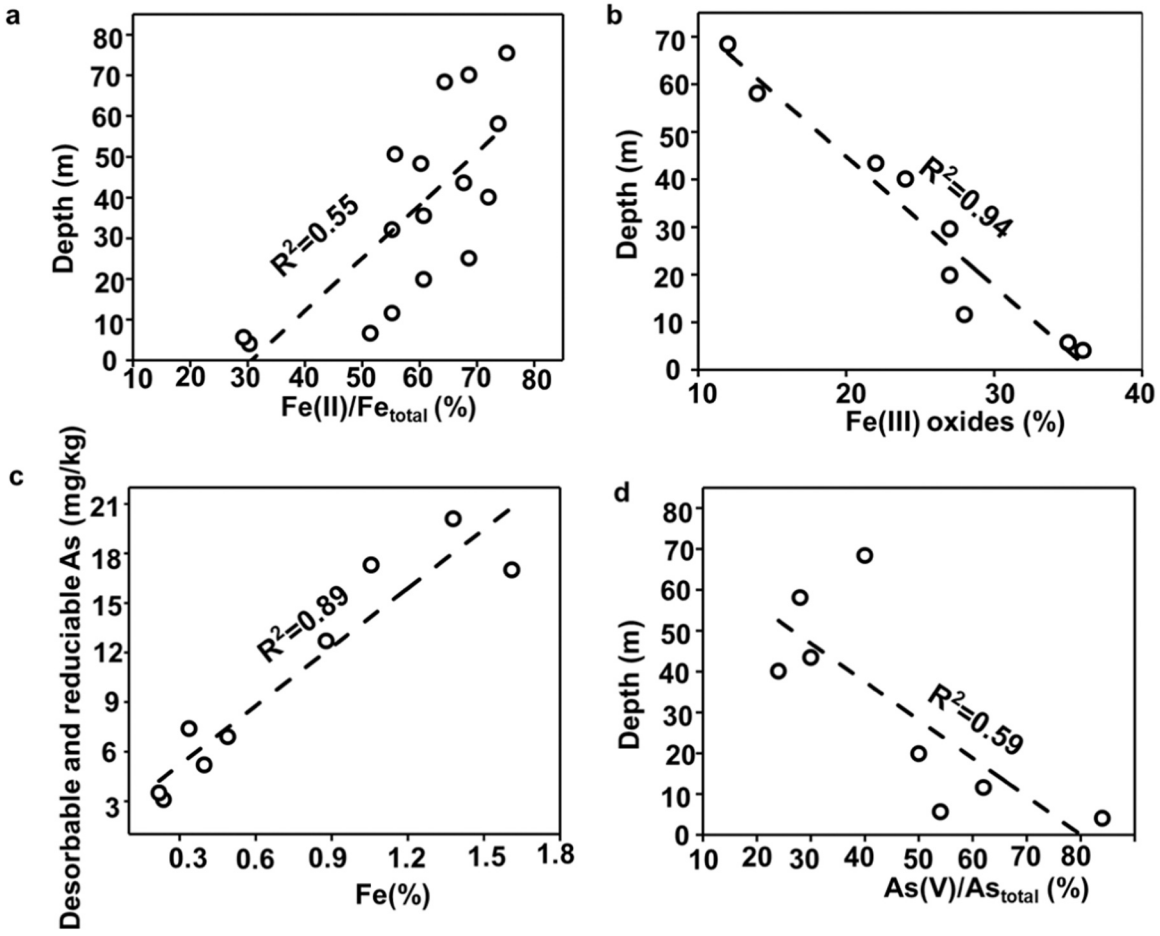

Fig. 6. Bivariate correlation between sample depth and ratio of Fe(II)/Fe from 2 M HCl extractions (a), bivariate correlation between sample depth and abundance of Fe(III) oxides (hematite and goethite) characterized by LCF in the Fe K-edge EXAFS range, correlation between sum of desorb-able(ligand-displaceable) and reducible As content and sum of goethite and hematite (calculated as Fe content) characterized by Fe K-edge EXAFS fitting (c), correlation between depth and arsenate fraction resulting from As K-edge derivative XANES LCF (d).

Table 2
Summary of extracted As contents (mg/kg) from each sequential step.

Depth (m)	S1	S2	S3	S4	S3 + S4	S5	As extracted	Total As
4.1	7.0	0.6	6.4	3.6	10	2.4	20.0	22
5.7	10.8	1.2	6.6	2.7	9.3	1.0	22.3	15
6.7	2.5	0.3	2.2	5.0	7.2	1.1	11.1	11
11.6	2.8	0.4	1.8	2.8	4.6	0.4	8.2	9
19.9	2.2	0.3	1.4	1.6	3	0.6	6.1	8
25.1	2.2	0.3	1.1	1.4	2.5	0.4	5.4	6
29.6	3.0	0.5	1.4	2.5	3.9	0.8	8.3	9
35.6	9.9	1.1	3.0	5.2	8.2	1.4	20.6	40
40.1	11.0	1.1	3.1	3.2	6.3	1.4	19.8	23
43.6	8.1	0.8	3.0	1.6	4.6	0.9	14.4	21
48.3	1.6	0.3	1.0	1.5	2.5	0.7	5.1	7
50.5	4.8	1.2	4.4	6.0	10.4	0.9	17.3	21
58.1	1.5	0.4	0.8	0.8	1.6	0.6	4.1	6.1
68.4	1.8	0.3	0.9	0.8	1.7	0.5	4.3	5.7
70.1	1.9	0.3	0.8	1.2	2	0.5	4.7	5.4
75.5	1.0	0.3	1.4	0.9	2.3	0.5	4.1	4.9
80.4	31.9	12.9	3.2	2.4	5.6	3.9	54.3	46

South and Southeast Asia such as the Red River Delta, the Mekong River Delta are controlled by depositional environments with reducing conditions widely developed in the Holocene fluvial sediments, while the Pleistocene aquifer are characterized by sub-oxic conditions (Postma et al., 2012; Gillispie et al., 2019; Viet et al., 2020).

Noticeably, redox heterogeneities exist in the sediments. Even though the reduced Fe, As and S species generally increase with depth, some sediment lenses show pronounced peaks, related to the redox heterogeneities in the sediments. For example, organic carbon-rich lenses including clay and peat layers have more reduced As, Fe and S species in comparison with surrounding sediments. High amounts of organic matter in those layers stimulates the in-situ reduction of As, Fe and S and therefore Fe sulfide formation.

4.2. Speciation and reactivity of Fe–S–As coupled minerals in the sediments profile

Dominant Fe(III) oxides in the sediments of the Hetao Basin are goethite and hematite, similar to sediments from the Red River Delta and the Mekong Delta (Burnol and Charlet, 2010; Postma et al., 2007; Postma et al., 2010; Stuckey et al., 2015). In contrast to the formation of secondary Fe(II) or Fe(II/III) solid phases such as siderite, vivianite, and magnetite which is well-documented in the floodplains of South and Southeast of Asia, in the sediments of the Hetao Basin (Horneman et al., 2004; Sø et al., 2018), only As containing Fe sulfides were detected. However, trace amounts of Fe sulfides do not appear to be the major sink of Fe(II), which is a consequence of reductive dissolution of the ample present Fe(III) oxides. This indicates that Fe(II) is most likely adsorbed/substituted back into clay minerals which can provide a large surface for Fe adsorption (Stumm and Sulzberger, 1992; Van Groeningen et al., 2020). The relatively higher adsorption affinity for Fe(II) is probably due to slightly alkaline pH conditions in the aquifers, in such adsorption of Fe(II) to clay minerals is favored at pH above 6.0 (Schultz and Grundl, 2004). This concept explains the lower average Fe concentration in the alluvial-lacustrine groundwater in the Yellow River catchment as well as decoupling of Fe and As concentration in the groundwater under reducing conditions (Guo et al., 2017; Pi et al., 2018).

Natural Fe(III) oxides are impure and are typically highly variable in crystallinity, incorporation or substitution of other elements in their structure is common, thus making predictions of their reactivities challenging (Sø et al., 2018). We used, a combination of quantification methods for our Fe(III) oxides and combined with Fe EXAFS LCF and As reactivities by sequential extractions. This enabled us to better understand of the As partition to Fe(III) oxides in the sediments. Correlations between Fe(III) oxides and desorbable and reducible As suggests that Fe (III) oxides are the main As carrier in the sediments. These findings corroborates with previous studies that the adsorption sites for As are limited and linked to the amount of Fe(III) oxides in aquifer sediments (Postma et al., 2016; Sø et al., 2018). The adsorption coefficient of As to Fe(III) oxides in the sediments of Hetao Basin is around 0.9×10^{-3}, based on the assumption that desorbable and reducible As are totally carried by Fe(III) oxides. A similar partition coefficient of As in Fe(III) oxides was documented for the Red River floodplain by Postma et al. (2016). The calculated adsorption capabilities of Fe(III) oxides for As provide the fundamental knowledge for modeling As mobilization in the groundwater especially in the alluvial-lacustrine aquifers draining the Yellow River and the Yangtze River.

Detection of mono Fe sulfides (mackinawite) in the primary sediments is consistent with the dark gray color found in the aquifer sediments, which is caused by Fe sulfides coating the sand particles (Hagiwara et al., 2011). Arsenic can form poorly crystalline arsenic sulfides that could adsorb to mackinawite (Farquhar et al., 2002). However, the adsorption efficiency of mackinawite for As is limited as indicated by As XANES analysis. This could be linked to the formation and stability of FeS in the groundwaters (Day et al., 2004). The further transformation of FeS to pyritie or greigite is a more likely process that provides the adsorption/incorporation sites and stable sinks for As. This was identified by the higher As content in the corresponding sediments than near-by layers and the existence of large proportions of As sulfides.

4.3. Significance of Fe–S–As coupled mineralization for geogenic groundwater As contamination

Redox cycling of Fe minerals in the redox front influences the partition of As. In the Hetao Basin, the groundwater table decreases during the irrigation season, allowing penetration of O_2 to cause the temporary formation of Fe(III) oxides by oxidation of Fe(II), therefore providing adsorption surfaces for dissolved As. Conversely, raising of the groundwater table and ensuing anoxic conditions will causes As release into groundwater via Fe(III) oxide reduction. Underlying the redox front, stable Fe and As reduction occurs simultaneously. Generally higher groundwater As concentrations are present in the shallow zone and less in the deep zone, even though the deep zone is more reducing. This can be due to lower abundance of Fe(III) oxides and desorbable and reducible As in the deep zone. The lower As concentration in the groundwater with less solid phase desorbable As and reducible As in the corresponding sediments intervals ($R^2 = 0.65$) (Fig. 7) further provides solid evidence that in-situ desorption of As from Fe(III) oxides causes groundwater As contamination. The decrease of Fe(III) oxide abundance and corresponding desorb-able/reducible As with depth can be related to the longer sediments reduction and flushing history. Sediments from deeper depths have longer exposure to reducing conditions than overlying sediments, corresponding to the accumulation of reduced phases (Fe(II), As(III)) and partial release of out of the system.

Redox heterogeneities in the sediment profile hinders the effort to estimate the redox reactions in the aquifer and thereby model groundwater As concentration. For example, localized formation of greigite and pyrite can very well provide a stable sink for As. Furthermore, S^0 detected in the sediments especially in the clay samples could lead to thiolation via the reaction between H_2S/S^0 and As species in the reduced sulfidic aquifer, which in turn can promote further As mobilization (Kumar et al., 2020; Planer-Friedrich et al., 2018; Stauder et al., 2005), Whether thioarsenate species exist in the groundwater and to what degree influences As mobility may also be related to the ratio of Fe, S and As in the sediments, which needs further investigation.

5. Conclusions

In this study, we have defined the redox profile of Fe–S–As in an alluvial-lacustrine inland Hetao basin. The sediment redox profile is generally controlled by physiographic features (e.g. groundwater table and sediment depths). Underlying the groundwater table, reduction of SO_4^{2-}, Fe and As co-occurs, while SO_4^{2-} reduction ratio is generally higher in the deep zone. Iron oxides seem to be the major carrier of As. The As mobilizes into groundwater mainly via in-situ desorption from Fe (III) oxides (goethite and hematite). The abundance of desorbable and reducible As content exhibited a decreasing trend with depth, which is most probably due to longer flushing history, during which part of As is flushed out of the system followed by reductive release into the groundwater. Iron sulfides are the main secondary minerals formed in the aquifer following changing redox and Fe(II) production. Among them, mackinawite was evidenced as having a limited adsorption/incorporating ability for As, while greigite and pyrite provide a more stable sink for As under reducing conditions. The heterogenous

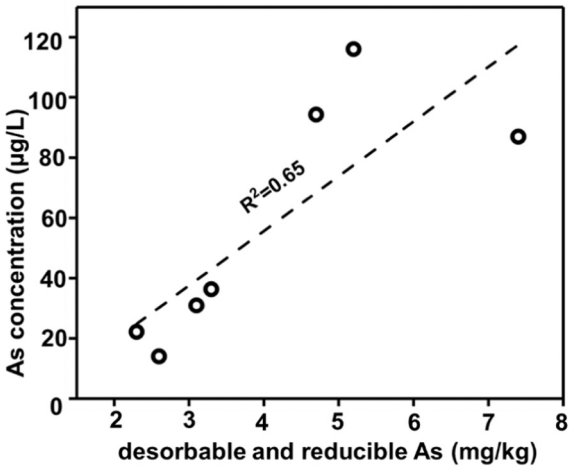

Fig. 7. Bivariate relationships between desorbable and reducible As in sediments and As concentration in the groundwater.

distribution and low contents of Fe sulfides formed in sediment lenses might contribute to the lower groundwater As concentrations under reducing conditions. The influences of such small-scale redox heterogeneity and their role for large-scale groundwater As pollution need further research.

CRediT authorship contribution statement

H.Y. Wang: investigation, writing–original draft, funding acquisition. **J. Göttlicher:** investigation, writing-review & editing. **J.M. Byrne:** investigation, writing–review & editing. **H. M. Guo:** writing–review & editing, funding acquisition. **L.G. Benning:** investigation, writing-review & editting. **S. Norra:** writing–review & editing, supervision, funding acquisition. The study is based on the Sino-German cooperation initiated by H. Guo and S. Norra and was inspired by their ideas.

Declaration of Competing Interest

The authors declare no conflict of interest.

Acknowledgments

The Authors are thankful for the technical assistance from Claudia Moessner (ICP-MS), Beate Oetzel (CSA), Sathish Mayanna (SEM-EDX). We Thank Ralf Steininger, Andrew Thomas for his support during collection of Fe, As and S K-edge XAS data at ANKA. The authors also acknowledge other members from CUGB group for their assistance during field trip to Hetao Basin and travel funding from GRACE graduate program at KIT. We are grateful for the constructive suggestios from three reviewers. The author Hongyan Wang is supported by Chinese scholarship Council (China) Grant no. 201606400055.

Appendix A. Supporting information

Supplementary data associated with this article can be found in the online version at doi:10.1016/j.jhazmat.2020.124924.

References

Bethke, C.M., Sanford, R.A., Kirk, M.F., Jin, Q., Flynn, T.M., 2011. The thermodynamic ladder in geomicrobiology. Am. J. Sci. 311, 183–210. https://doi.org/10.2475/03.2011.01.

Borch, T., Kretzschmar, R., Campbell, K., 2009. Biogeochemical redox processes and their impact on contaminant dynamics biogeochemical redox processes and their impact on contaminant dynamics. Environ. Sci. Technol. 15–23. https://doi.org/10.1021/es9026248.

Burnol, A., Charlet, L., 2010. Fe(II)-Fe(III)-bearing phases as a mineralogical control on the heterogeneity of arsenic in southeast Asian groundwater. Environ. Sci. Technol. 44, 7541–7547. https://doi.org/10.1021/es100280h.

Chen, C., Kukkadapu, R.K., Lazareva, O., Sparks, D.L., 2017. Solid-phase Fe speciation along the vertical redox gradients in floodplains using XAS and Mössbauer spectroscopies. Environ. Sci. Technol. 51, 7903–7912. https://doi.org/10.1021/acs.est.7b00700.

Davey, R.C., Macquaker, J.H.S., Siddiqi, M., Curtis, C.D., Williams, J.M., 1988. Applications of Mössbauer spectroscopy in the geochemistry of sedimentary rocks. Hyperfine Interact. 41, 771–774. https://doi.org/10.1007/BF02400504.

Day, P.A.O., Vlassopoulos, D., Root, R., Rivera, N., 2004. The influence of sulfur and iron on dissolved arsenic concentrations in the shallow subsurface under changing redox conditions. Proc. Natl. Acad. Sci. USA. https://doi.org/10.1073/pnas.0402775101.

Eiche, E., Kramar, U., Berner, Z., Norra, S., Berg, M., Neumann, T., 2009. Behaviour of As in sequential sediment extractions observed by muSy-XRF analysis,. Geochim. Et. Cosmochim. Acta 73 (supplement), 320.

Farquhar, M.L., Charnock, J.M., Livens, F.R., Vaughan, D.J., 2002. Mechanisms of arsenic uptake from aqueous solution by interaction with goethite, lepidocrocite, mackinawite, and pyrite: an X-ray absorption spectroscopy study. Environ. Sci. Technol. 36, 1757–1762. https://doi.org/10.1021/es010216g.

Fendorf, S., Michael, H.A., van Geen, A., 2010. Spatial and temporal variations of groundwater Arsenic in south and southeast Asia. Science 328, 1123–1127. https://doi.org/10.1126/science.1172974.

Frohne, T., Rinklebe, J., Diaz-Bone, R.A., Du Laing, G., 2011. Controlled variation of redox conditions in a floodplain soil: impact on metal mobilization and biomethylation of arsenic and antimony. Geoderma 160, 414–424. https://doi.org/10.1016/j.geoderma.2010.10.012.

Gillispie, E.C., Matteson, A.R., Duckworth, O.W., Neumann, R.B., Phen, N., Polizzotto, M. L., 2019. Chemical variability of sediment and groundwater in a Pleistocene aquifer of Cambodia: implications for arsenic pollution potential. Geochim. Cosmochim. Acta 245, 441–458. https://doi.org/10.1016/j.gca.2018.11.008.

Guo, H., Yang, S., Tang, X., Li, Y., Shen, Z., 2008. Groundwater geochemistry and its implications for arsenic mobilization in shallow aquifers of the Hetao Basin, Inner Mongolia. Sci. Total Environ. 393, 131–144. https://doi.org/10.1016/j.scitotenv.2007.12.025.

Guo, H., Liu, C., Lu, H., Wanty, R.B., Wang, J., Zhou, Y., 2013. Pathways of coupled arsenic and iron cycling in high arsenic groundwater of the Hetao basin, Inner Mongolia, China: an iron isotope approach. Geochim. Cosmochim. Acta 112, 130–145. https://doi.org/10.1016/j.gca.2013.02.031.

Guo, H., Wen, D., Liu, Z., Jia, Y., Guo, Q., 2014. A review of high arsenic groundwater in Mainland and Taiwan, China: distribution, characteristics and geochemical processes. Appl. Geochem. 41, 196–217. https://doi.org/10.1016/j.apgeochem.2013.12.016.

Guo, H., Jia, Y., Wanty, R.B., Jiang, Y., Zhao, W., Xiu, W., Shen, J., Li, Y., Cao, Y., Wu, Y., Zhang, D., Wei, C., Zhang, Y., Cao, W., Foster, A., 2016. Contrasting distributions of groundwater arsenic and uranium in the western Hetao basin, Inner Mongolia: implication for origins and fate controls. Sci. Total Environ. 541, 1172–1190. https://doi.org/10.1016/j.scitotenv.2015.10.018.

Guo, H., Zhou, Y., Jia, Y., Tang, X., Li, X., Shen, M., Lu, H., Han, S., Wei, C., Norra, S., Zhang, F., 2016. Sulfur cycling-related biogeochemical processes of arsenic mobilization in the western Hetao Basin, China: evidence from multiple isotope approaches. acs.est.6b03460 Environ. Sci. Technol. 50, 12650–12659. https://doi.org/10.1021/acs.est.6b03460.

Guo, H., Zhang, D., Ni, P., Cao, Y., Li, F., Jia, Y., Li, H., Wan, L., Wang, G., 2017. On the scalability of hydrogeochemical factors controlling arsenic mobility in three major inland basins of P.R. China. Appl. Geochem. 77, 15–23. https://doi.org/10.1016/j.apgeochem.2016.05.006.

Hagiwara, H., Akai, J., Terasaki, K., Yoshimura, T., Luo, H., 2011. Black colored sandy sediments caused by bacterial action, and the mechanism for arsenic enrichment of groundwater in Inner Mongolia. Appl. Geochem. 26, 380–393. https://doi.org/10.1016/j.apgeochem.2010.12.011.

Horneman, A., van Geen, A., Kent, D.V., Mathe, P.E., Zheng, Y., Dhar, R.K., O'Connell, S., Hoque, M.A., Aziz, Z., Shamsudduha, M., Seddique, A.A., Ahmed, K.M., 2004. Decoupling of As and Fe release to Bangladesh groundwater under reducing conditions. Part I: evidence from sediment profiles. Geochim. Cosmochim. Acta 68, 3459–3473. https://doi.org/10.1016/j.gca.2004.01.026.

Islam, F.S., Gault, A.G., Boothman, C., Polya, D. a, Charnock, J.M., Chatterjee, D., Lloyd, J.R., 2004. Role of metal-reducing bacteria in arsenic release from Bengal delta sediments. Nature 430, 68–71. https://doi.org/10.1038/nature02638.

Jeong, H.Y., Han, Y., Park, S.W., Hayes, K.F., 2010. Aerobic oxidation of mackinawite (FeS) and its environmental implication for arsenic mobilization. Geochim. Cosmochim. Acta 74, 3182–3198. https://doi.org/10.1016/j.gca.2010.03.012.

Jia, Y., Guo, H., Jiang, Y., Wu, Y., Zhou, Y., 2014. Hydrogeochemical zonation and its implication for arsenic mobilization in deep groundwaters near alluvial fans in the Hetao Basin, Inner Mongolia. J. Hydrol. 518, 410–420. https://doi.org/10.1016/j.jhydrol.2014.02.004.

Keon, N.E., Swartz, C.H., Brabander, D.J., Harvey, C., Hemond, H.F., 2001. Validation of an arsenic seqential extraction method for evaluating mobility in sediments. Environ. Sci. Technol. 35, 2778–2784. https://doi.org/10.1021/es001511o.

Kocar, B.D., Borch, T., Fendorf, S., 2010. Arsenic repartitioning during biogenic sulfidization and transformation of ferrihydrite. Geochim. Cosmochim. Acta 74, 980–994. https://doi.org/10.1016/j.gca.2009.10.023.

Kumar, N., Noël, V., Planer-friedrich, B., Besold, J., Lezama, J., Bargar, J.R., Brown, G.E., Fendorf, S., Boye, K., 2020. Redox heterogeneities promote thioarsenate formation and release into groundwater. Environ. Sci. Technol. 54, 3237–3244. https://doi.org/10.1021/acs.est.9b06502.

Larsen, O., Postma, D., Jakobsen, R., 2006. The reactivity of iron oxides towards reductive dissolution with ascorbic acid in a shallow sandy aquifer (Rømø, Denmark). Geochim. Cosmochim. Acta 70, 4827–4835. https://doi.org/10.1016/j.gca.2006.03.027.

Lemonte, J.J., Stuckey, J.W., Sanchez, J.Z., Tappero, R., Rinklebe, J., Sparks, D.L., 2017. Sea level rise induced arsenic release from historically contaminated coastal soils. Environ. Sci. Technol. 51, 5913–5922. https://doi.org/10.1021/acs.est.6b06152.

Lovley, D.R., Chapelle, F.H., Woodward, J.C., 1994. Use of dissolved H2 concentrations to determine distribution of microbially catalyzed redox reactions in anoxic groundwater. Environ. Sci. Technol. 28, 1205–1210. https://doi.org/10.1021/es00056a005.

McArthur, J.M., Ravenscroft, P., Safiulla, S., Thirlwall, M.F., 2001. Arsenic in groundwater: testing pollution mechanisms for sedimentary aquifers in Bangladesh. Water Resour. Res. 37, 109–117. https://doi.org/10.1029/2000WR900270.

Mihaljevic, M., 2019. Microbial sulfidogenesis of arsenic in naturally contaminated wetland soil. Geochim. Cosmochim. Acta 267, 33–50. https://doi.org/10.1016/j.gca.2019.09.021.

Nordstrom, D.K., 2002. Worldwide occurrences of arsenic in ground water. Science 296, 64–65. https://doi.org/10.1007/b101867.

O'Day, P.A., Rivera, N., Root, R., Carroll, S.A., 2004. X-ray absorption spectroscopic study of Fe reference compounds for the analysis of natural sediments. Am. Mineral. 89, 572–585. https://doi.org/10.2138/am-2004-0412.

Perez, J.P.H., Freeman, H.M., Brown, A.P., Van Genuchten, C.M., Dideriksen, K., S'Ari, M., Tobler, D.J., Benning, L.G., 2020. Direct visualization of arsenic binding on green rust sulfate. Environ. Sci. Technol. 54, 3297–3305. https://doi.org/10.1021/acs.est.9b07092.

Perez, J.P.H., Schiefler, A.A., Rubio, S.N., Reischer, M., Overheu, N.D., Benning, L.G., Tobler, D.J., 2021. Arsenic removal from natural groundwater using 'green rust': solid phase stability and contaminant fate. J. Hazard. Mater. 401, 123327 https://doi.org/10.1016/j.jhazmat.2020.123327.

Pi, K., Wang, Y., Xie, X., Ma, T., Su, C., Liu, Y., 2017. Role of sulfur redox cycling on arsenic mobilization in aquifers of Datong Basin, northern China. Appl. Geochem. 77, 31–43. https://doi.org/10.1016/j.apgeochem.2016.05.019.

Pi, K., Wang, Y., Postma, D., Ma, T., Su, C., Xie, X., 2018. Vertical variability of arsenic concentrations under the control of iron-sulfur-arsenic interactions in reducing aquifer systems. J. Hydrol. 561, 200–210. https://doi.org/10.1016/j.jhydrol.2018.03.049.

Pi, K., Wang, Y., Postma, D., Ma, T., Su, C., Xie, X., 2018. Vertical variability of arsenic concentrations under the control of iron-sulfur-arsenic interactions in reducing aquifer systems. J. Hydrol. 561, 200–210. https://doi.org/10.1016/j.jhydrol.2018.03.049.

Planer-Friedrich, B., Schaller, J., Wismeth, F., Mehlhorn, J., Hug, S.J., 2018. Monothioarsenate occurrence in bangladesh groundwater and its removal by ferrous and zero-valent iron technologies. Environ. Sci. Technol. 52, 5931–5939. https://doi.org/10.1021/acs.est.8b00948.

Podgorski, J., Berg, M., 2020. Global threat of arsenic in groundwater. Science 850, 1–31.

Polizzotto, M.L., Harvey, C.F., Li, G., Badruzzman, B., Ali, A., Newville, M., Sutton, S., Fendorf, S., 2006. Solid-phases and desorption processes of arsenic within Bangladesh sediments. Chem. Geol. 228, 97–111. https://doi.org/10.1016/j.chemgeo.2005.11.026.

Postma, D., Larsen, F., Minh Hue, N.T., Duc, M.T., Viet, P.H., Nhan, P.Q., Jessen, S., 2007. Arsenic in groundwater of the Red River floodplain, Vietnam: controlling geochemical processes and reactive transport modeling. Geochim. Cosmochim. Acta 71, 5054–5071. https://doi.org/10.1016/j.gca.2007.08.020.

Postma, D., Jessen, S., Hue, N.T.M., Duc, M.T., Koch, C.B., Viet, P.H., Nhan, P.Q., Larsen, F., 2010. Mobilization of arsenic and iron from Red River floodplain sediments, Vietnam. Geochim. Cosmochim. Acta 74, 3367–3381. https://doi.org/10.1016/j.gca.2010.03.024.

Postma, D., Larsen, F., Thai, N.T., Trang, P.T.K., Jakobsen, R., Nhan, P.Q., Long, T.V., Viet, P.H., Murray, A.S., 2012. Groundwater arsenic concentrations in Vietnam controlled by sediment age. Nat. Geosci. 5, 656–661. https://doi.org/10.1038/ngeo1540.

Postma, D., Pham, T.K.T., Sø, H.U., Hoang, V.H., Vi, M.L., Nguyen, T.T., Larsen, F., Pham, H.V., Jakobsen, R., 2016. A model for the evolution in water chemistry of an arsenic contaminated aquifer over the last 6000 years, Red River floodplain, Vietnam. Geochim. Cosmochim. Acta 195, 277–292. https://doi.org/10.1016/j.gca.2016.09.014.

Poulton, S.W., Canfield, D.E., 2005. Development of a sequential extraction procedure for iron: implications for iron partitioning in continentally derived particulates. Chem. Geol. 214, 209–221. https://doi.org/10.1016/j.chemgeo.2004.09.003.

Rancourt, D.G., Ping, J.Y., 1991. Voigt-based methods for arbitrary-shape static hyperfine parameter distributions in Mössbauer spectroscopy. Nucl. Inst. Methods Phys. Res. B 58, 85–97. https://doi.org/10.1016/0168-583X(91)95681-3.

Ravel, B., Newville, M., 2005. ATHENA, ARTEMIS, HEPHAESTUS: data analysis for X-ray absorption spectroscopy using IFEFFIT. J. Synchrotron Rad. 12, 537–541. https://doi.org/10.1107/S0909049505012719.

Schaefer, M.V., Guo, X., Gan, Y., Benner, S.G., Griffin, A.M., Gorski, C.A., Wang, Y., Fendorf, S., 2017. Redox controls on arsenic enrichment and release from aquifer sediments in central Yangtze River Basin. Geochim. Cosmochim. Acta 204, 104–119. https://doi.org/10.1016/j.gca.2017.01.035.

Schultz, C., Grundl, T., 2004. pH dependence of ferrous sorption onto two smectite clays. Chemosphere 57, 1301–1306. https://doi.org/10.1016/j.chemosphere.2004.09.023.

Shaheen, S.M., Rinklebe, J., Frohne, T., White, J.R., DeLaune, R.D., 2016. Redox effects on release kinetics of arsenic, cadmium, cobalt, and vanadium in Wax Lake Deltaic freshwater marsh soils. Chemosphere 150, 740–748. https://doi.org/10.1016/j.chemosphere.2015.12.043.

Sø, H.U., Postma, D., Vi, M.L., Pham, T.K.T., Kazmierczak, J., Dao, V.N., Pi, K., Koch, C. B., Pham, H.V., Jakobsen, R., 2018. Arsenic in Holocene aquifers of the Red River floodplain, Vietnam: effects of sediment-water interactions, sediment burial age and groundwater residence time. Geochim. Cosmochim. Acta 225, 192–209. https://doi.org/10.1016/j.gca.2018.01.010.

Sø, H.U., Postma, D., Hoang, V.H., Vi Mai, L., Pham Thi Kim, T., Pham Hung, V., Jakobsen, R., 2018. Arsenite adsorption controlled by the iron oxide content of Holocene Red River aquifer sediment. Geochim. Cosmochim. Acta 239, 61–73. https://doi.org/10.1016/j.gca.2018.07.026.

Stauder, S., Raue, B., Sacher, F., 2005. Thioarsenates in sulfidic waters. Environ. Sci. Technol. 39, 5933–5939. https://doi.org/10.1021/es048034k.

Stollenwerk, K.G., Breit, G.N., Welch, A.H., Yount, J.C., Whitney, J.W., Foster, A.L., Uddin, M.N., Majumder, R.K., Ahmed, N., 2007. Arsenic attenuation by oxidized aquifer sediments in Bangladesh. Sci. Total Environ. 379, 133–150. https://doi.org/10.1016/j.scitotenv.2006.11.029.

Stuckey, J.W., Schaefer, M.V., Benner, S.G., Fendorf, S., 2015. Reactivity and speciation of mineral-associated arsenic in seasonal and permanent wetlands of the Mekong Delta. Geochim. Cosmochim. Acta 171, 143–155. https://doi.org/10.1016/j.gca.2015.09.002.

Stumm, W., Sulzberger, B., 1992. The cycling of iron in natural environments: considerations based on laboratory studies of heterogeneous redox processes. Geochim. Cosmochim. Acta 56, 3233–3257. https://doi.org/10.1016/0016-7037(92)90301-X.

Sun, J., Quicksall, A.N., Chillrud, S.N., Mailloux, B.J., Bostick, B.C., 2016. Arsenic mobilization from sediments in microcosms under sulfate reduction. Chemosphere 153, 254–261. https://doi.org/10.1016/j.chemosphere.2016.02.117.

Thomasarrigo, L.K., Mikutta, C., Byrne, J., Barmettler, K., Kappler, A., Kretzschmar, R., 2014. Iron and arsenic speciation and distribution in organic flocs from streambeds of an arsenic-enriched peatland. Environ. Sci. Technol. 48, 13218–13228. https://doi.org/10.1021/es503550g.

Van Groeningen, N., ThomasArrigo, L.K., Byrne, J.M., Kappler, A., Christl, I., Kretzschmar, R., 2020. Interactions of ferrous iron with clay mineral surfaces during sorption and subsequent oxidation. Environ. Sci. Process. Impacts 22, 1355–1367. https://doi.org/10.1039/d0em00063a.

Viet, P.H., Lightfoot, A., Kipfer, R., Eiche, E., Kontny, A., Neumann, T., Glodowska, M., Patzner, M., Kappler, A., Rathi, B., Cirpka, O., Bostick, B., 2020. Spatial and temporal evolution of groundwater arsenic contamination in the Red River delta, Vietnam: interplay of mobilisation and retardation processes. Sci. Total Environ., 137143 https://doi.org/10.1016/j.scitotenv.2020.137143.

Viollier, E., Inglett, P.W., Hunter, K., Roychoudhury, A.N., Van Cappellen, P., 2000. The Ferrozine method revisited: Fe (II)/Fe (III) determination in natural waters. Appl. Geochem. 15, 785–790. https://doi.org/10.1016/S0883-2927(99)00097-9.

Wallmann, K., Hennies, K., König, I., Petersen, W., Knauth, H.D., 1993. New procedure for determining reactive Fe(III) and Fe(II) minerals in sediments. Limnol. Oceanogr. 38, 1803–1812. https://doi.org/10.4319/lo.1993.38.8.1803.

Wang, H.Y., Guo, H.M., Xiu, W., Bauer, J., Sun, G.X., Tang, X.H., Norra, S., 2019. Indications that weathering of evaporite minerals affects groundwater salinity and As mobilization in aquifers of the northwestern Hetao Basin, China. Appl. Geochem. 109, 104416 https://doi.org/10.1016/j.apgeochem.2019.104416.

Wang, H.Y., Byrne, J.M., Perez, J.P.H., Thomas, A.N., Goettlicher, J., Hofer, H.E., Mayanna, S., Kontny, A., Kappler, A., Guo, H.M., Benning, L.G., Norra, S., 2020. Arsenic sequestration in pyrite and greigite in the buried peat of As-contaminated aquifers. Geochim. Cosmochim. Acta 284, 107–119. https://doi.org/10.1016/j.gca.2020.06.021.

Wang, Y., Pi, K., Fendorf, S., Deng, Y., Xie, X., 2017. Sedimentogenesis and hydrobiogeochemistry of high arsenic Late Pleistocene-Holocene aquifer systems. Earth Sci. Rev. 0–1. https://doi.org/10.1016/j.earscirev.2017.10.007.

Wang, Y., Le Pape, P., Morin, G., Asta, M., King, G., Bartova, B., Suvorova, E., Frutschi, M., Ikogou, M., Pham, V.H.C., Le Vo, P., Herman, F., Charlet, L., Bernier-Latmani, R., 2018. Arsenic speciation in Mekong Delta sediments depends on their depositional environment. acs.est.7b05177 Environ. Sci. Technol.. https://doi.org/10.1021/acs.est.7b05177.

Zhang, Z., Guo, H., Liu, S., Weng, H., Han, S., Gao, Z., 2020. Mechanisms of groundwater arsenic variations induced by extraction in the western Hetao Basin, Inner Mongolia, China. J. Hydrol. 583, 124599 https://doi.org/10.1016/j.jhydrol.2020.124599.

Supplementary information

Acid digestion method used to determine As in the sediment

0.1 g of dried and grinded sample material was weighted into 100 mL Teflon tubes. 0.05 g of GXR-5 (Soil, USGS) and RGM-1 (Rhyolite, USGS) were additionally digested as certified references to check for accuracy. Two blank samples were digested at same time as control. Firstly, 1 mL Milli-Q water was added into tubes for avoiding heavy reactions of sediments with acid. Afterwards, 2 ml 65% HNO_3 (subboiled) was added and heated at 80 ℃ for 10 minutes. Then 1 mL $HClO_4$ (70%, normapure) and 5 mL HF (40%, suprapure) were added into tubes for digesting with cover at 120 ℃ for 18 h. Afterwards, the acid was evaporated until near dryness. Then 2 mL 65% HNO_3 (subboiled) were added and evaporated until dryness. The last step was repeated for 3 times. Finally, 2 mL HNO_3 were added and the adjusted to 50 mL in flasks using MiliQ-water.

Detailed XAS data collection and analysis information

The XAS data was collected at the synchrotron radiation facility of the Karlsruhe Institute of Technology. The storage ring operates at 2.5 GeV. spectra for As, Fe and S were collected under vacuum using Si(111) crystal pair as a monochromator with a fixed-beam exit. Higher-order harmonics were removed from incident beam using a grazing incidence mirror. Both transmission and fluorescence were collected in a range of -200 eV to 1000 eV with energy step of 0.35 eV. Every 20 min – 30 min was used for each scan. And several scans were collected, which depend on the data quality. Transmission spectra were collected using three ADC ionization chambers with 13 μm Kapton windows. The fluorescence spectra were collected using a Gresham 7-element (Li) detector. Arsenic and S K-edge spectra were collected using fluorescence mode, while Fe K-edge spectra were collected using transmission mode. Arsenic K-edge spectra were calibrated with Au foil (AuL_3 11919 eV), Fe K-edge spectra were calibrated with a Fe metal foil (Fe(0) 7112 eV). And sulfur K-edge XANES spectra was calibrated to the sulfate, white line of sulfate shows at 2481.4 eV. To prevent S species from beam damage, spectra were collected at different positions in thin layers.

Data reduction was performed using Athena [1]. Linear combination fitting (LCF) was conducted for the S K-edge on the XANES region (-20 eV to 30 eV), for the As K-edge on the 1^{st} derivatives of the XANES spectra (-20 eV to 30 eV), and for Fe K-edge in the EXAFS range (k = 3-10 Å, k^2-weighting). For all Fe reference compounds, the total number of contributing reference standards was limited to five. The sum was forced to equal 1.

Table S1 Sequential extraction scheme for selected sediments

Step	Target phase	Extractant	Conditions	Reference
F1	Ionically-bonded and strongly adsorbed	1.0 M NaH_2PO_4	40 mL, 24 h, pH 4-5, one repetition of each time duration, one water wash (40 mL)	[2]
F2	Co-precipitated with acid volatile sulfides, carbonates	1 M CH_3COONa /CH_3COOH	40 mL, 1 h, pH 4.5, one repetition, one water wash (40 mL)	[3]
F3	Co-precipitated with amorphous iron oxides and magnetite	0.2 M ammonium oxalate/0.17 M oxalic acid	40 mL, 2 h, pH 3, dark (wrapped in Al-foil), one repetition, one water wash (40 mL)	[2]
F4	Co-precipitated with crystalline Fe oxides	DCB: 0.5 M Na-Citrate +1 M $NaHCO_3$; 0.5 g $Na_2S_2O_4xH_2O$	35 mL Na-Citrate + 2.5 mL $NaHCO_3$ (heating to 85 °C), addition of 0.5 g $Na_2S_2O_4xH_2O$, 15 min at 80 °C, one repetition, one water wash (40 mL)	[2]
F5	Co-precipitated with pyrite and part of sheet silicates	16 M HNO_3	20 ml 16 M HNO_3, 2h, 25 °C, one repetition, one water wash (40 mL)	[2]

Table S2 Elemental compositions (atom ratios %) corresponding to EDS spectra in the Fig. 3.

Name	C	O	Fe	Si	Al	Ca	As	Cr	S	K
a	-	67.43	30.13	1.84	-	-	-	-	-	-
b	-	59.62	40.38	-	-	-	-	-	-	-
c	2.87	55.82	40.51	-	-	-		-	-	-
d	42.41	-	25.62	-	-	-	-	-	31.22	-
e	27.68	-	23.83	-	-	-			46.82	-

-: atom ratio less than 1%

Table S3 Hyperfine parameters obtained by fitting both samples. T – temperature, δ - isomer shift, ΔE_Q - quadrupole splitting, SDev – standard deviation, Skew – skew of fit, ε - quadrupole shift, B_{hf} - hyperfine magnetic field, RA – relative spectral abundance with associated error, χ^2 – goodness of fit. Hem – hematite, Greig –greigite, Gt - goethite

Depth (m)	**T K**	**Phase**	**δ mm/s**	**ΔE_Q mm/s**	***SDev (ΔE_Q) mm/s***	***Skew (ΔE_Q)***	**ε mm/s**	**B_{hf} T**	***SDev (B_{hf}) T***	***Skew (B_{hf})***	**RA %**	**±**	**χ^2**
29.6	20	Fe(II)	1.26	2.80	0.24	0.00					56.5	1.9	0.75
		Fe(III)	0.40	1.08	0.75	0.94					24.5	1.5	
		Gt	0.49				-0.15	50.3	2.4	0.0	19.0	2.3	
43.4	20	Fe(II)	1.26	2.80	0.31	0.00					52.0	1.9	0.57
		Fe(III)	0.36	0.83	0.49	0.42					26.6	1.4	
		Gt	0.48				-0.08	51.2	2.9	0.0	21.4	2.6	
68.4	20	Fe(II)	1.26	2.81	0.24	0.00					60.1	3.0	0.69
		Fe(III)	0.47	0.96	0.71	1.06					25.4	2.1	
		Gt	0.49				-0.13	51.8	2.7	0.0	14.5	3.6	
80.5	20	Fe(II)	1.27	2.85	0.13	0.00					20.4	3.0	1.00
		Fe(III)	0.48	1.16	1.17	1.81					18.0	1.3	
		Fe(II)	1.24	2.70	0.41	0.00					24.8	2.9	
		Greig	0.57				-0.04	31.2	4.0	0.0	30.0	1.8	
		Hem	0.43				-0.01	53.1	2.0	0.0	6.8	0.8	

Table S4 Model compounds collection information

Compound	Natural	Source/synthesis reference
Fe model compounds		
chlorite	-[a]	natural[1]
biotite	-[a]	natural[1]
illite	-[a]	natural[1]
hornblende	-[a]	natural[1]
pyrite	FeS_2	natural[1]
Fe monosulphide	FeS	commercial (Fluka)
siderite	$FeCO_3$	natural[1]
maghemite	γ-Fe2O3	synthetic[2]
Magnetite	Fe_4O_3	synthetic[2]
hematite	α-Fe_2O_3	synthetic[2]
sulfate green rust	$[Fe^{II}_4Fe^{III}_2(OH)_{12}].[SO_4^{2-}.{}_mH_2O]^{2-}$	Synthetic[2]
goethite	α-FeO(OH)	synthetic[2]
greigite	Fe_3S_4	natural[1]
lepidocrocite	β-FeO(OH)	synthetic[2]
ferrihydrite	$Fe(OH)_3$	synthetic[2]
Fe(III)-citrate dehydrate	$C_6H_5FeO_7$	commercial (Roth)
Fe(II)-oxalate dehydrate	$C_2H_4FeO_5$	commercial (Sigma-Aldrich)
S model compounds		
greigite	Fe_3S_4	natural[1]
iron monosulphide	FeS	commercial (Fluka)
pyrite	FeS_2	natural[1]
gypsum	$CaSO_4.2H_2O$	natural[1]
sulfur	S_0	Commercial (Fluka)
As model compounds		
As(III)-ferrihydrite	$As_{0.01}(Fe(OH)_3)_{0.99}$	synthetic[3]
As(V)-ferrihydrite	$As_{0.02}(Fe(OH)_3)_{0.98}$	synthetic[3]
arsenopyrite	FeAsS	natural[1]
glutamylcysteinylgly thioarsenite	$As(C_{10}H_{17}N_3O_6S)_{2.6}(OH)_{0.6}$	synthetic[4]
realgar	As_4S_4	Natural[1]

[a]The minerals are characterized by XRD without chemical compositions analysis.

[1]The minerals are provided by minerals center of Karlsruhe Institute of Technology.

[2]minerals is provided by Thomas et al.,[4]

[3]chemicals are synthesized according to Dixit and Hering[5]

[4]chemicals are synthesized according to Miot et al.,[6]

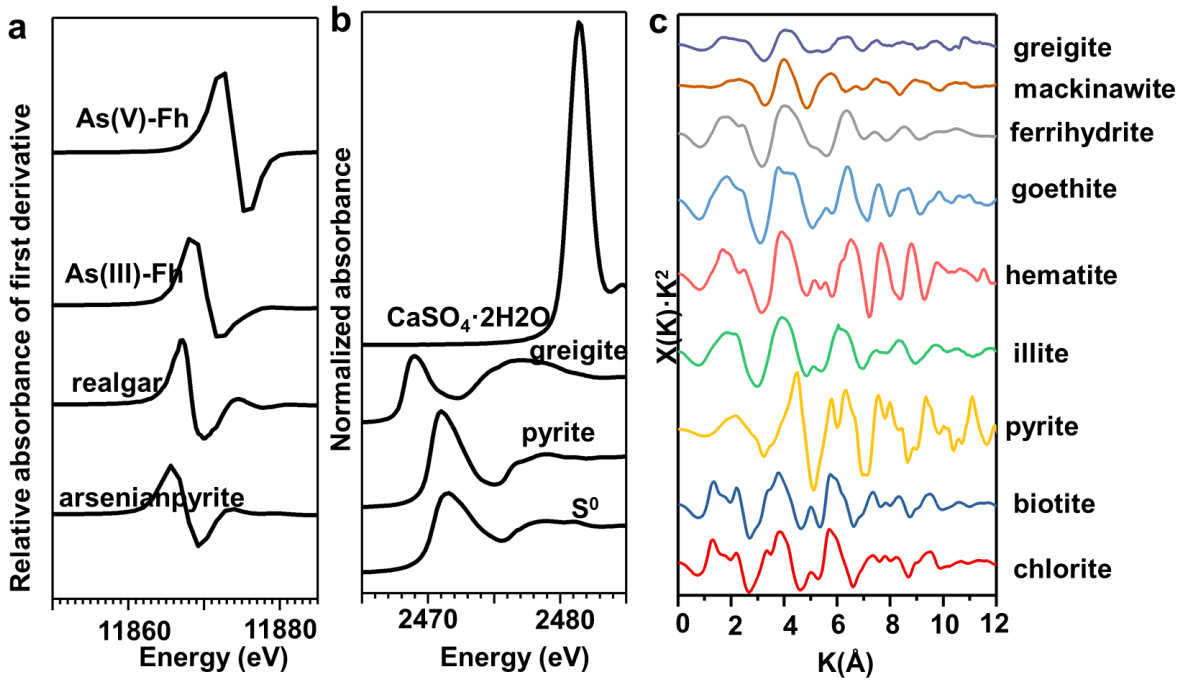

Supplementary Fig. 1 Model compounds XAS spectra for Fe, As and S used for samples fitting. As K-edge derivative XANES spectra of model compounds (As(V)-Fh: As(V) species was adsorbed onto ferrihydrite, As(III)-Fh: As(III) species was adsorbed onto ferrihydrite (a); sulfur K-edge XANES spectra of model compounds (b); Iron K-edge EXAFS spectra for model compounds (c).

Table S5 Total Fe and Fe(II) content extracted by 2 M HCl

Depth (m)	Fe(II)content (mg/kg)	Fe_T (mg/kg)	Fe(II)/Fe (%)
4.1	4537	14974	30
5.7	5851	19988	29
6.7	4802	9342	51
11.6	2353	4266	55
19.9	3268	5386	61
25.1	3225	4702	69
29.6	4214	7468	56
32.1	2761	4998	55
35.5	8441	13911	61
40.1	16354	22718	72
43.6	13256	19577	68
48.3	2571	4268	60
50.7	9202	16521	56
58.1	5867	7960	74
68.4	5431	8431	64
70.1	5026	7328	69
75.5	4850	6452	75
80.5	21456	27143	79

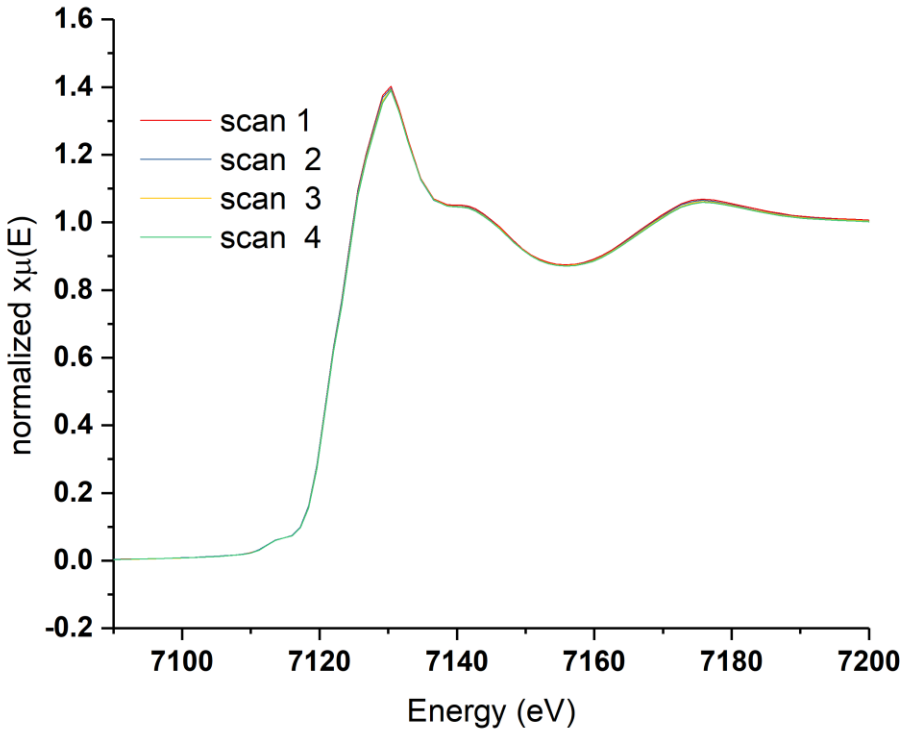

Supplementary Fig. 2 (Fig. S2) Parallel scans of Fe K-edge XANES spectra for an example of air-sensitive samples (sulfate green rust)

[1] B. Ravel, M. Newville, ATHENA, ARTEMIS, HEPHAESTUS: Data analysis for X-ray absorption spectroscopy using IFEFFIT, J. Synchrotron Radiat. 12 (2005) 537–541. https://doi.org/10.1107/S0909049505012719.

[2] N.E. Keon, C.H. Swartz, D.J. Brabander, C. Harvey, H.F. Hemond, Validation of an Arsenic Seqential Extraction Method for Evaluating Mobility in Sediments, Environ. Sci. Technol. 35 (2001) 2778–2784. https://doi.org/10.1021/es001511o.

[3] S.W. Poulton, D.E. Canfield, Development of a sequential extraction procedure for iron: Implications for iron partitioning in continentally derived particulates, Chem. Geol. 214 (2005) 209–221. https://doi.org/10.1016/j.chemgeo.2004.09.003.

[4] A. N. Thomas, E. Eiche, J. Göttlicher, R. Steininger, L. G. Benning, H. M. Freeman, K. Dideriksen, T. Neumann, Products of Hexavalent Chromium Reduction by Green Rust Sodium Sulfate and Associated Reaction Mechanisms, Soil Syst. 2 (2018) 58. https://doi.org/10.3390/soilsystems2040058.

[5] S. Dixit, J.G. Hering, Comparison of arsenic(V) and arsenic(III) sorption onto iron oxide minerals: Implications for arsenic mobility, Environ. Sci. Technol. 37 (2003) 4182–4189. https://doi.org/10.1021/es030309t.

[6] J. Miot, G. Morin, F. Skouri-Panet, C. Férard, E. Aubry, J. Briand, Y. Wang, G. Ona-Nguema, F. Guyot, G.E. Brown, XAS study of arsenic coordination in Euglena gracilis exposed to arsenite, Environ. Sci. Technol. 42 (2008) 5342–5347. https://doi.org/10.1021/es703072d.

Appendix 4 Arsenic sequestration in pyrite and greigite in the buried peat of As-contaminated aquifers

Available online at www.sciencedirect.com

ScienceDirect

Geochimica et Cosmochimica Acta 284 (2020) 107–119

Geochimica et Cosmochimica Acta

www.elsevier.com/locate/gca

Arsenic sequestration in pyrite and greigite in the buried peat of As-contaminated aquifers

H.Y. Wang [a,*], J.M. Byrne [b], J.P.H. Perez [c,d], A.N. Thomas [a], J. Göttlicher [e], H.E. Höfer [f], S. Mayanna [c], A. Kontny [a], A. Kappler [b], H.M. Guo [g], L.G. Benning [c,d], S. Norra [a]

[a] *Institute of Applied Geoscience, Working Group of Environmental Mineralogy and Environmental System Analysis, Karlsruhe Institute of Technology (KIT), 76131 Karlsruhe, Germany*

[b] *Geomicrobiology, Center for Applied Geosciences, University of Tuebingen, 72074 Tuebingen, Germany*

[c] *GFZ German Research Center for Geoscience, 14473 Potsdam, Germany*

[d] *Department of Earth Sciences, Freie Universität Berlin, 12249 Berlin, Germany*

[e] *Institute of Synchrotron Radiation, Karlsruhe Institute of Technology (KIT), 76131 Karlsruhe, Germany*

[f] *Institute of Geoscience, Goethe University, 60438 Frankfurt, Germany*

[g] *State key Laboratory of Biogeology and Environmental Geology, China University of Geoscience, 100083 Beijing, China*

Received 9 February 2020; accepted in revised form 15 June 2020; Available online 29 June 2020

Abstract

Detrital peat (organic carbon-enriched deposit) with high arsenic (As) content is widely distributed in sediments where groundwater As contamination exists. Iron sulfides often persist in these sediments under anoxic conditions. However, the mechanisms and pathways of formation of iron sulfides and its potential contribution in controlling As mobility are still poorly understood. In this study, we examined three As-contaminated peat sediments from the Hetao Basin in China to gain better understanding of the complex interplay between iron sulfides formation and As mobility. We employed high-resolution spectroscopic techniques, including X-ray absorption spectroscopy and ^{57}Fe Mössbauer spectroscopy, coupled with electron microscopy to determine the speciation of iron sulfides and the associated As in the peat sediments.

Pyrite (FeS_2) and metastable greigite (Fe_3S_4) persisted in peat as end-members of S and Fe diagenetic pathways. The Fe-rich phyllosilicates and decaying plant tissues provided the ideal micro-environments for pyrite and greigite nucleation. Pyrite formation most likely occurred via the polysulfides pathway in the surface water-sediments interface during early diagenetic process, while the relative enrichment of reactive Fe compared to sulfide possibly inhibited the transformation of greigite to pyrite in such Fe-rich sediments.

Our results revealed that the peat sediments could act as a stable sink for As immobilization under steady groundwater anoxic conditions, with As content up to 250 mg/kg and large proportions (40 to 60 wt.% As) sequestered in pyrite and greigite. Pyrite crystallites had up to 1 wt.% As content through the replacement of the S^{-I} sites. Greigite crystallites had a relatively constant As content ranging from ~500 to ~1400 mg/kg. Instead of being adsorbed or structurally incorporated, arsenic formed distinct arsenic sulfide phase in the greigite-enriched sediments, which was analogous to realgar. The transfer of As from iron sulfides to ferrihydrite temporarily retarded As release into groundwater under slightly oxic groundwater conditions. However, the reductive dissolution of ferrihydrite and potential subsequent As re-release could be a source of As in groundwater under disturbed redox conditions.

© 2020 Elsevier Ltd. All rights reserved.

Keywords: Peat; Arsenic; Greigite; Pyrite; Sediment biogeochemistry; Early diagenesis

* Corresponding author.
E-mail address: hongyan.wang@kit.edu (H.Y. Wang).

https://doi.org/10.1016/j.gca.2020.06.021
0016-7037/© 2020 Elsevier Ltd. All rights reserved.

1. INTRODUCTION

Over a hundred million people are exposed to groundwater with high levels of arsenic (As) (>10 μg/L) globally, particularly in South and Southeast Asia including the Ganges-Brahmaputra-Megha, Red River and Mekong Deltas and the basins belong to the Yangtze and Yellow River catchments (Winkel et al., 2008; Fendorf et al., 2010; Wang et al., 2019b). It is widely accepted that microbial reduction of Fe (oxyhydr)oxides coupled to organic carbon oxidation causes the release of Fe (oxyhydr)oxides-bound As into groundwater (Nickson et al., 1998; Islam et al., 2004; Guo et al., 2013). The reactivity and availability of organic matter, partitioning of As in solids and the presence of other redox-active species (e.g., NO_3^-, SO_4^{2-}) largely influence As speciation and partitioning between groundwater and solid phases (O'Day et al., 2004b; Langner et al., 2012; Stuckey et al., 2015a; Zhu et al., 2017; Smith et al., 2017).

Peat is a heterogeneous mixture of (partly) decayed plant materials that accumulate anaerobically (Naafs et al., 2019). Abundant reactive organic matter provides electrons for the reductive transformation of Fe (oxyhydr)oxides, thereby influencing the behavior of trace elements that are bound onto Fe (oxyhydr)oxides such as As. In the As contaminated aquifers in South and Southeast of Asia, peat formed in Holocene epoch or the last glacial period is widely embedded in the sediments (McArthur et al., 2001; Wang et al., 2018, 2019b). Influence of the buried peat for As mobilization has been extensively discussed in terms of reductive dissolution of Fe(III) (oxyhydr)oxides. On one hand, dissolved organic matter degraded from plants in the peat lenses can be transported to different locations by groundwater flow, stimulate microbial reduction of Fe(III) (oxyhydr)oxides and As (V) reduction and thereby releasing arsenic into groundwater (McArthur et al., 2001, 2004; Anawar et al., 2003; Fendorf et al., 2010). On the other hand, the detrital peat buried in the sediments can serve as a special sink for As. Following the reductive dissolution of Fe(III) (oxyhydr) oxides and As(V) species, mobilized As(III) species can be subsequently sequestrated by sulfides, with sulfide arising from reduced organic sulfide in peat or microbial reduction of SO_4^{2-} (Stuckey et al., 2015b; Wang et al., 2018; Knappová et al., 2019). Furthermore, recent research shows that reactive organic thiol groups formed by incorporating inorganic sulfide into organic carbon can adsorb As in contaminated peatlands, providing another sink for As (Langner et al., 2012, 2013; Wang et al., 2018). Therefore, the influence of peat for As behavior is complex and affected by Fe-C-S coupled mineralization pathways. Understanding the diagenetic process in the peat layers and related As speciation are vital to gain better understanding on the influence of peat sediments in As immobilization in contaminated anoxic environments.

Arsenic-Fe sulfides associations are common features in peat layers, and act an important role for As immobilization. Iron sulfides found in the natural sediments mainly include mackinawite (nominally "FeS"), greigite and pyrite (Wilkin and Ford, 2006; Pickard et al., 2017; Knappová et al., 2019). Recent research suggests that Fe sulfides are main As carriers in the detrital peat of As contaminated aquifer in South and Southeast of Asia. For example, arsenic is mainly sequestrated in pyrite found in peat from Mekong River Delta and Bangladesh (Lowers et al., 2007; Stuckey et al., 2015b; Wang et al., 2018). Several studies have been conducted to study the mechanisms of Fe sulfides formation as well as the adsorption/incorporation behavior of As in the laboratory scale (Benning et al., 2000; Bostick and Fendorf, 2003; Blanchard et al., 2007; Kirk et al., 2010; Le et al., 2017). However, the diagenetic formation process in natural settings and adsorption/incorporation mechanisms for As are still not sufficiently understood because Fe sulfides and related As species are difficult to characterize and quantify due to its oxygen-sensitive nature and poorly crystalline properties.

Based on the assumption that diagenetic process especially Fe sulfides formation in the peat can influence As partitioning in sediments and groundwater, we separated three peat lenses from the sediments of Hetao Basin, an important inland basin draining Yellow river with As contaminated groundwater. Using these, we seek to (1) define the S and Fe diagenetic minerals in peat lenses, (2) investigate As speciation in both peat sediments and specific Fe sulfides, and (3) evaluate the potential role of peat layers in controlling the toxicity and mobility of As in aquifers. The buried peat in the Hetao Basin formed either by over-flowed flood debris or swamps is analogous to other peat formed in As contaminated aquifers in South and Southeast Asia, therefore the research results can be applicable to comparable subsurface environments.

2. MATERIAL AND METHODS

2.1. Field area

The Hetao Basin is a typical inland basin lying in the central part of Inner Mongolia (China) with the Lang Mountains in the North and the Yellow River in the South, covering an area of about 13,000 km^2. In the early time of late Pleistocene (~120 ka) epoch, the Yellow River began to flow through the Hetao paleolake. At the same time, the paleolake started to shrink due to the cooling climate (Jia et al., 2016). Salt marshes as well as oxbow lakes were generated as a result of paleolake shrinkage and frequent movement of the Yellow River channels (Cai et al., 2019), resulting in the accumulation of organic matter. The study site was located in the flat plain of northwestern Hetao Basin which was one of most As contaminated area. The stratigraphy of the late Pleistocene and the Holocene covered a depth around 150 m, whereas the Holocene sediments primarily included alluvial-fluvial sediments with thicknesses of ~10 m (Deng et al., 2009). Further detailed information about the study area such as hydrological conditions were outlined in a previous study (Zhang et al., 2020).

2.2. Sediments collection, bulk geochemistry composition and mineral phase analysis

Two multilevel wells, K1 (41°0′9.00″N, 106°57′59.20″E) and K2 (41°1′2.10″N, 106°57′24.50″E), were selected in the study area. The wells were drilled in October 2015 by the China University of Geosciences (Beijing) (CUGB) using a circulatory drilling method. After bringing the cores to the surface, they were split into 10 cm sections according to lithology and color variations observed visually, and then capped and placed into N_2-purged Mylar bags. More detailed information about well construction and sediments sampling information has been reported by Zhang et al. (2020). Groundwater samples from different depths (sampling length: 1 m) were collected after the wells were constructed and then analyzed at CUGB. The geochemical and mineralogical composition of the sediments were analyzed at the Karlsruhe Institute of Technology (KIT). Methods for the groundwater sampling, geochemical analysis, and determination of elemental and organic carbon content and isotopic composition are detailed in the supplementary information (Supplementary text 1). Methods for mineralogical characterization of magnetically separated minerals, and sequential extractions of Fe-bearing phases in the bulk sediments are shown in the supplementary information (Supplementary text 2 and Supplementary Table S1). The magnetic susceptibility measurements of the peat sediments are described in detail in Supplementary text 3.

2.3. ^{57}Fe Mössbauer analysis

A section of peat was separated from each intact core for Mössbauer analysis at the University of Tübingen. Inside the glovebox (pure nitrogen atmosphere), dried powders of peat samples were loaded into Plexiglas holders (area 1 cm^2), forming a thin disc. Samples were kept in airtight jars under anoxic conditions at −20 °C until measurement. Holders were inserted into a closed-cycle exchange gas cryostat (Janis cryogenics) under a backflow of He to minimize exposure to air. Spectra were collected at 20 K using a constant acceleration drive system (WissEL) in transmission mode with a ^{57}Co/Rh source. All spectra were calibrated against a 7-μm thick α-^{57}Fe foil that was measured at room temperature. Analysis was carried out using Recoil (University of Ottawa) and the Voigt Based Fitting (VBF) routine (Rancourt and Ping, 1991). The half width at half maximum (HWHM) was constrained to 0.13 mm/s during fitting.

2.4. Scanning Electron Microscopy (SEM) and Electron probe microanalysis (EPMA)

Thin sections for SEM imaging and EPMA analysis were prepared at KIT. A section of peat was separated from intact cores, and embedded in an arsenic free-resin in the glovebox after drying. Sections of 1-mm thickness were cut and polished down to a thickness of 80 μm. Thin sections were stored in the glovebox until analysis.

Carbon-coated thin sections were used for SEM imaging and EPMA analysis. SEM images were acquired at the GFZ German Research Center for Geosciences using a Zeiss Ultra Plus FE-SEM at an acceleration voltage of 3 kV with10 μm aperture distance using an In-lens secondary electron detector. Following mineral observations using SEM, selected particles and areas were analyzed at Goethe University by wavelength spectrometer electron probe microanalysis (EPMA, JEOL 8900). The operating conditions were 20 keV accelerating voltage and 20nA beam current. Iron, S, Si, Ca, Mg and As concentrations were quantified using peak counting times of 10 s for Fe, S, Si, Ca, Mg, and 60 s for As. The detection limit for As was about 90 mg/kg. For As, S and Fe mapping, pixel size was set to 0.1 μm × 0.1 μm. The analysis volume for particles was approximately 0.2–0.3 μm based on the Monte Carlo simulations.

2.5. As, S and Fe K-edge X-ray absorption spectroscopic analysis

The speciation and local bonding environment of As, S and Fe in selected peat samples were characterized using X-ray absorption spectroscopy (XAS) analysis at the SUL-X beamline at the ANKA synchrotron radiation facility (KIT). Samples were collected from each peat and ground into powder after drying in the glovebox. A sample mass for Fe K-edge XAS analysis was calculated by the program XAFSmass and mixed with boron nitride (Sigma-Aldrich) prior to analysis (Klementiev, 2012). For As and Fe K-edge XAS analysis, powdered samples were suspended in deoxygenated water in the glovebox, drop-casted onto Kapton tape, and sealed using a second piece of Kapton tape. Arsenic K-edge EXAFS spectra for sample K2-28 was analyzed at the BM23 beamline of the European Synchrotron Radiation Facility (ESRF, Grenoble, France) using the same sample preparation method. For S K-edge XAS measurements, dried peat samples were directly loaded onto the Kapton tape surface. Three scans to 12 scans were collected per sample for each As, Fe and S K-edge XAS spectrum. Data reduction and analysis of XAS spectra were performed using Athena software package (Ravel and Newville, 2005). Experimental and data analysis procedures can be found in the supplementary information (Supplementary text 4).

3. RESULTS

3.1. Geochemical composition of peat sediments

Surface sediments (~10 m) from cores K1 and K2 were yellowish to brownish in color and fine-grained with a silt/-clay like texture, whereas gray aquifer sediments with interbedded brown/gray clay lenses were found at a depth of ~10 m (K1) and ~14 m (K2) to 82 m (maximum sampled depth) (Fig. 1). In borehole K1, a ~5 cm thick black peat band located between 80.4 and 80.5 m (K1-71) was composed of a poorly sorted mixture of fine sand, clay and small amounts of medium sand. In borehole K2, a ~5 cm poorly sorted clay peat band was found at a depth

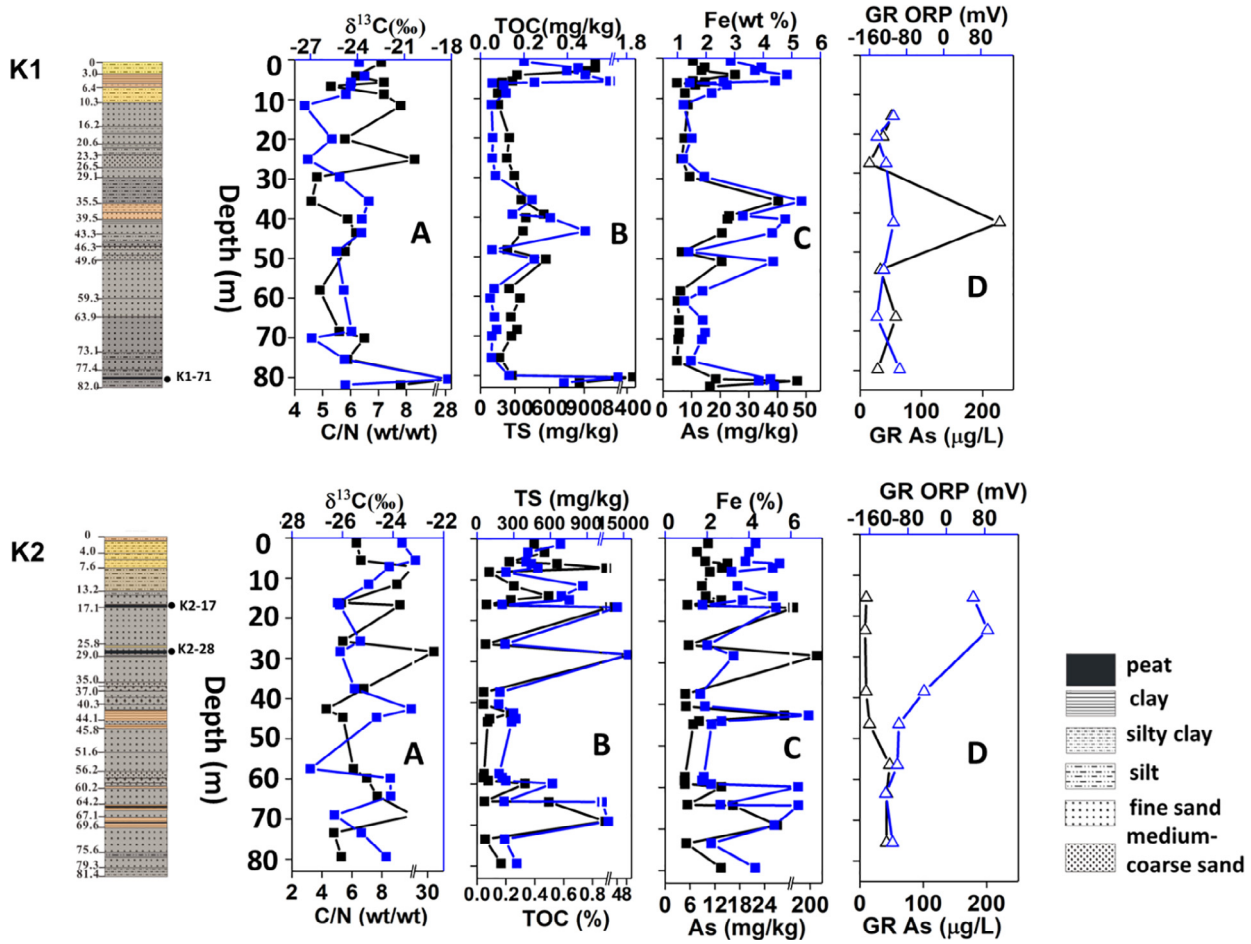

Fig. 1. Lithology and elemental content in the sediments profiles as well as groundwater redox conditions and As concentrations from different depths: (A) Isotope signature of organic carbon (δ^{13}Corg, blue) and ratio of organic carbon to total nitrogen (C/N, black); (B) total sulfur content (TS, blue) and total organic carbon (TOC, black); (C) total Fe (blue) and As content (black); and (D) groundwater redox conditions (GW ORP, blue) and As concentrations (black). Drawing color of the cores represents the visualized sediments colors, layers labeled with black dots (K1-71, K2-17, and K2-28) represent the analyzed peat sediments. (For interpretation of the references to colour in this figure legend, the reader is referred to the web version of this article.)

of 16.7–16.8 m (K2-17), and a peat layer composed of fine sand and visible detrital plant materials with thickness of at least of 10 cm was observed at a depth of 28.3–28.4 m (K2-28).

Arsenic content in the sediments was found to be between 4.7 mg/kg and 40.3 mg/kg (except for the peat layers) with generally higher content found in clay sediments (Table 1). Meanwhile, clay sediments had slightly higher Fe content (3.94% in average) than silt (2.86% in average) and sand (1.46% in average) (Table 1). Peat sediments showed significantly higher total organic carbon (TOC) and total sulfur (TS) content, and C/N ratios than in the underlying and overlying sediments (Fig. 1 and Table 1). Much higher As content was found in the peat lenses (up

Table 1
Geochemical compositions of studied peat sediments and comparison with other sediments.

Sample name	Depth(m)	As (mg/kg)	Fe (%)	TOC (%)	TS (mg/kg)	C_{org}/N ratio	δ^{13}Corg (‰)
K1-71	~80.4	46.9	3.85	1.70	8,836	29.1	−18.2
K2-17	~16.7	59.2	5.31	1.33	11,020	9.2	−26.1
K2-28	~28.3	256	3.27	9.52	155,970	31.6	−26.1
Clay/silty clay	–	18.6 ± 8.9	3.94 ± 0.72	0.40 ± 0.20	365 ± 156	5.9 ± 1.2	−23.7 ± 0.5
Silt	~	12.0 ± 5.1	2.86 ± 0.70	0.24 ± 0.14	376 ± 265	7.1 ± 2.4	−24.1 ± 0.5
Sand	~	6.0 ± 1.4	1.46 ± 0.26	0.06 ± 0.01	163 ± 67	6.2 ± 1.3	−25.7 ± 0.9

to ~250 mg/kg) in comparison with other sediments (Fig. 1 and Table 1). In comparison with peats K1-71 and K2-17, peat K2-28 had much higher organic matter as well as total S content (Table 1).

3.2. Fe-containing phases in the peat sediments

3.2.1. Fe K-edge XAS and ^{57}Fe Mössbauer analysis

The pre-edge inflection point near 7112 eV and primary inflection point near 7119 eV in the first derivative Fe K-edge XANES spectra suggested that Fe sulfides were abundant in the peat lenses (Supplementary Fig. S3) (O'Day et al., 2004a). The results of Fe K-edge extended X-ray absorption fine structure (EXAFS) linear combination fitting (LCF) revealed that, aside from phyllosilicates (~53% and ~66%), greigite (~23% and ~42%) was the primary Fe-bearing mineral phase in K2-17 and K1-71, respectively. Meanwhile, pyrite (~22%) and ferrihydrite (~17%) in combination with phyllosilicates (~59%) were the dominant Fe-bearing phases in K2-28 (Fig. 2 a and Table 2).

^{57}Fe Mössbauer spectroscopy was used to identify Fe-bearing mineral phases as a complementary technique to synchrotron-based Fe K-edge EXAFS (Fig. 2b). The parameters of the narrow sextet in the peat samples K2-17 and K1-71 were typical of greigite (magnetic hyperfine field of 31.2 T and 32.0 T, isomer shift: 0.59 and 0.57, quadrupole shift of 0.00 and −0.04) (Vandenberghe et al., 1992), comprising ~27% and ~30% of the Fe phases, respectively (Supplementary Table S6). Differences less than 10% in the greigite component between the Fe K-edge EXAFS and Mössbauer spectroscopy fits in peat sediments K2-17 and K1-71 is considered to be acceptable (Thomas-Arrigo et al., 2014; Chen et al., 2017).

Unfortunately, the similarity of phyllosilicates Fe(III) and pyritic Fe(II) in the Mössbauer spectra at 20 K can result to misidentification of pyrite in peat samples K2-17 and K2-28. However, the Fe K-edge EXAFS spectra of pyrite and phyllosilicates can be easily distinguished (O'Day et al., 2004a), and these fitting results matched the Mössbauer spectroscopy fits (Table 2 and Supplementary Table S6). Furthermore, an expected ferrihydrite sextet in the 20 K Mössbauer spectra was not observed, even in sample K2-28, while Fe (oxyhydr)oxides were detected by Fe K-edge EXAFS. The magnetic ordering temperature of ferrihydrite is strongly dependent on the mineral purity, crystallite size and crystallinity, and as such the absence of a ferrihydrite sextet in the Mössbauer spectra does not necessarily mean that it is absent, as shown using other spectroscopic measurements (Wang et al., 2016). The presence of ferrihydrite in the K2-28 peat sample was further confirmed by measurements of magnetic susceptibility, which decreased in value from −192 °C to 0 °C (Supplementary Fig. S2) (Pannalal et al., 2005).

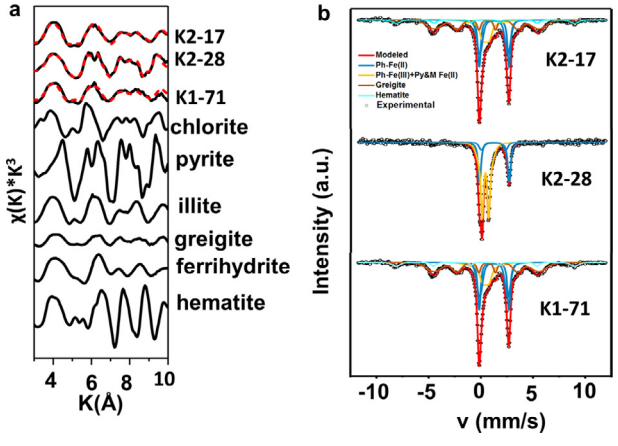

Fig. 2. (a) LCF fitting results of Fe K-edge EXAFS. Black lines represent experimental data for samples and model compound spectra used for fitting, and red dashed lines represent LCF fits. (b) ^{57}Fe Mössbauer spectra collected at 20 K for peat sediments, ph: phyllosilicates; py: pyrite; M: mackinawite.

3.2.2. Texture and morphologies of Fe-bearing phases (SEM-EDX analysis)

The Fe-bearing minerals texture and morphologies were evaluated according to SEM-EDX analysis based on the known minerals which were obtained by Fe K-edge XAS and Fe Mössbauer analysis.

Greigite aggregates nucleated in detrital silicates and decaying plant tissues, and less in gypsum/anhydrite (Fig. 3). The grain size ranged from ~80 nm to ~500 nm, whereas diverse crystallite habits were observed, including cuboidal, prismatic, and elongated particles. Neoformation of pyrite was also primarily occurred in confined spaces including plant tissues, phyllosilicates grains. The diameters of framboidal pyrites ranged from ~5 μm to ~40 μm (Fig. 3). Framboidal crystallites showed either octahedral, cubic (~2 μm in diameter) or spherical crystal habits (~1 μm in diameter). Massive pyrite crystals occurred with octahedral, cubic or irregular habits, with diameters up to ~10 μm. Ferrihydrite was found to be associated with pyrite particles.

3.3. Sulfur speciation in the peat sediments

Sulfur speciation in the peat sediments was analyzed by S K-edge XANES spectra. Based on the primary white line positions, the presence of reduced organosulfur species can be ruled out since they often have white line positions at >2472 eV (Manceau and Nagy, 2012). The primary inflection points at ~2469.1 eV and ~2471.1 eV in K2-17 and ~2469.1 eV in K1-71 revealed that inorganic sulfides were the primary sulfur-bearing phases, whereas the pronounced inflection points of ~2471.2 eV and ~2481.6 eV in peat sample K2-28 corresponded to inorganic sulfides and SO_4^{2-} from evaporites, respectively (Fig. 4). Iron monosulfide minerals (FeS) were not used in the XANES and XANES first derivative LCF fitting because their characteristic features were not observed in either Fe K-edge XAS analysis or sequential experiments (Fig. 2 a and Supplementary Table S2). Sulfur K-edge first derivative XANES LCF fitting showed that S^{2-} is the dominant S-bearing phase in K1-71 (~93%) and K2-17 (~70%). In sample K2-28, ~30% and ~60% of S was in the form of S^{-1} and zero-valent sulfur (S_0), respectively (Fig. 4 and Table 2).

Table 2
Summary of S, Fe and As K-edge XANES or EXAFS LCF fitting results.

Sample	Mineralogical composition (% mol S)				
	XANES first-derivative				
	Pyrite	Greigite	S_0	$CaSO_4 \cdot 2H_2O$	R^2
K2-17	14 (2.6)	70 (4.1)	15 (3)	1 (0.4)	0.091
K2-28	30 (2.0)	–	61 (2.9)	9 (0.4)	0.039
K1-71	–	93 (1.2)	5 (1.1)	2 (0.3)	0.058
Sample	**Mineralogical composition (% mol As)**				
	XANES first-derivative				
	Realgar	**Arsenopyrite**	**As (III)-Fh**	**As (V)-Fh**	**R^2**
K2-17	47 (6.9)	0 (4.2)	46 (2.1)	7 (1.5)	0.0245
K2-28	8(5.0)	61 (6)	3.8 (2.4)	27 (1.7)	0.0516
K1-71	41 (0.5)	–	50 (1.8)	10 (1.1)	0.0197
Sample	**Mineralogical composition (% mol Fe)**				
	EXAFS				
	Pyrite	**Greigite**	**Chlorite**	**Illite**	**Hematite**	**Ferrihydrite**	**R^2**
K2-17	3 (0.8)	23 (2.5)	19 (1.5)	47 (3.9)	8 (0.9)	–	0.0469
K2-28	23 (0.9)	–	39 (1.4)	18 (3.1)	-	21 (6.4)	0.0445
K1-71	–	42 (4.5)	24 (2.8)	29 (3.7)	5 (6.8)	–	0.1581

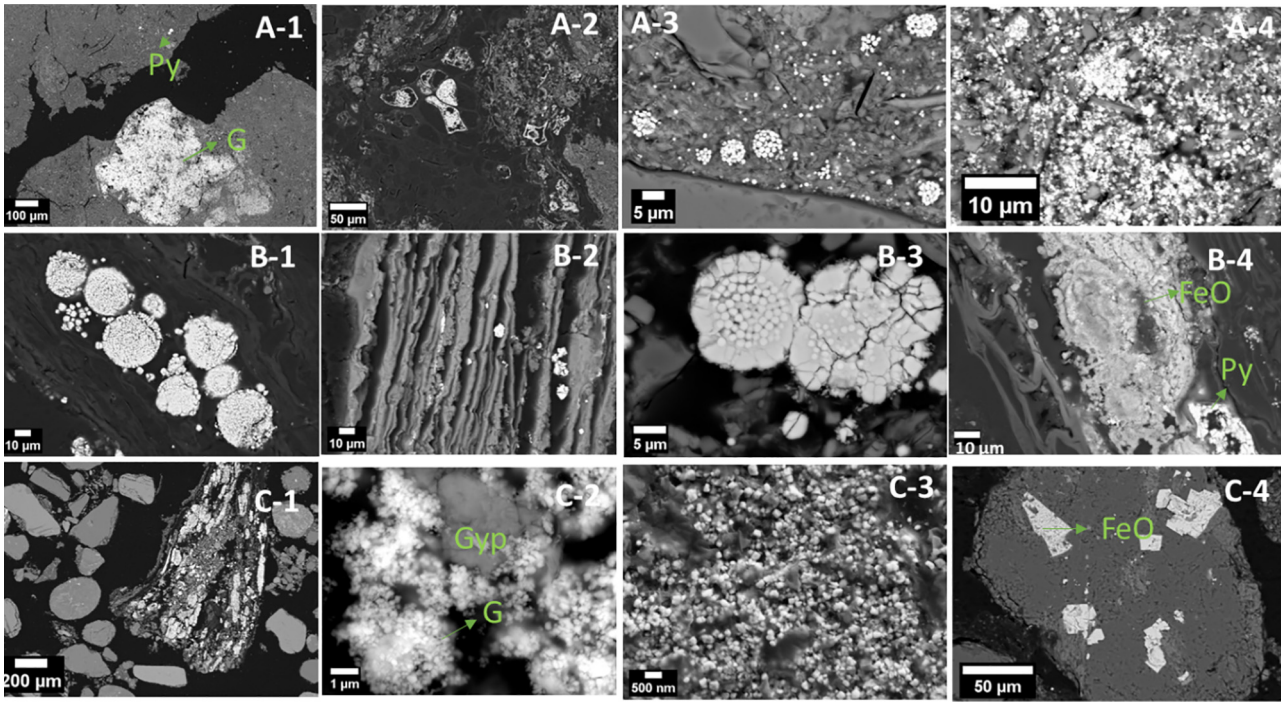

Fig. 3. Representative images of peat samples (A) K2-17, (B) K2-28 and (C) K1-71. (A-1) Representative greigite (G) and framboidal pyrite (Py) areas as indicated. (A-2) Greigite/pyrites nucleation in plant cells. (A-3) and (A-4) Nucleation of pyrites/greigite in phyllosilicates. (B-1) Framboidal and massive pyrites nucleation in plant tissues. (B-2) Massive pyrites nucleation in the phyllosilicates. (B-3) Framboidal pyrites nucleation in phyllosilicates. Overgrowth rims and interior crystallites were visible. (B-4) Mixture of ferrihydrite and pyrites in plant tissues/cells. (C-1) Greigite nucleation in phyllosilicates. (C-2) Greigite (G) nucleation in gypsum/anhydrite (Gyp). (C-3) Scattered electron images to show greigite grains. (C-4) Clastic iron oxides (FeO) in the sediment matrix.

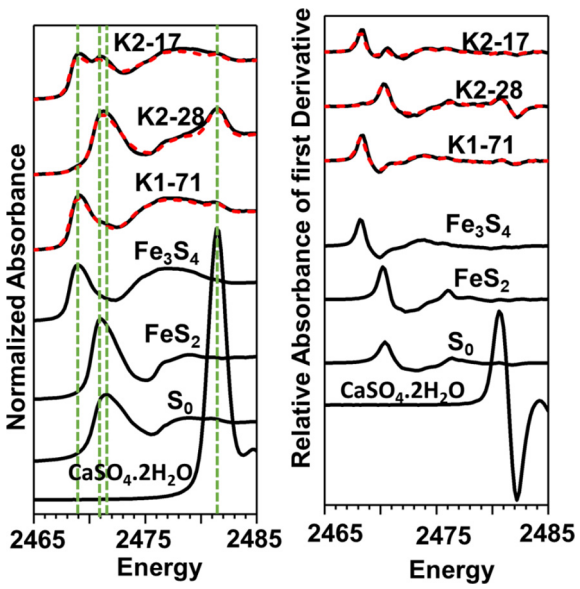

Fig. 4. Results of LCF fitting for S K-edge XANES and first derivative K-edge XANES spectra. Black lines represent experimental data, whereas red dashed lines represent the fits. Green dashed lines represent inflection points of selected model compounds. (For interpretation of the references to colour in this figure legend, the reader is referred to the web version of this article.)

3.4. Arsenic speciation and distribution in the peat sediments

3.4.1. As K-edge XAS analysis

The peat sediments of K1-71 and K2-17 both had white line energies near 11870 eV, which most likely indicates As (III) species were coordinated by sulfide (Smith et al., 2005). Arsenian pyrite/arsenopyrite detected in sample K2-17 do not seem to be major sinks for As due to the absence of the associated white line at ~11867.6 eV and the minimal pyrite content (<5%) (Fig. 5 A and Table 2). The first shells of the Fourier-transformed EXAFS spectra of K2-17 and K1-71 were comparable with the As(III)-O bond distance (~1.7 Å), while the second shell was consistent with the As(III)-S bond distance (~2.3 Å) (Bostick and Fendorf, 2003) (Fig. 5 D). First derivative K-edge XANES LCF fitting shows that ~40% of As is in the form of As-sulfide compounds in K2-17 and K1-71 while around 50% of As is in the form of arsenite (Table 2).

In peat K2-28, two inflection points occurred at ~11868 eV and ~11874 eV (Fig. 5 A), suggesting that the sample was mainly composed of arsenopyrite/arsenian pyrite (~11868 eV) and arsenate (~11874 eV). First derivative As K-edge XANES LCF fitting showed that ~61% and ~7% of As was presented as arsenopyrite/arsenian pyrite and As(V) species, respectively (Table 2).

3.4.2. Arsenic content and distribution in pyrite and greigite

Arsenic content of the pyrite and greigite grains was measured by EPMA and summarized in Table 3. Arsenic content in the pyrite grains ranged from <90 mg/kg (detection limit of EPMA) to ~11,000 mg/kg in both K2-17 and K2-28, respectively. Weak linear least squares fit was obtained for the As:S atomic ratio in the pyrite grains ($R^2 = 0.26$) (Fig. 6). Framboidal rims with over-grown pyrite crystallites contained more As than the framboid centers evidenced by two framboid measurements (Supplementary Table S5). Arsenic distributions in pyrites were heterogeneous, while the spatial distribution of As fluorescence intensities in the framboids showed a different picture compared to S and Fe (Fig. 7). Ferrihydrite aggregates had average As content about 4000 mg/kg, which was comparable with the average As content in pyrite measured using EPMA in peat K2-28 (Supplementary Table S5).

In contrast to pyrite, arsenic had a relatively homogeneous distribution in the greigite grains ranging from 500 to 1400 mg/kg (Table 3). Spatial As distribution was similar to the distribution of S and Fe fluorescence intensities (Fig. 7). Unfortunately, the result obtained from EPMA analysis may slightly underestimate the As content in the pyrite and greigite, while the total weight percent of S and Fe is 80% and 93% (on average) for greigite and pyrite, respectively (Supplementary Table S5). Except Fe (oxyhydr)oxides and sulfides, Fe-bearing phyllosilicates, especially clay minerals such as illite and chlorite, can also incorporate/adsorb As (Fakhreddine et al., 2015). However, our results showed that the influence from phyllosilicates was limited, as shown by the S/Fe atom ratios of pyrite and greigite which were similar to the stoichiometric ratios (Table 2). Furthermore, the distribution patterns of elements including Si, Mg and K, which are the main components of phyllosilicates, do not show any correlations with As distributions (Supplementary Fig. S4).

4. DISCUSSION

4.1. Diagenetic formation of Fe sulfides

The main minerals in the peat sediments include quartz, feldspar, carbonates and clay minerals, which has similar composition with the other sediments in the cores (Wang et al., 2019a). This suggests that the peat sediments have the same provenance with other sediments. Furthermore, the Fe sulfides found in the peat are likely of authigenic origin which can only be transported via small scales because they are susceptible to oxidation (Lowers et al., 2007). Therefore, the Fe sulfides found in the peat sediments were formed *in situ*.

Two proposed mechanisms, which are still under debate, can explain this pyrite formation via mackinawite (nominally "FeS") transformation, either by "FeS" reacting with polysulfides/elemental sulfur (S_0) (Eq. (1)) or "FeS" reacting with H_2S (Eq. (2)) (Benning et al., 2000):

$$FeS + S_0 \rightarrow FeS_2 \quad \text{or} \quad FeS + S_n^{2-} \rightarrow FeS_2 + S_{n-1}^{2-} \tag{1}$$

$$FeS + H_2S \rightarrow FeS_2 + H_2 \tag{2}$$

Reaction between S_0 precipitates and mackinawite [Eq. (1)] is most likely the dominant mechanism of pyrite formation since large proportions of S_0 (60% of total S) are detected together with pyrite. S_0 could have formed though sulfide oxidation coupled with Fe(III) reduction in such Fe-enriched sediments. Formation of pyrite via the polysulfides/S_0 pathway is typical in the oxic-anoxic transition

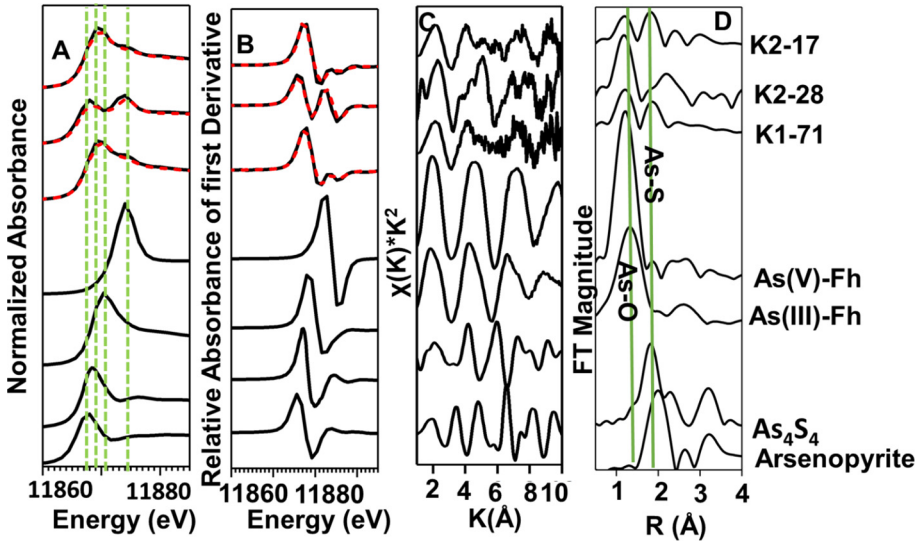

Fig. 5. As K-edge (A) XANES and (B) first-derivative XANES spectra of peat sediments and selected model compounds. The red dashed lines represent fits and the green dashed lines represent inflection points of selected model compounds (i.e., As(III)/As(V) adsorbed onto ferrihydrite, realgar (As_4S_4), arsenopyrite). (C) The k^2 weighted x(k) EXAFS spectra and their corresponding Fourier-transformations (D) The green lines represent the As-O and As-S bonding distances. (For interpretation of the references to colour in this figure legend, the reader is referred to the web version of this article.)

Table 3
Arsenic content in pyrite and greigite grains in the peat sediments based on the EPMA analyses.

Sample name	Mineral	S/Fe (avg. atomic %)	Min [As] (mg/kg)	Max [As] (mg/kg)	Average [As] ± SD (mg/kg)	n
K2-17	Pyrite	2.00	<90	11,040	5205 ± 5155	8
	Greigite	1.24	460	1380	1024 ± 341	5
K2-28	Pyrite	2.00	170	11,450	3760 ± 3,523	22
K1-71	Greigite	1.31	480	1270	895 ± 321	8

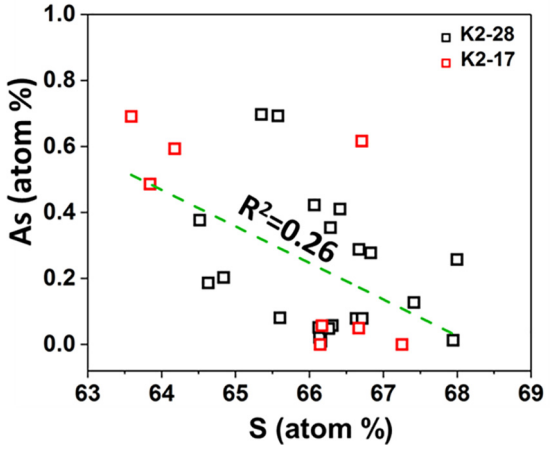

Fig. 6. Sulfur *vs* As atomic ratio measured by EPMA in peat samples.

zone of sediments (Berner, 1970; Neumann et al., 2005; Koeksoy et al., 2019), In the early diagenetic stage, the degradation of organic matter in the saturated water provides electrons for the reductive dissolution of SO_4^{2-} and Fe(III). This is followed by the subsequent precipitation of "FeS" upon saturation of Fe(II) and S(-II), and thereby resulting in the formation of pyrite via "FeS" reacting with S_0. The inhomogeneous framboid and euhedral pyrite sizes distribution could indicate unsteady geochemical conditions (Wilkin et al., 1996, 1997). The overgrowth of framboid, as well as the filled texture, is usually related to the secondary diagenetic growth of pyrite after formation in the surface water-sediment interface during early diagenetic process (Wilkin and Barnes, 1997), and the growth rate is limited by the sulfide supply, which can be constrained by labile organic matter in the sulfidic conditions or availability of SO_4^{2-} in porewater.

Greigite is a metastable iron sulfide mineral that is suggested to form as an intermediate during the oxidative transformation of mackinawite to pyrite (Vasiliev et al., 2008; Rickard and Luther, 2007; Pickard et al., 2017). However, the formation pathway and preservation mechanisms of this metastable mineral phase are still not fully understood, even though it has been increasingly recognized as an important sedimentary mineral. There have been few studies that show transformation of mackinawite to pyrite can be inhibited in natural sediments settings (Wilkin and Ford, 2006; Holmkvist et al., 2011; Burton et al., 2011). This is the case in one of the peats (K1-71) from Hetao Basin, wherein greigite is shown in the sample. In compar-

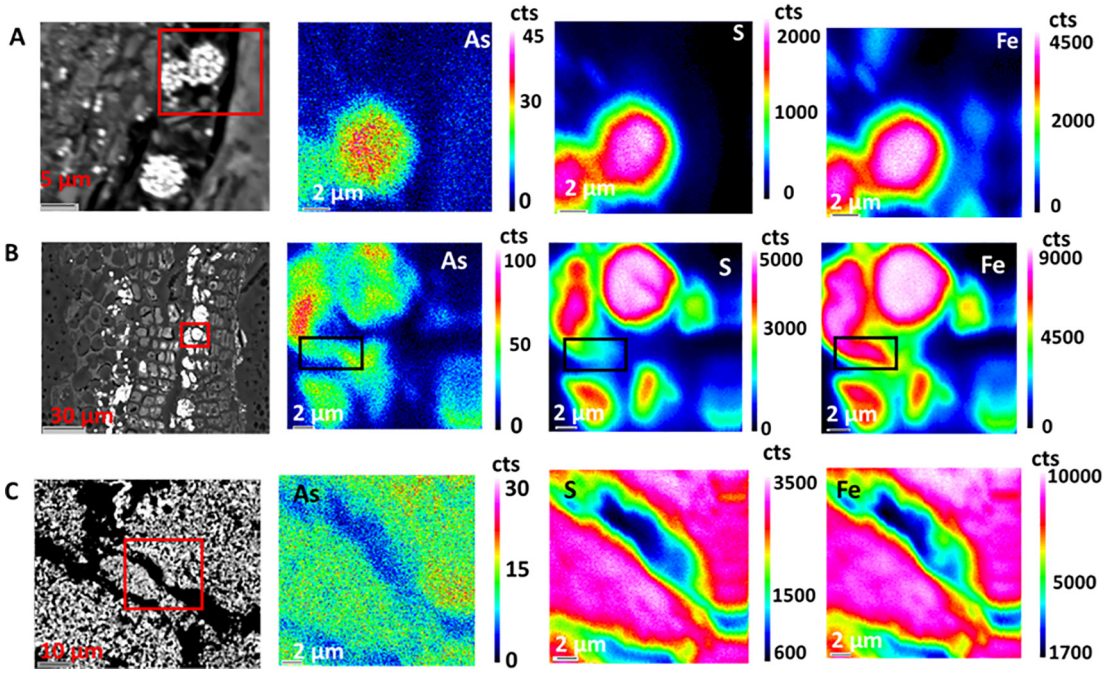

Fig. 7. Elemental mapping images of S, Fe and As elements obtained by EPMA, mapping area is indicated by red rectangle. (A) Map of framboidal pyrites area in sample K2-17. (B) Map of pyrites area in sample K2-28 which has nucleated in plant tissues, mapping area is indicated by a black rectangle corresponding to ferrihydrite (C) Map of greigite area in sample K1-71. (For interpretation of the references to colour in this figure legend, the reader is referred to the web version of this article.)

ison with pyrite-dominant peats, greigite-dominant peats have less organic matter and sulfur content, whereas the Fe content is comparable. This can be attributed to the likely precipitation of mackinawite which could remove sulfide from the pore water. The excess Fe^{2+} could exhaust sulfide, therefore, preventing polysulfide/S_0 formation and the subsequent transformation of greigite to pyrite. The lower sulfide flux in greigite-dominant layers compared to pyrite-dominant layers can be related to the limited labile organic carbon content or lower SO_4^{2-} concentration. This further emphasizes the importance of polysulfides/S_0 for the transformation of metastable iron sulfide precursors to pyrite under anoxic conditions in natural sediments. However, formation of greigite from a mackinawite precursor also requires an oxidant (Wilkin and Barnes, 1997; Schippers and JØrgensen, 2002; Hunger and Benning, 2007). In the surface water-sediments interface, penetration of oxidants such as O_2 and NO_3^- or metabolic activities of the SO_4^{2-} reducing bacteria probably favors the oxidation of FeS into greigite while polysulfides/S_0 is limited (Rickard, 1969; Picard et al., 2018; Mansor et al., 2019).

Phyllosilicates and decaying plant tissues provide the ideal micro-environments for pyrite/greigite nucleation and growth. Reactive Fe^{2+} provided by Fe-rich phyllosilicates via chemical or microbial reduction can induce supersaturation and precipitation of mackinawite on the silicates surface and subsequent transformation into pyrite/greigite. Some sulfate reducing bacteria such as *Desulfovibrio sp.* can reduce organic sulfur species into inorganic sulfides, which can also drive mackinawite formation in tissues (Altschuler et al., 1983). In addition, plant tissues can provide active surface area and decrease the oversaturation required for Fe sulfide nucleation (Rickard et al., 2007). Since organic sulfur is not detected in the S K-edge XANES spectra (<5%) of the peat samples, it suggests that microbial reduction of organic sulfur could have provided the inorganic sulfide needed for the formation of the mackinawite precursor. This result is contrary with previous study which has shown that inorganic sulfide is coupled with organic carbon as thiol functional groups, which in turn can sequester metalloids such as As (Langner et al., 2012; Wang et al., 2018). This might be a result of the differences in the ratio of reactive Fe to sulfur. The high abundance of reactive iron can remove inorganic sulfide in such Fe-rich sediments, thereby inhibiting transformation of inorganic sulfide to thiol functional groups.

4.2. Arsenic incorporation into Fe sulfides

Although relatively weakly correlated, the liner relationship between the S and As atomic ratios suggests that As possibly substitutes for S in the crystal structure of pyrite to form arsenian pyrite. The incorporation of As into pyrites is further evidenced by the As K-edge derivative XANES fits. In the pyrite-dominant peat sediments, our XANES data showed that approximate 60% of As exists as As(-I). The pyrite sequestration mechanism for As is consistent with previous studies of pyritic As sequestration mechanisms in natural sediments at low temperatures (Savage et al., 2000; Lowers et al., 2007). Arsenic content in the pyrite particles is between <90 mg/kg and 11,000 mg/kg with an average value around 5000 mg/kg,

showing that pyrite plays an important role for As sequestration in peat sediments. The similar maximum pyrite As concentrations in sediments from Bangladesh and the Hetao Basin suggests that the maximum As content incorporated into pyrite grains is around 1 wt.% under typical aquifer conditions (Lowers et al., 2007). The heterogeneous distributions of As in pyrite can be related to pyrite growth rates as well as contact time with porewater. The slightly higher As concentrations found in the framboid overgrowth rims as well as massive pyrites could be related to longer crystallization time, leading to enhanced As incorporation from the surrounding pore water into the pyrite structure (Lowers et al., 2007). Moreover, the resulting arsenian pyrites are still expected to be able to adsorb pore water As in the form of As(III) or As(V) species, or form As-S precipitates (Bostick and Fendorf, 2003; Qiu et al., 2018). This is consistent with our field observation that As concentration is relatively low in the groundwater with blackish-suspended particles, which likely corresponds to pyrite.

To our knowledge, adsorption and/or incorporation of As by greigite in both lab-scale batch reactions and in engineered and natural aquatic environments are still poorly investigated. The average As content of greigite particles as measured by EPMA, when multiplied by the amount of greigite determined in our samples, is comparable to the fraction of As bound in As sulfide (Supplementary text 5). Therefore, our results show that greigite is an important sink for As in the peat sediments with relatively lower S and organic carbon content and is primarily coordinated to sulfur within these particles, which is analogous to realgar evidenced by As K-edge XANES fitting. During greigite formation, oxidation of mackinawite coupled with As(III) species reduction may cause the surface precipitation of greigite and realgar. The findings in our study is consistent with the model predictions by Gallegos et al., (2008), where they argued that the formation of greigite is thermodynamically favorable by the reaction of As(III) species and mackinawite. Realgar and orpiment are also potential As carrier phases in the sulfidic sediments (O'Day et al., 2004a). However, greigite formation also uses up the available sulfide, therefore limiting As sulfides (i.e., realgar, orpiment) formation. Furthermore, it can also be constrained by relatively lower As concentrations in the pore water since As sulfide formation needs high porewater As concentration (O'Day et al., 2004b; Langner et al., 2012).

4.3. Significance of peat sediments for as mobilization process in aquifers

Our study clearly shows that Fe sulfides including greigite and pyrite formed in peat lenses could be important As sinks in contaminated aquifers. Sulfide flux controls Fe sulfides formation, while the sulfide flux would be in turn controlled either by labile organic matter in peat or SO_4^{2-} flux in the SO_4^{2-} limited groundwater (Lowers et al., 2007). In comparison to Fe (oxyhydr)oxides, greigite and pyrite are more thermodynamically stable under these sub-oxic conditions. Therefore, As release caused by reductive dissolution of iron (oxyhydr)oxides would not happen in the groundwater, and competitive adsorption between dissolved phosphate and silica and As on the reactive surfaces of Fe sulfides also cannot occur.

However, oxidation of arsenian pyrite to ferrihydrite-As (V) species can be ongoing process under slightly oxic conditions, as we have observed in the peat layer K2-28 (Fig. 1). Transferring As from surface or structure of arsenian pyrite onto ferrihydrite can temporarily retards the As release, which is supported by the similar average As content found in the ferrihydrite and pyrite as well as low As concentrations (<10 μg/L) in the groundwater (Fig. 1). However, ferrihydrite can potentially be reduced under disturbed groundwater redox conditions, which may cause elevated As concentration in the groundwater, since Fe sulfides re-formation is constrained by labile organic carbon. Groundwater redox conditions in draining delta or basins of South and Southeast Asia frequently experience anthropogenic perturbations, as well as seasonal fluctuations (Harvey et al., 2002; Fendorf et al., 2010), making Fe sulfides as an As source with respect to potential As remobilization. In recent years, *in situ* formation of Fe sulfides is suggested to remediate groundwater As pollution (Keimowitz et al., 2007; Pi et al., 2017). However, it is not suggested to apply it in such naturally unmanaged aquifer.

Previous studies also suggested that reactive organic carbon can be transported to other area by groundwater flow, therefore stimulating As release following by Fe (oxyhydr) oxides and As(V) species reduction (McArthur et al., 2001, 2004; Fendorf et al., 2010), but there is no solid evidence to prove that. Our study indicates that the labile organic matter buried in the peat sediments from aquifer can already be exhausted by early diagenetic Fe and S reduction. Our findings are consistent with the results found by Stuckey et al. (2015b), wherein organic matter leached from Mangrove deposits from Mekong delta cannot be able to simulate Fe (oxyhydr)oxides reduction.

5. SUMMARY AND CONCLUSION

Detrital peat formed from swamps or excessive flood debris is common in the As-contaminated aquifer of South and South-east Asia. To investigate the mineral diagenesis and sequestration behavior for As in these organic carbon-rich deposits, three peat lenses were retrieved from two cores with depths up to 80 m in the Hetao Basin.

Simultaneous microbial reduction of organic and inorganic sulfate favored Fe sulfide nucleation in the decaying plant tissues and phyllosilicates. Greigite and pyrite formed in surface water-sediment interface as the diagenetic minerals were stable in peat sediments under anoxic conditions. Excessive Fe(II) compared to sulfide due to lower sulfide flux potentially inhibited pyrite formation in the sulfidic porewater.

Peat sediments show a stable sink for As under steady anoxic conditions with As concentrations up to 250 mg/kg. Pyrite crystallites can have As content up to 11,000 mg/kg, with a majority of the As(-I) substitutes for

S(-I) in the pyrite structure. Arsenic content in the greigite grains is relatively homogeneous, ranging from ~500 to ~1400 mg/kg. We suggest that As forms distinct As sulfide precipitates in greigite-rich peats, as indicated by our As K-edge XAS data.

Anthropogenic perturbations and seasonal fluctuation of groundwater tables can largely change the groundwater redox conditions, for example, recharge of surface water caused by groundwater extraction infiltrates O_2 into groundwater. The increase of redox potential can induce Fe sulfides (e.g. pyrite and greigite) transfer to Fe (oxyhydr)oxides and temporarily retard As release into groundwater. However, reductive dissolution may in turn release As from the newly-formed iron (oxyhydr)oxide phase, as there is insufficient organic matter for transformation of these phases to Fe sulfide minerals and sequestration of As.

Declaration of Competing Interest

The authors declare that they have no known competing financial interests or personal relationships that could have appeared to influence the work reported in this paper.

ACKNOWLEDGEMENT

XRF, XRD, CSA, as well as HR-ICP-MS and IR-MS analysis were performed at KIT. The authors give thanks to Beate Oetzel, Claudia Moessner and Gesine Preuss for their technical assistance. We thank Ralf Steininger for his support during the collection of Fe, As and S K-edge XAS data at ANKA. The authors also acknowledge the CUGB group for their assistance during the field trip to the Hetao Basin and travel funding provided from the GRACE graduate program at KIT. We are also grateful for the advice from Elisabeth Eiche for C isotope analysis and Nicolas Börsig for XAS fitting analysis. The As K-edge XAS data of K2-28was collected at the BM23 beamline at ESRF (experiment no. EV-338), and the authors thank Sakura Pascarelli for assistance during beamtime. We further acknowledge the financial support from the Helmholtz Recruiting Initiative (award number I-044-16-01) awarded to L.G.B. J.P.H.P. and A.N.T. are supported by the European Union's Horizon 2020 Marie Skłodowska-Curie Innovative Training Network Grant No. 675219, and H.Y.W is supported by Chinese scholarship Council Grant No. 201606400055. Finally, we are grateful for the insightful comments from EIC Prof. Jeffrey Catalano, AE Prof. Caroline Peacock and three anonymous reviewers.

APPENDIX A. SUPPLEMENTARY MATERIAL

Supplementary data to this article can be found online at https://doi.org/10.1016/j.gca.2020.06.021.

REFERENCES

Altschuler Z. S., Schnepfe M. M., Silber C. C. and Simon F. O. (1983) Sulfur diagenesis in Everglades peat and origin of pyrite in coal. *Science* **221**(4607), 221–227.

Anawar H. M., Akai J., Komaki K., Terao H., Yoshioka T., Ishizuka T., Safiullah S. and Kato K. (2003) Geochemical occurrence of arsenic in groundwater of Bangladesh: sources and mobilization processes. *J. Geochem. Explor.* **77**(2–3), 109–131.

Benning L. G., Wilkin R. T. and Barnes H. L. (2000) Reaction pathways in the Fe–S system below 100 °C. *Chem. Geol.* **167**(1–2), 25–51.

Berner R. A. (1970) Sedimentary pyrite formation. *Am. J. Sci.* **268** (1), 1–23.

Blanchard M., Alfredsson M., Brodholt J., Wright K. and Catlow C. R. A. (2007) Arsenic incorporation into FeS2 pyrite and its influence on dissolution: a DFT study. *Geochim. Cosmochim. Acta* **71**(3), 624–630.

Bostick B. C. and Fendorf S. (2003) Arsenite sorption on troilite (FeS) and pyrite (FeS2). *Geochim. Cosmochim. Acta* **67**(5), 909–921.

Burton E. D., Johnston S. G. and Bush R. T. (2011) Microbial sulfidogenesis in ferrihydrite-rich environments: Effects on iron mineralogy and arsenic mobility. *Geochim. Cosmochim. Acta* **75** (11), 3072–3087.

Cai M., Ye P., Yang X. and Li C. (2019) Vegetation and climate change in the Hetao Basin (Northern China) during the last interglacial-glacial cycle. *J. Asian. Earth. Sci.* **171**, 1–8.

Chen C., Kukkadapu R. K., Lazareva O. and Sparks D. L. (2017) Solid-phase Fe speciation along the vertical redox gradients in floodplains using XAS and Mössbauer spectroscopies. *Environ. Sci. Technol.* **51**(14), 7903–7912.

Deng Y., Wang Y. and Ma T. (2009) Isotope and minor element geochemistry of high arsenic groundwater from Hangjinhouqi, the Hetao Plain, Inner Mongolia. *Appl. Geochem.* **24**(4), 587–599.

Fakhreddine S., Dittmar J. and Phipps D., et al. (2015) Geochemical triggers of arsenic mobilization during managed aquifer recharge. *Environ. Sci. Technol.* **49**(13), 7802–7809.

Fendorf S., Michael H. A. and van Geen A. (2010) Spatial and temporal variations of groundwater arsenic in South and Southeast Asia. *Science* **328**(5982), 1123–1127.

Gallegos T. J., Han Y. S. and Hayes K. F. (2008) Model predictions of realgar precipitation by reaction of As (III) with synthetic mackinawite under anoxic conditions. *Environ. Sci. Technol.* **42**(24), 9338–9343.

Guo H., Liu C., Lu H., Wanty R. B., Wang J. and Zhou Y. (2013) Pathways of coupled arsenic and iron cycling in high arsenic groundwater of the Hetao basin, Inner Mongolia, China: An iron isotope approach. *Geochim. Cosmochim. Acta* **112**, 130–145.

Harvey C. F., Swartz C. H., Badruzzaman A. B. M., Keon-Blute N., Yu W., Ali M. A., Jay J., Beckie R., Niedan V., Brabander D., Oates P. M., Ashfaque K. N., Islam S., Hemond H. F. and Ahmed M. F. (2002) Arsenic mobility and groundwater extraction in Bangladesh. *Science* **298**(5598), 1602–1606.

Holmkvist L., Ferdelman T. G. and Jorgensen B. B. (2011) A cryptic sulfur cycle driven by iron in the methane zone of marine sediment (Aarhus Bay, Denmark). *Geochim. Cosmochim. Acta*, 3581–3599.

Hunger S. and Benning L. G. (2007) Greigite: a true intermediate on the polysulfide pathway to pyrite. *Geochem. Trans.* **8**(1), 1.

Islam F. S., Gault A. G., Boothman C., Polya D. A., Charnock J. M., Chatterjee D. and Lloyd J. R. (2004) Role of metal-reducing bacteria in arsenic release from Bengal delta sediments. *Nature* **430**(6995), 68.

Jia L., Zhang X., Ye P., Zhao X., He Z., He X., Zhou Q., Li J., Ye M., Wang Z. and Meng J. (2016) Development of the alluvial and lacustrine terraces on the northern margin of the Hetao Basin, Inner Mongolia, China: Implications for the evolution of the Yellow River in the Hetao area since the late Pleistocene. *Geomorphol* **263**, 87–98.

Keimowitz A. R., Mailloux B. J., Cole P., Stute M., Simpson H. J. and Chillrud S. N. (2007) Laboratory investigations of enhanced sulfate reduction as a groundwater arsenic remediation strategy. *Environ. Sci. Technol.* **41**(19), 6718–6724.

Kirk M. F., Roden E. E., Crossey L. J., Brealey A. J. and Spilde M. N. (2010) Experimental analysis of arsenic precipitation during microbial sulfate and iron reduction in model aquifer sediment reactors. *Geochim. Cosmochim. Acta* **74**(9), 2538–2555.

Klementiev, K.V., 2012. XAFSmass. A program for calculating the mass of XAFS samples.

Knappová M., Drahota P., Falteisek L., Culka A., Penížek V., Trubač J., Mihaljevič M. and Matoušek T. (2019) Microbial sulfidogenesis of arsenic in naturally contaminated wetland soil. *Geochim. Cosmochim. Acta* **267**, 33–50.

Koeksoy E., Sundman A., Byrne J. M., Lohmayer R., Planer-Friedrich B., Halevy I., Konhauser K. O. and Kappler A. (2019) Formation of green rust and elemental sulfur in an analogue for oxygenated ferro-euxinic transition zones of Precambrian oceans. *Geology* **47**(3), 211–214.

Langner P., Mikutta C. and Kretzschmar R. (2012) Arsenic sequestration by organic sulphur in peat. *Nat. Geosci.* **5**(1), 66.

Langner P., Mikutta C., Suess E., Marcus M. A. and Kretzschmar R. (2013) Spatial distribution and speciation of arsenic in peat studied with microfocused X-ray fluorescence spectrometry and X-ray absorption spectroscopy. *Environ. Sci. Technol.* **47**(17), 9706–9714.

Le P. P., Blanchard M., Brest J., Boulliard J. C., Ikogou M., Stetten L., Wang S., Landort G. and Morin G. (2017) Arsenic incorporation in pyrite at ambient temperature at both tetrahedral SI and octahedral FeII sites: evidence from EXAFS-DFT analysis. *Environ. Sci. Technol.* **51**(1), 150–158.

Lowers H. A., Breit G. N., Foster A. L., Whitney J., Yount J., Uddin M. N. and Muneem A. A. (2007) Arsenic incorporation into authigenic pyrite, Bengal Basin sediment, Bangladesh. *Geochim. Cosmochim. Acta* **71**(11), 2699–2717.

Manceau A. and Nagy K. L. (2012) Quantitative analysis of sulfur functional groups in natural organic matter by XANES spectroscopy. *Geochim. Cosmochim. Acta* **99**, 206–223.

McArthur J. M., Banerjee D. M., Hudson-Edwards K. A., Mishra R., Purohit R., Ravenscroft P., Cronin A., Howarth R. J., Chatterjee A., Talukder T., Lowry D., Houghton S. and Chadha D. K. (2004) Natural organic matter in sedimentary basins and its relation to arsenic in anoxic ground water: the example of West Bengal and its worldwide implications. *Appl. Geochem.* **19**(8), 1255–1293.

McArthur J. M., Ravenscroft P., Safiulla S. and Thirlwall M. F. (2001) Arsenic in groundwater: testing pollution mechanisms for sedimentary aquifers in Bangladesh. *Water Resour. Res.* **37**(1), 109–117.

Mansor M., Berti D., Hochella M. F., Murayama M. and Xu J. (2019) Phase, morphology, elemental composition, and formation mechanisms of biogenic and abiogenic Fe-Cu-sulfide nanoparticles: a comparative study on their occurrences under anoxic conditions. *Am. Min.* **104**(5), 703–717.

Naafs B. D. A., Inglis G. N., Blewett J., McClymont E. L., Lauretano V., Xie S., Evershed R. P. and Pancost R. D. (2019) The potential of biomarker proxies to trace climate, vegetation, and biogeochemical processes in peat: a review. *Glob Planet Change* **179**, 57–79.

Neumann T., Rausch N., Leipe T., Dellwig O., Berner Z. and Böttcher M. E. (2005) Intense pyrite formation under low-sulfate conditions in the Achterwasser lagoon, SW Baltic Sea. *Geochim. Cosmochim. Acta* **69**(14), 3619–3630.

Nickson R., McArthur J., Burgess W., Ahmed K. M., Ravenscroft P. and Rahmanñ M. (1998) Arsenic poisoning of Bangladesh groundwater. *Nature* **395**(6700), 338.

O'Day P. A., Rivera, Jr, N., Root R. and Carroll S. A. (2004a) a) X-ray absorption spectroscopic study of Fe reference compounds for the analysis of natural sediments. *Am. Mineral.* **89**(4), 572–585.

O'Day P. A., Vlassopoulos D., Root R. and Rivera N. (2004b) b) The influence of sulfur and iron on dissolved arsenic concentrations in the shallow subsurface under changing redox conditions. *Proc. Natl. Acad. Sci.* **101**(38), 13703–13708.

Pannalal S. J., Crowe S. A., Cioppa M. T., Symons D. T., Sturm A. and Fowle D. A. (2005) Room-temperature magnetic properties of ferrihydrite: a potential magnetic remanence carrier? *Earth Planet. Sci. Lett.* **236**(3–4), 856–870.

Pi K., Wang Y., Xie X., Ma T., Liu Y., Su C., Zhu Y. and Wang Z. (2017) Remediation of arsenic-contaminated groundwater by in-situ stimulating biogenic precipitation of iron sulfides. *Water Res.* **109**, 337–346.

Picard A., Gartman A., Clarke D. R. and Girguis P. R. (2018) Sulfate-reducing bacteria influence the nucleation and growth of mackinawite and greigite. *Geochim. Cosmochim. Acta* **220**, 367–384.

Pickard D., Mussmann M. and Steadman J. A. (2017) Sedimentary sulfides. *Elements* **13**(2), 117–122.

Qiu G., Gao T., Hong J., Luo Y., Liu L., Tan W. and Liu F. (2018) Mechanisms of interaction between arsenian pyrite and aqueous arsenite under anoxic and oxic conditions. *Geochim. Cosmochim. Acta* **228**, 205–219.

Rancourt D. G. and Ping J. Y. (1991) Voigt-based methods for arbitrary-shape static hyperfine parameter distributions in Mössbauer spectroscopy. *Nucl. Instrum. Methods Phys. Res.: Beam Interact. Mater. Atoms* **58**(1), 85–97.

Ravel B. and Newville M. (2005) ATHENA, ARTEMIS, HEPHAESTUS: data analysis for X-ray absorption spectroscopy using IFEFFIT. *J. Synchrotron Radiat.* **12**(4), 537–541.

Rickard D. T. (1969) The microbiological formation of iron sulfides. *Stockholm Contrib. Geol.* **20**, 49–66.

Rickard D. and Luther G. W. (2007) Chemistry of iron sulfides. *Chem. Rev.* **107**(2), 514–562.

Rickard D., Grimes S., Butler I., Oldroyd A. and Davies K. L. (2007) Botanical constraints on pyrite formation. *Chem. Geol.* **236**(3–4), 228–246.

Savage K. S., Tingle T. N., O'Day P. A., Waychunas G. A. and Bird D. K. (2000) Arsenic speciation in pyrite and secondary weathering phases, Mother Lode gold district, Tuolumne County, California. *Appl. Geochem.* **15**(8), 1219–1244.

Schippers A. and Jørgensen B. B. (2002) Biogeochemistry of pyrite and iron sulfide oxidation in marine sediments. *Geochim. Cosmochim. Acta* **66**(1), 85–92.

Smith P. G., Koch I., Gordon R. A., Mandoli D. F., Chapman B. D. and Reimer K. J. (2005) X-ray absorption near-edge structure analysis of arsenic species for application to biological environmental samples. *Environ. Sci. Technol.* **39**(1), 248–254.

Smith R. L., Kent D. B., Repert D. A. and Böhlke J. K. (2017) Anoxic nitrate reduction coupled with iron oxidation and attenuation of dissolved arsenic and phosphate in a sand and gravel aquifer. *Geochim. Cosmochim. Acta* **196**, 102–120.

Stuckey J. W., Schaefer M. V., Benner S. G. and Fendorf S. (2015a) Reactivity and speciation of mineral-associated arsenic in seasonal and permanent wetlands of the Mekong Delta. *Geochim. Cosmochim. Acta* **171**, 143–155.

Stuckey J. W., Schaefer M. V., Kocar B. D., Dittmar J., Pacheco J. L., Benner S. G. and Fendorf S. (2015b) Peat formation concentrates arsenic within sediment deposits of the Mekong Delta. *Geochim. Cosmochim. Acta* **149**, 190–205.

Thomas-Arrigo L. K., Mikutta C., Byrne J., Barmettler K., Kappler A. and Kretzschmar R. (2014) Iron and arsenic

speciation and distribution in organic flocs from streambeds of an arsenic-enriched peatland. *Environ. Sci. Technol.* **48**(22), 13218–13228.

Vandenberghe R. E., De Grave E., De Bakker P. M. A., Krs M. and Hus J. J. (1992) Mössbauer effect study of natural greigite. *Hyperfine Interact.* **68**(1–4), 319–322.

Vasiliev I., Franke C., Meeldijk J. D., Dekkers M. J., Langereis C. G. and Krijgsman W. (2008) Putative greigite magnetofossils from the Pliocene epoch. *Nat. Geosci.* **1**(11), 782.

Wang H. Y., Guo H. M., Xiu W., Bauer J., Sun G. X., Tang X. H. and Norra S. (2019a) Indications that weathering of evaporite minerals affects groundwater salinity and As mobilization in aquifers of the northwestern Hetao Basin, China. *Appl. Geochem.* **109** 104416.

Wang X., Zhu M., Koopal L. K., Li W., Xu W., Liu F., Zhang J., Liu Q., Feng X. and Sparks D. L. (2016) Effects of crystallite size on the structure and magnetism of ferrihydrite. *Environ. Sci.: Nano.* **3**(1), 190–202.

Wang Y., Le Pape P., Morin G., Asta M. P., King G., Bártová B., Suvorova E., Frutschi M., lkogou M., Cong Pham V. H., Le Vo P., Herman, Charlet F. and Bernier-Latmani L. B. (2018) Arsenic speciation in Mekong Delta sediments depends on their depositional environment. *Environ. Sci. Technol.* **52**(6), 3431–3439.

Wang Y., Pi K., Fendorf S., Deng Y. and Xie X. (2019b) Sedimentogenesis and hydrobiogeochemistry of high arsenic Late Pleistocene-Holocene aquifer systems. *Earth-Sci. Rev.* **189**, 79–98.

Wilkin R. T., Arthur M. A. and Dean W. E. (1997) History of water-column anoxia in the Black Sea indicated by pyrite framboid size distributions. *Earth Planet. Sci. Lett.* **148**(3–4), 517–525.

Wilkin R. T., Barnes H. L. and Brantley S. L. (1996) The size distribution of framboidal pyrite in modern sediments: an indicator of redox conditions. *Geochim. Cosmochim. Acta* **60** (20), 3897–3912.

Wilkin R. T. and Ford R. G. (2006) Arsenic solid-phase partitioning in reducing sediments of a contaminated wetland. *Chem. Geol.* **228**(1–3), 156–174.

Wilkin R. T. and Barnes H. L. (1997) Formation processes of framboidal pyrite. *Geochim. Cosmochim. Acta* **61**(2), 323–339.

Winkel L., Berg M., Amini M., Hug S. J. and Johnson C. A. (2008) Predicting groundwater arsenic contamination in Southeast Asia from surface parameters. *Nat. Geosci.* **1**(8), 536.

Zhang Z., Guo H. M., Liu S., Weng H. C., Han S. B. and Gao Z. P. (2020) Mechanisms of groundwater arsenic variations induced by extraction in the western Hetao Basin, Inner Mongolia, China. *J. Hydrol.* **583**(124599), 1–13.

Zhu Y. G., Xue X. M., Kappler A., Rosen B. P. and Meharg A. A. (2017) Linking genes to microbial biogeochemical cycling: lessons from arsenic. *Environ. Sci. Technol.* **51**(13), 7326–7339.

Associate editor: Caroline L. Peacock

Supplementary material

Supplementary text 1

Methods for the bulk sediment geochemical composition characterization and groundwater analysis

Sub-sediments samples were frozen, dried and homogenized by mechanical grinding. Geochemical analysis for trace element composition was determined by means of energy dispersive X-Ray spectrometry (EDX; Epsilon 5, PANanalytical). Results were regularly checked by standard materials (SOIL-5, n=4; GXR-6, n=4; GXR-2, n=4; SL-1 n=4) with precision better than 5 % and afterwards corrected to certified values. Major elements (K, Na, Si, Ca, Mg, Fe, Mn) were analyzed by wavelength dispersive X-ray spectrometry (WDX; S4 Explorer, Bruker AXS) after making glass beads. The measurement accuracy (within 5 %) was regularly checked against a standard AGV-1 (USGS).

Arsenic content in the sediments was measured with hydride generation flow injection atomic absorption spectroscopy (HG-FIAAS) measurement with a Perkin Elmer AAnalyst200 coupled with a FIMS-400 hydride generation system and autosampler following sediment digestion. Around 0.1 g of each dried sediment sample was weighed into 100 mL Teflon tubes and mixed with 1 mL of Milli-Q water to avoid strong reactions between sediments and acid. Afterwards, 2 ml of 65 % HNO_3 (super pure) was added and the mixture heated at 80 °C for around 10 minutes. Then 1 mL $HClO_4$ (normal pure) and 5 mL HF (super pure) were added into the tubes and the samples digested under cover at 120 °C for 18 h, afterwards the acid was evaporated until the sample near dryness. Then the remains were added to 2 mL 65 % HNO_3 and evaporated until dryness. The last step was repeated 3 times. Finally, to these digested solutions 2 mL HNO_3 were added and then these were diluted to 50 mL with ultrapure water. Using the same procedure 0.05 g of the standards GXR-5 (Marine sediment, USGS) and RGM-1 (Rhyolite, USGS) as well as two blank samples were digested in parallel as controls.

Total carbon (TC), total organic carbon (TOC) and total sulfur (S) contents were determined with a carbon/sulfur analyzer (CSA; CS 2000 MultiLine F/SET-3, Eltra). Inorganic carbon was removed by repeated addition of 20 % HCl (Suprapure, Merke) and reacting at 60 °C. Measurement accuracy (100 ± 2 %) was regularly checked by analyzing a steel standard 92400-3050.

Total nitrogen (TN) and carbon of de-carbonated samples (2 % HCl, Suprapur©, Merck) were measured for part of samples with an elemental analyzer (EuroEA3000, HekaTech). Results of C and TN analyses were used to calculate

molar C/N ratios. The measurement accuracy and reproducibility for both elements (± 5 %) were checked with the reference standards BBOT (HekaTech) and GBW 07043 (office of CRN′S China).

The $\delta^{13}C_{org}$ signature for de-carbonated samples was measured using an elemental analyzer (EuroEA3000, EuroVector, Italy) in continuous flow mode, which was connected an isotope ratio mass spectrometer by an open split (IRMS, IsoPrime, Fa. GV Instrument, UK). All of $\delta^{13}C_{org}$ de-carbonated samples were reported relative to the Vienna Pee Dee Belemnite (‰ VPDB). The measurement accuracy is controlled by repeated samples measurements for 3 times and standards with precision better than ± 0.1‰ (UREA, n = 12; USGS 24, n = 44; NBS 18 n = 12).

The groundwater samples were analyzed by CUGB, the methods were shown in Guo et al., (2016). Specifically, all groundwater samples were filtered through 0.20 μm membrane filters in the field. Water samples for major cation and trace element analysis were acidified with ultrapure 6 M HNO_3 to pH < 2.0. Arsenic concentration is analyzed by inductively coupled plasma mass spectrometry (ICP-MS). Oxidation reduction potential (ORP) were measured in field site using multiparameter portable meter (HI 9828, HANNA).

Supplementary text 2

Characterizing minerals in the bulk peat layers by X-ray powder Diffraction and magnetic separates by synchrotron powder X-ray diffraction

Samples were freeze-dried and homogenized by manual grinding. Mineralogy of the core samples was determined by X–ray powder diffraction (XRD) analysis (Kristalloflex D500, Siemens, Germany) at conditions of 40 kV and 25 mA. Cu Kα1-radiation was used at angles between 2° and 80°. Peak identification was performed by EVA program (Bruker) by database PDF 2002.

Magnetic minerals were separated from peat layer K1-71 referred from Reinholdsso et al., (2013). About 2 g of grinded sediments were suspended in the methanol and stirred. The magnetic minerals were concentrated by placing a handy magnet. Afterwards, the concentrated magnetic aggregates were transferred into a small glass vials which were filled with methanol. Sodium pyrophosphate was used to disaggregate the separates. After around 2 min ultrasonic oscillation in the ultra-sonic bath, handy magnet was taped to the outside of the vial, which was shaken and left to stand so that non-magnetic material sank to the bottom, the material attracted to the side of the vial where the magnet was taped was recovered by a spoon and placed into a new vial. Minerals of magnetic separates were characterized by synchrotron powder X-ray Diffraction at SUL-beamline at ANKA with an incident beam energy of 12,735 eV. Peak identification was also performed by EVA program (Bruker) using database of PDF 2002.

Supplementary text 3

Temperature-dependent magnetic susceptibility measurement

Temperature-dependent magnetic susceptibility of peat sediments were measured with KYL-2 Kappabridge combined with CS-L cryostat and CS-2 furnace (Geofyzika/Agico). The measurement temperature varies from -192 ℃ to 700 ℃.

Supplementary text 4

Detailed XAS data collection and analysis information

XAS data is collected at ANKA synchrotron facility in Karlsruhe Institute of Technology. The storage ring operates at 2.5 GeV. Spectra was collected under vacuum. Collecting information for model compounds are shown in **Table EA-4**.

The incident X-ray beam was scanned through As and Fe K-edges (edge set at 11874 eV for As and 7112 eV for Fe) using Si (111) crystal pair as a monochromator with a fixed-beam exit. Fe K-edge spectra was collected in transmission mode, whereas As K-edge XAS spectra was collected in fluorescence mode. Transmission spectra were collected using three ADC IC-Type ionization chambers with Kapton windows, and fluorescence spectra were collected using a Gresham 7-element (Li) detector. As K-edge spectra was calibrated with Au foil, whereas Fe K-edge spectra was calibrated with Fe metal foil.

S K-edge XANES data was collected in fluorescence mode, the beam was calibrated to the sulfate excitation energy of Na_2SO_4 at 2481.4 eV. To prevent S species from beam damage, spectra were collected at different positions in thin layers.

Data reduction and analysis of EXAFS spectra were performed using Athena (Ravel and Newville, 2005). For liner combination fitting (LCF) was conducted on XANES and derivative XANES (-20 eV to 30 eV), and Fe K-edge XAFS (k = 3-10 Å, k^3-weighting) regions. For all Fe reference compounds, the total number of contributing reference standards was limited to five. The sum was forced to equal 1.

The k^2-weighted χ(k) As K-edge EXAFS spectra was Fourier-transformed over a k-range of 3 to 10 Å by a Hanning window with a dk value of 1, afterwards transforming the spectra to R-space.

Supplementary text 5

Calculation of As content adsorbed/incorporated by greigite

Average As content in the greigite particle is 1000 mg/kg and 900 mg/kg in sample K2-17 and K1-71 resulting from average As content measured by EPMA.

Atom ratio of Fe in the greigite is 23 % (± 2.5) and 42 % (± 4.5) in sample K2-17 and K1-71 resulting from Fe K-edge XAFS fitting, whereas total Fe content in K2-17 and K1-71 is 5.31 % and 3.85 %, respectively.

Total As content in the K2-17 and K1-71 is 59 mg/kg and 47 mg/kg, respectively.

1. Estimation of As content adsorbed/incorporated into greigite in the sample K2-17 (1) and weight percent to total As content (2)

1000 mg/kg * 5.31 *23 /10000 * 296/168= 21.5 mg/kg (1) 21.5 mg/kg / 59 mg/kg *100= 36.4 %

2. Estimation of As content adsorbed/incorporated into greigite in the peat K1-71 (1) and weight percent to total As content (2)

900 mg/kg * 3.85 *42/10000 * 296/168= 25.6 mg/kg (1) 25.6 mg/kg / 47 mg/kg *100= 54.4 % (2)

Supplementary Table S1 Sequential extraction scheme for Fe related phases in the peat samples referred from Keon et al., (2001) and Poulton and Canfield (2005).

Step	Target phases	Extractant	Conditions
F1	Ionically boned	1.0 M NaH_2PO_4	40 mL, 24 h, pH 4-5, one repetition of each time duration, one water wash
F2	Co-precipitated with FeS, carbonates	1 M CH_3COONa /CH_3COOH	40 mL, 1 h, pH 4.5, one repetition, one water wash
F3	Co-precipitated with amorphous iron oxides, magnetite and greigite as well	0.2 M ammonium oxalate/0.17 M oxalic acid	40 mL, 2 h, pH 3, dark (wrapped in Al-foil), one repetition, one water wash
F4	Co-precipitated with crystalline Fe oxides	DCB: 0.5 M Na-citrate +1 M $NaHCO_3$; 0.5 g $Na_2S_2O_4xH_2O$	35 mL Na-Citrate + 2.5 mL $NaHCO_3$ (heating to 85 °C), addition of 0.5 g $Na_2S_2O_4xH_2O$, 15 min at 80 °C, one repetition, one water wash
F5	Co-precipitated with pyrite and part of sheet silicates	16 M HNO_3	20 ml 16 M HNO_3, 2h, 25 °C, one repetition, one water wash

Supplementary Table S2 Sequential extraction results for Fe related phases (mg/kg) in peat layers.

Samples Name	F1	F2	F3	F4	F5
K2-17	537	93	18176	2397	2929
K2-28	807	91	5183	727	13697
K1-71	748	1185	23893	2356	1887

Supplementary Table S3 Model compounds collection information

Compound	Natural	Source/synthesis reference
Fe model compounds		
chlorite	-[a]	natural[1]
biotite	-[a]	natural[1]
illite	-[a]	natural[1]
hornblende	-[a]	natural[1]
pyrite	FeS_2	natural[1]
Fe monosulphide	FeS	commercial (Fluka)
siderite	$FeCO_3$	natural[1]
maghematite	γ-Fe2O3	synthetic[2]
magnetite	Fe_4O_3	synthetic[2]
hematite	Fe_2O_3	synthetic[2]
sulfate green rust	$[Fe^{II}_4Fe^{III}_2(OH)_{12}].[SO_4^{2-}.mH_2O]^{2-}$	synthetic[5]
goethite	α-FeO(OH)	synthetic[2]
greigite	Fe_3S_4	natural[1]
lepidocrocite	β-FeO(OH)	synthetic[2]
ferrihydrite	$Fe(OH)_3$	synthetic[2]
Fe(III)-citrate dehydrate	$C_6H_5FeO_7$	commercial (Roth)
Fe(II)-oxalate dehydrate	$C_2H_4FeO_5$	commercial (Sigma-Aldrich)
S model compounds		
greigite	Fe_3S_4	natural[1]
iron monosulphide	FeS	commercial (Fluka)
pyrite	FeS_2	natural[1]
gypsum	$CaSO_4.2H_2O$	natural[1]
sulfur	S_0	Commercial (Fluka)
As model compounds		
As(III)-ferrihydrite	$As_{0.01}(Fe(OH)_3)_{0.99}$	synthetic[3]
As(V)-ferrihydrite	$As_{0.02}(Fe(OH)_3)_{0.98}$	synthetic[3]
arsenopyrite	FeAsS	natural[1]
glutamylcysteinylgly thioarsenite	$As(C_{10}H_{17}N_3O_6S)_{2.6}(OH)_{0.6}$	synthetic[4]
Realgar	As_4S_4	Natural[1]
Orpiment	As_2S_3	Natural[1]

[a]The minerals are characterized by XRD without chemical compositions analysis.

[1]The minerals are provided by minerals center of Karlsruhe Institute of Technology.

[2]minerals provided by Thomas et al., (2018), which is synthesized according to Cornell and Schwertmann (2003).

[3]chemicals are synthesized according to Dixit and Hering (2003)

[4]chemicals are synthesized according to Miot et al., (2009)

[5]minerals provided by Thomas et al., (2018), which is synthesized according to Géhin et al., (2002).

Supplementary Table S4 As and S K-edge XANES fitting results

Sample	Mineralogical composition (% mol S)					Mineralogical composition (% mol As)				
	XANES					XANES				
	Greigite	Pyrite	S_0	$CaSO_4 \cdot 2H_2O$	R^2	realgar	arsenopyrite	As (III)-Fh	As (V)-Fh	R^2
K2-17	70 (1.0)	17 (2.2)	11 (3.5)	2 (0.3)	0.017	49 (8.7)	0 (7.3)	45 (3.8)	6 (1.7)	0.0072
K2-28	-	35 (1.9)	54 (1.9)	11 (3.1)	0.0097	8 (5.0)	61 (6)	3.8 (2.4)	27 (1.7)	0.0166
K1-71	92 (0.7)	-	6 (0.6)	2 (0.2)	0.0058	39 (2.1)	-	53 (4.7)	8 (1.3)	0.0063

Supplementary Table S5 Electron probe analyses of selected pyrite and greigite particles from peat layers.

Sample name	mineral	Fe (wt%)	As (wt %)	S (wt %)	Total (wt %)	Fe (atom %)	As (atom %)	S (atom %)	S/Fe (atom)	Morphology
K2-28	pyrite	45.5	0.651	52.1	98.3	33.22	0.35	66.29	2.00	massive
		41.2	0.454	51.4	93.0	31.31	0.26	68	2.17	massive
		44.4	0.140	49.0	93.5	34.14	0.08	65.6	1.92	massive
		43.6	0.312	46.4	90.3	34.9	0.19	64.63	1.85	framboid-filled
		43.5	0.341	46.7	90.5	34.67	0.2	64.84	1.87	framboid-over growth rim
		45	0.764	51.1	96.9	33.36	0.42	66.07	1.98	massive
		44.8	0.509	52.5	97.8	32.72	0.28	66.83	2.04	massive
		45.6	0.759	52.6	99.0	33.03	0.41	66.41	2.01	framboid-open
		45.4	0.533	52.8	98.7	32.91	0.29	66.67	2.03	massive
		42.7	0.088	49.2	92.0	33.03	0.05	66.27	2.01	framboid-over growth rim
		42.5	0.100	49.3	92.0	32.86	0.06	66.31	2.02	framboid-over growth rim
		44.5	0.017	50.1	94.6	33.69	0.01	66.16	1.96	framboid-open
		44.5	0.038	50.2	94.7	33.67	0.02	66.14	1.96	framboid-open
		43.2	0.139	50.2	93.5	32.92	0.08	66.63	2.02	framboid-over growth rim
		42.8	0.137	49.8	92.7	32.91	0.08	66.71	2.03	framboid-over growth rim
		44.0	0.090	49.8	93.9	33.52	0.05	66.13	1.97	framboid-filled
		43.7	0.084	49.7	93.5	33.43	0.05	66.26	1.98	framboid-filled
		44.3	0.024	54.3	98.6	31.81	0.01	67.95	2.14	massive
		44.2	0.235	53.4	97.8	32.03	0.13	67.41	2.1	massive
		40.1	1.140	45.8	87.0	32.9	0.7	65.35	1.99	massive
		40.3	1.145	46.4	87.8	32.72	0.69	65.57	2.00	massive
		38.8	0.573	42.0	81.4	34.23	0.38	64.52	1.88	massive
	Fe (oxyhydr)oxides	52.3	0.407	14.1	68.1	-	-	-	-	-
		46.0	0.462	10.6	58.4	-	-	-	-	-
K2-17	pyrite	40.6	bdl	47.3	87.9	32.58	--	66.15	2.03	framboid-open
		42.0	bdl	50.6	92.6	32.06	--	67.25	2.1	
		43.4	0.099	49.2	92.8	33.53	0.06	66.17	1.97	
		43.5	0.087	50.3	93.8	33.08	0.05	66.67	2.02	
		41.2	1.104	43.5	85.8	34.59	0.69	63.59	1.84	
		41.6	0.98	45.4	87.9	33.71	0.59	64.18	1.9	
		41.8	1.084	50.2	93.0	31.87	0.62	66.71	2.09	
		39.1	0.81	45.5	85.5	31.5	0.49	63.84	2.03	
	greigite	44.1	0.081	31.9	76.2	41.99	0.06	52.94	1.26	-
		39.3	0.046	28.8	68.2	39.36	0.03	50.31	1.28	
		52.2	0.125	36.2	88.5	44.77	0.08	54.04	1.21	
		50.6	0.138	34.9	85.7	44.87	0.10	53.88	1.2	
		51.3	0.122	37.2	88.6	43.78	0.08	55.24	1.26	
K1-71	greigite	47.8	0.072	36.5	84.4	42.84	0.05	56.93	1.33	-
		44.8	0.127	33.6	78.6	43.25	0.09	56.48	1.31	
		48.9	0.048	37.8	86.8	42.54	0.03	57.18	1.34	
		42.0	0.051	32.1	74.1	42.79	0.04	56.95	1.33	
		43.6	0.082	33.9	77.6	42.37	0.06	57.40	1.35	
		43.3	0.120	30.7	74.2	41.45	0.09	51.20	1.24	
		41.1	0.090	30.2	71.4	43.68	0.07	55.85	1.28	
		43.1	0.126	31.8	75.0	43.63	0.10	55.99	1.28	

bdl: below than the detection limit (~ 90 mg/kg).

Supplementary Table S6 Hyperfine parameters obtained by fitting both samples. T – temperature, δ - isomer shift, ΔE_Q - quadrupole splitting, SDev – standard deviation, Skew – skew of fit, ε - quadrupole shift, B_{hf} - hyperfine magnetic field, RA – relative spectral abundance with associated error, χ^2 – goodness of fit. Hem – hematite, Greig – greigite, Gt - goethite.

Sample	**T**	**Phase**	**δ**	**ΔE_Q**	***SDev (ΔE_Q)***	***Skew (ΔE_Q)***	**ε**	**B_{hf}**	***SDev (B_{hf})***	***Skew (B_{hf})***	**RA**	**±**	**χ^2**
	K		mm/s	mm/s	mm/s		mm/s	T	T		**%**		
6_K2_17	20	Fe(II)	1.27	2.88	0.13	0.00					20.7	2.5	2.51
		Fe(III)	0.46	1.07	1.12	2.45					33.6	1.6	
		Fe(II)	1.19	2.76	0.37	0.00					11.5	2.7	
		Hem	0.47				-0.07	53.4	1.0	0.0	7.1	0.5	
		Greig	0.59				0.00	32.0	3.2	0.0	27.1	1.3	
7_K2_28	20	Fe(II)	1.27	2.84	0.14	0.00					29.4	4.7	0.71
		Fe(III)	0.41	0.77	0.40	1.84					62.7	5.5	
		Fe(II)	1.19	2.34	0.31	0.00					7.9	6.0	
5_K1_71	20	Fe(II)	1.27	2.85	0.13	0.00					20.4	3.0	1.00
		Fe(III)	0.48	1.16	1.17	1.81					18.0	1.3	
		Fe(II)	1.24	2.70	0.41	0.00					24.8	2.9	
		Greig	0.57				-0.04	31.2	4.0	0.0	30.0	1.8	
		Hem	0.43				-0.01	53.1	2.0	0.0	6.8	0.8	

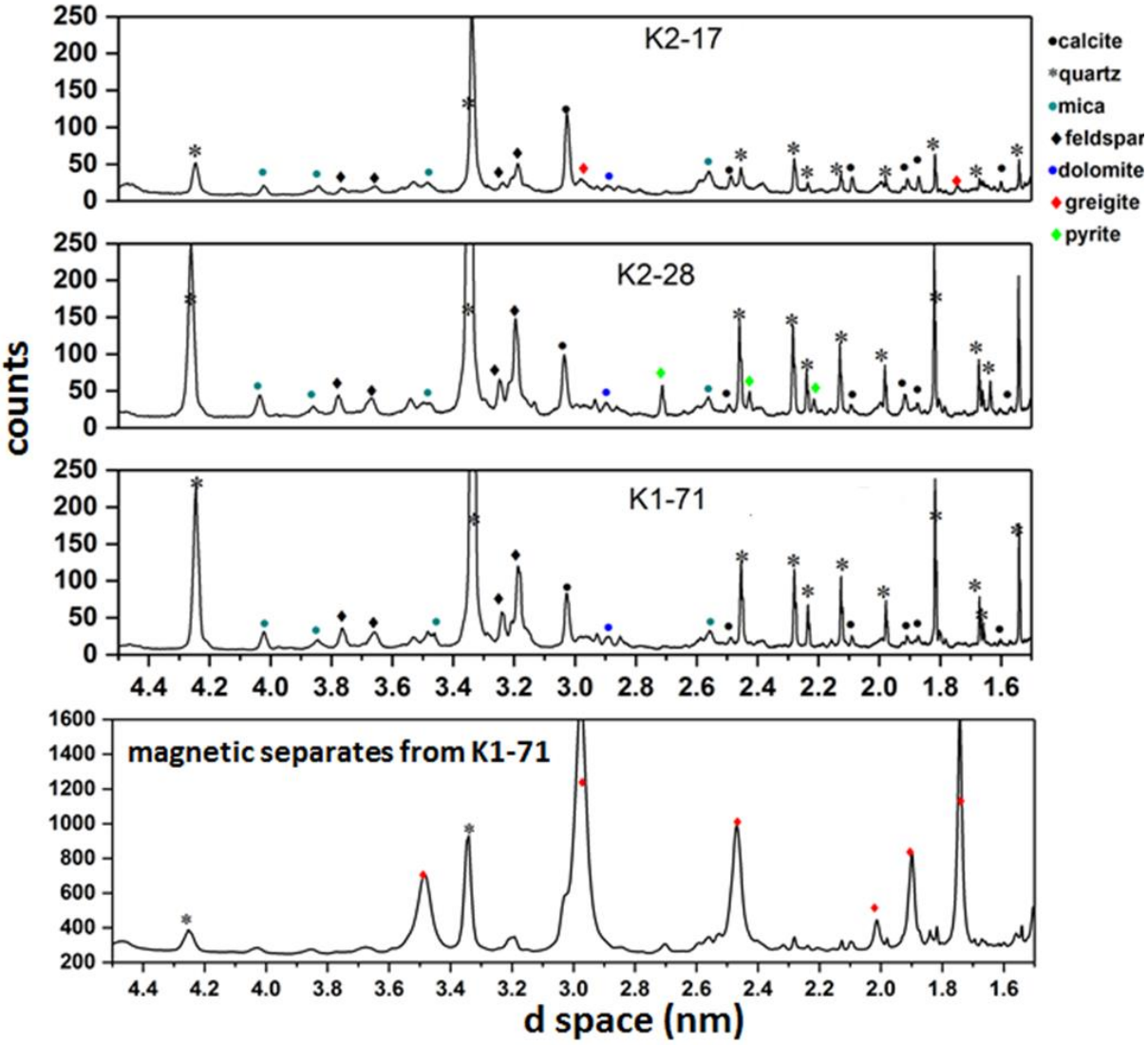

Supplementary Fig. S1 XRD pattern of peat samples and Synchrotron XRD pattern for magnetic separates from sample K1-71.

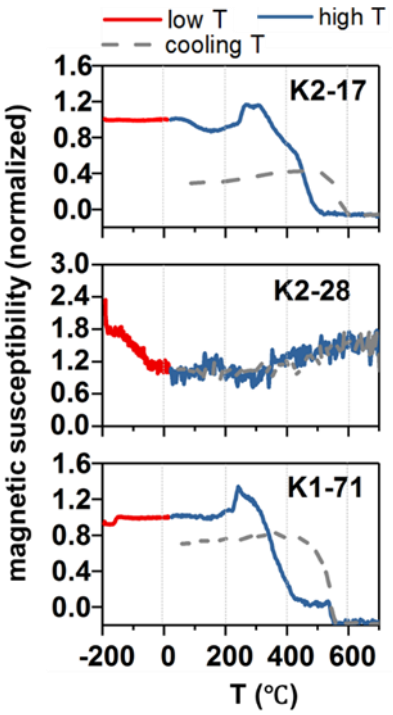

Supplementary Fig. S2 Thermomagnetic curves of magnetic susceptibility for peat sediments

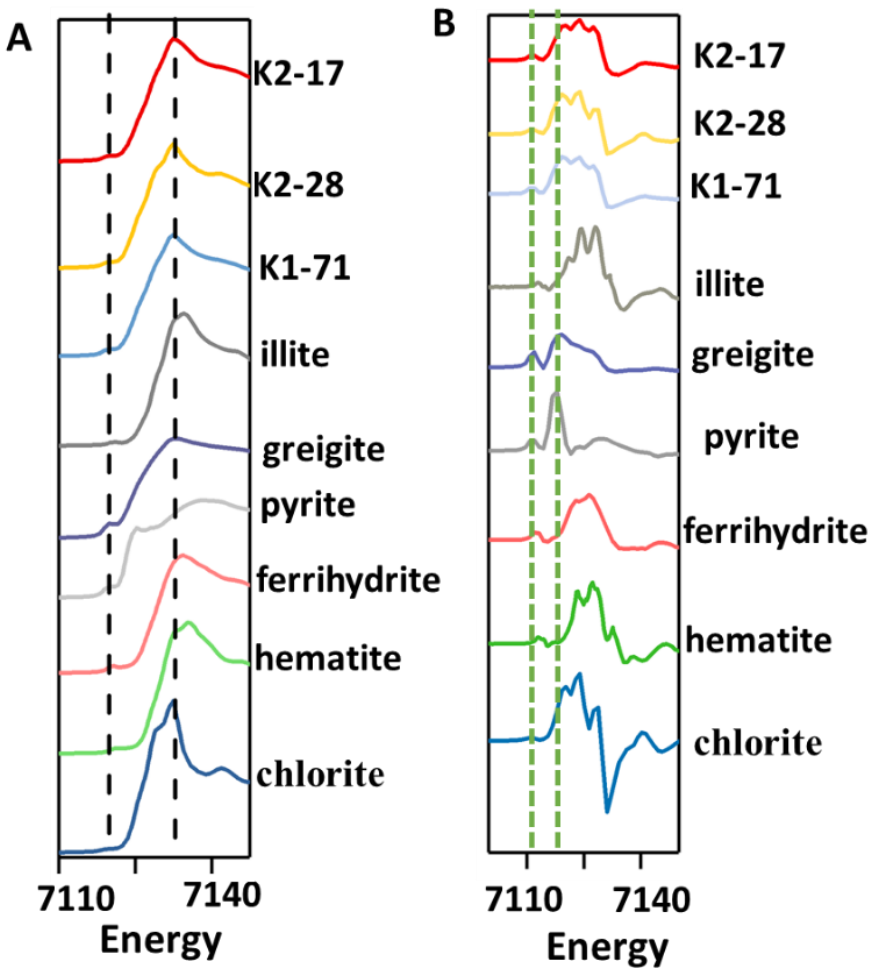

Supplementary Fig. S3 Fe K-edge XANES (A) and first-derivative XANES (B) spectra of peat samples and selective model compounds. The dashed lines in the XANES and derivative XANES spectra indicate that pre-edge inflection point and primary edge inflection points of peat sediments.

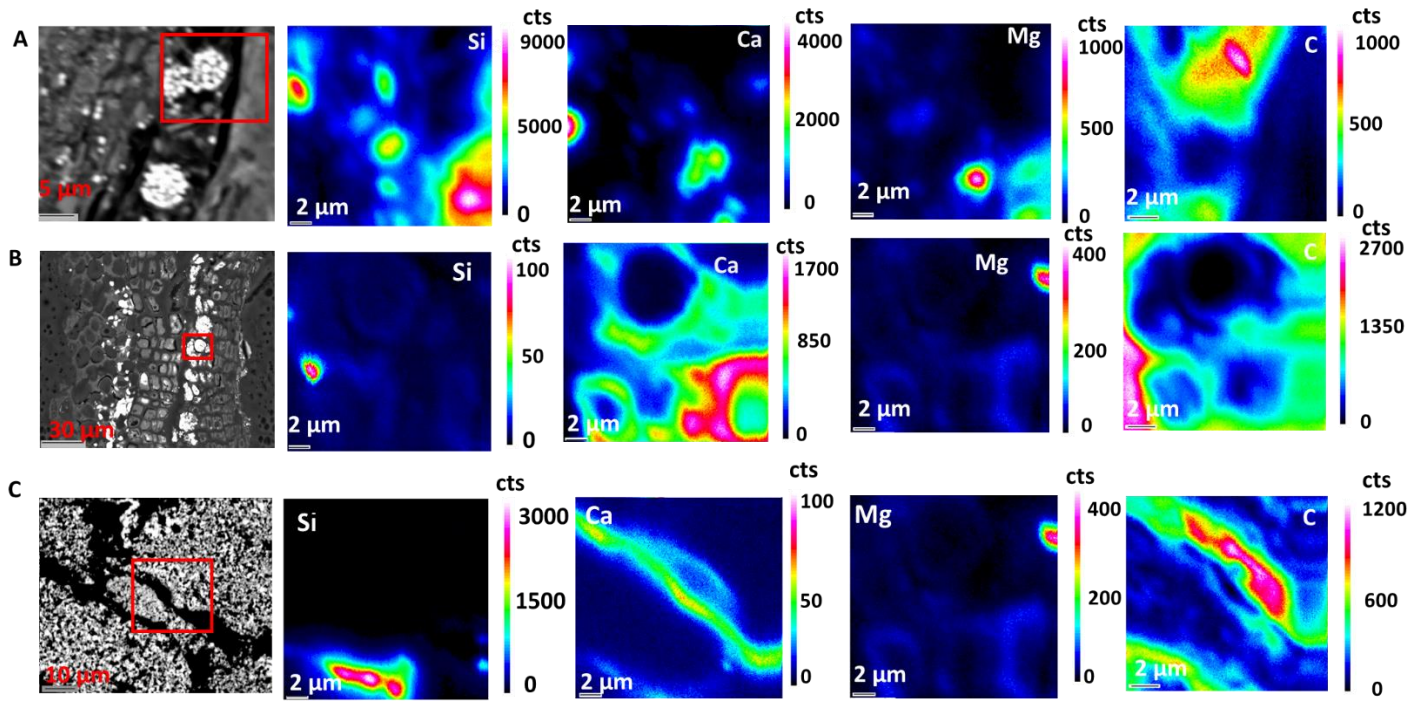

Supplementary Fig. S4 Elemental mapping images of Si, Ca and Mg and carbon obtained by electron probe microanalysis (EPMA), mapping area is indicated by red rectangle. (A) Map of framboidal pyrite aggregates in sample K2-17. (B) Map of framboidal and massive pyrite which nucleates in plant cells in K2-28 (C) Map of greigite in sample K1-71.

References

Cornell, R. M., Schwertmann, U. (2003). The iron oxides: structure, properties, reactions, occurrences and uses. *John Wiley & Sons*.

Dixit, S., Hering, J. G. (2003). Comparison of arsenic (V) and arsenic (III) sorption onto iron oxide minerals: implications for arsenic mobility. *Environl scie & technol*, 37(18), 4182-4189.

Géhin, A., Ruby, C., Abdelmoula, M., Benali, O., Ghanbaja, J., Refait, P., Génin, J. M. R. (2002). Synthesis of Fe (II-III) hydroxysulphate green rust by coprecipitation. *Solid State Sci*, *4*(1), 61-66.

Guo, H., Zhou, Y., Jia, Y., Tang, X., Li, X., Shen, M., Lu, H., Han S. B., Wei, C., Norra, S., Zhang, F. (2016). Sulfur cycling-related biogeochemical processes of arsenic mobilization in the western Hetao Basin, China: Evidence from multiple isotope approaches. *Environ sci & technol*, 50(23), 12650-12659.

Keon, N. E., Swartz, C. H., Brabander, D. J., Harvey, C., Hemond, H. F. (2001). Validation of an arsenic sequential extraction method for evaluating mobility in sediments. *Environ sci & technol*, *35*(13), 2778-2784.

Ravel, B. and Newville, M.A.T.H.E.N.A., 2005. ATHENA, ARTEMIS, HEPHAESTUS: data analysis for X-ray absorption spectroscopy using IFEFFIT. *J. Synchrotron Radiat*, 12(4), 537-541.